NUMERICAL MODELLING OF TWO-DIMENSIONAL SHALLOW-WATER FLOWS

BY

SAMI A AL-SANEA

M.Sc., D.I.C.

THESIS SUBMITTED FOR THE DEGREE OF

DOCTOR OF PHILOSOPHY

IN THE FACULTY OF ENGINEERING

UNIVERSITY OF LONDON

Mechanical Engineering Department

Imperial College of Science and Technology

London SW7 2BX

October , 1981

To

MY PARENTS,

BROTHER and

SISTER

GOD GRANT ME THE SERENITY
TO ACCEPT THE THINGS I CANNOT CHANGE;
THE COURAGE TO CHANGE THE THINGS I CAN;
AND THE WISDOM TO KNOW THE DIFFERENCE.

R. Niebuhr

ABSTRACT

This thesis describes a numerical model for predicting the behaviour of steady, two-dimensional and homogenous shallow-water flows. The flow is dependent primarily on the inertial forces, gravitational forces and channel-wall stresses.

The elliptic governing non-linear, depth-averaged differential equations are solved in a fixed and staggered cartesian-coordinate system using a finite-difference iterative procedure. The hydrodynamic variables are solved by a point-by-point (Jacobi) implicit scheme over the entire flow domain and the depth by a two-dimensional linear-equation solver. The free-surface position as well as the velocities are obtained after successive corrections based on the satisfaction of the conservation laws.

The model applies no restriction on the value of Froude number, i.e. to whether the flow is supercritical, subcritical or mixed. The locations of transition from supercritical to subcritical and vice versa are an outcome of the solution.

Certain notable features are introduced into the computational scheme, e.g. the use of the upstream values of depth when evaluating the fluxes across the cell faces and accounting for the depth variation into the formulation of the depth-correction equation. Also, the surface elevations are retained in the convective terms, a requirement needed for better accuracy especially at moderate and high Froude number values.

Simple experimental measurements are made of the supercritical flow and supercritical flow with hydraulic jumps in open channels. The main objective of these measurements is to provide data against which

the numerical model may be validated.

The numerical procedure is validated by comparing predicted results with analytical solutions, published data, computations by others and the present measurements. Some cases include comparisons made with the analogous two-dimensional compressible-gas flows. Good agreement is obtained in most cases considered and this demonstrates the applicability and accuracy of the numerical technique used.

P R E F A C E

The work reported in this thesis is the major result of my research activities in the Heat Transfer Section of the Mechanical Engineering Department, Imperial College of Science and Technology, during the period July 1977 to April 1981. These activities involved the development and validation of finite-difference calculation procedures for the prediction of fluid-dynamic and heat-transfer problems. The main objectives were to investigate and produce better and more economical procedures.

Prior to this period, after the completion of a one-year M.Sc. course in Heat Transfer Engineering in the same Section, I was engaged in team work for about six months to develop a computer code for the prediction of the flow inside a natural-draft cooling tower. The work was carried out at CHAM Ltd. (Concentration, Heat And Momentum).

For more than half the research period, I used the 2/E/FIX (Two-dimensional, Elliptic and Fixed Grid) computer code (Pun and Spalding, 1976), which was based on the SIMPLE (Semi-Implicit Method for Pressure-Linked Equations) pressure-correction technique of Patankar and Spalding (1972), but differed from SIMPLE in the way the finite-difference equations were solved.

My initial work concerned familiarising myself with finite-difference techniques and the SIMPLE algorithm used in the Heat Transfer Section. The computer code, 2/E/FIX, was employed for this purpose and was also used in a study to test various ideas, put forward by Prof. D.B.Spalding and Dr. W.M.Pun for the improvement of computing efficiency. Out of this study, a paper was produced and presented at the Conference on Laminar and Turbulent Flow,

Swansea,UK,July 1978 (AL-Sanea, et al, 1978).

Attention was then focussed on the development and validation of a numerical procedure for predicting two-dimensional shallow-water flows. The prediction of continuous flows was successfully achieved; however, for discontinuous flows, the solution procedure was found to be inadequate. The computer code was then changed to a more suitable one which used a "whole-field" approach instead of the "line-by-line" approach to the solution procedure. This computer code, called STABLEXT (Steady Three-dimensional Analyser of Boundary Layer Extended), was a general code based on the SIMPLE procedure for the prediction of three-dimensional parabolic and partially parabolic flows, developed originally at CHAM Ltd. This code was first experimented with and then modified, without loosing its general structure, to handle the problem of two-dimensional shallow-water flows. The features that were found to be important in describing both continuous and discontinuous flows were built into the model. To supplement the available experimental data, with which to validate the numerical procedure, I performed some experiments of supercritical flow and also supercritical flow with hydraulic jumps in channels of rectangular cross-section.

* * * * * * *

I would like now to express my gratitude to all those people who have directed and helped me in various ways during the course of my studies; I am indebted to all those from whom I have learnt. Firstly, I would like to thank my supervisor, Professor D.B.Spalding, for his constant and sincere interest; his skilful guidance through difficult periods is very much appreciated. Most of the achievements of the present study are largely due to his ideas and suggestions.

I am also grateful to Dr. W.M.Pun for the many discussions we

have had on all aspects of the work. My close association with him extends from my M.Sc. and third-year undergraduate projects. Throughout all this time, he has been a constant source of advice and encouragement. The interest of Dr. A.S.C.Ma is also appreciated.

My stay at Imperial College was enriched by the help, suggestions and the many discussions on both social and scientific matters with my colleagues and post-doctoral workers. These include: Tony Green, Ian Jennions, Urban Svensson, Bassam Younis, Ali Hadid, Luen Tong Tam, Ayodeji Demuren, S. Parameswaran, Amin Baghdadi, Ahmed Abdelmeguid, Pavlos Tagarakis, Richard Sun, George Carroll, Paul Shepherd and the many others. Thanks are also due to Mr. Bob King for his help in taking and processing the photographs of the experimental rig.

I would like to thank Sue Farmiloe, Maggie Dean and Frith Oliver for their assistance in adminstrative work, and Mr. Peter Dale for his help with various computer problems. Thanks are also due to Miss E.M.Archer and the rest of the staff in the Mechanical Engineering Library for providing excellent library survices.

I am indebted to the members of staff in the Hydraulics Section, laboratory technicians and to the library staff, of the Civil Engineering Department for allowing me use of their facilities.

Finally, I wish to acknowledge the partial support and assistance of the Science Research Council and CHAM Limited during the early period of my research; I have also benefitted from my early association with the expert engineers of the latter.

* * * * * * *

I would like to extend my gratitude to my parents, brother and sister, who have encouraged me through all the stages of my life and offered all possible support in making my education at school and college possible. My gratitude to them can not be expressed in words. I wonder if I can ever return some of the kindness they have shown me.

London Sami A. AL-Sanea

TABLE OF CONTENTS

	PAGE NUMBER
ABSTRACT	1
PREFACE	3
TABLE OF CONTENTS	7
LIST OF FIGURES	13
LIST OF TABLES	17
NOMENCLATURE	18
1. INTRODUCTION	22
1.1 The Problem Considered	22
1.2 Practical Relevance	23
1.2.1 Direct Applications of Shallow-Water Equations	23
1.2.2 Similarity to Floating Warm-Water Layers	27
1.2.3 Analogy to Compressible-Gas Flows	29
1.3 Present Study	31
1.3.1 Method of Calculation	31
1.3.2 Objectives	33
1.4 Outline of the Thesis	33
2. REVIEW OF PREVIOUS WORK	35
2.1 Introduction	35
2.2 Flow Classification	35
2.3 Continuous Shallow-Water Flows	35
2.3.1 Theoretical Work	36
2.3.2 Experimental Studies	48
2.4 Discontinuous Shallow-Water Flows	50
2.4.1 Experimental Studies and Control-Volume Analysis	50
2.4.2 Numerical Studies	55
2.4.3 Concluding Remarks	57
2.5 Analogous Flows	57
2.5.1 Studies of Gas-Hydraulic Analogy	57
2.5.2 Relevant Compressible-Gas Flows	63
2.5.3 Floating Warm-Water Layer and Other Analogous Flows	68
2.6 Status of Existing Information	70
2.7 Closure	71

		PAGE NUMBER
3.	MATHEMATICAL FORMULATION	72
	3.1 Introduction	72
	3.2 The Governing Differential Equations in General Form	72
	3.2.1 Derivation of Two-Dimensional Shallow-Water Equations	72
	3.2.2 Closure of the Equations	77
	3.2.3 Order of Magnitude Estimates	79
	3.3 The Governing Differential Equations Solved	84
	3.3.1 Basic Assumptions	84
	3.3.2 The Resulting Governing Equations	85
	3.3.3 Boundary and Initial Conditions	86
	3.3.4 Dependent Variables Solved	88
	3.4 Closure	88
4.	THE NUMERICAL SOLUTION PROCEDURE	90
	4.1 Introduction	90
	4.2 Determination of the Finite-Difference Equations	91
	4.2.1 The Finite-Difference Grid and Location of Flow Variables	91
	4.2.2 Control Volumes	94
	4.2.3 The Momentum Equations	94
	4.2.4 The Depth-Correction Equations	102
	4.3 Solution of the Finite-Difference Equations	107
	4.3.1 General Concept	107
	4.3.2 Point-By-Point Algorithm	107
	4.3.3 Two-Dimensional Linear-Equation Solver	108
	4.3.4 Summary of the Solution Steps	111
	4.4 Auxiliary Information	112
	4.4.1 Boundary Conditions	112
	4.4.2 Initial Conditions	113
	4.4.3 Treatment of Source Terms	114
	4.4.4 Convergence of the Procedure	115
	4.4.5 Stability of the Procedure	115
	4.4.6 Influence of Grid Size	120
	4.5 Summary of Main Features of the Procedure	121
	4.6 Closure	123

		PAGE NUMBER
5.	EXPERIMENTAL WORK	124
	5.1 Introduction	124
	5.2 One-Dimensional Measurements	125
	5.2.1 General Aspects	125
	5.2.2 Experimental Flume	125
	5.2.3 Experimental Procedure	127
	5.2.4 Experimental Accuracy	129
	5.2.5 Experimental Results	129
	5.3 Two-Dimensional Measurements	133
	5.3.1 General Aspects	133
	5.3.2 Experimental Flume	133
	5.3.3 Preparation and Setting-up Procedure	137
	5.3.4 Flow Measurements	138
	5.3.5 Experimental Procedure	139
	5.3.6 Experimental Accuracy	141
	5.3.7 Experimental Results	142
	5.4 Summary	149
6.	PREDICTIONS OF CONTINUOUS FLOWS	151
	6.1 Introduction	151
	6.1.1 General Concept	151
	6.1.2 Method of Presentation	152
	6.2 Subcritical Laminar Channel Flow	153
	6.2.1 Introduction	153
	6.2.2 Problem Specification	153
	6.2.3 Details of the Computations	155
	6.2.4 Results and Discussion	158
	6.2.5 Grid-Dependence Check	162
	6.3 Subcritical Laminar Square-Cavity Flow	162
	6.3.1 Introduction	162
	6.3.2 Problem Specification	162
	6.3.3 Details of the Computations	163
	6.3.4 Results and Discussion	167
	6.3.5 Grid-Dependence Check	167

		PAGE NUMBER
6.4	Spread of Depth Discontinuity in Supercritical Flows	170
6.4.1	Introduction	170
6.4.2	Problem Specification	170
6.4.3	Details of the Computations	174
6.4.4	Results and Discussion	176
6.4.5	Grid-Dependence Check	176
6.4.6	Concluding Remarks	181
6.5	Supercritical Flow Past Abrupt Channel Expansions	181
6.5.1	Introduction	181
6.5.2	Problem Specification	181
6.5.3	Details of the Computations	188
6.5.4	Results and Discussion	190
6.5.5	Grid-Dependence Check	191
6.5.6	Friction-Factor Investigation	197
6.5.7	Concluding Remarks	197
6.6	Closure	198
7.	PREDICTIONS TO COMPARE WITH EXPERIMENTAL RESULTS	199
7.1	Introduction	199
7.2	One-Dimensional Study	200
7.2.1	Introduction	200
7.2.2	Problem Specification	200
7.2.3	Details of the Computations	204
7.2.4	Presentation of the Results	206
7.2.5	Discussion of the Results	207
7.2.6	Friction-Factor Investigation	212
7.2.7	Grid-Dependence Check	214
7.2.8	Concluding Remarks	216
7.3	Two-Dimensional Study	217
7.3.1	Introduction	217
7.3.2	Problem Specification	217
7.3.3	Calculations with Supercritical Outlet Conditions	218
7.3.3.1	Details of the Computations	218
7.3.3.2	Presentation of the Results	220
7.3.3.3	Discussion of the Results	221
7.3.3.4	Friction-Factor Investigation	230

		PAGE NUMBER
7.3.3.5	Grid-Dependence Check	231
7.3.3.6	Concluding Remarks	231
7.3.4	Calculations with Subcritical Outlet Conditions	235
7.3.4.1	Background and General Concept	235
7.3.4.2	Details of the Computations	236
7.3.4.3	Presentation of the Results	238
7.3.4.4	Discussion of the Results	238
7.3.4.5	Friction-Factor Investigation	242
7.3.4.6	Grid-Dependence Check	244
7.3.4.7	Concluding Remarks	244
7.4	Closure	245
8.	CALCULATION OF TRANSONIC FLOWS USING THE HYDRAULIC ANALOGY	246
8.1	Introduction	246
8.2	The Analogy between Free-Surface and Compressible-Gas Flows	246
8.2.1	Background and General Concept	246
8.2.2	Mathematical Analysis	247
8.3	Simulation of Overexpanded Transonic Free Jets	252
8.3.1	Introduction	252
8.3.2	Problem Specification	252
8.3.3	Details of the Computations	256
8.3.4	Presentation of the Results	258
8.3.5	Discussion of the Results	259
8.3.6	Grid-Dependence Check	263
8.3.7	Concluding Remarks	266
8.4	Simulation of Supersonic Flow Impingement on a Blunt Body	267
8.4.1	Introduction	267
8.4.2	Problem Specification	267
8.4.3	Details of the Computations	272
8.4.4	Presentation of the Results	275
8.4.5	Discussion of the Results	286
8.4.6	Grid-Dependence Check	288
8.4.7	Concluding Remarks	293
8.5	Closure and General Remarks	294

	PAGE NUMBER
9. CONCLUSIONS	296
9.1 Achievements of the Present Study	296
9.2 Suggestions for Future Work	298
REFERENCES	300
APPENDIX A - DERIVATION OF TWO-DIMENSIONAL SHALLOW-WATER EQUATIONS	313
APPENDIX B - DERIVATION OF THE DEPTH-CORRECTION EQUATIONS	318
APPENDIX C - DEPTH-CORRECTION EQUATION AND ADJUSTMENT PROCEDURE FOR LOW FROUDE NUMBER FLOWS	323
APPENDIX D - TABULATED EXPERIMENTAL DATA FOR 1D FLOWS	328
APPENDIX E - TABULATED EXPERIMENTAL DATA FOR 2D FLOWS	331

LIST OF FIGURES

FIGURE NUMBER	TITLE	PAGE NUMBER
1.1	SOME RELEVANT SHALLOW-WATER FLOWS	25
2.1	FLOW CLASSIFICATION CHART FOR PRESENTATION OF THE LITERATURE REVIEW	36
3.1	DEFINITION OF BOTTOM HEIGHT, DEPTH, MEAN WATER LEVEL AND WATER SURFACE	75
4.1	LOCATION OF THE VARIABLES ON THE FINITE-DIFFERENCE GRID	93
4.2	DEFINITION OF THE CONTROL VOLUMES	93
4.3	NEAR-BOUNDARY CONTROL VOLUMES	95
4.4	GRID NOMENCLATURE USED TO DEVELOP THE FINITE-DIFFERENCE EQUATIONS	95
5.1	SCHEMATIC DIAGRAM (NOT TO SCALE) OF EXPERIMENTAL FLUME FOR 1D FLOWS	126
5.2	EXPERIMENTAL SURFACE PROFILES OF 1D FLOWS	132
5.3	SCHEMATIC DIAGRAM (NOT TO SCALE) OF EXPERIMENTAL FLUME FOR 2D FLOWS	134
5.4	OVERALL VIEW OF THE EXPERIMENTAL FLUME	135
5.5	PERSPECTIVE VIEWS OF THE SURFACE FOR RUN 1 LOOKING AT DIFFERENT ANGLES	145
5.6	PERSPECTIVE VIEWS OF THE SURFACE FOR RUN 2 LOOKING AT DIFFERENT ANGLES	146
5.7	VIEW OF THE FLOW BEHIND THE SEPARATING WALL	147
5.8	LOCATIONS OF THE TOE OF HYDRAULIC JUMPS VERSUS TAILWATER DEPTH	148
6.1	LAMINAR DEVELOPING FLOW IN A STRAIGHT OPEN CHANNEL; SHOWING GEOMETRY, COORDINATES, AND BOUNDARY CONDITIONS	159
6.2	VELOCITY-VECTOR PLOT FOR DEVELOPING OPEN-CHANNEL FLOW	159
6.3	VELOCITY DISTRIBUTION OF THE LAMINAR DEVELOPING FLOW IN A STRAIGHT OPEN CHANNEL	160
6.4	GRID-DEPENDENCE CHECK, OPEN-CHANNEL FLOW	161
6.5	CAVITY, SHOWING GEOMETRY, COORDINATES, AND BOUNDARY CONDITIONS	165
6.6	INITIAL FIELD VALUES FOR THE VELOCITIES	165
6.7	VELOCITY-VECTOR PLOT FOR FREE-SURFACE CAVITY FLOW. ($Re = 1$, $Fr_{ref} = 0.01$)	168
6.8	STREAM-FUNCTION CONTOURS FOR FREE-SURFACE CAVITY FLOW. ($Re = 1$, $Fr_{ref} = 0.01$)	168
6.9	u-VELOCITY PROFILES ACROSS THE VERTICAL CENTRE-PLANE, FREE-SURFACE CAVITY FLOW. ($Re = 1$, $Fr_{ref} = 0.01$)	169

FIGURE NUMBER	TITLE	PAGE NUMBER
6.10	SPREAD OF DEPTH DISCONTINUITY, SHOWING GEOMETRY, COORDINATES AND BOUNDARY CONDITIONS	173
6.11	THEORETICAL ANALYSIS OF THE ANGLE OF SPREAD OF A POINT DISTURBANCE	173
6.12	PERSPECTIVE VIEWS OF SURFACE ELEVATION; SPREAD OF DEPTH DISCONTINUITY, CASES 1,2 AND 3	177
6.13	CONTOUR PLOTS OF DEPTH; SPREAD OF DEPTH DISCONTINUITY, CASES 1,2 AND 3	178
6.14	DEPTH DISCONTINUITY; WAVE ANGLE VERSUS FROUDE NUMBER	179
6.15	GRID-DEPENDENCE CHECK; SPREAD OF DEPTH DISCONTINUITY (CASE 2, Fr = 3.19)	180
6.16	FLOW SITUATION; SUPERCRITICAL FLOW PAST ABRUPT EXPANSION	186
6.17	PERSPECTIVE VIEWS OF SURFACE ELEVATION; SUPERCRITICAL FLOW PAST ABRUPT EXPANSION, Fr_{in} = 2.0	192
6.18	VELOCITY-VECTOR PLOT FOR ABRUPT EXPANSION, Fr_{in} = 2.0	192
6.19	DIMENSIONLESS DEPTH CONTOURS FOR ABRUPT EXPANSION; COMPARISON WITH EXPERIMENTAL DATA, Fr_{in} = 2.0	193
6.20	NORMALIZED STREAM-FUNCTION CONTOURS AND Fr_x CONTOURS FOR ABRUPT EXPANSION , Fr_{in} =2.0	193
6.21	GRID-DEPENDENCE CHECK; ABRUPT EXPANSION	194
6.22	GRID USED TO PREDICT SUPERCRITICAL FLOW PAST ABRUPT EXPANSION	195
6.23	FRICTION-FACTOR INVESTIGATION; ABRUPT EXPANSION	196
7.1	WATER-SURFACE PROFILES OF 1D HYDRAULIC JUMPS AT DIFFERENT h_t AND FOR FIXED q	208
7.2	CHARACTERISTIC CURVES OF HYDRAULIC JUMPS	209
7.3	LOCATIONS OF THE BEGINNING OF THE HYDRAULIC JUMPS VERSUS TAILWATER DEPTH	210
7.4	WATER-SURFACE PROFILES OF 1D HYDRAULIC JUMPS AT DIFFERENT q AND FOR FIXED h_t	211
7.5	FRICTION-FACTOR INFLUENCE FOR 1D HYDRAULIC JUMPS	213
7.6	GRID-DEPENDENCE CHECK FOR 1D HYDRAULIC JUMPS	215
7.7	CROSS-STREAM DEPTH PROFILES FOR RUN 1	222
7.8	DEPTH DISTRIBUTION ALONG THE SIDE WALLS FOR RUN 1	225
7.9	COMPUTED VELOCITY-VECTOR PLOT AND STREAMLINES FOR RUN 1	225
7.10	CROSS-STREAM DEPTH PROFILES FOR RUN 2	226
7.11	DEPTH DISTRIBUTION ALONG THE SIDE WALLS FOR RUN 2	229
7.12	FRICTION-FACTOR INVESTIGATION FOR RUN 1	232
7.13	GRID-DEPENDENCE CHECK FOR RUN 1	233

FIGURE NUMBER	TITLE	PAGE NUMBER
7.14	GRID USED TO PREDICT MERGING OF TWO SUPERCRITICAL STREAMS FOR RUN 1	234
7.15	PERSPECTIVE VIEWS OF THE SURFACE ELEVATIONS FOR VARIOUS TAILWATER DEPTHS (RUN 1)	239
7.16	VELOCITY-VECTOR PLOT FOR RUN 1 AND h_t = 10.4 cm	239
7.17	COMPUTED DEPTH CONTOURS FOR RUN 1 AND h_t = 10.4 cm	240
7.18	COMPUTED STREAMLINES AND FROUDE-NUMBER CONTOURS FOR RUN 1 AND h_t = 10.4 cm	240
7.19	HYDRAULIC-JUMP MOVEMENT WITH VARIOUS TAILWATER DEPTHS (RUN 1)	241
7.20	HYDRAULIC-JUMP MOVEMENT WITH VARIOUS TAILWATER DEPTHS (RUN 2)	241
7.21	FRICTION-FACTOR INVESTIGATION FOR RUN 1 WITH SUBCRITICAL OUTLET CONDITIONS: SHOWING HYDRAULIC-JUMP LOCATION FOR h_t = 9.4 cm	243
7.22	GRID-DEPENDENCE CHECK FOR RUN 1 WITH SUBCRITICAL OUTLET CONDITIONS: SHOWING HYDRAULIC-JUMP LOCATION FOR h_t = 9.4 cm	243
8.1	DIAGRAMATIC VIEWS OF AN OVEREXPANDED FREE JET	253
8.2	PERSPECTIVE VIEWS OF THE SURFACE ELEVATIONS FOR THE SIMULATION OF OVEREXPANDED JETS (M_n = 1.92, PRESSURE RATIO = 0.51, γ = 1.4)	260
8.3	VELOCITY-VECTOR PLOT FOR THE SIMULATION OF OVEREXPANDED JETS (M_n = 1.92, PRESSURE RATIO = 0.51, γ = 1.4)	260
8.4	COMPUTED DEPTH CONTOURS NORMALIZED TO h_n ; SIMULATION OF OVEREXPANDED JET (M_n = 1.92, PRESSURE RATIO = 0.51, γ = 1.4)	261
8.5	COMPUTED STREAMLINES AND FROUDE-NUMBER CONTOURS; SIMULATION OF OVEREXPANDED JET (M_n = 1.92, PRESSURE RATIO = 0.51, γ = 1.4)	261
8.6	COMPARISON OF RIEMANN WAVE PARAMETERS FOR M_n (= Fr_n) OF 1.92; OVEREXPANDED FREE JETS	262
8.7	COMPUTED CENTRE-PLANE DEPTH VARIATIONS; SIMULATION OF OVEREXPANDED JET (M_n = 2.0, PRESSURE RATIO = 0.55, γ = 1.4)	264
8.8	COMPUTED DEPTH VARIATIONS AT THREE CROSS-STREAM LOCATIONS; SIMULATION OF OVEREXPANDED JET (M_n = 2.0, PRESSURE RATIO = 0.55, γ = 1.4)	265
8.9	FLOW IMPINGEMENT ON A BLUNT BODY SHOWING GEOMETRY AND BOUNDARY CONDITIONS	268
8.10	PERSPECTIVE VIEWS OF THE SURFACE ELEVATIONS OF FLOW IMPINGEMENT ON A BLUNT BODY (Fr_{in} = M_{in} = 5.0, γ = 1.4)	277
8.11	VELOCITY-VECTOR PLOT OF FLOW IMPINGEMENT ON A BLUNT BODY (Fr_{in} = M_{in} = 5.0, γ = 1.4)	278

FIGURE NUMBER	TITLE	PAGE NUMBER
8.12	COMPUTED DEPTH CONTOURS NORMALIZED TO h_{in} ; SIMULATION OF FLOW IMPINGEMENT ON A BLUNT BODY ($Fr_{in} = M_{in} = 5.0$, $\gamma = 1.4$)	279
8.13	COMPUTED STREAMLINES AND FROUDE-NUMBER CONTOURS; SIMULATION OF FLOW IMPINGEMENT ON A BLUNT BODY ($Fr_{in} = M_{in} = 5.0$, $\gamma = 1.4$)	280
8.14	COMPARISON OF THEORETICAL, NUMERICAL, AND EXPERIMENTAL SHOCK STANDOFF DISTANCES IN FRONT OF A 180° WEDGE (BLOCK) PLACED NORMAL TO THE FREE STREAM	281
8.15	SHOCK-WAVE LOCATIONS OF FLOW IMPINGEMENT ON 180° WEDGE AT DIFFERENT FREE-STREAM MACH NUMBERS	282
8.16	SHOCK-WAVE AND SONIC-LINE LOCATIONS OF FLOW IMPINGEMENT ON 180° WEDGE AT FREE-STREAM MACH NUMBER OF 1.37	283
8.17	SHOCK-WAVE AND SONIC-LINE LOCATIONS OF FLOW IMPINGEMENT ON 180° WEDGE AT FREE-STREAM MACH NUMBER OF 5.0	284
8.18	PRESSURE DISTRIBUTION ON THE FACE NORMAL TO FREE STREAM OF A 180° WEDGE	285
8.19	CENTRE-PLANE DEPTH RATIO ACROSS THE BOW SHOCK	285
8.20	COMPUTED CENTRE-PLANE DEPTH VARIATIONS FOR $Fr_{in} = 2.8$; FLOW IMPINGEMENT ON A RECTANGULAR BODY	289
8.21	COMPUTED CROSS-STREAM DEPTH VARIATIONS AT $x/B = 1.0$ FOR $Fr_{in} = 2.8$; FLOW IMPINGEMENT ON A RECTANGULAR BODY	290
8.22	GRID USED TO PREDICT FLOW IMPINGEMENT ON A RECTANGULAR BODY FOR FREE-STREAM FROUDE NUMBER BETWEEN 2 AND 5.8	291
8.23	GRID USED TO PREDICT FLOW IMPINGEMENT ON A RECTANGULAR BODY FOR FREE-STREAM FROUDE NUMBER BETWEEN 1.3 AND 1.9	292
B1	DEPTH-CORRECTION CELL	318
C1	RELAXATION FACTOR FOR DEPTH VARIATION VERSUS FROUDE NUMBER	326

LIST OF TABLES

TABLE NUMBER	TITLE	PAGE NUMBER
1.1	COMPARISON OF THE FEATURES OF SHALLOW-WATER FLOWS WITH FLOATING WARM-WATER LAYERS	28
1.2	GAS-WATER FLOW ANALOGY	29
2.1	SUMMARY OF THE EXPERIMENTAL STUDIES ON SHALLOW-WATER FLOWS	51
2.2	STUDIES OF GAS-HYDRAULIC ANALOGY	62
3.1	TERMS IN THE GENERAL u-MOMENTUM EQUATION IN DIMENSIONLESS FORM	82
4.1	LINEARISED-SOURCE TERMS FOR THE DEPTH-AVERAGED SHALLOW-WATER FLOWS	114
5.1	TEST CONDITIONS FOR 1D FLOW EXPERIMENTS	131
5.2	TEST CONDITIONS FOR 2D FLOW EXPERIMENTS	143
6.1	COMPUTATIONAL DETAILS FOR SUBCRITICAL LAMINAR CHANNEL FLOW	158
6.2	COMPUTATIONAL DETAILS FOR SUBCRITICAL LAMINAR CAVITY FLOW	166
6.3	COMPUTATIONAL DETAILS FOR SPREAD OF DEPTH DISCONTINUITY IN SUPERCRITICAL FLOWS	175
6.4	COMPUTATIONAL DETAILS FOR SUPERCRITICAL FLOW PAST ABRUPT EXPANSION	190
7.1	COMPUTATIONAL DETAILS FOR ONE-DIMENSIONAL HYDRAULIC JUMPS	206
7.2	COMPUTATIONAL DETAILS FOR PREDICTING RUN 1 OF THE 2D EXPERIMENTS WITH SUPERCRITICAL OUTLET CONDITIONS	221
7.3	COMPUTATIONAL DETAILS FOR PREDICTING RUN 1 OF THE 2D EXPERIMENTS WITH SUBCRITICAL OUTLET CONDITIONS	237
8.1	COMPARISON BETWEEN SHALLOW-WATER AND COMPRESSIBLE-GAS FLOW EQUATIONS	250
8.2	STUDIES OF TWO-DIMENSIONAL (PLANE) TRANSONIC FREE JETS	254
8.3	COMPUTATIONAL DETAILS FOR PREDICTING TWO-DIMENSIONAL OVEREXPANDED FREE JET	258
8.4	SELECTED STUDIES OF TWO-DIMENSIONAL (PLANE) SUPERSONIC FLOW IMPINGEMENT ON RECTANGULAR BODIES	270
8.5	COMPUTATIONAL DETAILS FOR PREDICTING FLOW IMPINGEMENT ON A RECTANGULAR BODY	275

NOMENCLATURE

SYMBOL	MEANING
a	area of a control volume face; speed of sound;
A	coefficient in the finite-difference equations;
a,b,B,N & E	coefficients in the recurrence relation of the h' equation;
b	narrow channel width (Section 6.5);
B	block half width (Section 8.4);
c	wave speed;
C	Chézy's coefficient; convective flux in the finite-difference equations;
C_d	discharge coefficient of sluice gate;
C_f	wall shear-stress coefficient;
C_p & C_v	specific-heat capacity at constant pressure, and at constant volume, respectively;
C_s	free-surface shear-stress coefficient;
d	height of opening below sluice gate;
D	diffusive flux in the finite-difference equations; coefficient in the finite-difference equations;
E	total energy head (Section 7.2);
f	Coriolis parameter; denoting a function of;
Fr	$= u / (gh)^{\frac{1}{2}}$, the Froude number;
g	gravitational acceleration;
h	depth of flow;
h_4	headwater depth (Sections 5.2 and 7.2);
h_5	depth below sluice gate (Sections 5.2 and 7.2);
h_c	critical depth ;
h_j	$= h_2 - h_1$, height of hydraulic jump;
h_t	tailwater depth;
H	a reference depth;
i	energy slope (friction slope);
L	channel length; a reference length (Chapter 3); length of hydraulic jump (Section 7.2); shock standoff distance (Section 8.4);
m	mass flux across a finite-difference cell; hydraulic mean depth;
M	$= u / (\gamma p / \varrho)^{\frac{1}{2}}$, the Mach number;

SYMBOL	MEANING
n	Manning's roughness coefficient;
n,s,e & w	locations midway between grid nodes;
N,S,E,W & P	finite-difference node locations;
p	pressure;
q	discharge per unit width;
R	= V / fL , the Rossby number (Chapter 3); a quantity denoting residual (Chapter 4);
Re	= ρ V L / μ , the Reynolds number;
RELAXϕ	under-relaxation factor for the variable ϕ;
s	channel slope;
S_U	one part of the linearized source term in the finite-difference equations;
S_P	the other part of the linearized source term;
S^{ϕ}	source term in the transport equation for ϕ;
t	time;
T	temperature;
u,v	velocity components in the x- and y-directions respectively;
U	lid velocity (Section 6.3); inlet u-velocity (Section 6.4);
U_0 & V_0	relative wind velocity components in the x- and y-directions respectively;
V	a reference velocity (Chapter 3); volume of finite-difference cell (Chapter 4);
x	coordinate direction;
$\bar{x}$	= x/ Y. Re (Section 6.2);
x_{stem} & y_{stem}	shock standoff distance and shock half width respectively (Section 8.3);
y	coordinate direction;
Y	relates to channel width; square-cavity side length (Section 6.3);
z	coordinate in the vertical direction (normal to x-y plane);
z_b	channel bed above a horizontal datum;

GREEK SYMBOLS	MEANING
α	wave angle relative to flow direction;
β	volumetric-expansion coefficient;
γ	ratio of specific heats (= C_p / C_v);
Γ	transport coefficient;
δx, δy	length and width (respectively) of a finite-difference cell;
Δ	an increment of;
η	surface elevation relative to mean-water level;
μ	dynamic viscosity;
ρ	density;
Σ	signifies summation;
τ	shear stress;
ϕ	general variable;
ψ	stream function;

SUBSCRIPTS

1,2	relate to streams 1 and 2; relate to toe and end of 1-D hydraulic jump respectively;
3	denotes inlet conditions for 1-D flows (measured at 15 cm from sluice gate);
a	ambient; air; atmospheric;
b	relates to channel bed;
i	relates to grid node N, S, E or W;
in	relates to inlet plane; relates to free stream (infinity);
n	relates to nozzle exit plane (Section 8.3);
n,s,e & w	define variables midway between grid nodes;
N,S,E,W & P	define variables at the grid nodes;
new	relates to variable value immediately after solving the difference equations;
0	relates to total; stagnation; headwater;
old	relates to variable value prevailing at previous iteration;
ref	relates to a reference value;
s	relates to flow surface;

SUBSCRIPTS	MEANING
t	relates to tailwater conditions;
xx,xy,xz, yy and zy	relate to plane normal to flow direction and the flow direction respectively;
*	defining a dimensionless quantity;

SUPERSCRIPTS

u,v,Ø	denote coefficient of finite-difference equations for the respective variable;
*	estimated value; derived from an estimated value;
'	correction to be added to estimated value;
-	mean value; depth-averaged value.

CHAPTER 1

INTRODUCTION

1.1 THE PROBLEM CONSIDERED

Numerical modelling techniques have progressed rapidly in the last decade or so for solving a variety of engineering and environmental problems. This was made possible by the advent of fast and large digital computers, before which investigations were limited to a few analytical and experimental approaches which were known to suffer from severe drawbacks as far as approximations involved, applicability and economy were concerned. Examples of such engineering problems, in the field of fluid mechanics, are shallow-water flows, which belong to a more general class known as free-surface flows which are regarded as two-phase flows where the phases are completely separated. Typical examples are water flows in hydraulic structures in general, tidal motion in shallow seas and estuaries, and flows in shallow wind-stirred bays, lakes, etc. These flows are of considerable importance in the environment as indeed in hydraulics engineering practice; they are of scientific interest too because of the analogy to compressible-gas flows. Although methods do exist for the solution of these flows, they are either limited in applicability, expensive to use or mainly applied for solving problems in the field of gas-dynamics.

This thesis describes the development and application of a numerical model, which is both extendable and economical, for predicting steady shallow-water flows in one- and two-dimensions. The flow is regarded as either laminar or inviscid with a hydrostatic pressure distribution in the vertical (these assumptions lie within the frame-

work of the shallow-water approximations); the stresses with the channel surfaces, if present, are accounted for by empirical friction formulae. A variety of flow situations in which the flow is wholly subcritical, wholly supercritical and a mixture of the two are investigated; a few compressible-gas flow problems are also simulated. These applications form the main basis for the physical validation of the model and demonstrate the well-known analogy with comressible-gas flows.

1.2 PRACTICAL RELEVANCE

1.2.1 Direct Applications of Shallow-Water Equations

Shallow-water flows are found largely in the environment, such as in lakes and coastal waters, where horizontal dimensions are much larger than the depth. They are also found in irrigation canals, natural and man-made cooling ponds and in partially filled conduits. Typical shallow-water and some analogous flows and the situations in which they occur include:

(a) Shallow wind-stirred bays, lakes, estuaries, etc. The interest in this area is largely motivated by environmental considerations and the need for prediction of man-made alterations to nature by the construction of harbours, barrages and emission of thermal and chemical effluents.

(b) The "hurricane draw-down" problem and its effects on the cooling-water intake for a power station as the hurricane passes over shallow coastal-waters.

(c) The movement of tidal waves in terrestrial waters and its effects

on navigation, construction of engineering works and indeed on the cooling capacity of a water body used as a heat disposal from power stations

(d) Wind-induced circulation in lakes.

(e) Various flows in hydraulic-engineering structures, such as flows in channels, spillways, etc. Informations of the flow are needed for an efficient design, e.g. in the design of an open-channel transition for high velocity flows.

(f) The spread of an oil slick over a water surface.

(g) Shallow-liquid flow in partially filled conduits.

(h) Waves approaching beaches including the breaking of such waves.

(i) Airflow over mountains and the spread of cool air over the earth's surface beneath masses of warmer air.

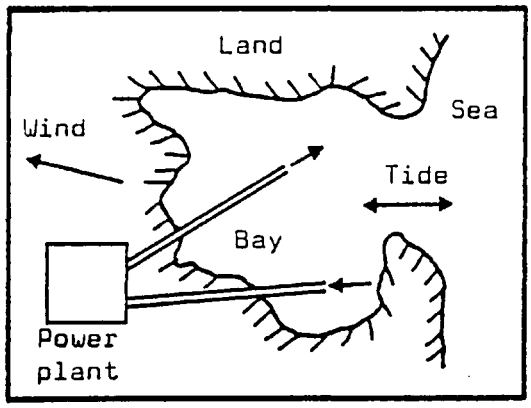
(j) Density currents in reservoirs.

(k) The occurrence of hydraulic jumps and bores which link two different types of flow regimes. This constitutes one of the most interesting phenomena in the field of hydraulic engineering. An internal jump may occur if a density gradient exists between two fluids.

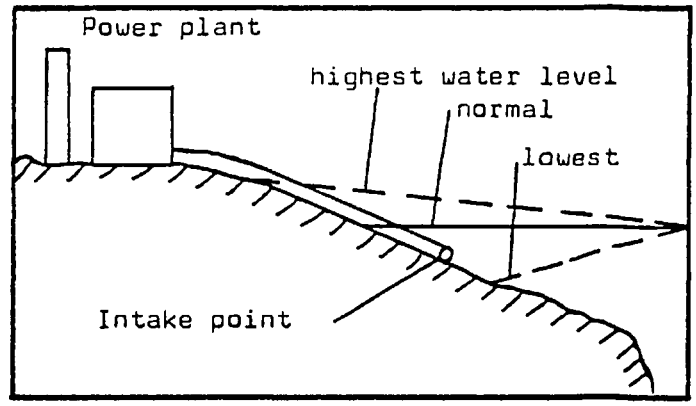
(l) The propagation of a "tsunami" wave towards the coast. Such a wave is generated by the sudden rise in sea level above the seismic centre due to deformation of the sea bottom caused by such an earthquake.

Some of these flows are illustrated in Figure 1.1.

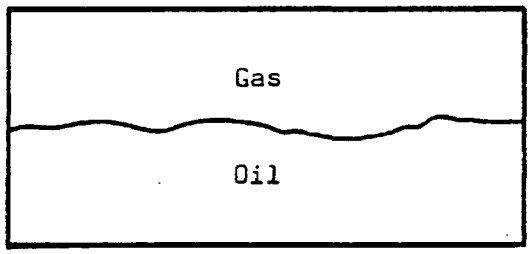
To adequately design structures, estimating the cooling capacity of a lake, to give an advance warning of the threat of an oil slick,



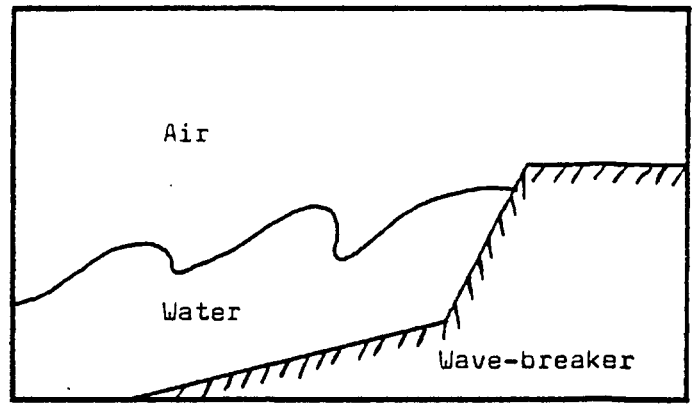
Cooling-water reservoir



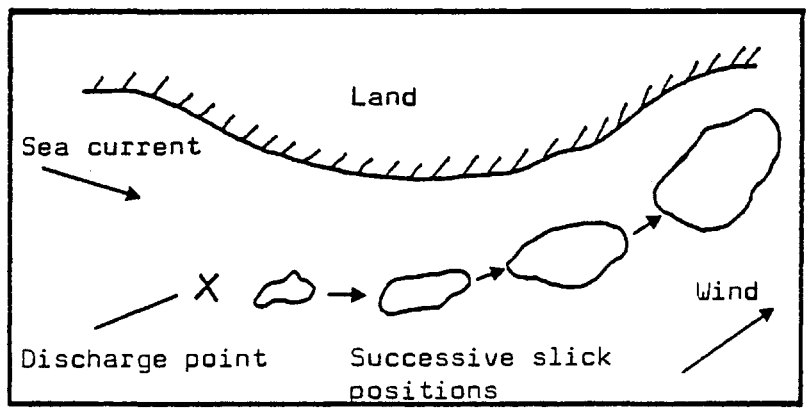
Hurricane draw-down problem



Flow of oil in an oil pipe line

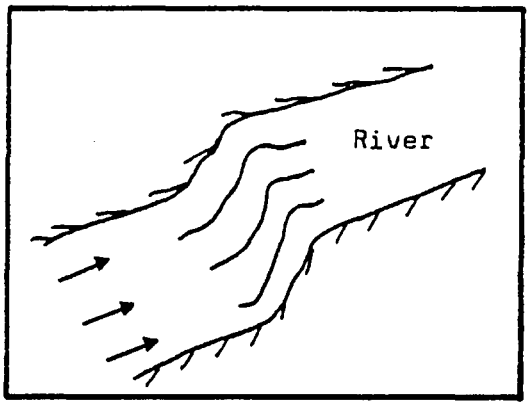


Wave breaking on beaches

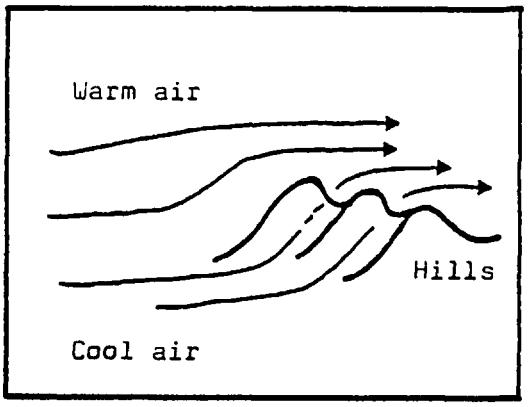


Spread of oil slick

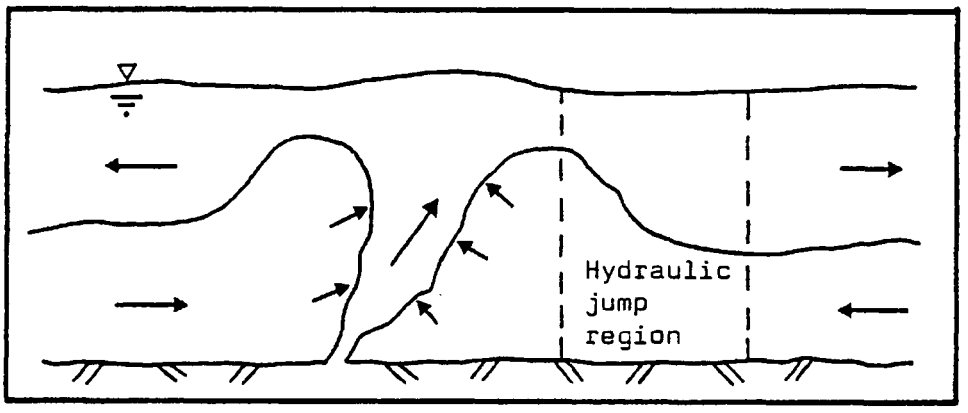
FIGURE 1.1 : SOME RELEVANT SHALLOW-WATER FLOWS



Hydraulic jump or bore in rivers



Air flow over hills



Internal hydraulic jump in highly buoyant jets

FIGURE 1.1 : (Continued)

a hurricane or flooding etc. involve detailed information regarding the flow in the above situations. Analytical methods do not produce sufficiently accurate information because of the approximations involved and they certainly do not exist for complex geometrical configurations. The use of hydraulic models is tedious and expensive. The development of numerical models which are computationally cheap, general, and easy to use will therefore be valuable for such calculations.

The importance of shallow-water flow studies is very much augmented by the similarity and analogy they have with a variety of other flows found in both the environment and in engineering practice. Such flows are classified and discussed next.

1.2.2 Similarity to Floating Warm-water Layers

Similarities exist between shallow-water flows and those of floating warm-water layers (as indeed with fresh-water layers floating over saline layers). While the former flows are characterized by the Froude number, which is the ratio of the inertial to the gravitational forces, the latter flows are characterized by the densimetric Froude number, which is the ratio of the inertial to the buoyancy forces. Hydraulic jumps, which are associated with shallow-water flows, have their counterparts in floating warm-water layers, as internal hydraulic jumps, which usually link the near and far fields of the thermal discharges of power plants into bodies of water. Knowledge of the flow field is required to assess the impact of a power station on the environment as well as the cooling efficiency of the receiving water flows. The basic similarities and differences of these two flows are summarized in Table 1.1.

Shallow-water flows	Floating warm-water layers
• Characterized by Froude number = $\frac{\text{inertial force}}{\text{gravitational force}}$	• Characterized by densimetric Froude number = $\frac{\text{inertial force}}{\text{buoyancy force}}$
• Supported by solid mass	• Supported by cooler (denser) liquid mass
• Bottom friction important	• Entrainment important
• Hydraulic jump	• Internal hydraulic jump

TABLE 1.1 : COMPARISON OF THE FEATURES OF SHALLOW-WATER FLOWS WITH FLOATING WARM-WATER LAYERS

A mathematical model which is developed to calculate shallow-water flows can be easily adapted to calculate floating-layer flows in general, such as the oil slick flow and the heated surface discharge. All that is needed is:

(i) The friction at the solid boundaries to be replaced by an appropriate entrainment formula, except, of course, for the oil slick flow.

(ii) A density gradient ($\Delta\rho/\rho$), given by $\beta\,\Delta T$ (where β is the volumetric expansion) when there is a temperature difference, now multiplies the depth-gradient terms in the momentum equations.

1.2.3 Analogy to Compressible-Gas Flows

The equations that govern the flow of shallow water are analogous to those governing the flow of a compressible fictitious gas of γ (= C_p / C_v) = 2, where the C's are the specific heats at constant pressure and constant volume. This is often termed the "hydraulic analogy to comressible-gas flows" and will be discussed in detail in Chapter 8. Hydraulic jumps are analogous to shock waves although the former occur over much longer physical lengths. The analogy may be described as shown in Table 1.2.

Analogous quantity	Shallow-water flows	Compressible gas flows
Flow conditions	• Frictionless • Total head(h_0)	• Adiabatic process • Enthalpy
Fluid	• Incompressible; water	• Compressible gas; γ = 2
Wave velocity	• Wave celerity ($c = \sqrt{gh}$)	• Acoustic velocity ($a = \sqrt{\gamma p/\rho}$)
Shock wave	• Hydraulic jump	• Shock wave
Flow	• Supercritical • Subcritical • Critical line	• Supersonic • Subsonic • Sonic line
Characteristic ratios	• Froude number ($Fr = V/c$) • Depth ratio (h/h_0) • Depth ratio • Total pressure ratio ($P/P_0 = h^2/h_0^2$)	• Mach number ($M = V/a$) • Density ratio (ρ/ρ_0) • Temperature ratio (T/T_0) • Pressure ratio (p/p_0)

TABLE 1.2 : GAS-WATER FLOW ANALOGY

Measurements and flow visualizations in flumes and water tables have been reported in the literature to study and demonstrate the behaviour of analogous compressible-gas flows. These only give an interesting qualitative study since an exact, and hence a quantitative agreement, is only possible when γ equals 2. No gas is known in nature with such a value for γ ; for example, the value of γ for air equals 1.4.

The above limitation is true as far as experiments with water are concerned; however, as far as a numerical model is concerned, there is no need for γ to be assigned a realistic value and indeed it can be assigned to any value even if fictitious. If a mathematical model for compressible-gas flows is at hand, a direct analogy with shallow-water flows can be achieved simply by setting $\gamma = 2$, i.e. solving for the fictitious gas in the model. On the other hand, if a mathematical model for shallow-water flows is developed, as in the present study, it can be made to simulate the inviscid flow of a compressible gas with any value of γ , for example air in which $\gamma = 1.4$, with a minor adjustments to the equations. In other words, the analogy with the compressible-gas flow equations can be made in a straightforward manner, with small modifications needed to the shallow-water equations.

It is to be concluded from the above that any progress in solving the shallow-water equations can be made immediately applicable to the solution of compressible-gas flows as will be shown and demonstrated in a few test cases in Chapter 8. This highlights another important and practically relevant aspect of the subject studied in this thesis.

1.3 PRESENT STUDY

1.3.1 Method of Calculation

The theoretical calculation of two-dimensional shallow-water flows involves the simultaneous solution of a set of non-linear partial-differential equations which govern the conservation of mass and momentum. If the transport of other flow properties, such as temperature, concentration, etc., is to be accounted for, an additional conservation equation for each must be added. This system of equations is complex, and in general, not amenable to closed-form analytical solutions. Therefore, attention is directed towards the development of numerical solution procedures which can provide accurate and reliable predictions of real flow situations.

In the present study these equations, in steady state and depth-averaged form, are solved by an implicit finite-difference scheme based on the "SIMPLE" (Semi-Implicit Method for Pressure-Linked Equations) algorithm of Patankar and Spalding (1972). SIMPLE is an iterative pressure-correction procedure in which the velocity fields are calculated from a "guessed" pressure field, and then, "pressure-corrections" are computed from the continuity relations. These pressure-corrections are used to adjust both the pressure and velocity fields. This process is performed iteratively until the hydrodynamic fields are obtained. In free-surface flows, the terms pressure and pressure-correction are translated into depth and depth-correction respectively.

Other specific features of the present calculation procedure are:

(a) The finite-difference form of the momentum equations are solved by an implicit Jacobi point-by-point method.

(b) The depth-correction equations are formulated over the whole field and solved by a two-dimensional linear-equation solver (Spalding, 1979).

(c) The use of upstream depths in evaluating the mass fluxes across the finite-difference control-volume faces.

(d) An implicit account of depth variations in the formulation of the depth-correction equations.

The computations of shallow-water flows are often complicated by the presence of discontinuities such as bores and hydraulic jumps, in which case, both supercritical and subcritical flow regions are present in the flow domain. Supercritical flows are associated with surface waves and characterized by the hyperbolic nature of the governing equations; surface disturbances only travel downstream and the flow is controlled by upstream conditions. On the other hand, the changes in velocities and depth in subcritical flows are usually much less pronounced and the flow is characterized by the elliptic nature of the equations; surface disturbances travel in all directions and the flow is controlled by downstream conditions. However, in this study, the set of equations is solved by the same solution scheme; the adjustment procedure is made general and independent of Froude number.

From the numerical point of view the hydraulic jump is modelled as a discontinuity, this is physically realistic only when the width of the actual jump is much smaller than the reference length. The discontinuity is not treated explicitly, but comes out of the

computation as steep gradients in the flow properties spreading over a few grid lines. This procedure of computing is known as the "shock-capturing technique".

1.3.2 Objectives

The present study concerns the development and application of a general numerical solution procedure for the prediction of steady two-dimensional shallow-water flows. The objectives of this work are as follows:

(a) To develop a mathematical model and solution procedure capable of predicting shallow-water flows.

(b) To assess the mathematical accuracy and physical realism of the numerical procedure by comparing predictions with analytical solutions, published data and reliable solutions by others.

(c) To carry out an experimental investigation of the supercritical flow of water in channels to supplement the existing experimental information.

(d) To predict the experimental results and hence to further validate the numerical model.

1.4 OUTLINE OF THE THESIS

The main body of the thesis consists of nine chapters, the first of which describes the introductory material. Chapter 2 contains a review of the previous work in which other mathematical models and experimental investigations on the subject in general are described. The mathematical formulation of the present work is laid in Chapter 3.

The numerical solution procedure is detailed in Chapter 4. The experimental investigation carried out is reported in Chapter 5. Chapter 6 contains the predictions of continuous flows which concentrates on a step by step verification of the solution procedure, based on analytical solutions where possible. The predictions to compare with own experimental results are presented in Chapter 7 which contains discontinuous flows. The hydraulic analogy to compressible-gas flows is described in Chapter 8; two test cases of transonic flows are simulated, the first considers the Mach-stem flow of over-expanded free jets, while the second case simulates the impingement of two-dimensional supersonic flows on blunt bodies.

The conclusions from this thesis are given in Chapter 9; the achievements of the present study are stated, and some suggestions for future work are made. This concludes the main part of the thesis. The remaining sections contain a list of the cited references, and appendices that provide supplementary information to that given in the main text.

C H A P T E R 2

REVIEW OF PREVIOUS WORK

2.1 INTRODUCTION

The purpose of this chapter is to review the various theoretical procedures applied to shallow-water flows and analogous flows; it also summarizes the available experimental data. The chapter is concluded with remarks on the status of the existing information.

2.2 FLOW CLASSIFICATION

Owing to the diversity of the subject reviewed and in order to help clarify and present the literature review, the subject is classified as follows:

(a) Continuous shallow-water flows.

(b) Discontinuous shallow-water flows.

(c) Analogous flows.

This classification is shown in Figure 2.1. Some of the work, the results of which are used for comparison in the present study, are discussed further in Chapters 6,7 and 8.

2.3 CONTINUOUS SHALLOW-WATER FLOWS

Continuous flows are flows without hydraulic jumps or bores, in which the flow can either be wholly subcritical or wholly supercritical. These flows range from uniform flows, which scarcely occur in practice but are very simple to analyse, to varied flows with various physical processes which are most commonly encountered in practice.

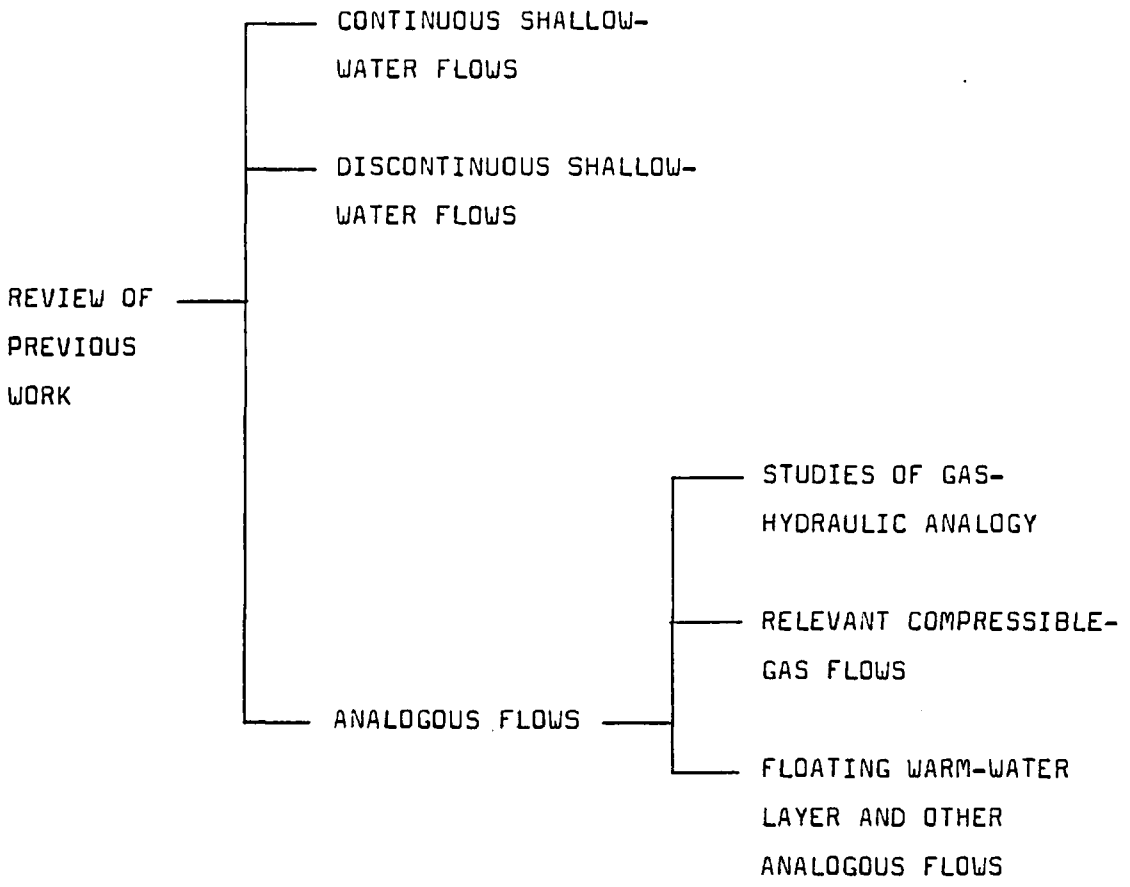


FIGURE 2.1 : FLOW CLASSIFICATION CHART FOR PRESENTATION OF THE LITERATURE REVIEW

2.3.1 Theoretical Work

Many different mathematical formulations, based on various assumptions, and solution procedures for continuous flows exist in the literature. Spalding (1975) has extensively reviewed this subject and discussed the various problems involved and the assumptions made, in a course of lectures on the transfer of heat in rivers, bays, lakes and estuaries (see also Spalding, 1976). This study covered a much wider area than continuous shallow-water flows. Simplified models of analysis are classified according to flow dimensionality and behaviour. Some methods, finite-difference techniques, of modelling these flows

are proposed. It is not intended here to review all these but to concentrate on studies that are representative of the various approaches.

Theoretical work on continuous shallow-water flows can be broadly divided into the following categories:

(i) Empirical Formulae

Empirical formulae have been developed in the past to determine the uniform-flow velocity, and hence the discharge, for a given cross-section in an open-channel flow. These uniform-flow formulae are also assumed to be applicable to varied flows, and usually offer a simple means of modelling channel-friction forces.

Uniform-flow formulae

The most widely used formulae are the well known Chézy, Manning and Darcy formulae. These formulae involve surface-roughness coefficients which can conveniently be evaluated from tabulated values for the particular channel-bed type and condition. Such tables are given extensively by, for example, Posey (1949), Chow (1959), and King and Brater (1963). Spalding (1975) suggested the use of an empirical-friction factor (C_f) with values between 0.001 and 0.003, corresponding to smooth to rough surfaces respectively. This factor has been successfully used by, e.g. McGuirk and Rodi (1978) and Demuren (1979). The value C_f is related to C (Chézy's C), n (Manning's n) and f (coefficient appearing in Darcy's formula) by:

$$C_f = \frac{g}{C^2} = \frac{n^2 g}{m^{\frac{1}{3}}} = \frac{f}{8} \qquad ,(2.1)$$

where m is the hydraulic mean depth (= depth in shallow flows).

One-dimensional gradually-varied-flow equation

This equation relates the depth, velocity and slope along a prismatic channel. It is derived for steady flow over a sloping channel, using the energy and continuity principles, and is given by:

$$\frac{dh}{dx} = \frac{s - i}{1 - Fr^2} \qquad ,(2.2)$$

where s is the channel slope (+ ve along the flow direction) and i is the energy slope determined empirically using a uniform-flow formula.

Equation (2.2) can be used to describe the characteristics of various types of surface profile. It cannot normally be integrated directly, as i is a function of u and h. The solution is often obtained by a numerical integration. A comprehensive study of the different methods of computation and of surface-profile classification is given by Chow (1959).

(ii) Analytical Studies

Very few analytical methods can be devised to adequately simulate shallow-water flows, indeed, as is the case with the majority of fluid-dynamics problems. This is mainly due to the complexity of the governing equations and geometrical configurations of real flows. However, analytical methods can be developed for certain idealized flow situations. They can also be very useful for validating numerical schemes.

Schlichting (1968) presented an analytical solution for the two-dimensional, laminar developing flow in a straight open channel. The problem is treated as the development of boundary layers along the walls.

The depth variations in the channel are assumed negligible and hence the solution is valid for flows at very small Froude numbers. This study is considered in Section 6.2.

The theoretical wave speed c, = $(gh)^{\frac{1}{2}}$, for small amplitude waves is used extensively to validate different numerical schemes for transient, one-dimensional inviscid flows. A small and sharp depth discontinuity can be set up, at t = 0, in the middle of a horizontal and rectangular open channel closed at both ends. The discontinuity then propagates at speed c (as compression and rarefaction wave fronts in opposite directions) and reflects from both ends, in a similar fashion to a pressure wave in a shock tube. Such a problem has been considered, as a test case, by many investigators dealing with numerical modelling of unsteady free-surface and two-phase flows (in the absence of interphase friction); see, for example, Vliegenthart (1969), Kawahara et al (1978) and Baghdadi (1979). The last author has also considered an analytical relation (derived from simple control-volume analysis using the continuity and momentum relations for 1-D inviscid flow) for the constant speed of the surge-wave propagation formed by the sudden closure of a channel carrying a uniform flow. If the wave is of small height (compared to the mean depth of flow) the velocity of the wave relative to the undisturbed liquid becomes c.

In two-dimensional steady flows, a small discontinuity in the surface elevation propagates downstream at a half angle (α), with respect to the main flow direction, given analytically by:

$$\alpha = \sin^{-1} (1/Fr) \qquad .(2.3)$$

The relation given by equation (2.3) is analogous to the Mach angle in

compressible-gas flows. This wave propagation in space is similar to that propagating in time for the 1-D problems mentioned above. Such a study is considered in Section 6.4.

The simple wave equations have also been used for some idealized flow situations for which analytical solutions could be developed. The wave equations, referred to here, are the linearized shallow-water equations in the absence of viscous terms, Coriolis term, and damping effects. For one-dimensional problems, these are:

$$\frac{\partial^2 u}{\partial t^2} = c^2 \frac{\partial^2 u}{\partial x^2} \quad ,$$

$$\frac{\partial^2 \eta}{\partial t^2} = c^2 \frac{\partial^2 \eta}{\partial x^2} \qquad ,(2.4)$$

where $c^2 = gh$, η is the surface elevation relative to the mean-water level (h), and $\eta \ll h$.

Wang and Connor (1975) considered, as a test case, an analytical solution for u and η for the above set of equations for the problem of a standing wave in a rectangular prismatic channel. The channel, of length L, is closed at one end (x = L) and at the open end (x = 0), the water level is forced up and down according to a sinosoidal function in time. Good agreement was obtained with their numerical model.

(iii) Method of Characteristics

The method of characteristics (MOC), developed originally for the computation of supersonic-gas flows, has been used in the computation of shallow-water flows. Basically, the governing equations are replaced by equivalent equations in characteristic form (compatibility equations), along characteristic curves (Mach lines or wavelets). The

method has also been extended to handle discontinuities; in such a case, it is matched with the jump relations across the shock.

Analysis of supercritical flows in open channels was first carried out in detail by Preiswerk (1940). He used the MOC to study the supercritical flow of water in a Laval nozzle.

Ippen (1951) studied the supercritical flow in rectangular channels with oblique standing waves and expansion waves created by the deflection of the channel boundary. He used the MOC as a graphical aid of solution and approximated the wave angle by the value of $\sin^{-1} 1/Fr$ for gradual surface changes. For standing waves of appreciable heights, the method was modified with respect to the wave angle and the energy dissipation involved.

Based on Ippen's work, Rouse et al (1951) used the MOC to determine the surface contours in abrupt and curved-wall expansions. The results compared well with their measurements.

Liggett and Vasudev (1965) solved the equations of 2-D shallow-water theory while including the usually neglected terms of slope and friction in formulating the MOC. The characteristics equations were integrated using finite-difference approximations. The method was applied to flow in channel expansion and the results were compared to those obtained from the frictionless, zero-slope solution. The latter assumptions were found to be adequate for design purposes.

Bagge and Herbich (1967) carried out a similar study to the above in a straight flaring expansion. They showed that even a moderate change in slope would have a significant effect on the flow. The method was limited to the initial assumption of frictionless flow; no comparison with data was made.

Dakshinamoorthy (1977) compared results obtained by the MOC, for

Fr between 1.5 and 6.0, with the experimental data of Herbich and Walsh (1972) for the supercritical flow in straight flared expansions. His solution, incorporating the friction effect, has yielded an improved agreement with the data as compared to the MOC solutions of the latter authors which neglected the channel-frictional resistance.

Katopodes and Strelkoff (1979) used the MOC in unsteady two-dimensional applications. They simulated a 2-D wave emerging from a partially failed dam and propagating on the dry bed of the valley downstream of the structure. The flow resistance was evaluated using the Manning formula.

(iv) Finite-Difference Methods

The finite-difference methods (FDM) are the most general and widely used methods for predicting shallow-water flows, as indeed in the various fields of fluid dynamics. An early detailed study of several finite-difference schemes, as applied to the solution of shallow-water equations, was made by Liggett and Woolhiser (1967). The equations solved were for unsteady shallow-water in one dimension. The difference equations were obtained by expanding each term in a Taylor series. Implicit methods were found to be the most stable over a wide range of parameters.

A similar study to the above was made by Dronkers (1969). Implicit and explicit schemes were examined for tidal flows in both one and two dimensions. The time step in implicit FDM's is independent of stability requirements and is a function of the required accuracy of the results only.

Leendertse and Gritton (1971) presented a finite-difference approximation for the time-dependent depth-averaged equations describing

the 2-D flow in a well-mixed tidal estuary. The discrete values of the variables were described on a space-staggered grid. The time interval was considered over two successive operations with a mixed implicit/explicit method (simpler than implicit methods; more stable than explicit methods). The "effective-stress" terms were neglected in the analysis. Techniques were used to suppress the generation and transmission of disturbances due to the time-dependent boundary changes. The water velocities and water levels were computed and then used in the mass-balance equation to obtain the waste-constituent transport.

Kuipers and Vreugdenhil (1973) used the unsteady model of Leendertse, above, for application to steady-flow cases (i.e. time-dependent approach, using steady boundary conditions). The occurrence of non-linear instability was suppressed by a smoothing process applied after each half time step, in which the quantities u and v were replaced by a weighted-mean values. The weighting factors were chosen by experience and with no reference to a physical basis. It was shown that this smoothing process could be interpreted as the addition of diffusion terms to the momentum equations.

Flokstra (1977) indicated the importance of the so called "effective stresses" (normally neglected in the majority of the applications to shallow-water flows) in giving rise to recirculation within a flow. These stresses consist of three contributions: viscous stresses, turbulent stresses and stresses due to the non-uniform vertical velocity distributions of u and v (dispersion terms). The first stresses can be neglected but the other two are important in particular flow situations, as were shown by order of magnitude estimates. It was suggested that two separate closure models should be used for these two stresses, in terms of the mean velocities and depth, based on physical foundations.

Various closure expressions for the turbulent stresses have been put forward. Wang and Connor (1975) used a constant eddy-viscosity approximation, but was mainly used for the reason of suppressing non-linear instabilities. More sophisticated models were also used, which describe the Reynolds stresses by additional differential equations; many of these turbulence models are reviewed by Launder and Spalding (1972). Rodi (1978) conducted a survey of existing turbulence models with particular emphasis on their hydraulics applications. The "K - ε" model was found to offer the best compromise between width of applicability and computational economy.

Rastogi and Rodi (1975) applied the K- ε model, in a depth-averaged form, to a steady warm-water jet issuing over the entire depth of a co-flowing river of rectangular cross-section. The water depth was taken constant and the boundary-layer approximations were applied. This approximation made the differential equations parabolic and were solved by a marching-integration procedure.

McGuirk and Rodi (1978) extended the above study by applying the K- ε depth-averaged model to a more complex flow situation; namely, the near field of a side discharge into open-channel flow. The elliptic differential equations, required to describe flows with recirculation zones, were solved iteratively using the algorithm of Patankar and Spalding(1972).

The dispersion terms are often neglected in the mathematical formulation of the depth-integrated equations. These are neglected on the assumption that the vertical profiles are uniform or nearly so. Rastogi and Rodi (1978) presented comparisons of 2-D and 3-D predictions for the flow situation mentioned above (Rastogi & Rodi, 1975); the 3-D results were integrated over the water depth. Good agreement was found at high densimetric Froude numbers which justified the neglect of the dispersion terms in 2-D models. However, the agreement between 2-D and 3-D predic-

tions was shown to deteriorate as Fr decreases (below a value of about 5). This is because the 2-D depth-averaged model does not account for the stratification and secondary motion induced by buoyancy.

Closure equations for the dispersion terms can be obtained by prescribing vertical profiles for the horizontal velocities and then carrying out the integration over the depth (Zienkiewicz and Heinrich, 1979). These model formulations allow the study of return currents in the vertical direction such as in wind-induced flow circulation in lakes.

While all the above studies use the "rigid-lid" approximation, to filter out all surface gravity-waves , the modelling becomes more complicated in situations where this assumption can not be applied. Demuren (1979) employed the downstream marching-integration procedure for the computation of velocities and surface elevations of the super-critical flow of water in open channels of varying cross-sections. The shallow-water approximations were used and the depth was determined by the "pressure" correction technique of Patankar and Spalding (1972).

Other means of locating a free surface or an interface are possible. Maxwell (1977) employed the particle-tracking technique to investigate the behaviour of the free surface in 2-D unsteady flows. Awn (1979) extended the same work in which the technique was employed to track the interface location in compressible flow situations. In stratified two-phase flows, Baghdadi (1979) used the volumetric form of the continuity equation in his studies of 1-D unsteady flows. The depth of flow of one phase can be found from the determination of the volume fraction of the particular phase.

Multi-layer models are used as simplified and alternatives to 3-D models, for the computation of flows with velocity variation in the vertical direction and for density-stratified flows. The system consists of

a series of single layers, stacked vertically one upon another, with transfer of mass, momentum, and energy from one layer to the next. The governing equations are being integrated over the depth of each layer. Simons (1972) used a four-layer model to study the circulation in Lake Ontario under stratified conditions and strong wind stresses. The problem of interaction between the layers was not discussed. Cheng et al (1976) presented a detailed discussion on how the layers can be delineated, and the transport of mass, momentum and energy at the interfaces specified.

(v) Finite-Element Methods

Finite-element methods (FEM), which are widely used for solving linear equations in structural mechanics, have also been used recently for the computation of the depth-averaged equations applicable to shallow-water flows.

An early application of the method was made by Grotkop (1973) for the tidal computation of the North Sea. The flow variables at a new time step were linked by linear equations with those at an earlier time. The water levels at the open boundaries were prescribed values that depended on time in a cosine variation. Convergence and stability were found to diminish with increased time step and relative importance of the convection terms. In such applications, the convection terms are usually of little importance and hence the "rigid-lid" approximation is widely used and justified accordingly.

A similar application to that used above was made by Brebbia and Partridge (1976). Two schemes, implicit and explicit, were investigated. Both schemes produced similar results, however, the implicit scheme was more expensive per time step than the explicit one but accommodated larger

time steps. The two schemes became unstable for a value of Chezy's coefficient greater than 60 $m^{\frac{1}{2}}$ / s (i.e. for small values of friction). Small oscillations were also produced by the imposition of a tidal inlet which propagated through the flow field. Procedures to dampen these effects were proposed.

Kawahara et al (1978) used the FEM for the analysis of the tsunami (tidal) wave propagation problem. The time was discretized by employing a two-step explicit method which was adopted from the Lax-Wendroff finite-difference method. The scheme was applied to the Tokachi Oki earthquake tsunami propagation problem; as initial conditions, the tide elevation (tsunami) was assumed to take the same shape as the upheaval of the sea bottom. Coriolis force and bottom friction effects were neglected. The results compared fairly well with the observed data.

Zienkiewicz and Heinrich (1979) introduced a formulation of the shallow-water equations which accounted for the effect of return current in the vertical direction. This formulation allows the study of, for example, wind driven flows in lakes. This was done by weighting the momentum equations by suitable vertical velocity distribution functions and integrating through the depth. The FEM was used and the model applied to a few flow situations; no comparison with data was made.

Detailed formulations of the FEM's and their application to shallow-water equations can be found in, for example, Wang & Connor(1975).

The main disadvantages of the FEM's are the requirement for more comupter storage and time as compared to the FDM's. Weare (1976) compared, on theoretical grounds, the computational costs of some finite-element and finite-difference methods used to solve the depth-averaged shallow-water equations. He showed that the unit cost (per node) of the FEM's increases with the band-width of the computational mesh, whereas

for the FDM's the unit cost (per grid point) is independent of the size of the grid. He concluded: "It is essential that the disadvantage of a band-width dependent efficiency should be overcome before the full potential of the FEM's can be realized in hydraulic applications".

The main advantage of the FEM's over the FDM's is the improved resolution of irregular boundaries and internal obstacles. However, advances to overcome this limitation in FDM's have been made recently, Moult et al (1978) and Spalding (1981). A special practice (a blockage-ratio technique) was introduced in order to modify the form of the finite-difference equations, and allowed an irregular boundary to be accurately approximated.

2.3.2 Experimental Studies

Experimental studies on shallow-water flows are reviewed below. These can be found summarized in Table 2.1.

Preiswerk (1940) carried out measurements of surface profiles in supercritical-water flow through a Laval nozzle designed to produce, at its exit, a parallel flow of Froude number = 2.

Rouse et al (1951) discussed the problems involved in the design of channel expansions for supercritical flows with both gradual and abrupt expansions. They carried out experimental measurements of the surface elevations and used the method of characteristics to compare the results. In Section 6.5, the flow at an abrupt expansion is studied in more detail. Arumugam (1955) performed similar experiments in a channel with an abrupt expansion on one side and a wall of varying angle on the other.

Ippen and Dawson (1951) measured the surface profiles in both subcritical and supercritical flows in channels with straight-wall and

circular-arc contractions. This was an attempt to minimize the energy losses, wave heights and disturbances in the downstream channel. Measurements of supercritical flow in curved channels for both rectangular and trapezoidal cross-sections were made by Knapp (1951).

Herbich and Walsh (1972) carried out depth measurements in supercritical flows in flared expansions. The channel slope was varied from 0% to 15% with a wall expansion angle up to 30^{o}; a Froude number up to 8.4 was investigated. Only a few results were presented and compared with those obtained from the method of characteristics. The discrepancy in the results was attributed to the neglect of friction in the theory. For slopes greater than 15% , air entrainment became influential and resulted in a considerable increase in depth.

Kuipers and Vreugdenhil (1973), in validating their numerical model, applied it to several flow situations where experimental data had been taken from hydraulic model studies. One of the studies simulated the flow pattern in a river bend which consisted of a half circle with joining straight parts. The mean-radius-to-width ratio was 2.5 and was considered to represent a weak curvature to which a 2-D depth-averaged numerical model was applied. The velocities were measured by a current meter and the inlet Froude number was 0.46. Shukry (1950) performed measurements of velocity distribution and surface elevation for subcritical flow in strongly-curved open channels. He studied flows in 180^{o} bends for mean-radius-to-width ratios between 0.5 and 3.0. However, such flows can only be analysed by using 3-D models, since secondary flows are significant. It was found that the strength of the secondary flow decreases by increasing the Reynolds number, radius-width ratio, and the depth-width ratio. The ratio of radius-width = 3.0 was recommended as the minimum ratio at which the bend action effects are negligible.

Magalhaes (1974) carried out an experimental investigation of a supercritical flow merging with a deeper uniform subcritical stream flowing in the same direction. The work was concerned with the characteristics of the hydraulic jump forms and the diffusion process of the resulting subcritical streams downstream of the jump. However, his results were not sufficiently complete for use in verifying numerical results.

Demuren (1979) performed systematic experimental measurements of the supercritical flow of water in open horizontal channels of varying cross-sections. The channel side walls consisted of one convex wall (radius of curvature = 6 m), the other wall was either concave (radius of curvature = 6.2 m) or straight at an angle of 0^{o}, 5^{o} or 7^{o} to the flow. The range of Froude numbers investigated was 1.85 to 2.2; the initial aspect ratio was 8. Detailed measurements of depth profiles at successive cross-stream locations were presented.

Table 2.1 provides a summary of the above experimental studies.

2.4 DISCONTINUOUS SHALLOW-WATER FLOWS

Discontinuous flows are those with hydraulic jumps (sometimes called rapidly-varied flows). They contain two distinct flow regions, namely, supercritical and subcritical in which the flow is transformed rapidly from the former to the latter.

2.4.1 Experimental Studies and Control-Volume Analysis

One of the earliest and most systematic studies of the normal hydraulic jump was reported by Bakhmeteff and Matzke (1936). They carried out one-dimensional measurements of hydraulic jumps and covered a range of Froude number between 1.9 and 8.8. The results of the "verti-

Author (s)	Year	Application
Preiswerk	1940	Laval nozzle for Fr = 2.
Shukry	1950	Subcritical flow in a 180° bend; strong and weak curvatures (radius-width ratio = 0.5 to 3).
Rouse et al	1951	Channel expansions (gradual and abrupt) for Fr = 1 to 8.
Ippen & Dawson	1951	Channel contractions (straight-wall and curved-wall) for sub- and supercritical flows.
Knapp	1951	Curved channels with supercritical flows.
Arumugam	1955	Channel with abrupt expansion on one side and a wall of varying angle on the other (super-critical).
Herbich & Walsh	1972	Supercritical flow in flared-expansions and varying-slope channel (Fr up to 8.4).
Kuipers & Vreu-gdenhil	1973	Subcritical flow in a 180° bend; weak curva-ture (radius-width ratio = 2.5), Fr = 0.46.
Magalhaes	1974	Supercritical flow merging with subcritical flow, both flowing in the same direction.
Demuren	1979	Supercritical flow in varying channel cross-sections, Fr = 1.85 to 2.2.

TABLE 2.1 : SUMMARY OF THE EXPERIMENTAL STUDIES ON SHALLOW-WATER FLOWS

cal elements" of the jump, such as jump height, were presented in terms of Fr. These were compared with theoretical values based on control-volume analysis. They also presented the "longitudinal elements" of the jump, such as the length of the jump and the profile of the surface roller.

Stoker (1948) presented a detailed discussion of the problem of the development of breakers on a sloping beach, and the identical problem of the formation of bores in rivers due to tidal action. The differential equations of the nonlinear shallow-water theory (which are now termed "depth-averaged equations") were presented. He pointed out their analogy with the one-dimensional unsteady flow of a compressible gas.

He also used the method of characteristics to study the propagation of 1-D surface waves in shallow water: the motion on each side of the shock is satisfied by the resulting ordinary-differential equations, these are "connected" through a shock discontinuity which is satisfied by the shock relations derived analytically.

Ippen and Harleman (1956) undertook a series of experiments to verify the hydrodynamic theory of both oblique hydraulic jumps and expansion waves. The position of the standing waves and associated depth changes were measured and compared to theory, the range of Fr covered was 2 to 7. The fundamental theoretical relationships of both the oblique jumps and expansion waves were derived using the continuity and momentum principles (in the direction normal to the wave front) together with a geometrical relationship obtained from a velocity-vector diagram. In general, good agreement between theory and experiment was obtained.

Wilson (1967) carried out a semi-empirical analysis to study the sensitivity of the hydraulic-jump location to a change in tailwater depth in rectangular channels. The problem was rationalised by using a "position-sensitivity parameter" defined as the displacement of the jump toe along the channel per unit change in elevation of the tailwater, given that conditions upstream of the jump remain constant. The analysis showed that, while the "position sensitivity" is dependent upon the Froude number, channel-bed slope and the energy gradient, the sensitivity can be reduced by increasing both the channel-bed slope and Froude number. The results were compared with laboratory tests and showed fair agreement.

Sluice gates are often used for controlling the discharge, and indeed, as a means of measuring the flow rate. Henry (1950), Franke and Valentin (1969) developed formulae to determine the discharge below gates

for both free and submerged flows. These formulae were verified by their experimental measurements.

Effects of the state of flow development on hydraulic jumps

Leutheusser and Kartha (1972) studied the effects of the state of flow development, of the supercritical stream, on the hydraulic-jump characteristics. Experiments were performed on hydraulic jumps with Fr as large as 30, having either fully developed or undeveloped inflow velocity profiles. The results showed that, up to Fr = 10, the inflow velocity profile has no observable effect on the sequent-depth ratio (depths on either side of the jump). For Fr greater than 10, however, the sequent-depth ratios for the developed inflow fall below those for the undeveloped inflow for the corresponding Froude numbers. The lengths of the jumps with developed inflow are about 35% greater than those of jumps with undeveloped inflow.

Leutheusser and Alemu (1979) continued the above study by investigating the effects of the state of flow development on the flow separation under hydraulic jumps. They showed that the flow separation extends downstream beyond the conventionally defined end section of the jump. The size of the separation cavity is much larger for hydraulic jumps with undeveloped inflow than those with fully developed inflow.

Turbulence characteristics of hydraulic jumps

Rouse et al (1959) simulated the hydraulic jump in an air duct (air model) shaped according to the profile of the jump and measured the turbulence characteristics of jumps by means of the hot-wire anemometer. The results were then correlated in accordance with the momentum and energy equations. Similar measurements were made in actual hydraulic jumps by Resch and Leutheusser (1972). The results were presented in terms of turbulence intensity and Reynolds stress distributions in the jump region

for Fr = 2.85 and 6.0, for both fully developed and undeveloped upstream flow conditions. The turbulence levels of the former condition were found to be slightly higher.

Spatial and radial hydraulic jumps

The hydraulic jump is often used to dissipate energy. Its formation at a particular position is aided by appurtenances such as sills, baffles, adverse bottom slopes, etc. Herbrand (1973) studied the formmation of the so called spatial hydraulic jump at abrupt channel expansions and proposed an empirical formula useful for practical design purposes. It was found that the spatial jump requires a smaller tailwater depth than the classical jump with the same entrance values. Although the flow is two-dimensional, it has always been modelled using the one-dimensional formulation neglecting wall friction.

Khalifa and McCorquodale (1979), and France (1981) carried out experiments on the radial hydraulic jump within gradually diverging channels. The problem is similar to the radially expanding flow of a jet discharging vertically downwards against a flat plate before forming a circular jump, Koloseus and Ahmad (1969). The results showed that the relative energy loss in the radial (circular) jump is approximately 15% higher than in a parallel-sided channel for the same Froude number, i.e. the radial jump is a better energy dissipator. The length of the radial jump is approximately 30% less than the rectangular jump; the sensitivity of the jump location to a change in the tailwater depth, and the sequent-depth ratio were also found to be less for the radial jump. In all studies, theoretical relationships were derived for the sequent depth ratio (in terms of Froude number and the sequent-radius ratio) by considering the jump formed as a sector of a circular jump, applying the continuity and momentum principles, and assuming a particular shape of the jump surface profile.

Rajaratnam (1967) gave a detailed theoretical and experimental analysis of hydraulic jumps by assessing the works of various contributors to the subject.

2.4.2 Numerical Studies

Very few attempts have been made towards the numerical computation of discontinuous shallow-water flows. Computer codes which solve for either subcritical or supercritical flows often fail to solve for the two flows together. This is mainly due to the difference in the physical nature of the two flow regimes. Thus, special prctices are needed to overcome this difficulty. Positive steps towards this objective have been very limited which is in surprising contrast with the advances made in the numerical modelling of the analogous compressible-gas flows with shock waves (discontinuities).

Spalding (1978) proposed efficient finite-difference procedures for computing transonic flow problems in both streamline-coordinate and fixed-grid systems. He has also bridged the gap in modelling compressible-gas flows and their analogous shallow-water flows. These procedures were refined and made more general and are the basis of the technique used in this thesis.

Leendertse (1970) and Abbott (1974) used finite-difference methods to calculate two-dimensional nearly-horizontal flows. They discussed the problems associated with the numerical computation of discontinuities, in which numerical techniques may develop "parasitic waves", which often lead to instabilities. Two approaches were proposed to overcome this difficulty. One approach is to "fit" the jump by introducing the specific local laws of the discontinuity and matching the continuous parts on either side using these laws, simultaneously locating the discontinuity.

Another approach is to add artificial viscosity in a similar manner to that used in the numerical computation of shocks. However, both approaches add extra complication and cost of computation especially for two-dimensional flows.

Pandolfi and Zannetti (1977) extended the analogy between compressible flow and shallow-water motion to well beyond the usual comparison of equations. They developed some "numerical experiments" which represented different physical shallow-water problems. Their results were obtained by computer codes developed for solving problems in gasdynamics. Details of the modifications are not reported, however, the scheme used was a time-marching finite-difference technique with second-order accuracy. The approach used in computing the hydraulic jump, which was regarded as a discontinuity, was the "shock-fitting technique". The paper gives a summary of the works and applications made by the authors in this field.

Forbes and Schwartz (1981) carried out similar work to that of Pandolfi and Zannetti by extending the classical blunt-body problem of gasdynamics to an analogous problem arising in shallow-water flows. They considered a blunt object, such as a bridge pier, immersed in a supercritical-water stream, supporting a detached shock-wave, or bore. However, the problem was formulated inversely, that is, the free-stream Froude number and the shape of the shock wave were specified in advance. It was then required to determine the values of the variables downstream and the shape of the body as Taylor-series expansions about the shock wave. The shock conditions were used to relate flow quantities on the upstream and downstream sides of the shock.

Zienkiewicz and Heinrich (1979) pointed out the close analogy between the numerical computations of shallow-water and compressible-gas flows. However, positive steps towards its application have not been made.

2.4.3 Concluding Remarks

(i) The majority of the theoretical works are limited to one-dimensional analysis and the use of simplifying assumptions.

(ii) On the numerical side, very few attempts have been made to utilize the advances achieved in modelling the analogous transonic flows.

(iii) Detailed experimental measurements are lacking.

2.5 ANALOGOUS FLOWS

2.5.1 Studies of Gas-Hydraulic Analogy

The analogy between shallow-water flow with a free surface and two-dimensional compressible-gas flow has long been appreciated. The water channel is being used as an instrument for the investigation of compressible-flow phenomena because of the ease and low cost of construction as compared to a transonic wind-tunnel.

Selected studies on the gas-hydraulic analogy are presented next. These studies are summarized in Table 2.2 at the end of this section, together with the main concluding remarks.

Preiswerk (1940) conducted a detailed mathematical study of the hydraulic analogy to a fictitious gas with a specific-heat ratio (γ) of 2. The theory was confirmed experimentally by application to the case of Laval expansions for water, a problem directly analogous to the supersonic flow through Laval nozzles.

Ippen (1942) carried out a similar study to that of Preiswerk in open-channel flows, using concepts based upon supersonic aerodynamics with the limitation of $\gamma = 2$. However, the author argued that

many flow phenomena do not depend very strongly on the value of δ .

Orlin et al (1947) constructed a water channel to investigate the hydraulic analogy to flows through nozzles and about circular cylinders extending from subsonic to supersonic velocities. The effects of δ were shown to be not very large, especially in subsonic-compressible flows, and could be taken into account in the interpretation of the experimental data.

Gilmore et al (1950) made a study of shock-wave interactions using the hydraulic analogy. They took measurements of hydraulic-jump intersections on a water table. Considerable disagreement was found between their theory and experiment which they attributed to the differences between hydraulic jumps and compression waves in gases, and to the relative thickness of the waves studied by the hydraulic analogy.

Black and Mediratta (1950) operated a small water channel but failed to get good quantitative correlation with aerodynamic values between hydraulic jumps and shock waves, however the agreement was good for continuous flows. It was found possible to use hydraulic jumps to simulate qualitatively most of the features of gas flow with shock waves, such as the flow in a Laval nozzle or past a supersonic aerofoil.

Ippen and Harleman (1950) produced an extensive investigation of the hydraulic analogy in a three-part report. Part (i) of this report covered a review of previous experimental work and the design of suitable experimental equipment for hydraulic-analogy research. In part (ii) they included studies of the basic hydraulic shock wave designed to verify the theory of oblique hydraulic shocks. Two modifications of the "direct" hydraulic analogy were developed which led to an improved quantitative correlation between analogous air and water phenomena. Charts were produced for the Mach numbers (M) in air and modified Froude numbers (Fr) that gave identical shock angles for flows

over different angle wedges. If the results of the modified Fr are interpreted as corresponding to air flow with M, the depth ratio will equal the density ratio, and thus all quantities determined from this density ratio will be identical with the aerodynamic analysis. In part (iii) of the report, Ippen and Harleman covered studies of expansion zones which complemented the shock wave studies. They also carried out experimental measurements and theoretical studies, using the hydraulic theory and the modified analogy, of supersonic aerofoils (circular arc and half-diamond shapes). Comparison to aerodynamic theory and supersonic wind-tunnel measurements on geometrically similar aerofoils showed satisfactory agreement, hence establishing the validity of the analogy for these applications. A shadowgraph photographic technique was used and resulted in clear photographs of shock wave patterns.

Crossley and Harleman (1952) obtained hydraulic experimental measurements on wedge profiles in the transonic range by employing towed-model techniques in a water channel. The direct hydraulic analogy (water depth corresponds to gas density with $\gamma = 2$) together with the use of transonic-similarity rules (to apply the results to air flows) was found to be a satisfactory method of analyzing hydraulic experimental data.

Laitone (1952) presented photographs of the water surface waves corresponding to shock waves in front of wedges and circular cylinders. The analogy was restricted to flows in which the water depth was very shallow; the shock waves or hydraulic jumps considered were of the weak type having a negligible increase in entropy. Broude (1956) set up a water table and made use of the gas-hydraulic analogy to study the flow of water over wing contours and obtained good quantitative results.

Bryant (1956) conducted a rigorous mathematical treatment of the governing equations for non-rectangular channel cross-sections.

This was in an attempt to remove the restriction of the hydraulic analogy to $\gamma = 2$. He concluded that this was mathematically possible for a one-dimensional analogy (for both steady and unsteady subsonic and transonic flows) with weak shocks, but he ruled out the possibility of constructing a satisfactory two-dimensional hydraulic analogy for specific-heat ratios other than 2.

Loh (1959) considered the one-dimensional unsteady-flow hydraulic analogy. The equations are presented for channels with cross sections other than a simple rectangle in order to represent a gas flow of the desired γ. The time scale for events taking place in a water channel is much longer than in gas flows. This makes the hydraulic analogy a relatively easy way in which to observe and study transient effects in gasdynamics, e.g. unsteady flow in ducts and flow in reciprocating engines. In general, the scheme is to use water channels (often triangular, in order to model better the ratio of specific heats, simulating γ of 1.5) to reproduce the wave phenomena existing in the inlet and exhaust manifolds of reciprocating engines.

Hoyt (1962) reviewed the subject of the hydraulic analogy for compressible-gas flow and classified the review according to application.

Saiva (1964) used a towed-model hydraulic-analogy tank to investigate the transonic flow over two-dimensional wedge profiles. He applied the transonic-similarity laws to transfer the experimental hydraulic data to the corresponding prototype gas flow. The transonic-similarity parameter was modified to allow for the effect of the development of boundary layer along the walls of the model profile. The discrepancies in the results obtained were attributed to the fact that steady flow conditions had not been reached in the relatively short tank. Werlé (1973) surveyed the principal methods of visualizing flows applicable to studies of liquids and their hydraulic analogy to gases. The study

included clear photographs representing various flow phenomena to which hydrodynamic visualization has contributed.

Tuck (1978) reviewed the hydrodynamic problems of ships in restricted waters. He also discussed the nature of the aerodynamic analogy for shallow-water flow, since ships are slender bodies moving in a fluid medium dynamically similar to air.

Kedziur et al (1978) simulated the process of depressurization in a pressurized-water reactor (PWR) in the case of a hypothetical blowdown accident. The downcomer of a PWR was treated approximately as a two-dimensional plane region (unwrapped). The flow was simulated experimentally using the hydraulic analogy of free-surface waves in a shallow-water bed and compared to numerical (finite-difference) simulations of the flow of an ideal gas with $\gamma = 2$. The comparison showed very satisfactory agreement.

Table 2.2 gives a summary of the above cited studies.

Concluding Remarks

The status of the present information concerning the gas-hydraulic analogy can be summarized as follows:

- As a qualitative device, the analogy provides a simple method of obtaining information on complex gas flows.
- Both success and failure, in terms of quantitative agreement with theory, are reported in the literature. Failure possibly arises from one or more of the following causes:
  - Violation of the basic assumptions of the gas-hydraulic analogy. The water flow is assumed: inviscid, under hydrostatic pressure, of negligible surface tension, without body forces, etc. The gas is assumed inviscid and the concept of a perfect gas is assumed to hold.

Author (s)	Year	Application
Preiswerk	1940	Laval nozzles (experiments and theory, method of characteristics).
Ippen	1942	Open-channel flows in general (theory, method of characteristics).
Orlin	1947	Circular cylinders and nozzles (experiments).
Gilmore et al	1950	Shock-wave interactions using the hydraulic analogy (experiments and theory).
Black & Mediratta	1950	Laval nozzles and supersonic aerofoils (experiments).
Ippen & Harleman	1950	Wedges (deflected channel side wall, for both compressions and expansions) and supersonic aerofoils (experiments and theory).
Crossley & Harleman	1952	Towed-model techniques for wedge profiles (experiments and theory).
Laitone	1952	Wedges and circular cylinders (experiments).
Broude	1956	Wing contours (experiments).
Bryant	1956	Non-rectangular channel cross-sections (mathematical treatment of equations, theory).
Loh	1959	1-D unsteady flow for non-rectangular cross-sections, applicable to flows in reciprocating engines (mathematical treatment of equations, theory).
Hoyt	1962	General review of the subject according to type of application.
Saiva	1964	Towed-model techniques for wedge profiles (experiments and theory).
Werlé	1973	Various hydrodynamic visualizations.
Tuck	1978	Ships in restricted waters, equivalence to aerofoils in air (discussion).
Kedziur et al	1978	Pressurized-water reactor, blowdown accident (model experiments and numerical study).

TABLE 2.2 : STUDIES OF GAS-HYDRAULIC ANALOGY

- The change in internal energy for a gas is not equivalent to the change in internal energy for water.
- The analogy only corresponds to a "hydraulic gas" with $\gamma = 2$.

- Methods have been devised whereby experimental hydraulic data may be transferred to a corresponding real-gas flow. These require great care in the experiment and in the interpretation of the results.

2.5.2 Relevant Compressible-Gas Flows

Advances made in the numerical computation of compressible-gas flows have overshadowed those made in the field of free-surface shallow-water flows. This is because of the prominence of space technology in the last two decades or so.

Two numerical techniques have emerged. One is known as the "shock-capturing technique" which requires no special treatment in dealing with discontinuities; the shock is "captured" by the computation and comes out as steep gradients in the dependent variables spread over few mesh points. The other technique is known as the "shock-fitting technique" which treats the discontinuities explicitly and considers them as internal boundaries between two continuous regions where a regular solution is valid. The two continuous regions are then matched by "fitting" the shock conditions across the boundaries. Detailed studies on such flows can be found in, for example, Murman (1972), Hall (1976), and Roache (1976). The scheme used in the present study belongs to the first technique.

Some studies of two-dimensional overexpanded free jets are very briefly discussed and summarized in Table 8.2 (Chapter 8). Selected studies of two-dimensional supersonic flow impingement on rectangular bodies are summarized in Table 8.4. These are briefly reviewed here together with some others.

Approximate methods

Moeckel (1949) predicted the location of detached shock waves ahead of plane or axially-symmetric bodies for free-stream Mach numbers (M_{in}) between 1.15 and 3.6 for $\gamma = 1.4$. He developed an approximate method, based on a simplified form of the continuity relation and assumed that: (i) the form of the shock from the axis to its sonic point,

is adequately represented by an hyperbola asymptotic to the free-stream Mach lines; and (ii) the sonic line between the shock and the body is straight and inclined at an angle that depends only on M_{in}. With these assumptions, the location of the shock will be independent of the body shape ahead of the sonic point. He also presented a simple geometric method for estimating the shock location. The predicted shock locations compared well with available experimental data, belonging to different nosed-shape bodies, at M_{in} 1.2 and 1.5.

Experimental studies

Griffith (1952) performed an experimental study of the flow around wedges in the transonic range using a shock tube and a Mach-Zehnder interferometer. Detached shocks for wedges of between 10^{o} and 90^{o} and 180^{o} total included angle were observed for $1.16 < M_{in} < 1.80$. The experiments show that the shape of the detached shock and its detachment distance from the sonic point on a wedge depend only on the body thickness and the Mach number when the shock is not near to attachment. Measurements of pressure over the wedge incline show that identical distributions exist for a considerable range of supersonic flows.

Method of integral relations

The method of integral relations (MIR) is based on dividing the flow domain into strips and reducing the governing partial-differential equations to a system of ordinary-differential equations on the basis of assumed profile shapes. However, the shock wave is treated as an internal boundary on which boundary conditions must be specified. This is done in terms of two unknown parameters describing both the location and shape of the shock. The process starts with an assumed solution at the stagnation point, and it is a requirement that it satisfies the imposed conditions in the critical region. If this is not met, the stagnation-

point solution must be revised and the integration process repeated and when satisfied a unique solution is determined.

The MIR was used by Xerikos and Anderson (1962) to study supersonic flow impingement on various blunt bodies for both plane and axisymmetric flows. They also considered the case of a rectangular body for M_{in} = 5.8 in air. The results presented did not include any comparison. Bazzhin (in Hayes and Probstein, 1966) applied the same method for the impingement on a rectangular body at M_{in} of 5.0 and 20.0 in air.

Time-marching finite-difference methods

Time-marching finite-difference methods of various orders of accuracy have been proposed for the calculation of comressible-flow problems. Taylor et al (1972) compared the accuracy and the performance of first, second and third-order schemes, with exact solutions for 1-D flows with shock waves. The results demonstrated that the first and third-order schemes have the optimum overall performance and offer the best overall accuracy. The third-order schemes, however, have the disadvantage of requiring about twice the amount of computer time as the first-order schemes. Srinivas et al (1976) carried out an assessment of a similar but more detailed study. The study showed that the use of third or fourth-order schemes does not offer any specific advantage. The second order schemes are, however, susceptible to oscillations and nonlinear instabilities and are in need of certain modifications to be of practical use. First-order schemes, on the other hand, are resistant to nonlinear instability but one has to accept smearing of the discontinuities. Grid refinement and distribution then become important factors affecting the accuracy of such schemes.

The problem of supersonic flow impingement on rectangular bodies has often been used to test the various schemes. Burstein (1966) employ-

ed a second-order scheme incorporating an explicit artificial viscosity to stabilize the calculation. He produced results with free-stream Mach numbers (M_{in}) = 4.23 in air and 10.0 for γ = 1.17. Palumbo and Rubin (1972) used a second-order scheme for calculating the supersonic flow ahead of a two-dimensional rectangular body as well as in the laminar near wake. The flow was viscous with a heat conducting wall; M_{in} = 2.0 in air. Harten and Zwas (1972) used a hybrid scheme for such shock computation. The scheme was constructed from a first-order accuracy operator which dominated the shock regions and a second-order accuracy operator applied in smooth regions, this was in order to overcome nonlinear instabilities and post-shock oscillations. The values of M_{in} and γ were 4.23 and 1.4 respectively. Srinivas and Gururaja (1977) used a first-order scheme for M_{in} = 4.23 in air.

Whilst the results of the above schemes are in general agreement with each other the computer time required to obtain a solution, as reported by different authors, is measured in hours. In a recent paper by Landrum and Miller (1981), the authors assessed different methods for the prediction of supersonic flow over bodies. They concluded that the finite-difference method is superior as far as accuracy and applicability are concerned. However, the method was of the shock-fitting and time-marching type, which is not one of the best finite-difference methods. The authors concluded that there still exists a need for a fast method that can account for predominant nonlinear effects.

Space-marching finite-difference methods†

Surprisingly, very few authors have used these methods to solve transonic-flow problems. This may be because of the difficulties asso-

† The term space-marching is used to distinguish it from the time-marching methods of the previous section; the steady-state equations are solved here.

ciated with solving such flows in the steady state in which the equations are of a mixed hyperbolic/elliptic nature. The authors usually revert to the more expensive methods of the last section, in which the equations are hyperbolic in time.

Singhal (1977) used a space-marching finite-difference method to predict the compressible flow in axial turbomachinery cascades. The flow was treated as isentropic since the Mach numbers considered were not very high. The computations were conducted in a streamline-coordinate system.

Jennions (1980) used a similar approach, based on the pressure-correction technique, for the computation of impingement of axisymmetric supersonic jets on cones. The transonic flows considered have a predominant flow direction and the method employed is of the "shock-capturing" technique, with the shock-jump relations being explicitly input into the solution procedure. A distinction was made in solving for the subsonic and supersonic regions when formulating the pressure-correction equations and the corresponding adjustment procedure. The model was validated by comparing with analytical solutions and experimental data for various flow situations. However, difficulties were experienced in obtaining a solution for the impingement on cones of half angle greater than about 40^{o}.

The main advantage of these methods, as compared to the time-marching ones, is a huge saving in the computer time required to obtain a solution. The prediction procedure detailed in this thesis falls into this category.

2.5.3 Floating Warm-Water Layer and Other Analogous Flows

(i) Continuous warm-water layer flows

Various theoretical and experimental investigations of surface thermal discharges have been carried out in the last decade. Many of these are extensively reviewed by Jirka et al (1975) and Dunn et al(1975).

More recent studies, employing efficient finite-difference techniques (marching integration along the predominant flow direction and the use of the pressure-correction approach of Patankar and Spalding, 1972), have been made by, for example, Demuren (1979), McGuirk and Rodi (1979). Demuren used a depth-averaged mathematical formulation and employed different calculation procedures depending on the relative importance of the buoyancy forces. The effects of turbulence were modelled through entrainment relations derived from experimental data. McGuirk and Rodi employed a simplified 3-D model for the computation of 3-D heated surface jets discharging into stagnant water. The turbulent shear stresses and heat fluxes were determined by the "K-ε" turbulence model (see Launder and Spalding, 1972). The results of each study, as compared to experimental data, showed satisfactory agreement in general.

(ii) Layer-flow with internal hydraulic jumps (discontinuities)

In the above studies, attention was restricted to the supercritical jet-flow region. Generally, the local Froude number decreases in the downstream direction; when it reaches a value near unity, the flow develops into a subcritical stratified two-layer flow which is then controlled by downstream conditions. This flow transition occurs in the form of an internal hydraulic jump.

Long (1954) photographed the phenomenon of the internal hydraulic

jump in a two-fluid system consisting of salt-water and a mixture of carbon-tetrachloride and a commercial cleaning fluid. In his experiments, an obstacle was drawn by a motor at uniform speed along the bottom of the channel. The occurrence of internal hydraulic jumps was demonstrated for a range of obstacle velocities.

The governing equations for the internal hydraulic jump were derived, on the basis of control-volume analysis, by Yih and Guha (1955). The analysis was based on the assumption that the pressure distribution at the interface is hydrostatic and that the interfacial shear as well as shear at the bottom of the channel can be neglected. They also carried out experiments in a flume with a two-layer system consisting of water and stanisol (oil with a specific gravity of 0.777) or a mixture of stanisol and carbon-tetrachloride (with a specific gravity of 1.59). Good agreement was obtained between theory and experiments for the conjugate-depth ratio of the jumps.

Wilkinson and Wood (1971) performed experiments on an internal hydraulic jump of a two-layer flow consisting of a warm-water layer flowing over a cooler layer.

Jirka and Harleman (1979) studied the problem of a plane buoyant jet discharging vertically into a two-dimensional channel of confined depth. The integral method was employed to analyse the buoyant jet region with the usual boundary-layer approximations and the assumption of a variable entrainment coefficient. The properties of the surface impingement and internal jump regions were determined on the basis of control-volume analyses. The jump length was estimated, based on experiments, and used to match the near and far field regions. Experiments in a laboratory flume were made for the simulation of such buoyant discharges.

(iii) Other analogous flows

Hydraulic jumps have also been observed in the atmosphere (density jumps). Houghton and Kasahara (1968) applied the 1-D "shallow-water" equations to an investigation of steady fluid flows over an isolated ridge. The scheme is of the time-marching finite-difference approach.

Other flows of the layer type, analogous to shallow-water flows, are the oil-slick problem. For a study and review of the subject see, for example, Hoult (1972) and Stolzenbach et al (1977). Allen and Thanarajah (1977) carried out experiments in an open-water-channel placed in a wind tunnel. Oils, covering a wide range of viscosity, were introduced at the upstream end of the wind tunnel and their subsequent movements were studied under differing wind velocities.

2.6 STATUS OF EXISTING INFORMATION

The status of the existing information on shallow-water flows and analogous flows may be summarized as follows:

(1) Few experimental studies, on continuous shallow-water flows, are available that could be used to validate mathematical models.

(2) Experimental studies of discontinuous shallow-water flows are not sufficiently detailed, especially for 2-D flows, to allow adequate comparisons with mathematical models.

(3) Analytical solutions can be developed, that can provide reliable means of comparison with numerical solutions, for certain idealized flow situations.

(4) Simple control-volume analyses are used extensively to provide theoretical values of flow variables across discontinuities, and also to develop empirical formulae useful for design purposes.

(5) Sufficient experimental data and reliable numerical solutions on transonic flows are available, which may be used for comparison with analogous shallow-water flows.

(6) Most mathematical models developed for predicting shallow-water flows are limited in applicability, especially in dealing with mixed supercritical/subcritical flows.

(7) Most of the studies on the gas-hydraulic analogy are limited to comparisons of equations and on a qualitative basis. This is mainly due to the limitation of a specific-heat ratio of 2.

(8) The advances made in numerical techniques for computing transonic flow problems have not been exploited, at least positively, in computing discontinuous shallow-water flows. However, most of the methods which do exist for the solution of transonic flows are either limited in applicability or very expensive to use.

2.7 CLOSURE

In this chapter, theoretical and experimental studies of shallow-water flows and analogous flows were reviewed. The review was conducted according to a flow classification; namely, continuous shallow-water flows, discontinuous shallow-water flows, and analogous flows. At present, it appears that a need still exists for computationally cheap, fairly general and accurate procedures for computing such flows. Coordination in modelling shallow-water flows and compressible flows is desirable.

C H A P T E R 3

MATHEMATICAL FORMULATION

3.1 INTRODUCTION

The first task in analysing any flow situation is to consider the general physical laws that describe the fluid-dynamics of the flow. These laws are the well-known conservation laws, in partial differential form, of mass, momentum and scalar properties and any other auxiliary relations that may be required. In most cases, only a few features need to be considered, in the general laws, when simulating a certain flow situation. A numerical model should take full account of the features that play an important role in describing the flow. On the other hand, certain terms and equations may well be left out of the general system when these are believed to be irrelevant to, or of little influence on, the physical flow. The task of the modelling is then reduced to formulating these conservation equations into a suitable form to be solved by an efficient scheme and by supplying the appropriate initial and boundary conditions.

This chapter presents the equations which describe two-dimensional shallow-water flows. The equations are first introduced in the most general form covering a wide range of applications which have been listed in Chapter 1 as being of practical relevance. They are then reduced to a form suited to the current study. All assumptions and simplifications are clearly stated.

3.2 THE GOVERNING DIFFERENTIAL EQUATIONS IN GENERAL FORM

3.2.1 Derivation of Two-Dimensional Shallow-Water Equations

In general, free-surface flows can be three-dimensional, time-dependent and turbulent. However, for shallow-water flows, it is often

reasonable to assume that both vertical velocities and accelerations (compared to gravity) are negligible. Accordingly, the vertical equilibrium equation reduces to the hydrostatic pressure balance. It is further assumed that surface tension is negligible and the fluid is incompressible and homogenous.

The general three-dimensional Navier-Stokes equations for continuity and momentum can thus be written, in rectangular coordinates (x,y,z) for a fluid body on a rotating earth, as:

Conservation of Mass

$$\frac{\partial u}{\partial x} + \frac{\partial v}{\partial y} = 0 \qquad ,(3.1)$$

Conservation of u-Momentum

$$\frac{\partial u}{\partial t} + \frac{\partial}{\partial x}(u^2) + \frac{\partial}{\partial y}(uv) = - \frac{1}{\rho} \frac{\partial p}{\partial x} + f v + \frac{1}{\rho} \left(\frac{\partial \tau_{xx}}{\partial x} + \frac{\partial \tau_{xy}}{\partial y} + \frac{\partial \tau_{xz}}{\partial z} \right) \qquad ,(3.2)$$

Conservation of v-Momentum

$$\frac{\partial v}{\partial t} + \frac{\partial}{\partial x}(uv) + \frac{\partial}{\partial y}(v^2) = - \frac{1}{\rho} \frac{\partial p}{\partial y} - f u + \frac{1}{\rho} \left(\frac{\partial \tau_{xy}}{\partial x} + \frac{\partial \tau_{yy}}{\partial y} + \frac{\partial \tau_{zy}}{\partial z} \right) \qquad ,(3.3)$$

Conservation of w-Momentum

$$0 = - \frac{1}{\rho} \frac{\partial p}{\partial z} - g \qquad ,(3.4)$$

The symbols in the above equations represent:

u,v	the two velocity components in the x-and y-directions respectively,
x,y,z	perpendicular coordinate directions,
t	time,
ρ	the fluid density,
p	the static pressure,
g	the gravitational acceleration,
f	Coriolis parameter = $2\omega \sin\theta$, where ω is the angular velocity of the earth and θ is the latitude,
τ_{xx} , etc.	the fluid stresses.

The above equation system is still three-dimensional, with $u = \{ x,y,z,t \}$ and $v = \{ x,y,z,t \}$. The problem can be reduced to two-dimensions by integrating equations (3.1) to (3.4) vertically over the flow domain shown in Figure 3.1 and by defining depth-averaged quantities. The flow is bounded below by a rigid, fixed surface $z = z_b (x,y)$ and by a free surface $z = z_b (x,y) + h(x,y,t)$ above a horizontal datum-plane and subjected to atmospheric pressure (p_a), where h is the water depth. The integration will be carried out from the bottom to the surface, i.e. from z_b to $z_b + h$. The depth-averaged quantities are defined by the following relations:

$$\bar{u} = \frac{1}{h} \int_{z_b}^{z_b+h} u \, dz \, , \quad \bar{v} = \frac{1}{h} \int_{z_b}^{z_b+h} v \, dz \quad \text{and} \quad \overline{\tau} = \frac{1}{h} \int_{z_b}^{z_b+h} \tau \, dz \qquad .(3.5)$$

On integrating the equation system, making use of Leibnitz's rule and the kinematic boundary-conditions at the surface and bottom, (Appendix 1), there results the depth-averaged conservation equations:

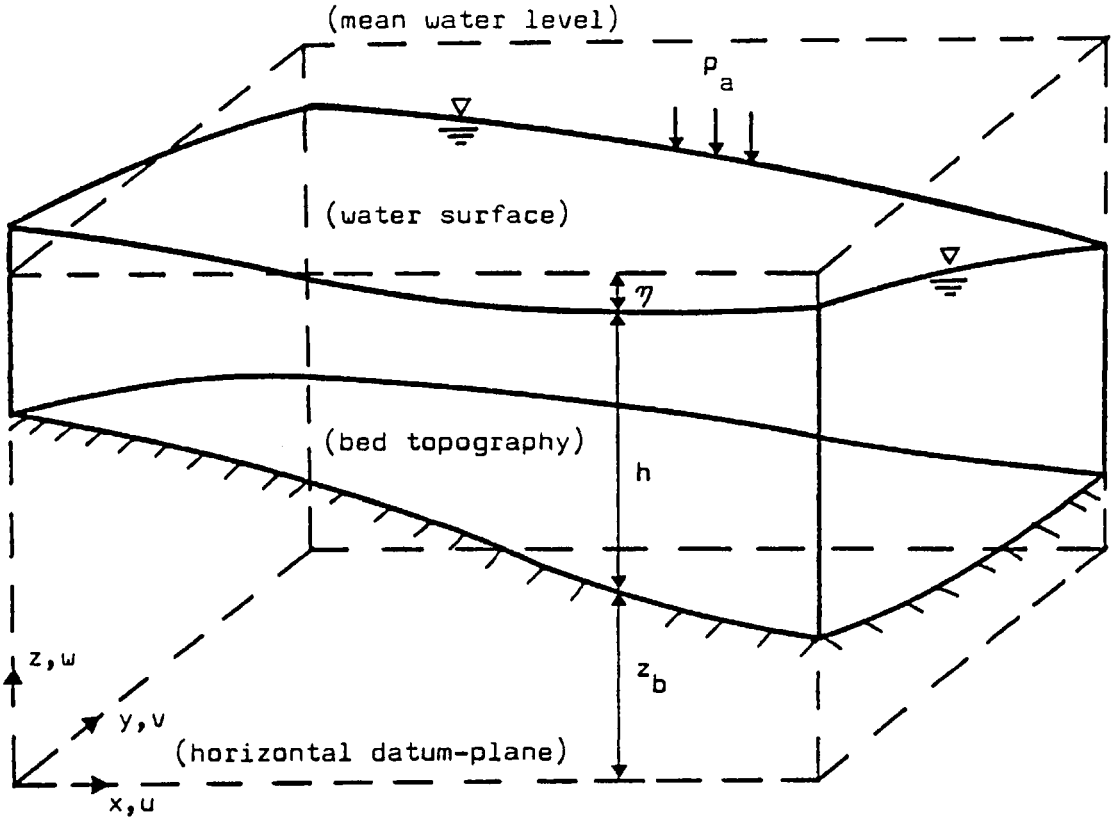


FIGURE 3.1 : DEFINITION OF BOTTOM HEIGHT, DEPTH, MEAN WATER LEVEL AND WATER SURFACE

Continuity

$$\frac{\partial h}{\partial t} + \frac{\partial}{\partial x}(h \bar{u}) + \frac{\partial}{\partial y}(h \bar{v}) = 0 \qquad ,(3.6)$$

u-Momentum

$$\frac{\partial}{\partial t}(h \bar{u}) + \frac{\partial}{\partial x}(h \bar{u}^2) + \frac{\partial}{\partial y}(h \bar{u} \bar{v})$$

$$= - gh \frac{\partial}{\partial x}(z_b + h) - \frac{h}{\rho} \frac{\partial p_a}{\partial x} + f h \bar{v}$$

$$+ \frac{1}{\rho}(\tau_{sx} - \tau_{bx}) + \frac{1}{\rho} \frac{\partial}{\partial x}(h \overline{\tau}_{xx}) + \frac{1}{\rho} \frac{\partial}{\partial y}(h \overline{\tau}_{xy})$$

$$,(3.7)$$

v-Momentum

$$\frac{\partial}{\partial t}(h \bar{v}) + \frac{\partial}{\partial x}(h \bar{u} \bar{v}) + \frac{\partial}{\partial y}(h \bar{v}^2)$$

$$= - gh \frac{\partial}{\partial y}(z_b + h) - \frac{h}{\rho} \frac{\partial p_a}{\partial y} - f h \bar{u}$$

$$+ \frac{1}{\rho}(\tau_{sy} - \tau_{by}) + \frac{1}{\rho} \frac{\partial}{\partial x}(h \overline{\tau}_{xy}) + \frac{1}{\rho} \frac{\partial}{\partial y}(h \overline{\tau}_{yy})$$

$$,(3.8)$$

where,

τ_{sx} and τ_{sy} are the surface shear-stresses in the x-and y-directions respectively and

τ_{bx} and τ_{by} are the bottom shear-stresses in the x-and y-directions respectively.

General Remarks

(i) The system of equations (3.6) to (3.8) represents a general form of the non-linear shallow-water equations. This will be reduced, in Section 3.3, to the form most suitable to the applications considered in this thesis. The significance of terms in the general equations is examined, for a variety of flow situations, by order of magnitude estimates in Section 3.2.3.

(ii) The vertical profiles of flow properties are assumed to be nearly uniform; hence depth-averaged values of the dependent variables are used. Accordingly, extra terms, called "dispersion" terms, are not present in this formulation. Such terms arise from depth integration of the transport equations when these profiles are not uniform.

(iii) The surface and bottom stress terms, τ_s and τ_b , in equations (3.7) and (3.8) result from the depth-integrated momentum transports, τ_{xx} , τ_{xy} , etc.

(iv) The equation system is closed when the surface, bottom and fluid stresses are expressed in terms of depth-averaged flow properties.

3.2.2 Closure of the Equations

A. Wind Stresses

The wind exerts shear stresses, τ_{sx} and τ_{sy} in the x-and y-directions respectively, on the water surface which may be calculated (see Spalding, 1975) from the following relations:

$$\tau_{sx} = C_s \rho_a U_0 \left(U_0^2 + V_0^2 \right)^{\frac{1}{2}} ,$$

$$\tau_{sy} = C_s \rho_a V_0 \left(U_0^2 + V_0^2 \right)^{\frac{1}{2}} \qquad ,(3.9)$$

where,

C_s is the surface shear-stress coefficient,

ρ_a is the density of the air,

U_0, V_0 are the velocity components of the wind relative to the flow averaged-velocity components in the x-and y-directions respectively.

B. Bottom Stresses

The bottom shear-stresses, τ_{bx} and τ_{by} in the x-and y-directions respectively, are calculated by relating them to the depth-averaged velocities via:

$$\tau_{bx} = C_f \rho \bar{u} \left(\bar{u}^2 + \bar{v}^2 \right)^{\frac{1}{2}} \quad ,$$

$$\tau_{by} = C_f \rho \bar{v} \left(\bar{u}^2 + \bar{v}^2 \right)^{\frac{1}{2}} \qquad ,(3.10)$$

where,

C_f is the bottom shear-stress coefficient.

The value of C_f is dependent on the bed roughness. For smooth to rough surfaces, its value varies between 0.001 to 0.003 (Spalding, 1975). This empirical friction-factor is related to Chezy's coefficient (C) by:

$$C_f = \frac{g}{C^2} \qquad ,(3.11)$$

where the dimension of C is $m^{\frac{1}{2}}/\ sec.$

C. Fluid Stresses

These are $\overline{\tau}_{xx}$, $\overline{\tau}_{xy}$ and $\overline{\tau}_{yy}$ in the momentum equations (3.7) and (3.8). In shallow flows, where horizontal dimensions greatly exceed vertical ones, these terms are negligible when compared to other terms in the equations. However, their neglect also depends upon the physical situation considered. In turbulent flow, these terms are retained and may be modelled by a constant eddy-viscosity coefficient multiplying the depth-averaged velocity gradients, or by the use of more advanced turbulence models. So far, the stress terms are retained in the equations only for generality and to facilitate order of magnitude estimates.

3.2.3 Order of Magnitude Estimates

Greater insight into the significance of the terms in the general equations may be gained by casting them into non-dimensional form. This also helps to establish the conditions under which the dynamic similarity of two systems can be achieved, by equating the numerical coefficients (dimensionless numbers) obtained from their normalized equations.

Consider the u-momentum equation given by (3.7). The stress terms $\overline{\tau}_{xx}$ and $\overline{\tau}_{xy}$ are expressed here for simplicity in terms of velocity gradients and fluid properties. They are given by $\mu\, \partial\bar{u}/\partial x$ and $\mu\, \partial\bar{u}/\partial y$, where μ is the laminar viscosity and is taken as a constant. The bars denoting depth-averaged quantities are left out for clarity, and a set of dimensionless quantities introduced and defined by asterisks in the following manner:

$$x_* = \frac{x}{L} \quad , \quad y_* = \frac{y}{L} \quad , \quad h_* = \frac{h}{H} \quad , \quad z_{b_*} = \frac{z_b}{H} \quad , \quad u_* = \frac{u}{V} \quad , \quad v_* = \frac{v}{V} \quad ,$$

$$t_* = \frac{t}{t_0} = \frac{t}{L/V} \quad , \quad p_{a_*} = \frac{p_a}{\varrho g H} \quad , \quad f_* = f\, t_0 = \frac{f\, L}{V} \quad ,$$

$$\tau_{sx_*} = \frac{1}{C_f} \frac{\tau_{sx}}{\varrho V^2} \frac{\varrho V^2}{\varrho_a U_0^2} \quad \text{and} \quad \tau_{bx_*} = \frac{1}{C_f} \frac{\tau_{bx}}{\varrho V^2} \qquad ,(3.12)$$

where,

L,H,V are constant reference values of length, depth and velocity respectively, to be chosen as characteristics of the system.

Now, if equations (3.12) are substituted in equation (3.7), the following equation is obtained:

$$\frac{HV^2}{L} \frac{\partial}{\partial t_*} (h_* u_*) + \frac{HV^2}{L} \frac{\partial}{\partial x_*} (h_* u_*^2) + \frac{HV^2}{L} \frac{\partial}{\partial y_*} (h_* u_* v_*)$$

$$= - \frac{gH^2}{L} h_* \left(\frac{\partial h_*}{\partial x_*} + \frac{\partial z_{b_*}}{\partial x_*} \right) - \frac{gH^2}{L} h_* \frac{\partial p_{a_*}}{\partial x_*} + \frac{HV^2}{L} f_* h_* v_*$$

$$+ C_f V^2 \left(\frac{\varrho_a U_0^2}{\varrho V^2} \tau_{sx_*} - \tau_{bx_*} \right) + \frac{HV}{L^2} \frac{\mu}{\varrho} \left[\frac{\partial}{\partial x_*} \left(h_* \frac{\partial u_*}{\partial x_*} \right) + \frac{\partial}{\partial y_*} \left(h_* \frac{\partial u_*}{\partial y_*} \right) \right]$$

.(3.13)

The dimensions of the above equation have not altered. Each term has a dimension of m^2/s^2 i.e. accelaration (or force per unit mass) times length, the length dimension arises when integrating the equation over the depth. Equation (3.13) can now be made dimensionless by dividing each term by HV^2/L to give:

$$\frac{\partial}{\partial t_*}\left(h_* u_*\right) + \frac{\partial}{\partial x_*}\left(h_* u_*^2\right) + \frac{\partial}{\partial y_*}\left(h_* u_* v_*\right)$$

$$= -\frac{1}{Fr^2} h_* \frac{\partial}{\partial x_*}\left(h_* + z_{b_*} + p_{a_*}\right) + \frac{1}{R} h_* v_*$$

$$+ C_f \frac{L}{H}\left(\frac{\rho_a U_0^2}{\rho V^2} \tau_{sx_*} - \tau_{bx_*}\right)$$

$$+ \frac{1}{Re}\left[\frac{\partial}{\partial x_*}\left(h_* \frac{\partial u_*}{\partial x_*}\right) + \frac{\partial}{\partial y_*}\left(h_* \frac{\partial u_*}{\partial y_*}\right)\right] \qquad ,(3.14)$$

where,

Fr is Froude number $= \frac{V}{(gH)^{\frac{1}{2}}}$ and represents the ratio of inertia forces to gravity forces,

R is Rossby number $= \frac{V}{fL}$ and represents the ratio of inertia forces to Coriolis forces and

Re is Reynolds number $= \frac{\rho VL}{\mu}$ and represents the ratio of inertia forces to the viscous forces.

The same dimensionless groups can be obtained for the y-direction momentum equation, equation (3.8). The continuity equation (3.6), when put in a dimensionless form, introduces no additional similitude conditions.

All derivatives in equation (3.14) have an order of magnitude of roughly unity. Hence, the significance of the individual terms can be decided by comparing the magnitude of the dimensionless coefficients. The meaning and significance of each term are displayed in Table 3.1.

Term	Dimensionless Form	Order of Magnitude
(1) Unsteady	$\frac{\partial}{\partial t_*} (h_* u_*)$	1 (unsteady flow) 0 (steady flow)
(2) Convection	$\frac{\partial}{\partial x_*} (h_* u_*^2) + \frac{\partial}{\partial y_*} (h_* u_* v_*)$	1
(3) Pressure gradient	$\frac{1}{Fr^2} h_* \frac{\partial}{\partial x_*} (h_* + z_{b_*} + p_{a_*})$	$1/Fr^2$ i.e. gH/V^2
(4) Coriolis	$\frac{1}{R} h_* v_*$	$1/R$ i.e. fL/V
(5) Wind stress	$C_f \frac{L}{H} \frac{\rho_a}{\rho} \frac{U_0^2}{V^2} \tau_{sx_*}$	$C_f \frac{L}{H} \frac{\rho_a}{\rho} \frac{U_0^2}{V^2}$
(6) Bottom stress	$C_f \frac{L}{H} \tau_{bx_*}$	$C_f \frac{L}{H}$
(7) Diffusion	$\frac{1}{Re} \left[\frac{\partial}{\partial x_*} (h_* \frac{\partial u_*}{\partial x_*}) + \frac{\partial}{\partial y_*} (h_* \frac{\partial u_*}{\partial y_*}) \right]$	$1/Re$ i.e. $\mu/\rho VL$

A. Order of Magnitude of Terms

TABLE 3.1 : TERMS IN THE GENERAL u-MOMENTUM EQUATION IN DIMENSIONLESS FORM

Term	Significance
(1) Unsteady	• Time-dependent flows in general: • tidal flows, • the hurricane problem, • wind-induced flows in lakes, where wind direction and magnitude change with time, • steady flows with time-dependent methods of calculation.
(2) Convection	• Unimportant in tidal flows(usually dominated by the driving force caused by tidal changes on the boundaries). • Unimportant in wind-driven circulation in wide shallow lakes(usually dominated by Coriolis forces, when Rossby number is small, and wind stresses).
(3) Pressure gradient	• The h-gradient term represents the tendency of layers with horizontal bottoms to have horizontal surfaces. • The z_b-gradient term represents the tendency of water to slide over sloping bottom surfaces. • The p_a-gradient term is significant, for example, in hurricane problems.
(4) Coriolis	• Important in large bodies of water, e.g. North Sea and Great Lakes.
(5) Wind stresses	• Important in large stretches of water with large ratio of wind to water speed, e.g. wind-induced circulation in lakes.
(6) Bottom stresses	• Important for shallow flows in general, especially for rough surfaces.
(7) Diffusion	• Not present in inviscid flows. • Can be neglected in shallow flows.

B. Significance of Terms

TABLE 3.1 : (Continued)

Equation (3.14) has the same solution for two geometrically similar systems when the dimensionless coefficients are numerically the same for the two systems. Depending on the flow situation considered, one or more dimensionless coefficients may be unimportant and hence these terms can be left out of the general equations. In shallow-water flows, only Froude number equality is needed to achieve dynamic similarity. In the analogy between shallow-water flows and two-dimensional inviscid, compressible-gas flows, it is a requirement that the Froude number and Mach number are equal in magnitude to achieve dynamic similarity for two geometrically similar systems. This will be demonstrated by using test cases and the implication discussed in Chapter 8.

3.3 THE GOVERNING DIFFERENTIAL EQUATIONS SOLVED

3.3.1 Basic Assumptions

So far, the only approximations made to the three-dimensional Navier-Stokes equations, in deriving the general shallow-water equations (equations 3.6 to 3.10), are:

(1) The assumption of a hydrostatic pressure distribution.

(2) The fluid is assumed incompressible and homogenous and gain or loss of mass from surface (rain, evaporation) or bottom (seepage) are not considered.

(3) The vertical velocity profiles are approximated to be uniform; hence depth-averaged values are used.

(4) The wind and bottom stresses are related to the square of the depth-averaged velocities by equations (3.9) and (3.10).

(5) The fluid stresses are expressed by a constant laminar-or eddy-viscosity coefficient multiplying the depth-averaged velocity gradients.

In the present study, it is further assumed (with reference to Table 3.1) :

(6) The flow is steady.

(7) A horizontal bed topography.

(8) Flow is over small stretches of water under calm conditions; hence negligible atmospheric-pressure variation and wind stresses.

(9) A large Rossby number, i.e. negligible Coriolis forces (see equation 3.14).

(10) That viscous terms are neglected unless otherwise stated, where the laminar viscosity is used.

3.3.2 The Resulting Governing Equations

Subject to the above assumptions, for fixed rectangular coordinates (x,y,z) of Figure 3.1, the system of equations (3.6) to (3.10) reduces to:

Conservation of Mass

$$\frac{\partial}{\partial x}\left(h\,\overline{u} \right) + \frac{\partial}{\partial y}\left(h\,\overline{v} \right) = 0 \qquad ,(3.15)$$

Conservation of u-Momentum

$$\frac{\partial}{\partial x}\left(h\,\overline{u}^{2} \right) + \frac{\partial}{\partial y}\left(h\,\overline{u}\,\overline{v} \right) = - gh\frac{\partial h}{\partial x} - C_f\,\overline{u}\left(\overline{u}^{2} + \overline{v}^{2} \right)^{\frac{1}{2}} \qquad ,(3.16)$$

Conservation of v-Momentum

$$\frac{\partial}{\partial x}\left(h \bar{u} \bar{v} \right) + \frac{\partial}{\partial y}\left(h \bar{v}^2 \right) = - gh \frac{\partial h}{\partial y} - C_f \bar{v} \left(\bar{u}^2 + \bar{v}^2 \right)^{\frac{1}{2}} \qquad .(3.17)$$

The general Transport Equation

The above set of equations can be represented by a single equation of the form:

$$\frac{\partial}{\partial x}\left(h \bar{u} \bar{\phi} \right) + \frac{\partial}{\partial y}\left(h \bar{v} \bar{\phi} \right) = S^{\phi} \qquad ,(3.18)$$

where $\bar{\phi}$ identifies the depth-averaged dependent variable and stands for 1, $\bar{u}$ and $\bar{v}$ in equations (3.15) to (3.17) respectively. S^{ϕ} is the general "source term" and represents the individual terms on the right-hand side of the same equation set. The source term is used to put all the equations into a standard form, which is solved by the solution procedure described in the next chapter.

3.3.3 Boundary and Initial Conditions

The equation set given by (3.15) to (3.17) is closed. But the mathematical formulation for a particular flow situation is complete only when the relevant boundary and initial conditions are specified.

(i) Boundary Conditions

The necessary boundary conditions are either the values or gradients of the dependent variables on the boundaries of the calculation domain. The proper specification of these conditions is of vital importance in simulating a flow situation correctly and are highly

dependent on whether the flow is supercritical or subcritical. When the flow is supercritical, it is controlled by upstream conditions (hyperbolic) and when the flow is subcritical, it is controlled by downstream conditions (elliptic). When the flow changes from supercritical to subcritical conditions, both upstream and downstream controls are active. The following physical boundaries are encountered in the present study:

Inlet

When conditions at the inlet boundary are supercritical, the distribution of both velocities and depth must be prescribed. For subcritical conditions, only the flow rate needs to be prescribed.

Outlet

When conditions at the outlet boundary are supercritical, values need not be specified. For subcritical conditions, the depth must be specified and acts as a downstream control. The velocities at the outlet boundary need not be specified and are determined by continuity.

Symmetry Plane

At a symmetry plane the normal velocities are set to zero, other variables are prescribed as having zero flux.

Wall

At a wall which is stationary and impervious, the velocity components and normal gradients of depth are set to zero.

Free-Stream Boundary

The free-stream boundary is usually located far enough away from the inside of the domain so that the conditions prevailing there would be the undisturbed free-stream conditions.

(ii) Initial Conditions

Dependent variables need to be given initial values in order to start the calculation. A good initial guess, based on insight to the flow situation, generally ensures quicker convergence and better stability of the solution scheme. However, the final results should not depend on these conditions when solving steady-state problems.

The details of the implementation of these boundary and initial conditions will be discussed along with other matters concerning the solution procedure in Chapter 4.

3.3.4 Dependent Variables solved

There are only three dependent variables, in the absence of the enthalpy equation, that characterize the isothermal modelling of steady two-dimensional shallow-water flows. These are the two depth-averaged velocity components u, v and depth of flow, h. The non-linear partial-differential equations (3.15) to (3.17) are used to solve for these variables using specified boundary conditions. A suitable numerical solution procedure is developed to perform this task as described in the next chapter.

3.4 CLOSURE

The information presented in this chapter is summarized below.

(a) The equations which describe the two-dimensional shallow-water flows are deduced from the general Navier-Stokes equations.

(b) The equation system is closed through appropriate expressions for the bottom and surface interactions.

(c) Order of magnitude estimates are conducted to determine the significance of terms in the transport equations for a variety of applications.

(d) Further relevant assumptions are stated in arriving at a set of differential equations suitable for the current applications.

(e) The boundary conditions necessary to complete the mathematical formulation are specified.

(f) The dependent variables solved are stated.

CHAPTER 4

THE NUMERICAL SOLUTION PROCEDURE

4.1 INTRODUCTION

In the previous chapter, the depth-averaged differential equations governing the flow of shallow water have been formulated. These equations are coupled and non-linear. Apart from a few simple and idealized flow situations, these equations are not amenable to analytical solution, and therefore, other means of solution are sought.

This chapter provides details of a general numerical procedure for solving shallow-water equations. The procedure is based on a finite-difference implicit scheme and utilizes a pressure-correction technique of Patankar and Spalding (1972). An upwind-difference scheme is employed and the hydrodynamic variables solved are the component velocities and depth.

A general description of the procedure is outlined in this section in order to give an overall picture before discussing the details in the following sections. The solution procedure consists of the following major steps:

(i) The flow domain is divided into discrete regions by constructing a staggered finite-difference grid. This yields "control volumes" for each flow variable.

(ii) The transformation of the partial-differential equations into algebraic ones (finite-difference equations) for each variable at each cell. This is accomplished by integrating the former equations over the control volumes and using assumptions for

the variation of the variables between grid nodes.

(iii) Solving the resulting set of finite-difference equations for the hydrodynamic variables by an appropriate algorithm.

(iv) The determination of the depth field. This is achieved by utilizing the widely used "SIMPLE" algorithm of Patankar and Spalding (1972), in which corrections based on continuity are made to the depth field, and corresponding corrections made to the velocity fields which are obtained from the solution of the momentum equations. By successive solution of the momentum and depth-correction equations, the velocities and depths are determined uniquely for given boundary conditions. The depth-correction values are obtained by using a suitable solver.

The remainder of the chapter consists of five main parts in which the solution procedure is detailed. In the next section, the finite-difference equations for the momentum and depth-correction are determined; this is followed by the solution procedure of these equations. Detailed account of auxiliary information is then given. A concluding section then summarizes the main features of the procedure.

4.2 DETERMINATION OF THE FINITE-DIFFERENCE EQUATIONS

4.2.1 The Finite-Difference Grid and Location of Flow Variables

The finite-difference grid consists of a set of orthogonally intersecting lines (grid lines) which form a lattice, in the x-y plane, covering the whole flow domain. The points of intersection

of the grid lines are called grid nodes which provide reference locations for identifying the flow variables. The depth, pressure, and any other scalar variable (if included in the model) are stored at the nodal points of the grid. The velocity components are calculated and stored at points midway between grid nodes. Figure 4.1 shows a portion of the grid and identifies the locations for each of the flow variables. The dashed enclosures in the figure show the manner in which the variables are grouped together for identification purposes. This grid arrangement is known as a staggered-grid system, introduced by Harlow and Welch (1965), and has the following advantages:

(i) The velocity components are stored at just the points at which they are required for the calculation of a continuity balance over the region surrounding a grid node. This also makes the velocities directly available for the calculation of convective fluxes.

(ii) The pressure gradients driving the velocities can be evaluated more conveniently.

The grid spacings need not necessarily be uniform over the flow domain but can vary so that it is possible to locate more grid nodes in regions where steep variations of flow properties are expected. However, once the grid density and dimensions have been set, they remain fixed during the solution process. The results of the computations are checked for grid independence by successively increasing the grid fineness. The grid refinement process is usually governed by computer storage limitation and economic considerations.

The discretization scheme has made it necessary, when a variable is required at points other than those at which it is stored, to use the weighted average of its neighbouring values.

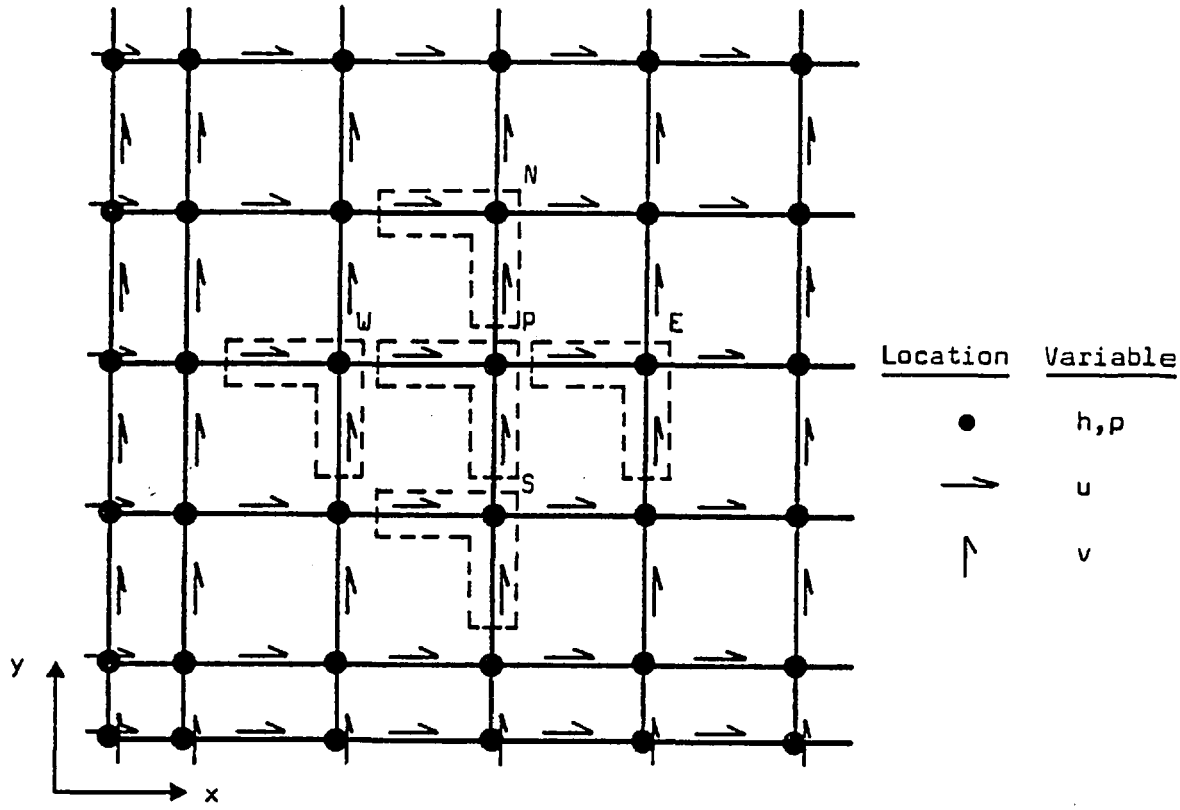


FIGURE 4.1 : LOCATION OF THE VARIABLES ON THE FINITE-DIFFERENCE GRID

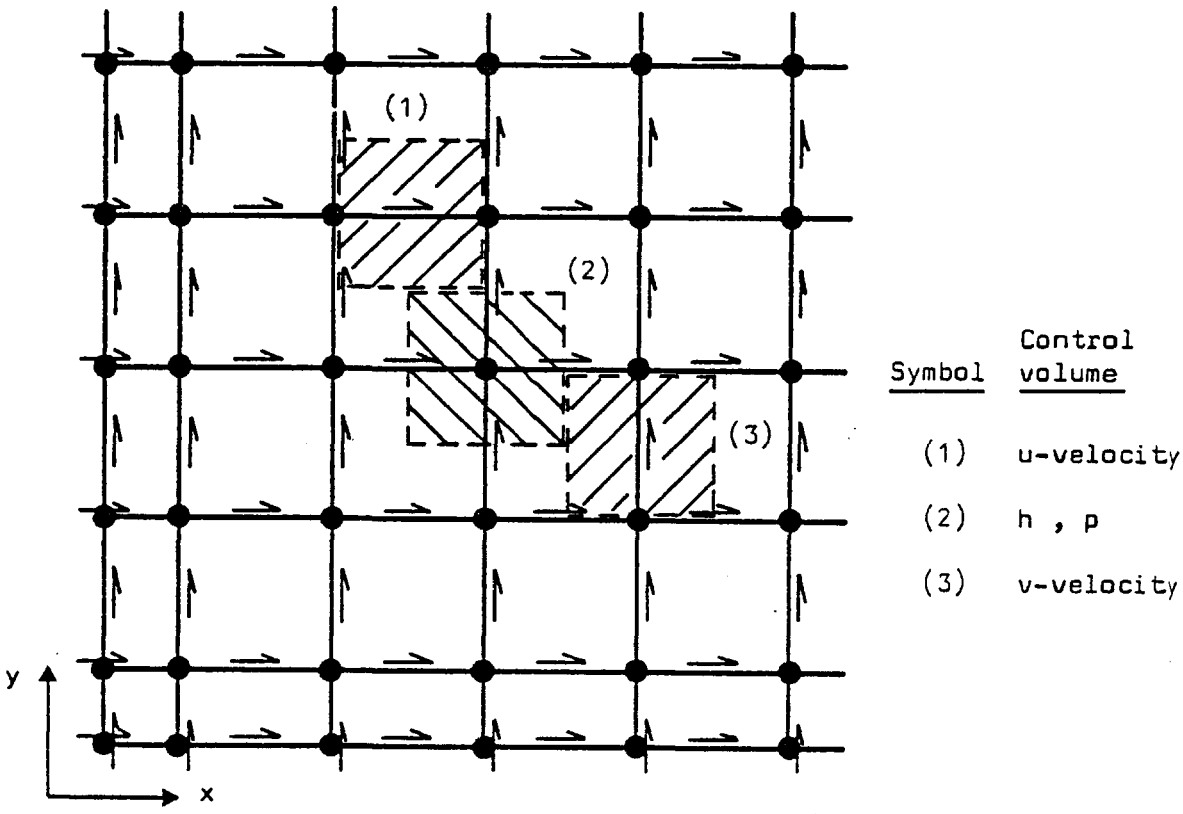


FIGURE 4.2 : DEFINITION OF THE CONTROL VOLUMES

4.2.2 Control Volumes

Control volumes are the regions, that surround the nodes of the grid system, over which the partial-differential equations are integrated to yield the finite-difference equations. Due to the staggered-grid configuration, there are three types of control volume belonging to the three different locations of the flow variables as shown in Figure 4.2. The figure shows the main control volumes for the variables stored at each grid node, u-velocity control volumes for the u-velocity storage locations and v-velocity control volumes for the v-velocity storage locations.

The control volumes corresponding to the near-boundary grid nodes are slightly different to those in the rest of the calculation domain, as illustrated in Figure 4.3. This difference is necessary so as to enable both the control-volume surfaces and the locations of the velocities normal to them, to coincide with the boundary itself. Control volumes are not needed for the boundary nodes, since the values of the variables there are either known or can be deduced from the values on the near-boundary nodes.

4.2.3 The Momentum Equations

General concept

The finite-difference equations are obtained by integrating the differential equations for each variable over the appropriate control volume. There being different control volumes for variables does not preclude a general form of the finite-difference equations being expressed in terms of a general variable ϕ , where ϕ stands

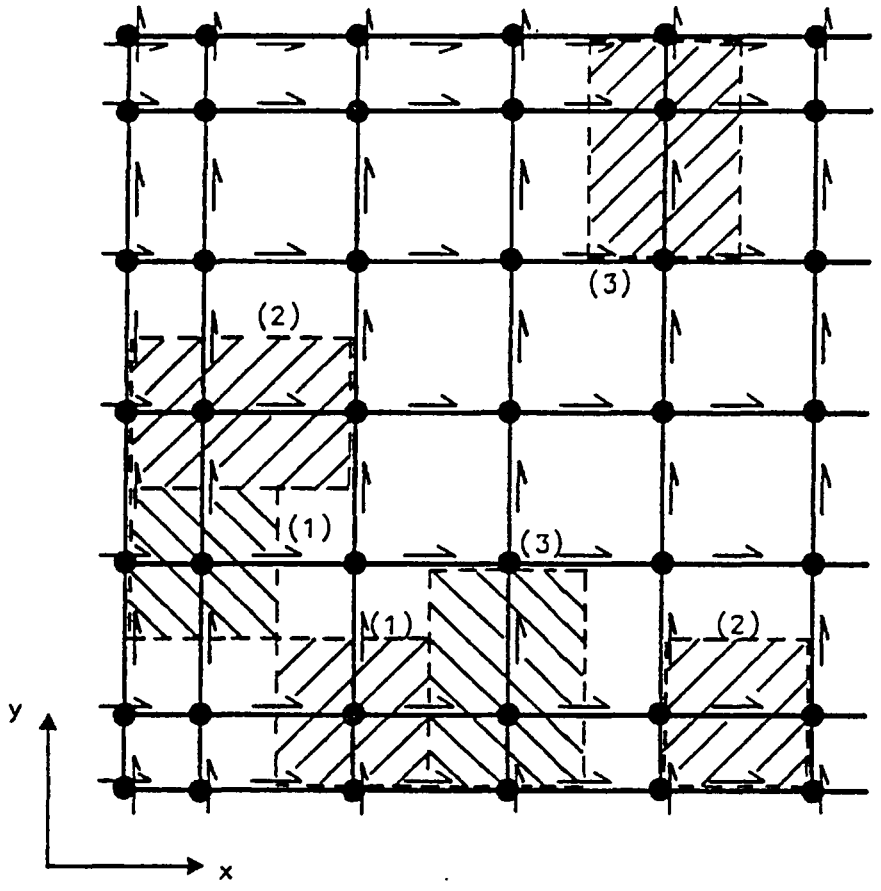


FIGURE 4.3 : NEAR-BOUNDARY CONTROL VOLUMES

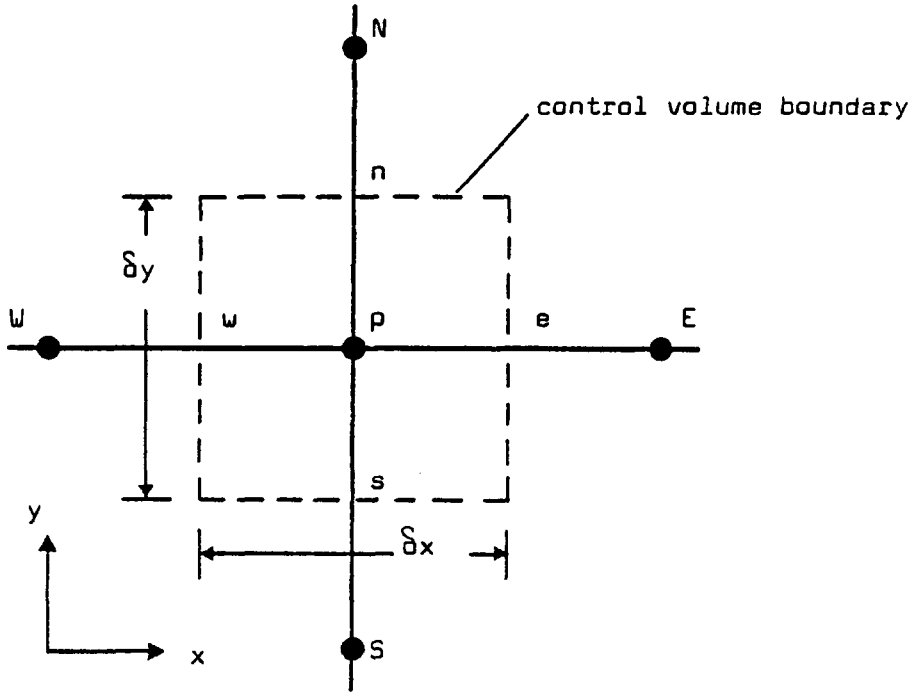


FIGURE 4.4 : GRID NOMENCLATURE USED TO DEVELOP THE FINITE-DIFFERENCE EQUATIONS

for u, v and any scalar variable in the equation set. Differences in the contents of each equation are contained in "source terms". Accordingly, the integration procedure will be developed, in this section, with reference to the transport equation written for the general variable ϕ and given by equation 3.18 in Section 3.3.2.

Figure 4.4 shows a typical cell enclosing the ϕ-node, P. Point P, the central node, has four neighbouring nodes N,S,E and W. The flow properties between these nodes, i.e. at the cell faces, are subscripted n,s,e and w accordingly. A finite-difference equation linking the value of ϕ at P to those at N,S,E and W, is obtained by integrating the differential equation 3.18 over the volume of the cell.

The basic decisions

In the integration, the following decisions are taken regarding the manner in which the variables vary between grid nodes:

(i) All flow properties are uniform over a cell face.

(ii) For the calculation of the source terms, that may depend on ϕ, the value of ϕ is considered uniform and equal to ϕ_P over the control volume surrounding the point P, and changes abruptly to ϕ_N , ϕ_S , ϕ_E or ϕ_W at the faces of the control volume.

(iii) For the diffusion terms, if present, ϕ is taken to vary linearly between nodes.

(iv) For the convection terms, an upwind-differencing scheme is employed. Accordingly, the value of ϕ convected across the face is the value at the neighbouring node from which the flow is approaching the face concerned.

(v) Similarly, in calculating the mass fluxes across the cell faces, the upstream depth values are used.

N.B. The decisions taken in (iv) and (v) above are needed for the numerical stability of the scheme, as will be discussed later. However, the effect of these on the accuracy of the results will diminish as the grid is made finer.

Areas of the cell faces

The areas of the cell faces which will be used in the finite-difference equations are:

$$a_n = \delta x\, h_n \qquad \text{(north face)} \quad ,$$

$$a_s = \delta x\, h_s \qquad \text{(south face)} \quad ,$$

$$a_e = \delta y\, h_e \qquad \text{(east face)} \quad ,$$

$$a_w = \delta y\, h_w \qquad \text{(west face)} \qquad .(4.1)$$

In equation 4.1, the subscripts for the depth values are merely used for the identification of the cell face under consideration. Rule (v) above should be obeyed, for example h_n can either be h_p or h_N, depending upon whether v_n is positive (upwards) or negative (downwards) respectively. This applies similarly to the other three faces. Hence, whenever an area (a) is used with a subscript n,s,e or w, it is to be remembered that it contains the value of the depth at the upstream side of the particular face.

The volume of the cell is given by:

$$V_p = \delta x\, \delta y\, h_p \qquad .(4.2)$$

Diffusions terms

The majority of the flow situations considered in this study are for inviscid flows. However, a few cases are considered with a constant viscosity. This has made it necessary to formulate the diffusion terms, as well, in the general finite-difference equations.

Consider, for example, the west face of the cell shown in Figure 4.4; ϕ is taken to vary linearly between P and W. Therefore, the diffusive flux for the west face can be written as:

$$\text{Diffusive flux} = \frac{1}{2} \delta y \, (h_P + h_W) \, \Gamma_{\phi,w} \, \frac{(\phi_W - \phi_P)}{(x_P - x_W)} \qquad ,(4.3)$$

where, $\Gamma_{\phi,w}$ is the exchange coefficient for the property ϕ at the west face divided by density.

Similar expressions can be written for the diffusive fluxes across the north, south and east faces.

Convection terms

The convective flux across the west face of the control volume is:

$$\text{Convective flux} = a_w \, u_w \, \phi_w \qquad ;(4.4)$$

the uniform density allows ρ to be eliminated.

In the present study, the "upwind-difference" formulation is used, see Spalding (1972). The value of ϕ_w is, therefore, taken to

be the nodal value prevailing at the upwind side of the face. Thus, ϕ_w is specified as:

$$\phi_w = \phi_W \quad \text{if} \quad u_w \geqq 0 \quad ,$$

$$\phi_w = \phi_p \quad \text{if} \quad u_w < 0 \qquad .(4.5)$$

The upwind-difference scheme is chosen because, in the flows considered, the convection contribution to the flux is predominant. The use, for example, of a central-difference scheme for such flows would lead to numerical instability and physically unrealistic results. The upwind-difference practice ensures positive or zero but never negative coefficients.

Similar expressions to (4.5) exist for the other cell faces.

Total flux

The expression for total flux across the west cell-face is therefore given by:

$$\text{Total flux} = (D_w + C_w)\,\phi_W - D_w\,\phi_p \quad \text{for} \quad C_w \geqq 0 \quad ;$$

$$\text{Total flux} = D_w\,\phi_W - (D_w - C_w)\,\phi_p \quad \text{for} \quad C_w < 0 \qquad ,(4.6)$$

where,

$$D_w = \frac{1}{2}\,\delta y\,(h_p + h_W)\,\sqrt{\phi,_w}\,/\,(x_p - x_W) \quad ,$$

$$C_w = a_w\,u_w \qquad .(4.7)$$

Expressions (4.6) can be written more compactly as:

$$\text{Total flux} = A_w^{\phi} \left(\phi_w - \phi_p \right) + C_w \phi_p \qquad ,(4.8)$$

where,

$$A_w^{\phi} = \text{Max} \left(D_w \ , \ D_w + C_w \right) \qquad ,(4.9)$$

with Max (X,Y) denoting the larger of either X or Y and the superscript ϕ signifying that the A's, for different ϕ's, may be different.

Total-flux expressions similar to (4.8) can be obtained for the other three cell faces.

Source terms

The source term S^{ϕ}, in equation (3.18), is integrated by assuming it to be constant over the control volume. The integrated value is then linearised so that it may be written as:

$$S^{\phi} V_p = S_U^{\phi} V_p + S_p^{\phi} V_p \phi_p \qquad .(4.10)$$

This linearisation enhances the stability of the numerical scheme. Further, if there is no dependence of the integral on ϕ_p, then S_p^{ϕ} is set equal to zero; otherwise, it is necessary that S_p^{ϕ} is always negative if stability is to be ensured.

The complete equation

The integration of the general transport equation is now complete. By suitably combining the total fluxes on the four cell faces, the net outflow of ϕ by diffusion and convection can be readily obtained. Equating this to the volume integral of the source term, S_P^{ϕ}, and making use of mass continuity, the finite-difference form of equation (3.18) is obtained as:

$$A_P^{\phi} \phi_P = A_N^{\phi} \phi_N + A_S^{\phi} \phi_S + A_E^{\phi} \phi_E + A_W^{\phi} \phi_W + S_U^{\phi} \quad ,(4.11)$$

where,

$$A_P^{\phi} = A_N^{\phi} + A_S^{\phi} + A_E^{\phi} + A_W^{\phi} - S_P^{\phi} \quad .(4.12)$$

Equation (4.11) may be abbreviated to:

$$\phi_P = \left[\sum_i \left(A_i^{\phi} \phi_i \right) + S_U^{\phi} \right] / A_P^{\phi} \quad ,(4.13)$$

where the summation is over the four neighbouring nodes, N,S,E and W.

The finite-difference equations for the velocity components can be expressed in the same form as equation (4.13) but contain an additional source term representing the depth gradient. Their coefficients, A_i^u and A_i^v, can be obtained directly from A_i^{ϕ} above by using appropriate interpolation.

These finite-difference forms of the momentum equations are solved by an algorithm described in Section 4.3.2.

4.2.4 The Depth-Correction Equations

General concept

The partial-differential equation for continuity (equation 3.15) when discretized, merely states the requirement that the inflows and outflows of mass are locally in balance for each control volume in the flow domain. This does not yield a finite-difference equation of the form of equation (4.13), because there is no variable for the mass conservation. Moreover, because the depth field is not known in advance, the velocities obtained from the solution of the momentum equations, u^* and v^*, do not in general satisfy mass continuity, and must be corrected to account for the error introduced by the guessed depth field, h^*. Therefore, it is necessary to derive a way of correcting the velocity and the depth fields simultaneously.

In the present method the mass continuity is enforced, as in the "SIMPLE" (Semi-Implicit Method for Pressure-Linked Equations) algorithm of Patankar and Spalding (1972), via a depth-correction (h') for which finite-difference equations need to be formulated and solved.

The depth-correction equation is developed by utilizing source terms from the finite-difference continuity equation and coefficients from truncated forms of the momentum equations.

Derivation

In each cycle of operations, the momentum equations are first solved with the depth-gradient terms evaluated from the existing, but as yet incorrect, depth field h^*, yielding the corresponding velocities

u^* and v^*, which in general, do not satisfy mass continuity. The new depth field, h, for the cycle is obtained by adding a correction, h', to h^*, viz:

$$h = h^* + h' \qquad .(4.14)$$

Since a change in depth at a point produces a change in the velocities near the point, then the final values of the velocities for the cycle, u and v, can similarly be written as:

$$u = u^* + u' \quad ,$$

$$v = v^* + v' \qquad ,(4.15)$$

where, u' and v' are the velocity corrections which need to be calculated.

Simple relationships between the velocity corrections and the depth corrections can be derived from approximate (truncated) forms of the momentum equations. These truncated forms of the momentum equations are obtained by eliminating all the terms on the right-hand side of equation (4.13) except the source term for the depth gradient. These velocity-corrections depth-corrections relationships are given by:

$$v'_n = D^v_n (h'_p - h'_N) \quad ,$$

$$v'_s = D^v_s (h'_S - h'_p) \quad ,$$

$$u'_e = D^u_e (h'_p - h'_E) \quad ,$$

$$u'_w = D^u_w (h'_W - h'_p) \qquad ,(4.16)$$

where the D coefficients are the same as those multiplying the corresponding depth-difference terms in the finite-difference equations used to obtain u^* and v^* earlier (i.e. equations (4.13) with $\emptyset$ standing for u and v in turn).†

The integrated continuity equation over the control volume shown in Figure 4.4, reads:

$$a_n v_n + a_s v_s + a_e u_e + a_w u_w = 0 \qquad ,(4.17)$$

where the a's are the areas of the cell faces containing upstream depths given by equation (4.1).

The h' equation

It is now a simple matter to substitute equations (4.14) and (4.15), with the velocity corrections replaced by depth corrections from equation (4.16), into the continuity equation above (equation 4.17). This yields, after grouping the coefficients, a depth-correction equation having the same form as equation (4.11) and given by:

$$A_p h'_p = A_N h'_N + A_S h'_S + A_E h'_E + A_W h'_W + S_U \qquad ,(4.18)$$

where,

---

† The complete expressions for these terms are of the following form:

$$v'_n = D^v_n (h'_p - h'_N) + \left[\sum_i A^v_i (v_i - v^*_i) \right] / A^v_p$$

where i indicates the summation over the neighbouring velocity locations.

$$A_N = a_n D_n^v - \text{Min}\,(0,\ \delta x\, v_n^*) \quad ,$$

$$A_S = a_s D_s^v - \text{Min}\,(0,\ -\delta x\, v_s^*) \quad ,$$

$$A_E = a_e D_e^u - \text{Min}\,(0,\ \delta y\, u_e^*) \quad ,$$

$$A_W = a_w D_w^u - \text{Min}\,(0,\ -\delta y\, u_w^*) \quad ,(4.19)$$

S_U assumes the significance of a mass source for the cell, resulting from the velocities u^* and v^*, which is to be eliminated.

A_P can be expressed in terms of the other coefficients.

Min (O,Y) denotes the smaller of either O or Y.

The full derivation and contents of all terms in equation (4.18) are given in Appendix B.

General remarks

(a) All coefficients are positive or zero; they are never negative.

(b) The depth correction at point P is linked to the corrections at the neighbouring nodes, namely N,S,E and W, as given by equation (4.18). In order to preserve the implicitness of these linkages, an implicit two-dimensional linear-equation solver is used to solve these equations, as described in Section 4.3.3.

(c) Solution of equation (4.18) for h' values allows the depths and velocities to be corrected via equations (4.14) to (4.16).

(d) In deriving the h' equation, which basically utilizes the continuity conservation equation and acts to reduce the mass source,

no conditions have been placed on whether the flow is subcritical or supercritical. Accordingly, the same equation is used for both flows and both have the same adjustment procedure.

(e) Two notable features are introduced in the formulation of the h' equation, these are:

(i) Upstream depths are used throughout in calculating the mass fluxes across the cell faces. These depths are included in the cell-face areas a_n , a_s , etc. of equations (4.19). For example, a_n is given by $\delta x\ h_P^*$ or $\delta x\ h_N^*$ depending on whether v_n^* is positive or negative. This feature is required to enhance the stability of the numerical scheme and arises from the fact that, for example, an increase in h_p pushes more fluid out of the cell and decreases the inflow and vice versa.

(ii) The h' equation is formulated generally, i.e. the corrections to the depths, which are used in the convection terms (mass fluxes), are taken into account. This arises from the substitution of expressions given by equation (4.14) for all the cell faces into the continuity equation (4.17). This feature is needed to procure convergence for flows in which variation in surface elevation is significant, i.e. as for most supercritical flows.†

(f) The general formulation of the h' equation has led to the following:

(i) The coefficients of the h' equation have extra terms added to the "conventional ones". These are the second terms given on the right-hand side of equations (4.19).

(ii) The coefficients are non-reciprocal, and require extra computer storage.

---

† For a description of a simpler, but restricted treatment, refer to Appendix C.

4.3 SOLUTION OF THE FINITE-DIFFERENCE EQUATIONS

4.3.1 General Concept

The previous section has shown how the partial-differential equations could be approximated by a set of algebraic equations ready to be solved by appropriate algorithms. These are equations (4.11) and (4.18) for the two hydrodynamic variables and the depth-correction equation respectively. The finite-difference equations are still, of course, coupled and non-linear and must be solved by an iterative process.

The non-linearity of the finite-difference equations arises from the fact that the coefficients are functions of the dependent variables themselves. However, the equations can be expressed in a linear form, but momentarily only, by evaluating the coefficients from the flow variables prevailing at the previous iteration and "freezing" their values throughout the current iteration. The final solution is usually obtained after a number of iterations and by re-evaluating the values of these coefficients at the beginning of every iteration using the up-dated values of the dependent variables. Moreover, the method and the frequency of updating the flow variables decide the scheme, i.e. the algorithm employed.

In the present work two different algorithms are used: a point-by-point algorithm for solving the momentum equations and a two-dimensional linear-equation solver for the depth-correction equations. The details of each algorithm are described in the next two sections.

4.3.2 Point-By-Point Algorithm

The two momentum equations for u and v are solved by a point-

by-point Jacobi implicit scheme. The value of ϕ_p , in equation (4.11) where ϕ_p stands for u or v at a centre location P, is equal to a linear expression of "known" quantities given by the right-hand side of the equation. These "known" quatities represent the values of the coefficients surrounding nodal values and surface elevation gradients taken from the previous iteration. After calculating all values of ϕ over the whole domain, they are put in store to replace the old ones.

This scheme is very simple to implement, cheap to compute and, indeed, similar to an explicit procedure. The distinction between this point-by-point implicit and explicit procedures, and alternative procedures (e.g. Gauss-Seidel), are given in, for example, Roache (1976) or Spalding (1980). Carroll (1980) reported a large saving of computer time by employing the point-by-point method as compared, for example, to the ADI (Alternating direction iteration) method. This saving was possible because the ADI scheme requires more operations per iteration and smaller under-relaxation factors to make the overall solution procedure converge.

Finally, it should be mentioned here that the result of this scheme does not depend on the visiting order in which the solution of the various equations is conducted. This is in contrast to the Gauss-Seidel procedure where continuous updating of the variables and coefficients takes place within the iteration.

4.3.3 Two-Dimensional Linear-Equation Solver

One of the simplest schemes, used to solve the momentum equations, was discussed in the previous section. This scheme is adequate because a very good solution is not needed for the hydrodynamic variables

at an early stage in the computation. It is best, for economic reasons and knowing that these velocities do not normally satisfy the continuity equation, to intersperse the solution with a continuity correction rather than to seek to fully satisfy momentum conservation with values that may significantly change in the course of adjustment.

The depth-correction equation is a more difficult and complicated equation to solve, compared to the momentum equations, and this will ultimately call for a stronger and more implicit algorithm.

Spalding (1979) has presented a simplified and straight-forward approach for deriving a family of procedures of strongly-implicit linear-equation solvers. The procedures are developed by choosing the form of the recurrence relation for the following equation:

$$a_p \phi_p = a_N \phi_N + a_S \phi_S + a_E \phi_E + a_W \phi_W + b \qquad ,(4.20)$$

in the present study, the recurrence relation chosen is:

$$\phi_p = N_p \phi_N + E_p \phi_E + B_p \qquad ,(4.21)$$

where,

ϕ_p is linked to ϕ_N and ϕ_E ;

N_p , E_p and B_p are new coefficients to be determined.

Equations for ϕ_S and ϕ_W can be written in the same form as equation (4.21) given by:

$$\phi_S = N_S \phi_p + E_S \phi_{SE} + B_S \qquad ,$$

$$\phi_W = N_W \phi_{NW} + E_W \phi_p + B_W \qquad .(4.22)$$

Substitution of equations (4.22) into (4.20), to eliminate ϕ_S and ϕ_W , gives:

$$\begin{aligned}(a_P - a_S N_S - a_W E_W) \phi_P = {} & a_N \phi_N + a_E \phi_E + b \\ & + a_S (E_S \phi_{SE} + B_S) \\ & + a_W (N_W \phi_{NW} + B_W) \end{aligned} \quad .(4.23)$$

Comparison of equation (4.23) with equation (4.21) yields recurrence relations for N_P , E_P and B_P as:

$$D_P = a_P - a_S N_S - a_W E_W \quad ,$$

$$N_P = a_N / D_P \quad ,$$

$$E_P = a_E / D_P \quad \text{and}$$

$$B_P = \left[b + a_S (E_S \phi_{SE} + B_S) + a_W (N_W \phi_{NW} + B_W) \right] / D_P \quad .(4.24)$$

The computational procedure for the depth-correction equations is therefore conducted as follows:

(i) Compute D_P , N_P and E_P , starting at the bottom-left-hand corner of the finite-difference grid and stepping node-by-node across the whole field, and store in two-dimensional arrays.

(ii) Compute B_P using the in-store values of ϕ_{SE} and ϕ_{NW} .

(iii) Compute ϕ_p , equation (4.21), starting at the top-right-hand corner of the grid and replace the old values in store.

(iv) Repeat steps (ii) and (iii) until convergence.

Remarks

- The above steps form part of the general operations performed every iteration, as described in the next section.
- In all cases considered in the present study, steps (ii) and (iii) are repeated no more than three times per iteration. It was found that a number greater than three, would almost always give faster convergence but, of course, be more expensive.
- The solver described above represents Spalding's "basic" solver.

4.3.4 Summary of the Solution Steps

The main steps of the present computational procedure can now be summarized as follows:

(i) Guess initial values of the variables in the field. This is only applicable to the first iteration (see next section for some relevant details); thereafter, the values in store, which are continually updated, are employed to start any new iteration.

(ii) Compute values of u^* over the whole field. This is achieved by solving the finite-difference form of the u-momentum equation, equation (4.11), using the point-by-point method and employing the existing depth field, i.e. h^*.

(iii) Compute values of v^* as in (ii) above.

(iv) Compute values of h' over the whole field. The continuity errors produced by u^* and v^* obtained from steps (ii) and (iii) are employed in equation (4.18) to calculate the depth-corrections by a two-dimensional linear-equation solver.

(v) Correct the depth and velocity fields. This is done by using h' values obtained from step (iv) above and the relations given by equations (4.14) to (4.16) to eliminate the continuity errors in all control volumes.

(vi) Repeat steps (ii) to (v) until convergence, i.e. until the errors in each equation reduce to practically zero.

4.4 AUXILIARY INFORMATION

4.4.1 Boundary Conditions

The different boundary conditions that are required to specify supercritical and subcritical flows are discussed in Section 3.3.3. An appropriate method of implementing these, in the finite-difference procedure, is given below along with the source term linearisation discussed in Section 4.4.3.

The values of the dependent variables must be specified at the boundaries before the set of the finite-difference equations can be solved. These boundary conditions, which determine the uniqueness of the solution for a given flow situation, are usually of two types:

(i) The value of ϕ is prescribed at the boundary. This is known to be the most stable of boundary conditions.

(ii) The value of ϕ on the boundary is deduced from the known gradient of ϕ at the boundary.

The incorporation of either type of boundary condition into the calculation procedure is easy, and achieved by modifying the coefficients and the source terms. For example, at stationary impervious walls, all velocities are set to zero. The depth gradients normal to walls are also set to zero. At symmetry planes, the velocity normal to the boundary and all other variable gradients are set to zero. At free-stream boundaries, as well as at inlet planes (for supercritical flows), the flow variables are prescribed. At the exit of the calculation domain, an additional boundary condition is needed for the depth. It is usually assumed that the exit depth is uniform, otherwise experimental values are specified. For supercritical conditions at the outlet boundary, these fixed values of depth do not have any influence on the flow upstream of this boundary.

4.4.2 Initial Conditions

The initial fields of velocities and depth must be specified before the calculation procedure can start. These conditions are highly problem dependent and will be discussed for every flow situation considered. It suffices to say here that using a good guess of the initial fields to start the solution with, based on experience and an insight to the flow situation, is advantageous as far as the stability, speed of convergence and hence economy are concerned. Their implementation is a straightforward task and only require filling the field variable arrays with the appropriate initial values.

4.4.3 Treatment of Source Terms

The phrase "source terms" is used to represent all the terms in the general ϕ-equation (3.18), apart from the convection terms and diffusion terms if present. This treatment enables the same computer code to be used for a wide variety of cases, with only the "source terms" needing modification. These, in the general case, may represent bed and side-wall friction, wind stresses, Coriolis forces, body forces, etc.

The source term, S^{ϕ}, is linearised in a similar manner to Patankar and Spalding (1972). This has been discussed briefly and given by equation (4.10). The linearisation permits the source term to depend on both current and previous iteration values of the variable concerned. The level of implicitness is thereby increased, leading to enhanced stability.

For the equation system solved in the present study (equations (3.15) to (3.17)), the source terms for the u- and v-momentum equations are shown in Table 4.1 below; they are composed of the depth gradients and the channel-surface stresses. The source terms for the depth-correction equation consist of the continuity errors which are to be eliminated as discussed in Section 4.2.4.

ϕ	S_U^{ϕ}	S_P^{ϕ}
u	$-gh\,\frac{\partial h}{\partial x}$	$-C_f\,(\overline{u}^2 + \overline{v}^2)^{\frac{1}{2}}$
v	$-gh\,\frac{\partial h}{\partial y}$	$-C_f\,(\overline{u}^2 + \overline{v}^2)^{\frac{1}{2}}$

TABLE 4.1 : LINEARISED-SOURCE TERMS FOR THE DEPTH-AVERAGED SHALLOW-WATER FLOWS

4.4.4 Convergence of the Procedure

A measure of how well the finite-difference equations are satisfied is determined by the degree of convergence of the numerical process. The convergence is monitored through the use of residuals. A residual of a variable ϕ at a node P, denoted by R_p , is defined as:

$$R_p = \phi_p \; A_p^{\phi} - \sum_i A_i^{\phi} \; \phi_i - S_U^{\phi} \qquad ,(4.24)$$

where ϕ_p is the value at the previous iteration. This is to be compared to equation (4.13).

To facilitate monitoring, the residuals are suitably normalised to the inlet momentum and flow rate for the momentum and depth-correction equations respectively. For a given grid, a solution that produces sufficiently small residuals everywhere in the flow field, for all the variables solved, is regarded as a converged one provided that the values of the dependent variables do not change by more than, say, 0.01 % during successive iterations.

The table of computational details, provided for each test case solved, gives the values required for a converged solution such as: the number of iterations performed, the sum of the absolute values of the residuals over the whole field ($\sum|R|$), the maximum depth correction (Max. h') and other relevant information.

4.4.5 Stability of the Procedure

The iterative procedure presented in this chapter, as indeed with all other procedures, does not always reduce the errors, remaining

in the equations, with each iteration. When the errors continue to increase or fluctuate, the solution procedure is unstable and may diverge. The instabilities are known to be caused by many factors, see for example, Runchal (1971) and Roache (1976). Such factors are discussed below.

Causes of instability

(i) Truncation errors. These are induced into the numerical solution by the finite-difference approximations. They will also affect the accuracy of the procedure, as discussed in the next section, and depend mainly on the grid size; if they grow fast enough they may lead to an unstable solution. Since the depth-correction equation is derived from truncated momentum equations, the correction may not promote convergence if the truncated terms are more important than the depth-gradient term. This form of truncation does not affect the accuracy of the procedure since the depth-corrections tend to zero as convergence is approached.

(ii) Perturbations. Initial conditions of the flow variables are needed to start the solution. Since these differ from the final solution, perturbations are likely to occur and, when large, instability may take place. Obviously, the closer the initial guess is to the solution the smaller the effect of these perturbations is on the stability and convergence speed.

(iii) Boundary conditions. The boundary conditions in which the value of the dependent variables are specified are known to be the most stable of all boundary conditions. Those in which the normal gradients of the variables are specified at the boundary

are less so. However, the majority of flow situations contain a mixture of these conditions. The instability introduced at the boundaries may arise due to, for example, a large difference between the depth specified at the inlet boundary and that specified at another boundary.

(iv) Coupling and non-linearity of the equations. This may give rise to large changes in the values of the finite-difference coefficients between successive iterations and may lead to instability and divergence.

Remedies to procure convergence

(i) Good initial guess of the flow variables based on experience and insight to the flow situation. This is a remedy for cause (ii) above.

(ii) Under-relaxing the effect of the boundary conditions on the solution. This is a remedy for cause (iii) above. The depth at the boundary is allowed to change to its final value, gradually, at every iteration or by moderate increments at the end of a number of iterations. The advantage of this technique is not only to enhance convergence but also to study the solution at, say, different inlet to outlet depth ratios or different free-stream Froude numbers, etc.

(iii) Under-relaxing the changes in flow variables. This is a satisfactory remedy for all causes of instability listed above and will almost always ensure convergence provided, of course, (i) and (ii) are satisfied, consistency in the formulation of the solution procedure, compatibility of boundary conditions, etc.

Momentum relaxation

The solution of the difference equations is taken as a linear combination of values before and after a given iteration, as follows:

$$\phi_{new} = (RELAX\phi) \phi^{*} + (1 - RELAX\phi) \phi_{old} \qquad ,(4.25)$$

where ϕ stands for u or v and RELAXϕ is the relaxation factor for u or v. With RELAXϕ < 1, the variation of ϕ between successive iterations is reduced and this improves the stability.

Relaxation of the depth-correction

The depth-correction values calculated for many of the flow situations are found to be too large to add directly to the in-store depths. The corrections are therefore under-relaxed before they are added to those prevailing in the field. This practice ensures that the solution is approached smoothly and is represented by:

$$h_{new} = h^{*} + (RELAXH) h' \qquad ,(4.26)$$

in which RELAXH is the relaxation factor for the depth-correction and takes a value between 0.0 and 1.0.

Remarks

(i) Equations (4.25) and (4.26) represent the operations often needed to under-relax the variations in the dependent variable values.

These operations are carried out immediately after the particular field values are calculated. This implies:

(a) The u's and v's, used in calculating the continuity errors for the h' equation sources and parts of the coefficients, are the relaxed ones.

(b) The corrections made to the velocities are those corresponding to the relaxed depth corrections.

(ii) The depth field is regarded and actually separated into:

(a) "Depth field" (h), with values used to calculate the mass fluxes.

(b) "Pressure field" (p), with values used to calculate the driving force in the momentum equations.

The two fields are analogous to the density and pressure fields respectively in compressible-gas dynamics.

The "pressure field" is obtained from the "depth field" as follows:

$$p_{new} = (RELAXP) h_{new} + (1 - RELAXP) p_{old} \qquad ,(4.27)$$

in which RELAXP is the relaxation factor for the "pressure" and takes a value between 0.0 and 1.0, and h_{new} is the value obtained from equation (4.26).

With RELAXP = 1, the depth and pressure fields will contain identical values; but when RELAXP $<$ 1, i.e. applying extra relaxation to the pressure variation as derived from the already relaxed depth variation, the two fields will contain different values during the solution process. As the solution progresses the pressure field starts to "catch up" with the depth field as

dictated by equations (4.27) and both will be identical, as they should be, when a converged solution is obtained.

(iii) See Appendix (C) for a variant to such a procedure which uses a simpler form of h' equation and different approach to obtaining the pressure and depth fields.

(iv) Negative depths, like negative densities, are physically unrealistic and give rise to negative areas and coefficients in the finite-difference equations. They may occur during the solution process, and lead to divergence, due to large corrections, especially in very shallow regions of the flow and when the relaxation factors are not well chosen. These depths are put to a very small but positive value whenever they appear so as the solution may continue and recover.

4.4.6 Influence of Grid Size

The solutions obtained by finite-difference methods are grid dependent except for very fine grids. It is, therefore, important to test that the solution obtained is independent of the grid size. Increasing the number of grid nodes improves the accuracy, but at the same time increases the computation time. Also convergence will be slowed down because the errors will be distributed over a greater number of nodes. The task is, therefore, to establish a grid with the smallest possible number of nodes for which the finite-difference solutions are essentially those of the original differential equations. This is achieved, in part, by obtaining solutions with an increasing number of grid nodes until a stage is reached where the solution exhibits negligible change with further increase in the number of grid

nodes. The solution is then regarded to be grid independent. Once this is achieved, the accuracy and physical realism of the whole scheme is to be tested by application to a variety of problems in which analytical solutions or experimental data are available. The grid size influence and grid distribution will be discussed when each problem is considered in turn.

4.5 SUMMARY OF MAIN FEATURES OF THE PROCEDURE

The details of the solution procedure for the two-dimensional shallow-water flows, have been explained. The main features of the procedure are now summarized with particular emphasis on its applicability and limitations. These are:

(i) A general numerical procedure based on a finite-difference implicit scheme.

(ii) Use of depth and velocities as the main hydrodynamic variables.

(iii) Derivation of finite-difference equations by integrating the differential equations over finite control volumes.

(iv) Use of a staggered grid which can be non-uniformly spaced.

(v) The coefficients of the finite-difference equations are formulated using an upwind-difference scheme.

(vi) Use of a point-by-point Jacobi method to solve the momentum equations in turn over the whole field.

(vii) The pressure-correction technique of Patankar and Spalding is utilized to determine the depth and velocity fields that satisfy the conservation laws.

(viii) The depth-correction equations are solved using the basic two-dimensional linear-equation solver of Spalding.

(ix) Use of upstream depths in evaluating the mass fluxes across the cell faces.

(x) Account of the depth variations in formulating the depth-correction equations.

(xi) Provision for separating the "pressure" and "depth" fields and relaxing their changes differently if required.

(xii) As far as the flow type is concerned, i.e. whether continuous (wholly supercritical or wholly subcritical) or discontinuous (flow with hydraulic jumps), the following features are pertinent to the numerical scheme:

(a) The same solution procedure is applicable to all types of flow; no limitations have been put on Froude number values.

(b) The depth-correction equations, and the resulting adjustments made to the depths and velocities, are the same for all types of flow. Neither flow-type identification nor different adjustment procedures are then needed to obtain a solution. This demonstrates the generality of the model as compared to other models which can handle only one flow regime.

(c) The scheme is of the "shock-capturing" type, a phrase borrowed from compressible-gas dynamics. This means the presence and location of a hydraulic jump are an outcome of the solution.

(d) The energy losses across hydraulic jumps are accounted for implicitly by solving the continuity and momentum equations alone. Physically, this energy is dissipated as heat but has a negligible effect on changing the water density. Once a

solution is obtained, the energy losses may be estimated by making use of the energy equation.

(e) The scheme, being two-dimensional and depth-averaged, is limited in the sense that it does not consider details of flow inside the hydraulic jumps or the shape and length of jumps. This is inevitable, however, and such limitations of the numerical model are often of little impotrance especially when the stretch of the channel, as is often the case, is much larger than the length of the jump.

(f) The physical length of a hydraulic jump is always finite; but as far as the numerical model is concerned, the jump is regarded as a sharp transition. However, because of numerical (false) diffusion, as with any other numerical solution procedure, this sharp transition will be smeared over a few grid nodes. In the present study, the smearing effect is substantially reduced by refining the grid system used.

4.6 CLOSURE

In this chapter the derivation of the finite-difference form of the depth-averaged partial-differential equations governing the flow of shallow water and their method of solution have been presented. Remarks on the capabilities and limitations of the numerical procedure have also been given. This completes the mathematical formulation of the problem.

As has been indicated, the solution procedure is general and flexible, and may be applied to calculate various flow situations governed by different boundary conditions. This is illustrated in Chapters 6, 7 and 8, where the procedure is applied to predict, respectively, continuous flows, flows with hydraulic jumps,and compressible-gas flows (with shock waves) using the hydraulic analogy.

C H A P T E R 5

EXPERIMENTAL WORK

5.1 INTRODUCTION

This chapter describes the experimental investigation that was conducted in the Hydraulics Laboratory of the Civil Engineering Department of Imperial College. The study provided data to supplement existing experimental information and to further validate the numerical solution procedure described in Chapter 4. Although many experimental studies of supercritical open-channel flows are reported in the literature, these are either insufficiently detailed or without adequate boundary-condition information. Besides these, little information exists regarding extensive surface-profile measurements or accurate recording of hydraulic-jump locations in both one- and two-dimensional flows.

This study examines the supercritical flow of water in straight, rectangular and horizontal open channels for one- and two-dimensional flow situations. The two-dimensional flow situation simulates the merging of two streams separated at the inlet by a thick wall. Hydraulic jumps were introduced into the test sections by raising the tailwater depth. Measurements of the surface elevation were taken, together with the recording of the hydraulic-jump locations, if present. The flow parameters varied were the inlet Froude number and the tailwater depth. The range of Froude numbers investigated were 3.88 to 4.68 and 2.04 to 3.71 for the one- and two-dimensional flows respectively; the flow Reynolds numbers (based on the inlet depth) were of the order of 2×10^4 and 8×10^4 respectively.

In this chapter, and for each of the one- and two-dimensional

cases, brief descriptions of the experimental flume and procedure are provided. The experimental results are then presented, with some of the results being further analysed when compared with the numerical solutions in Chapter 7. The chapter closes with a brief summary.

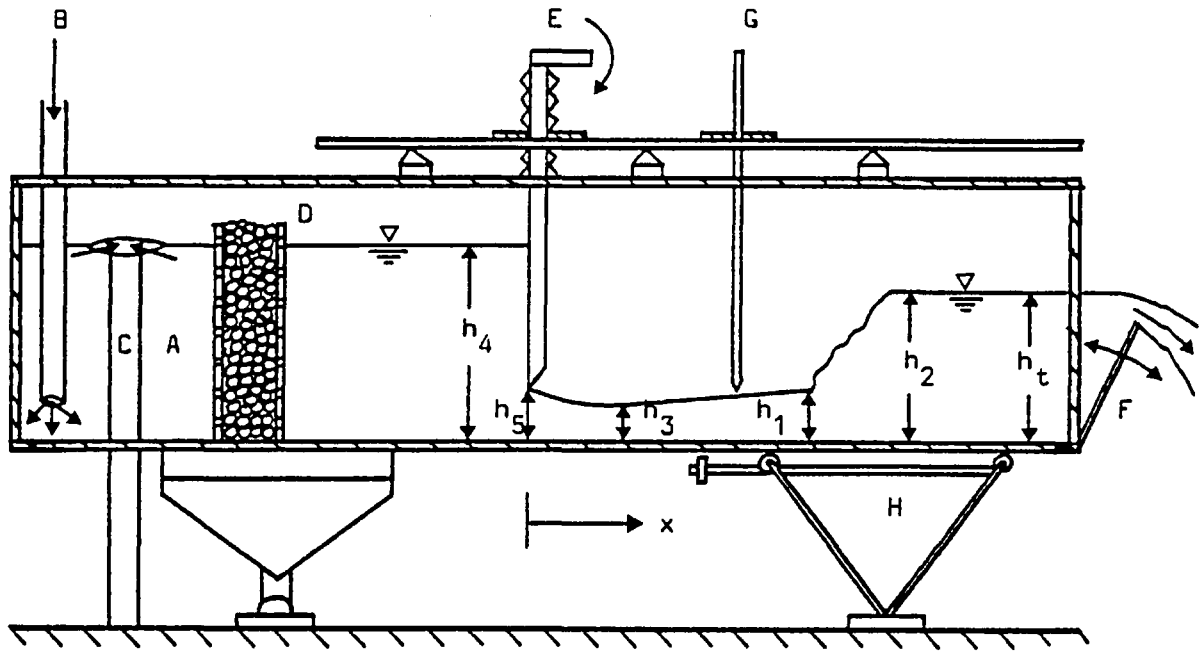
5.2 ONE-DIMENSIONAL MEASUREMENTS

5.2.1 General Aspects

The main objective of this study was to obtain measurements of the surface profiles for one-dimensional flows in a straight, rectangular and horizontal channel at different inlet Froude numbers (Fr) and tailwater depths (h_t); of primary importance was the accurate recording of the hydraulic-jump locations as influenced by a change in Fr or h_t.

5.2.2 Experimental Flume

A schematic diagram of the experimental flume employed in the present investigation is shown in Figure 5.1. The flume, of prismatic rectangular cross-section, was 4 m long, 0.104 m wide and 0.4 m deep; the test section (the distance from the sluice gate to the outlet boundary) was 2.7 m long. The wooden bottom of the flume was kept horizontal; the two vertical side walls were made of glass. Water was fed from a large reservoir on the roof of the laboratory building to the supply basin (A) by a vertical pipe (B) situated at the very beginning of the flume. The basin was provided with a regulated overflow (C) to control the upstream water head (h_4) and two vertical perforated plates (D) with pebbles in between to ensure the uniformity



A Supply basin (settling tank)

B Inlet pipe

C Regulated overflow

D Baffle

E Adjustable sluice gate

F Adjustable flap

G Depth gauge

H Tilting mechanism

FIGURE 5.1 : SCHEMATIC DIAGRAM (NOT TO SCALE) OF EXPERIMENTAL FLUME FOR 1D FLOWS

of the flow entering the channel. The supercritical flow necessary for the formation of a jump, was produced by an adjustable sluice (E); the depth below it being h_5 . The tailwater depth (h_t) was regulated, and thus the location of the jump was controlled by means of an adjustable flap (F) at the end of the flume. The water flowing through the system could be collected in a measuring tank from which it was returned to the laboratory circulating system. Two rails were mounted on top of the channel side walls and parallel to its bed. A depth gauge (G), reading to $\pm$ 0.01 cm, was free to move vertically through a turning knob and along the rails by a travelling carriage.

5.2.3 Experimental Procedure

The main objective of the study is stated in Section 5.2.1. The depth gauge was used to measure the thickness of the water layer in the test section.

Velocity measurements were not made, though it might have been desirable to do so, due to the shallowness of the flow and because the use of conventional measuring instruments, e.g. a pitot-static probe or a mini-current meter, would interfere with the flow itself. The instrument would act as a disturbance to the supercritical flow, thereby generating cross waves, and the measured velocity would not be the true velocity at that point in the absence of the instrument. The use of a device such as a Laser-Doppler anemometer would have been ideal, but this was not readily available.

Before taking the final measurements, some preliminary runs were made which demonstrated the effects of varying both upstream and downstream controls on the hydraulic-jump location. Precautions were also taken to level the channel with a spirit level and to seal the

small clearances, between the sluice gate and the side walls, with plasticine to prevent any leakage.

The flow rate was obtained by measuring the volumetric discharge in the measuring tank over a sufficiently long time interval.

The experimental procedure for each run made is given by the following steps:

(i) The depth below the sluice gate (h_5) was set to the desired value.

(ii) The water supply was turned on and the regulated overflow (C) was adjusted to give the desired upstream water head (h_4).

(iii) The flap (F) at the end of the flume was then adjusted to introduce a hydraulic jump in the test section.

(iv) Enough time was given for the flow to settle down at this stage. Then finer adjustments could be made to h_4 and/or h_t if required; if so, the system was left for a few minutes to settle down.

(v) The flow rate (q) was then measured by collecting the flow in the measuring tank for a period of 2 minutes.

(vi) The depth of flow was then measured with the depth gauge, at several intervals, along the channel and up to 2.4 m from the sluice.

(vii) Apart from the measurements made at (vi) above, and for every run, the depths h_1 , h_2 and h_t (Figure 5.1) were measured along with the two distances x_1 and x_2 ; h_1 and h_2 being the depths of flow just before and after the hydraulic jump respectively (these are termed the "conjugate" or "sequent" depths) and x_1 and x_2 being the distances from the sluice gate to the

toe and end of jump respectively.

(viii) At the end of the run, the flow rate was measured again.

5.2.4 Experimental Accuracy

Experimental inaccuracies could be attributed to the following factors:

(i) Error in measuring the flow rate. This was found to be very small; the discharge was measured at the beginning and at the end of each run with the maximum discrepancy found to be less than 0.4 % .

(ii) Error in measuring the depth. This was found, on reproducibility basis, to be less than $\pm$ 0.3 mm. Thus the maximum error was less than 2 % of the actual depth at a point.

(iii) Small oscillations of the position of the toe of the jump was observed. This was of the order of $\pm$ 4 cm.

(iv) Whereas the beginning of the jump was well defined, the end of it was much less clear. In the present study, the end of the jump was taken to be at the location where the depth, h_2 , had reached its maximum value. The difficulty lay in the fact that the surface in this region was undergoing continuous oscillation.

5.2.5 Experimental Results

Two sets of experimental measurements were made. Each set consisted of five runs, the depth below the sluice gate (h_5) was kept constant. Due to the presence of the so called "vena contracta",

at a short distance from the sluice, h_5 would not give a true representation of the inlet flow depth to the test section. A station was therefore chosen at 15 cm from the sluice (well away from the vena contracta) at which measurements were started. Variables, at this station, have been given subscript 3.

In Runs 1.1 to 1.5 (Set 1) the upstream depth (h_4) was kept unaltered. Thus, the investigations were carried out at a constant discharge (q) and constant inlet Froude number; the only parameter varied was the tailwater depth (h_t).

In Runs 2.1 to 2.5 (Set 2) the tailwater depth (h_t) was kept unaltered. The only parameter varied was the upstream depth (h_4). Thus, the investigations were carried out at a variable discharge, i.e. for variable inlet Froude number.

The above test conditions are summarized in Table 5.1. Figure 5.2 shows the measured surface profiles for all runs. It is clearly seen how h_t or q influences the location of the hydraulic jump. Analysis and discussion of the results are postponed till Chapter 7 where they are presented and compared with the numerical solutions. These results are given in tabular form in Appendix D.

	Upstream depth (h_4)	Depth below sluice (h_5)	$qx10^2$ (m^2/s)	Depth at x= 15 cm (h_3)	Fr at x= 15 cm	Tailwater depth (h_t)
Set 1 Runs :						
1.1	11.8	2.0	1.823	1.31	3.88	4.46
1.2	11.8	2.0	1.823	1.31	3.88	4.64
1.3	11.8	2.0	1.823	1.31	3.88	5.34
1.4	11.8	2.0	1.823	1.31	3.88	5.60
1.5	11.8	2.0	1.823	1.31	3.88	5.90
Set 2 Runs :						
2.1	16.6	2.0	2.196	1.31	4.68	5.90
2.2	14.7	2.0	2.046	1.31	4.36	5.90
2.3	13.5	2.0	1.951	1.31	4.16	5.90
2.4	12.7	2.0	1.893	1.31	4.03	5.90
2.5	11.8	2.0	1.823	1.31	3.88	5.90

Table 5.1 : Test conditions for 1D flow experiments

(All depths are in cms)

Set 1 : Constant discharge and inlet Froude number; variable tailwater depth.

Set 2 : Constant tailwater depth; variable discharge and inlet Froude number.

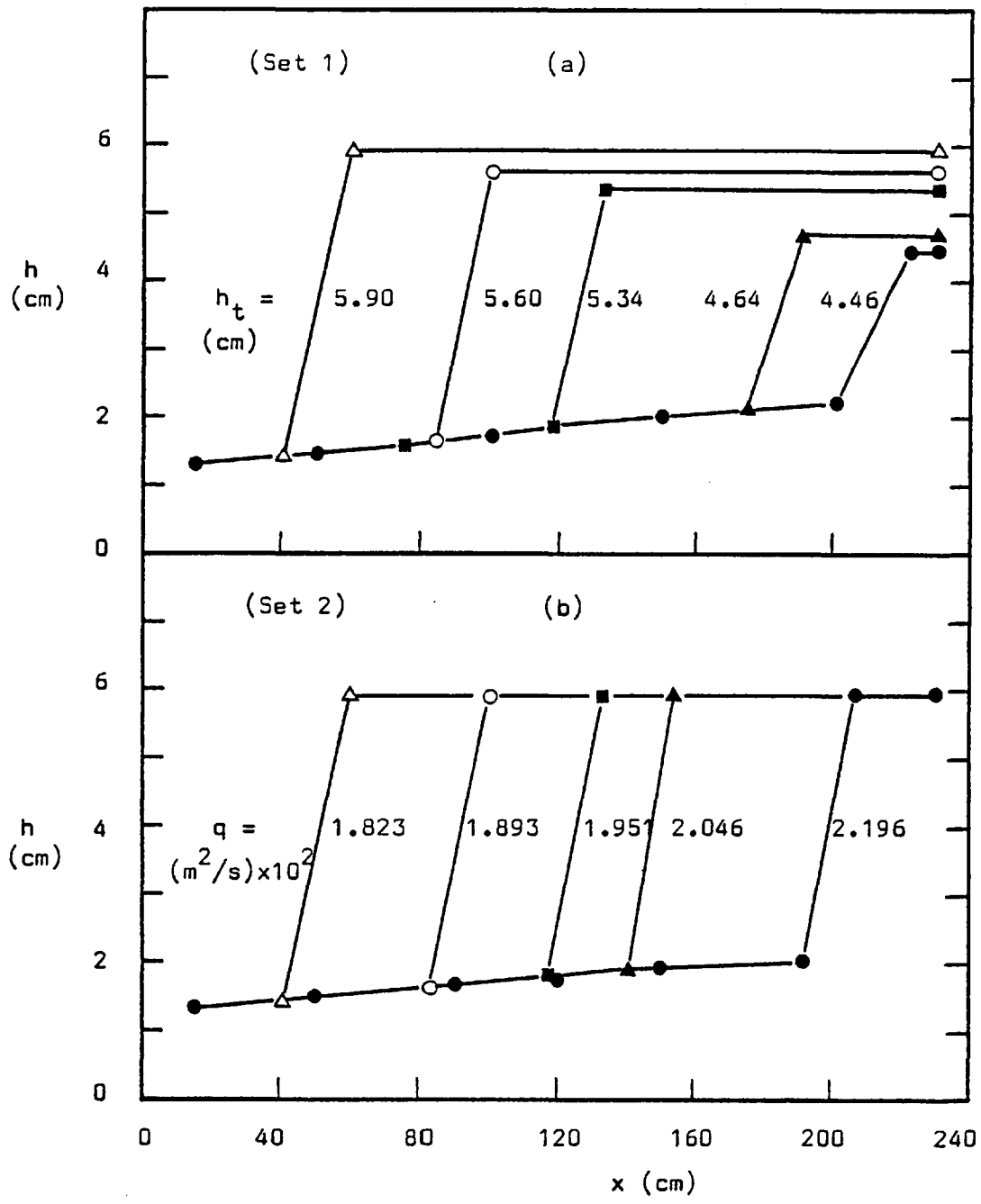


FIGURE 5.2 : EXPERIMENTAL SURFACE PROFILES OF 1D FLOWS

(a) Variable tailwater depth (h_t); constant q
(q = 1.823 E-2 m^2/s, h_3 = 1.31 cm, Fr_3 = 3.88)

(b) Variable discharge (q); constant h_t
(h_t = 5.9 cm, h_3 = 1.31 cm)

(h_3 is depth at 15 cm from sluice gate)

5.3 TWO-DIMENSIONAL MEASUREMENTS

5.3.1 General Aspects

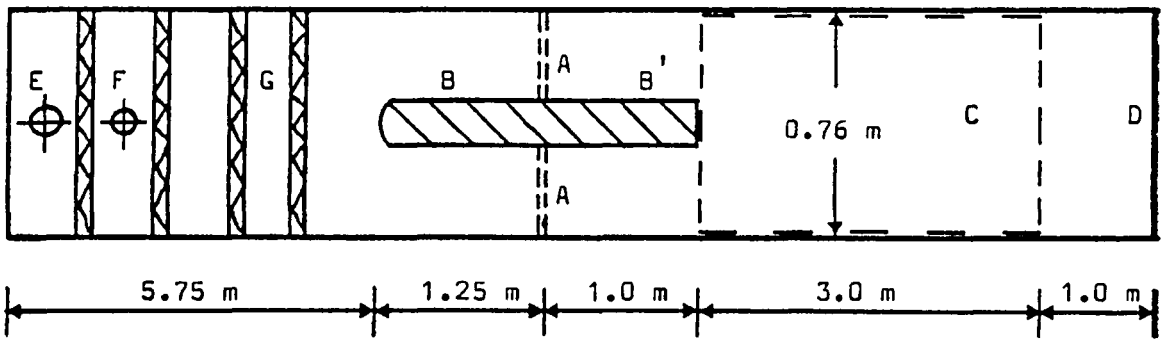
The main objectives of this study were to obtain depth measurements and to record hydraulic-jump locations for two-dimensional flows in a straight, rectangular and horizontal channel at different inlet Froude number and tailwater depths (h_t). The flow situation simulated the merging of two parallel supercritical streams flowing in the same direction and separated at the inlet by a thick wall. Conditions at the exit boundary could be either supercritical or subcritical. The latter conditions were obtained by imposing higher tailwater depths. A hydraulic jump was therefore introduced into the test section of the channel, the location of which depended on both the inlet and outlet conditions. For fixed inlet conditions, an increase in h_t would move the jump location upstream.

5.3.2 Experimental Flume

A schematic diagram of the experimental flume employed in the present investigation is shown in Figure 5.3 for the overall and the test-section plan views. These are augmented by the photograph given in Figure 5.4 which shows the flume in operation.

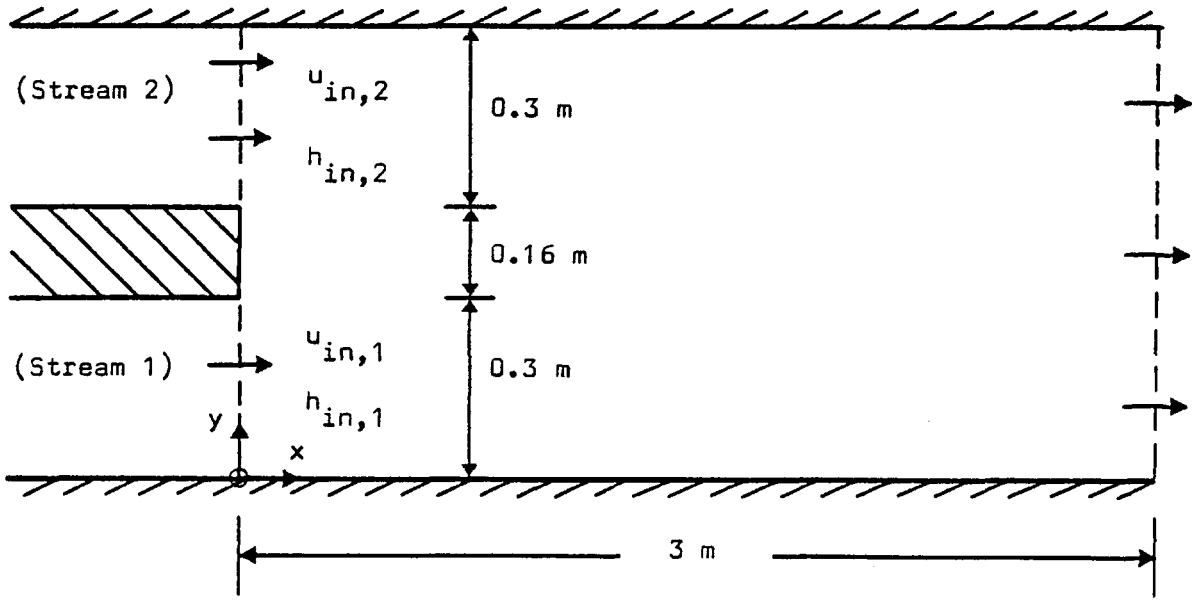
The metal flume, of prismatic rectangular cross-section, was 12.5 m long, 0.76 m wide and 0.45 m deep. This consisted of the following main arrangements:

(i) The settling chamber; this supplied the test section with a uniform-head flow. A number of cardboard honeycomb sheets (G), 0.1 m thick, were fitted across this chamber to smooth the flow.



A Sluice gates
B Separating wall
C Test section
D Tainter gate
E Large pipe inlet
F Small pipe inlet
G Baffles

(a) Overall plan view



(b) Test-section plan view

FIGURE 5.3 : SCHEMATIC DIAGRAM (NOT TO SCALE) OF EXPERIMENTAL FLUME FOR 2D FLOWS

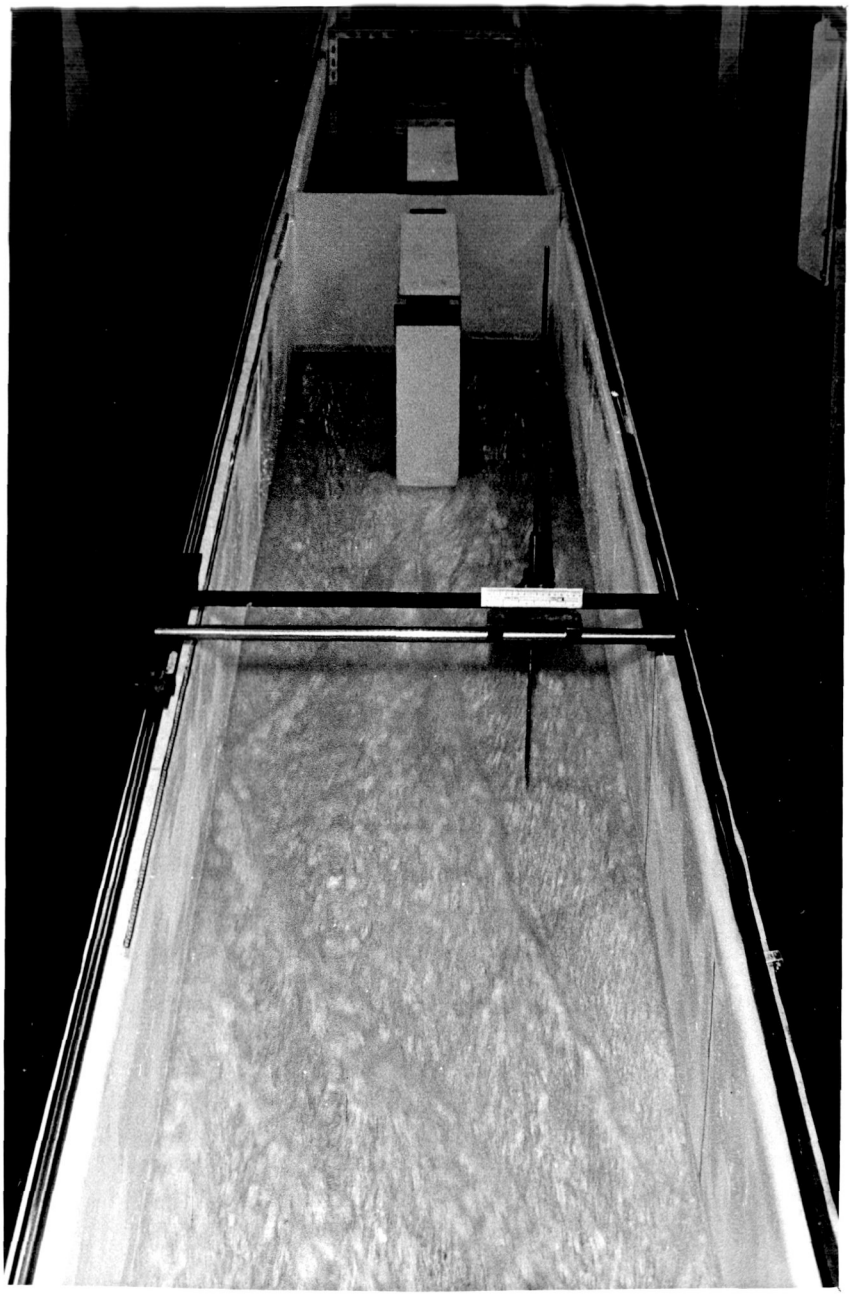


FIGURE 5.4 : OVERALL VIEW OF THE EXPERIMENTAL FLUME

(ii) Inlet pipes; the water was supplied to the flume at constant pressure from a large capacity tank, situated on the roof of the laboratory building, by two inlet pipes (E and F). Due to high flow rate of water needed to run the experiment, e.g. up to 55 Kg/Sec (Litre/Sec), the water was supplied by two vertical pipes of 10 cm and 20 cm inside diameters situated at the very beginning of the settling chamber. After passing through the flume, the water was then collected in the laboratory sump and pumped up to the main tank.

(iii) The sluice gate arrangement; this was a simple and economic wooden structure fitted inside the metal flume at a location more than halfway down the flume (7 m downstream). This mainly consisted of a wooden board (A), 18 mm thick and 0.76 m wide, which extended over the whole channel depth across its width. Two openings, each of 0.30 m wide, were made at the bottom corners of this board, 4 cm and 8 cm deep. The bottom of these opertures was tapered at 60° to the horizontal. A wall (B), 0.16 m thick and 1.25 m long, was fitted along the centre plane of the flume and attached at right angles to the board on its upstream side. A similar wall (B), 0.16 m thick and 1 m long, was fitted in the same way but on the downstream side of the board; this wall separated the two streams entering from the two openings and extended to 1 m downstream, to a station at which the test section started. All the joints were carefully sealed with plasticine.

(iv) Test section (C); the measurements were made over a 3 m stretch of the flume, starting at the section where the separating wall terminated and ending at 1 m upstream of the Tainter gate. The

width of the test section was, of course, the same as the inside width of the flume (0.76 m).

(v) Tainter gate (D); this was situated near the end of the flume and used to control, if desired, the tailwater level.

(vi) Outlet chamber; this was situated at the end of the flume (0.5 m downstream of the Tainter gate), 0.65 m long, 0.85 m wide and 0.65 m deep, from which the water was discharged into the sump of the laboratory through 0.3 m diameter pipe and then pumped up to the main tank.

Traversing mechanism

This consisted of two horizontal and parallel steel bars, attached to two steel blocks at the ends. These blocks could slide on two parallel rails mounted along the side walls of the channel, producing the longitudinal traverse (in the x-direction). The depth gauge, which provided movement in the vertical direction (z-direction) through a turning knob, could be moved by a carrier to provide the lateral traverse (y-direction).

5.3.3 Preparation and Setting-up Procedure

Due to the large flow rates used, all parts, fitted inside the flume, were securely fastened using wedges that were forced between the sluice gate arrangement and the channel side walls. The small clearances left, were carefully sealed with plasticine. All joints of the separating walls with the sluice, and indeed with the channel bed, were also sealed. Heavy weights were put on top of the separating walls, after they had been correctly aligned, to prevent any movement

due to the different pressures on their sides.

The flume had a tilting mechanism, operated both manually and electrically, which allowed adjustments in the slope of the channel. However, all the experiments were carried out with the bottom of the channel in a horizontal position. This was checked by a spirit level and also by trapping a layer of water and measuring its depth at different points for uniform thickness.

In running the flume, the cardboard honeycomb sheets fitted across the channel gave a uniform flow just upstream of the sluice gates. Also, a sheet of polystyrine was allowed to float on the water surface in the settling chamber to help to make the water surface smoother still. The upstream side of the separating wall facing the incoming main stream was rounded to provide a smoother flow for each sluice.

5.3.4 Flow Measurements

The depths of the flow inside the test section were measured using a point gauge, measuring to 0.1 mm. The heads of water upstream of the two sluice gates ($h_{0,1}$ and $h_{0,2}$) were measured by measuring tapes stuck vertically on the inside of the channel walls. The tail-water depth (h_t) was also measured, when the Tainter gate was used to control the downstream flow to induce a hydraulic jump in the flow. The location of the latter was recorded by measuring tapes, one along the channel with x=0 at the start of the test section (i.e. where the separating wall terminated) and the other tape across the channel and stuck on the traversing carriage with y=0 at the inside of the shallower stream (Stream 1).

Velocity measurements were not made, for the same reasons given in Section 5.2.3.

The coefficients of discharge (C_d) for each sluice and for each run were determined by measuring the height of the opening (d), the headwater depth (h_0), and using experimental charts for C_d . The flow rate per unit width (q) under each sluice gate was obtained via:

$$q = C_d \, d \, (2 \, g \, h_0)^{\frac{1}{2}} \qquad .(5.1)$$

Henry (1950) determined experimentally the discharge characteristics of a sharp-edged sluice gate for both a free and a submerged outflow of the gate, in which he constructed curves of C_d versus h_0 / d . The results were verified by an approximate theoretical approach using the continuity and energy equations utilizing the assumptions of hydrostatic pressure distribution throughout the flow, uniform velocity distribution in the vertical and no energy loss between the section just upstream of the gate and the vena contracra. However, even with these assumptions in the theoretical approach the agreement in determining C_d was remarkably good as compared to the experimental results; the maximum discrepancy for the range of h_0 / d used in the present work was less than 4 % .

5.3.5 Experimental Procedure

The main objectives of the study are given in Section 5.3.1. The experimental flume and flow measurements are described in the subsequent sections. Preliminary runs were made first, before taking the final measurements, which demonstrated the effects of varying

both upstream and downstream conditions on the flow behaviour and jump location. The test procedure employed to conduct the experiments for each run is outlined below.

(i) The channel bed was first checked for zero slope. The opening below the Tainter gate was made large, so that the gate would not interfere with the flow at this early stage.

(ii) The water supply from the two inlet pipes was turned on gradually and adjusted to give, roughly, the desired upstream water heads ($h_{0,1}$ and $h_{0,2}$ for Streams 1 and 2 respectively).

(iii) The system was left to run for a few minutes for the flow to settle down. Meanwhile, constant observations and finer adjustment to the flow were made to bring h_0 to the desired values. The system was then left for a few minutes more to settle down completely.

(iv) The elevation of the water surface was then measured with the point gauge, at predetermined intervals (at 5 to 20 cm intervals) in the longitudinal direction and up to 3 m downstream from the inlet of the test section, and at 2 to 4 cm intervals in the lateral direction.

(v) For the runs with hydraulic jumps, the Tainter gate was lowered down gradually and fixed momentarily in position. During the process, the tailwater depth (h_t) was seen to increase more and more till a hydraulic jump was formed. With a slight increase in h_t (by lowering the Tainter gate), the jump was forced to travel upstream and form at the downstream end of the test section. Adequate time (a few minutes) was given for the flow to settle down and then the location of the jump was recorded; h_t was measured with the point gauge at 1 m upstream

of the Tainter gate. For the same upstream conditions, the process was repeated for different values of h_t . Measurements and the run were terminated when the hydraulic jump reached about 0.4 m downstream of the inlet to the test section. Any further increase in h_t would drown the inlets of the sluice gates.

Each run (two runs in all) lasted for about 15 hours, the measurements were made in sessions of about 3 hours each, there being more than 600 measuring points for each run. The headwater depths (h_0) were checked at about 20 minute intervals with no noticeable difference found in their values.

5.3.6 Experimental Accuracy

Experimental inaccuracies could be attributed to the following factors:

(i) Error in measuring the depth; the maximum error found, on the basis of reproducibility of results, was about $\pm$ 0.5 mm. This has given a maximum error of about 1.5 % of an average depth of the flow.

(ii) Small variations in the headwater depth (h_0); the maximum variation observed over a period of 3 hours was about $\pm$ 1 mm out of heads of 20 cm and 36 cm for Run 1 and Run 2 respectively, thus the flow rate did not vary by more than 0.25 % over the period of investigation.

(iii) Small oscillations of the position of the toe of the hydraulic jump was observed. This was of the order of $\pm$ 6 cm.

(iv) The fact that the surface downstream of the hydraulic jump was

undergoing continuous oscillations has made it difficult to measure h_t very accurately. The maximum oscillation in h_t was found to be $\pm$ 2 mm; the range of h_t investigated was 9.4 cm to 15.8 cm.

5.3.7 Experimental Results

A. Upstream control only

The experimental measurements were first made where the flow was controlled by upstream conditions only, since the inlet conditions in all runs were supercritical. No downstream control was activated; the Tainter gate was not used and was positioned well above the water surface. The outlet boundary was at supercritical conditions.

Experimental measurements were made for two runs; namely, Run 1 and Run 2. In both runs, the heights of the openings below the sluice gates (d_1 and d_2) were kept unaltered at 4.1 cm and 8.15 cm for Streams 1 and 2 respectively. The only parameters varied were the headwater depths ($h_{0,1}$ and $h_{0,2}$). Thus the investigation carried out for each run, was at a different flow rate for each stream, i.e. at different inlet Froude number.

Table 5.2 summarizes the flow parameters used for each run. The inlet station to the test section was at x=0 (1 m downstream of the sluice gates where the separating wall terminated), see Figure 5.3. The cross-stream depth measurements started at x=0, the flow variables were all subscripted "in,1" and "in,2" specifying inlet conditions for Stream 1 and Stream 2 respectively. The bars over the variables were used to specify mean values for reference purposes only (since the measured depth profiles at the inlet were not exactly uniform). This

Parameters	Run 1	Run 2
$h_{0,1}$ (cm)	20.9	36.3
$h_{0,2}$ (cm)	20.0	35.8
d_1 (cm)	4.1	4.1
d_2 (cm)	8.15	8.15
C_{d1}	0.55	0.58
C_{d2}	0.51	0.54
q_1 (m^2/s) x100	4.57	6.29
q_2 (m^2/s) x100	8.28	11.73
$\bar{h}_{in,1}$ (cm)	3.09	3.09
$\bar{h}_{in,2}$ (cm)	5.52	5.58
$\bar{u}_{in,1}$ (m/s)	1.48	2.04
$\bar{u}_{in,2}$ (m/s)	1.50	2.10
$\bar{Fr}_{in,1}$	2.68	3.71
$\bar{Fr}_{in,2}$	2.04	2.84
h_t (cm)	A. Not fixed (supercritical outlet) B. Fixed (subcritical outlet) = 9.4,9.8,10.0,10.4, 10.8 and 11.2	A. Not fixed (supercritical outlet) B. Fixed (subcritical outlet) =11.6,12.4,13.8,14.8, 15.6 and 15.8

Table 5.2 : Test conditions for 2D flow experiments

Key : h_0 headwater depth
d opening height below sluice gate
C_d coefficient of discharge
q flow rate per unit width
$\bar{h}_{in}$ mean depth at inlet to test section
$\bar{u}_{in}$ mean velocity at inlet to test section
$\bar{Fr}_{in}$ mean Froude number at inlet to test section
$\bar{h}_t$ tailwater depth
Subscripts 1 and 2 : Streams 1 and 2 respectively

station, as will be seen in Chapter 7, is taken as the inlet boundary for the numerical computations.

The measured depth points were used to construct perspective views of the surface by means of a "MATMAP" package generated by the Imperial College computer laboratory. Figures 5.5 and 5.6 show such views for Runs 1 and 2 (slower and faster flows respectively). The plots, for each run, differ only in the angle of projection; slight exaggeration is shown in the surface elevation for clarity. The flow is characterized by the presence of a very shallow region directly downstream of the separating wall and as long as the entering streams remain supercritical. Such regions are often termed "dry regions", since the depth of flow there is practically zero. The width of the dry region starts as equal to the width of the separating wall, and then narrows as the entering streams start to expand. The depth increases sharply as the two streams hit each other, from which two main stationary waves emerge and spread out downstream at different angles. These waves reflect as they meet the channel side walls and give rise to a local increase in depth. Complicated flow patterns then follow as these reflected waves meet further downstream.

Figure 5.7 displays a photograph of the "dry region" which extends to a length approximately equal to the width of the separating wall for the flow parameters investigated.

More analysis and discussion of the results are postponed until Chapter 7 where the cross-stream depth profiles are plotted and compared with the numerical results.

The measurements are given in tabular form in Appendix E.

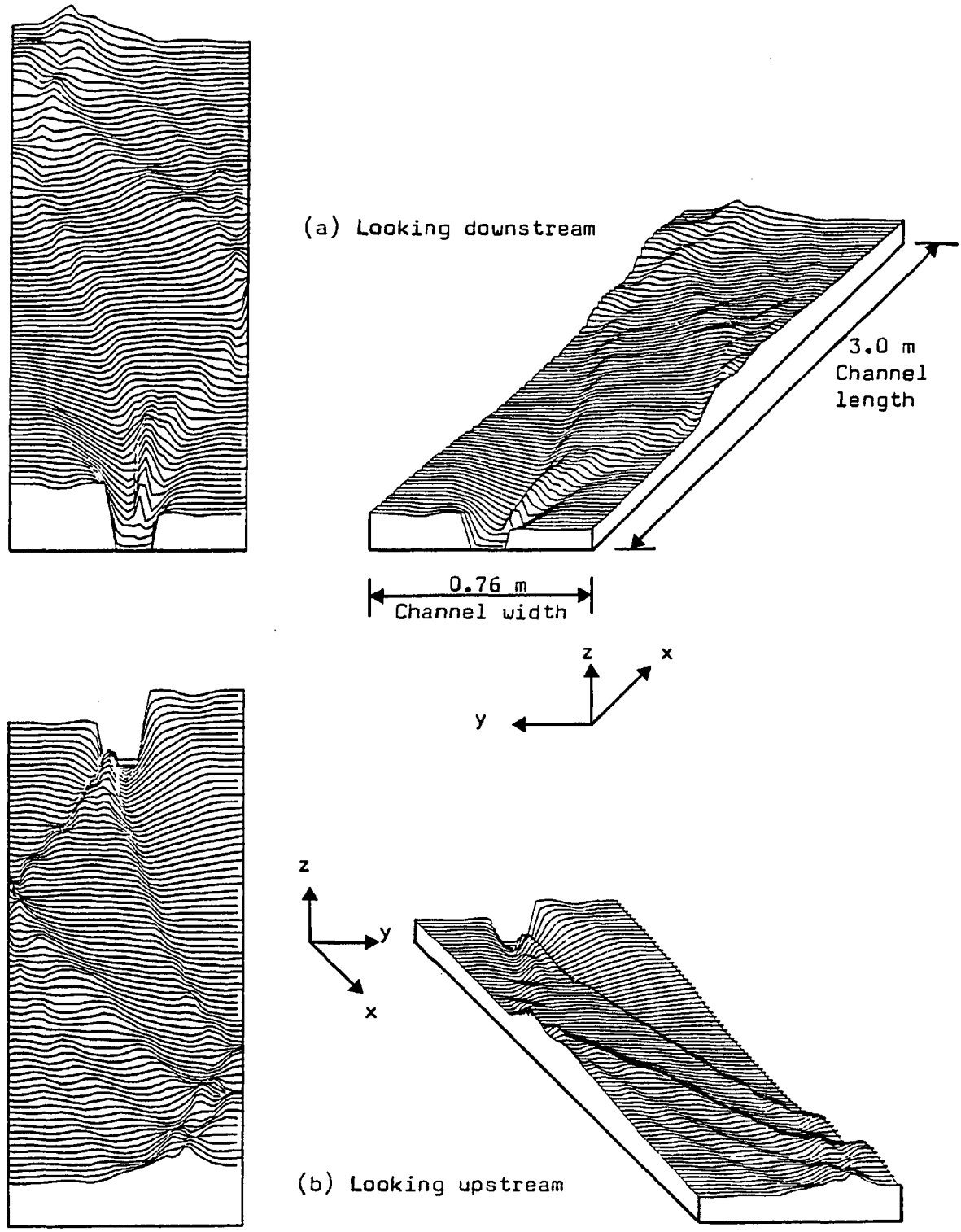


FIGURE 5.5 : PERSPECTIVE VIEWS OF THE SURFACE FOR RUN 1 LOOKING AT DIFFERENT ANGLES

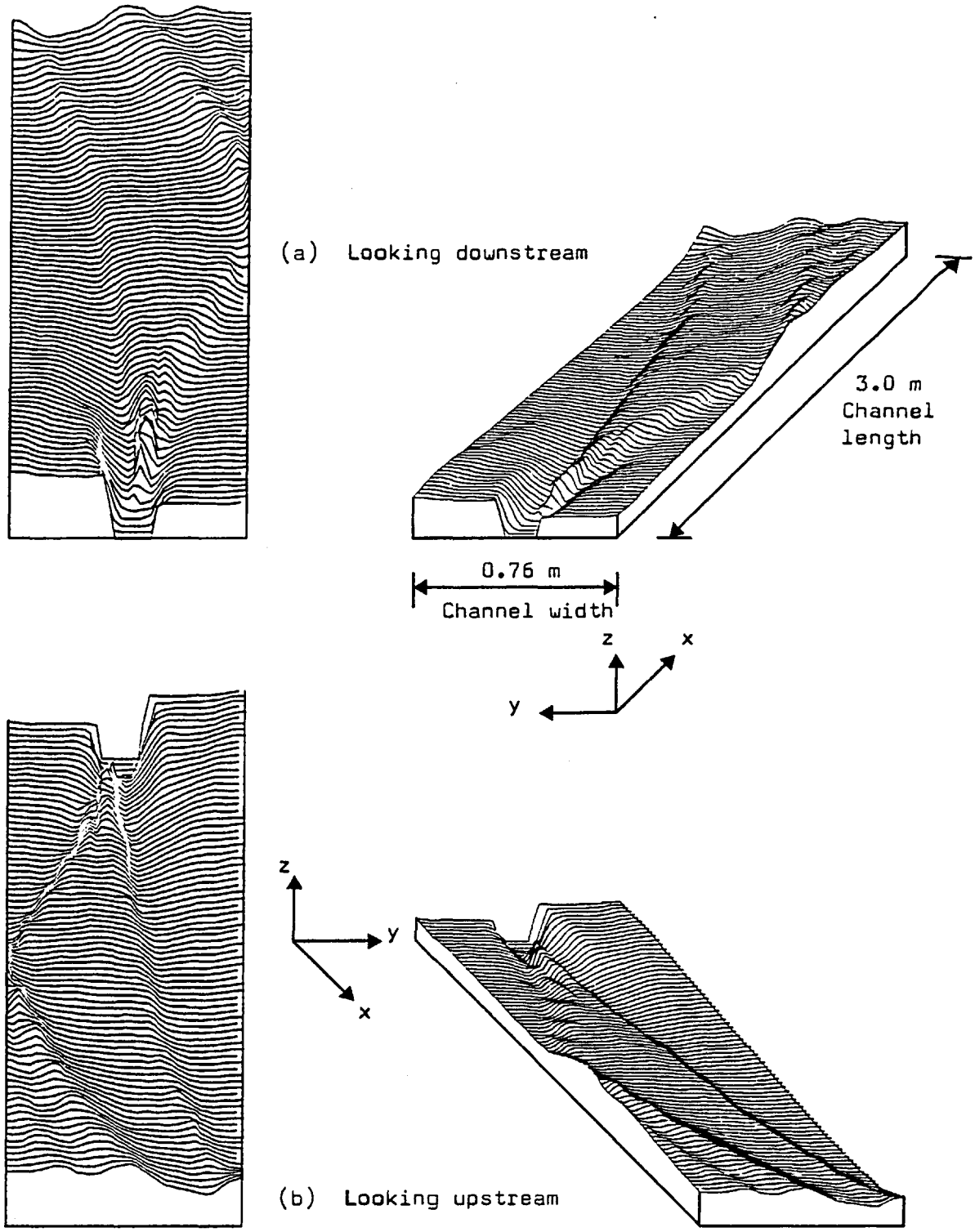


FIGURE 5.6 : PERSPECTIVE VIEWS OF THE SURFACE FOR RUN 2 LOOKING AT DIFFERENT ANGLES

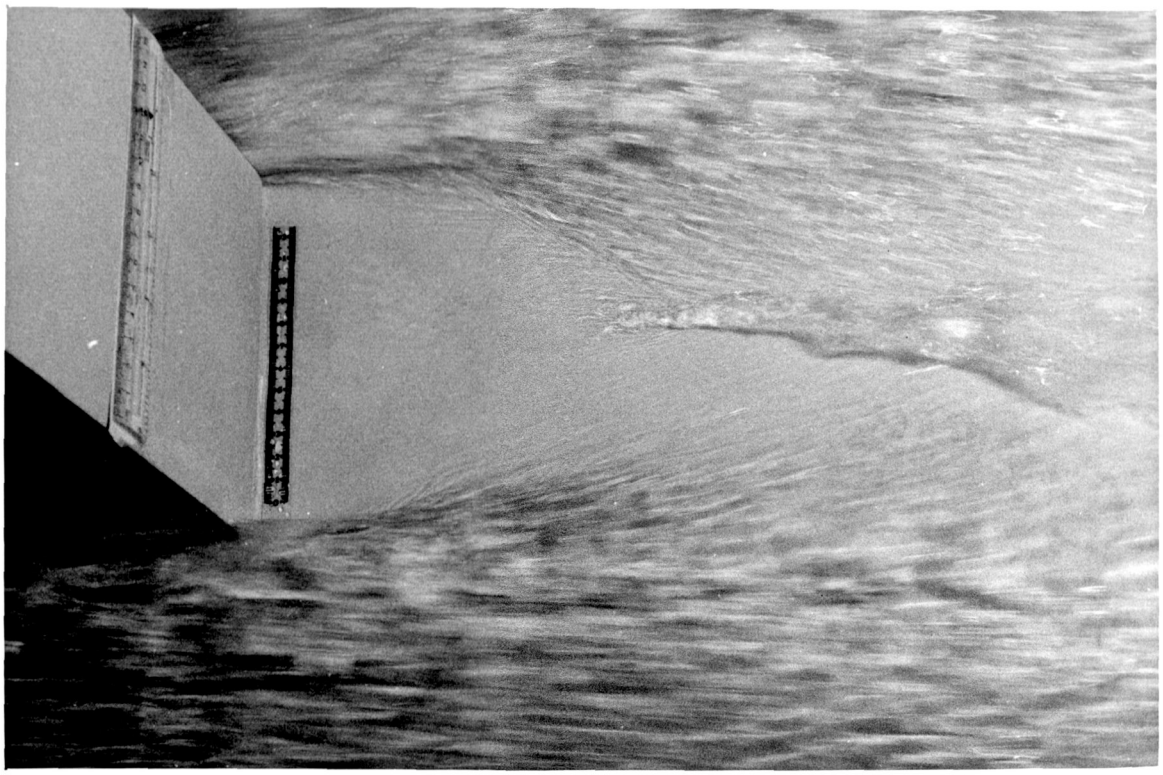


FIGURE 5.7 : VIEW OF THE FLOW BEHIND THE SEPARATING WALL

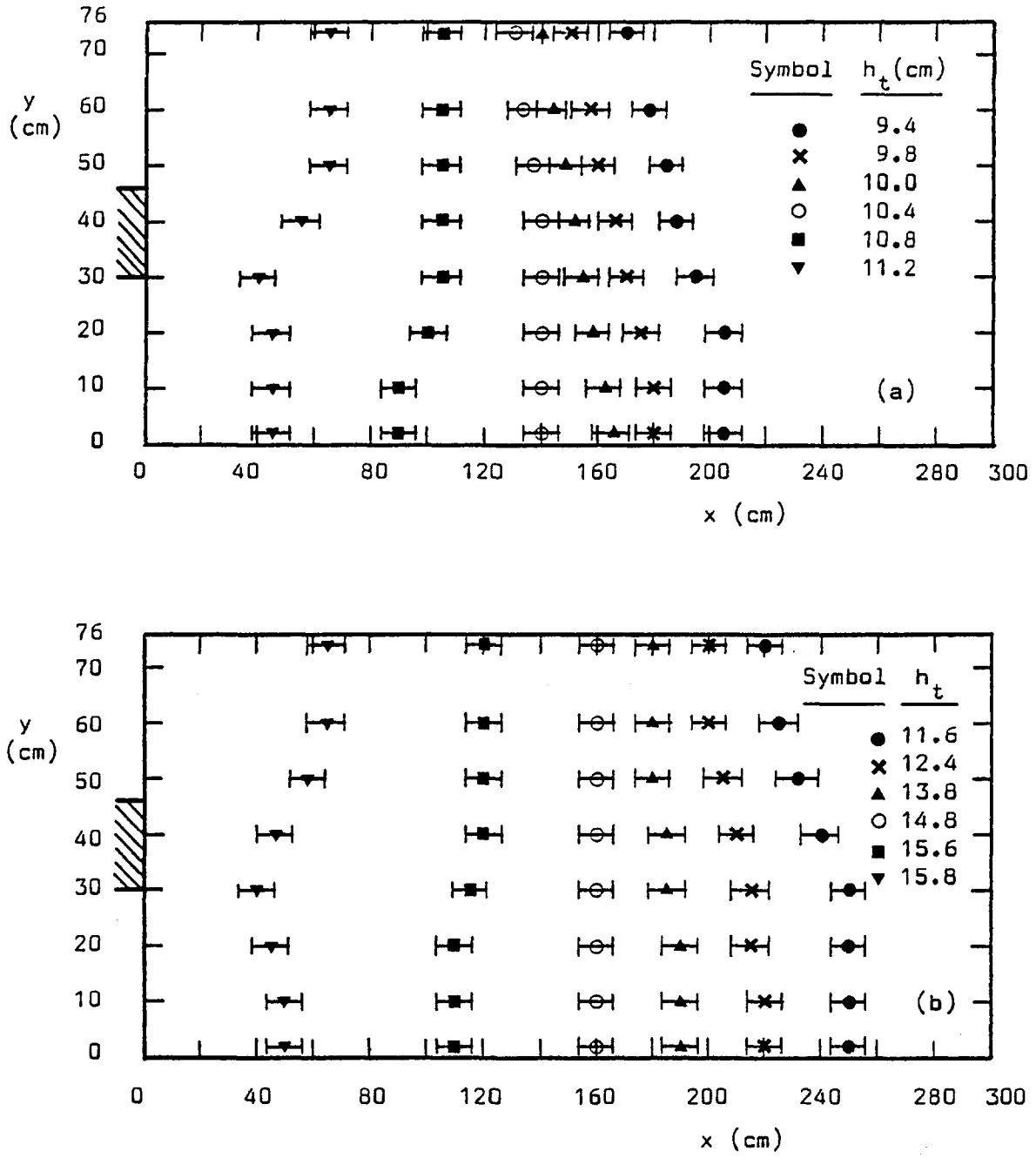


FIGURE 5.8 : LOCATIONS OF THE TOE OF HYDRAULIC JUMPS VERSUS TAILWATER DEPTH

(a) Run 1 (experiment)

(b) Run 2 (experiment)

B. Upstream and downstream controls

The measurements for Runs 1 and 2 were extended to include hydraulic jumps in the test section. Here, the downstream control was activated by the use of the Tainter gate. The tailwater depth (h_t) was accordingly adjusted to desired values that produced jumps in the flow (see Section 5.3.5, step (v)). The outlet boundary was, thus, at a subcritical condition. The upstream conditions were left unaltered for each run as given in (A) above. The surface upstream of the jump was, of course, unaffected by the presence of the jump, since the flow remained supercritical. On the downstream side of the jump, the surface oscillated slightly, but an average depth of h_t prevailed everywhere.

The flow situation described above is characterized and influenced by flow conditions prescribed on both upstream and downstream boundaries. Figures 5.8(a) and 5.8(b) show the locations of the toe of the hydraulic jump as being affected by altering h_t for Runs 1 and 2 (slower and faster flows respectively).

5.4 SUMMARY

In this chapter, the experimental investigations for each of the one-and two-dimensional flows have been discussed. The information presented is summarized as follows:

(i) The objectives and main parameters of the study have been stated.

(ii) The experimental flume has been described.

(iii) The experimental procedure and accuracy of the measurements have been given.

(iv) The experimental results have been presented; some in perspective views only.

The measurements in tabular form are given in Appendices D and E. In Chapter 7, these experimental results will be further analysed and compared with the predictions obtained from the numerical model.

CHAPTER 6

PREDICTIONS OF CONTINUOUS FLOWS

6.1 INTRODUCTION

6.1.1 General Concept

In Chapter 4, a numerical procedure for the prediction of two-dimensional shallow-water flows was presented. As with any other solution procedure, it should be capable of producing accurate results and to realistically simulate, considering the assumptions made, actual flow situations. The procedure should also be economic and readily extendable to account for extra physical processes if and when required. It is, therefore, in the present chapter and the following two chapters, that the procedure is examined and tested for such requirements, by application to a variety of flow situations.

The numerical model developed in this thesis is general, i.e. it solves for both *continuous and discontinuous* flows using the same solution and adjustment procedures. Continuous flows, the subject of this chapter, can be either subcritical or supercritical. Discontinuous flows are those with hydraulic jumps and are the subject of Chapters 7 and 8. Some of the problems predicted are ones for which analytical solutions and numerical solutions are available; these problems are therefore especially useful as tests of the computational accuracy of the procedure. Other problems are compared with experimental data as an assessment of the physical realism of the predictions.

All the computations presented were produced with the STABLEXT † (Steady Three-Dimensional Analyser of Boundary Layer Extended) Computer Program, appropriately modified to embody the solution procedure described in Chapter 4. The program is written in standard FORTRAN and requires no special features of a particular computer.

All the results presented are essentially grid independent; specific grid tests are reported for each case considered. The predictions were computed on various CDC machines using MNF compilers; the execution times are quoted in terms of CDC 6600 seconds.

In this chapter the numerical accuracy of the solution procedure is checked by comparing predictions of four flows; two of the comparisons are with analytical solutions. All four flows are continuous; two cases are for wholly subcritical flows and the other two simulate wholly supercritical flows, with one analytical solution falling in each category.

6.1.2 Method of Presentation

A uniform format will be adopted for the presentation of all problems studied in this chapter and in the following two chapters. For each test case the description is, in general, divided into the following parts:

(i) Introduction; in which the motivation for the study and the statement of the objectives are given.

(ii) Problem specification; in which the physical situation considered is described. This section also involves description of

† Program kindly lent by CHAM Ltd, London.

any theoretical considerations, if available, experimental data and solutions by others. The flow parameters studied and the information to be obtained are also stated.

(iii) Details of the computations; in which the equations solved, boundary conditions used, initial conditions, finite-difference grid employed and further information, are given.

(iv) Presentation of the results.

(v) Discussion of the results.

(vi) Further details; this mainly involves the grid-dependence check. It may also include, when relevant, a study of the effects on the predictions of the empirical friction-factors used and some parametric studies.

(vii) Concluding remarks.

6.2 SUBCRITICAL LAMINAR CHANNEL FLOW

6.2.1 Introduction

The objectives of this study are to validate the model and assess the accuracy of the numerical solution procedure for a simple flow situation in which the flow is wholly subcritical. The study is motivated by the existence of an analytical solution for such a flow.

6.2.2 Problem Specification

(a) Flow situation

Figure 6.1 shows the geometry of the flow in the inlet length

of a straight channel with flat parallel walls. Only one half of the physical domain is shown and solved for due to symmetry of flow on either side of the centre-plane of the channel; the channel half width being Y. A constant-property fluid is set in steady and laminar motion along the channel with a uniformly distributed velocity at the inlet section (u_{in}). Owing to viscous friction, a boundary layer will be formed on the wall and grow in the downstream direction; at a sufficient distance downstream it will become fully developed and the velocity profile will be parabolic.

(b) Theoretical consideration

Schlichting (1968) has analysed such a flow mathematically and produced velocity profiles for the laminar flow in the inlet section of the channel. This was achieved by, firstly, performing an integration in the downstream direction so that the boundary-layer growth is calculated for an accelerated external stream. Secondly, by integrating in the upstream direction and analysing the progressive deviation of the profile from its asymptotic parabolic distribution. Having obtained both solutions, they were joined at a section where both were still applicable.

(c) Flow parameters

The rate of development of the laminar velocity profiles in the channel depends on the Reynolds number of the flow (Re), where Re is based on the half width of the channel (Y). This dependence can be removed by normalizing the axial distance from the inlet with Re, thus:

$$\bar{x} = \frac{x}{Y\ Re} \qquad .(6.1)$$

For this study the flow parameters are chosen as follows:

u_{in} = 0.001 m/s

Y = 1.0 m

L = 24.0 m (channel length)

Re = 100.0

Further, the inlet depth (h_{in}) is taken as 0.1 m; this gives a value for the Froude number at the inlet (Fr_{in}) as:

$$Fr_{in} = \frac{u_{in}}{(g\ h_{in})^{\frac{1}{2}}} = 0.001$$

This small value of Froude number is needed together with the value of Reynolds number to ensure that the gravity and viscous forces predominate over the pressure forces, as is the case in developing flows in straight channel.

The result of this study, for the above parameters, is the predicted velocity distribution in the inlet section of the channel. These are to be compared with available analytical results.

6.2.3 Details of the Computations

(a) Equations solved

The equations solved are the continuity and the two momentum

equations given by (the bars denoting depth-averaged quantities are left out for convenience):

continuity equation

$$\frac{\partial}{\partial x}(hu) + \frac{\partial}{\partial y}(hv) = 0 \qquad .(6.2)$$

u-momentum equation

$$\frac{\partial}{\partial x}(h u^2) + \frac{\partial}{\partial y}(huv) = -gh\frac{\partial h}{\partial x} + \frac{\mu}{\rho}\left[\frac{\partial}{\partial x}\left(h\frac{\partial u}{\partial x}\right) + \frac{\partial}{\partial y}\left(h\frac{\partial u}{\partial y}\right)\right] \qquad .(6.3)$$

v-momentum equation

$$\frac{\partial}{\partial x}(huv) + \frac{\partial}{\partial y}(h v^2) = -gh\frac{\partial h}{\partial y} + \frac{\mu}{\rho}\left[\frac{\partial}{\partial x}\left(h\frac{\partial v}{\partial x}\right) + \frac{\partial}{\partial y}\left(h\frac{\partial v}{\partial y}\right)\right] \qquad .(6.4)$$

(b) Boundary conditions

The boundary conditions employed in the computations, for the flow geometry shown in Figure 6.1, are:

(1) Inlet plane :

$$u = u_{in}\ , \quad v = 0\ , \quad h = h_{in} \qquad .(6.5)$$

(2) Plane of symmetry :

$$\frac{\partial u}{\partial y} = v = \frac{\partial h}{\partial y} = 0 \qquad .(6.6)$$

(3) Channel wall :

$$u = v = \frac{\partial h}{\partial y} = 0 \qquad .(6.7)$$

(4) Exit plane : $$\frac{\partial u}{\partial x} = \frac{\partial v}{\partial x} = \frac{\partial h}{\partial x} = 0 \qquad .(6.8)$$

(c) Initial conditions

The conditions specified at the inlet plane are used as initial guesses for the field values, i.e. equations (6.5).

(d) Finite-difference grid

In order to examine the effects of grid size on the solution, three different finite-fifference grids were used: 10 x 7 , 14 x 12 and 19 x 18 (in the x- and y-directions respectively); all with uniform spacings. As will be demonstrated later, the 14 x 12 grid is adequate to ensure grid-independent results.

(e) Other details

Under-relaxation factors were applied on all the variables u, v and h; 0.8 for u,v and 0.3 for h were found to be the optimum values.

Residuals for u and v were normalized by the total momentum flow-rate at the inlet; the mass residuals were normalized by the total mass flow-rate. The solution was obtained after 120 iterations of the flow field. This was found to be sufficiently converged by monitoring the residuals and the values of the variables at a pre-selected point in the flow field for every iteration. To enhance the monitoring further, the whole-field variable values were also printed out at intervals. On termination, the normalized sum of the absolute residuals over the whole field were found to be 3.0 E-2, 1.1 E-3 and 2.6 E-4 for u, v and the continuity error; the maximum

depth-correction (Max. h') normalized to h_{in} was 1.5 E-10. A summary of these details and other information is contained in Table 6.1.

VARIABLE	VALUE
Re	100
Fr_{in}	0.001
Grid	19 x 18
Type of grid spacing	Uniform
Number of iterations	120
RELAXU, RELAXV, RELAXH, RELAXP	0.8, 0.8, 0.3, 1.0
Overall normalized continuity error	2.6 E-4
Max. normalized h'	1.5 E-10
Computer time in CDC 6600 seconds	38

TABLE 6.1 : COMPUTATIONAL DETAILS FOR SUBCRITICAL LAMINAR CHANNEL FLOW

6.2.4 Results and Discussion

The velocity-vector plot is displayed in Figure 6.2. This confirms the qualitative description of the problem, in that the plug velocity profile prescribed at the inlet is developed downstream to a fully-developed parabolic profile. The decrease of velocity near the wall which is due to friction is compensated by a corresponding increase near the symmetry plane.

Figure 6.3 shows some of the cross-stream u-velocity profiles at different stations compared with the analytical solution of Schlichting. The parabolic profile is found at about $100\ \overline{x} = 20$ (see equation (6.1)). The agreement between computed and analytical solutions is good.

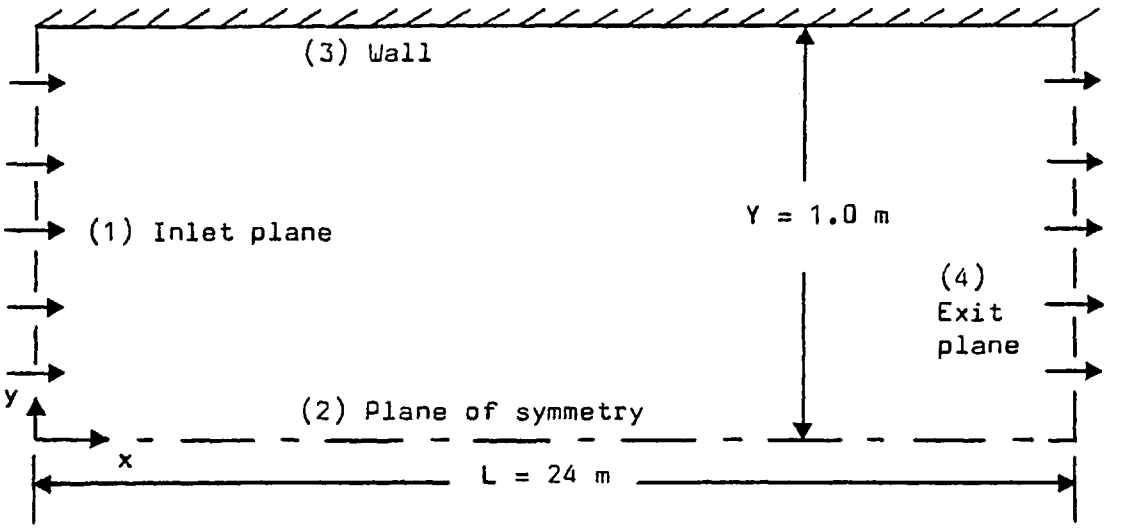


FIGURE 6.1 : LAMINAR DEVELOPING FLOW IN A STRAIGHT OPEN CHANNEL; SHOWING GEOMETRY, COORDINATES, AND BOUNDARY CONDITIONS

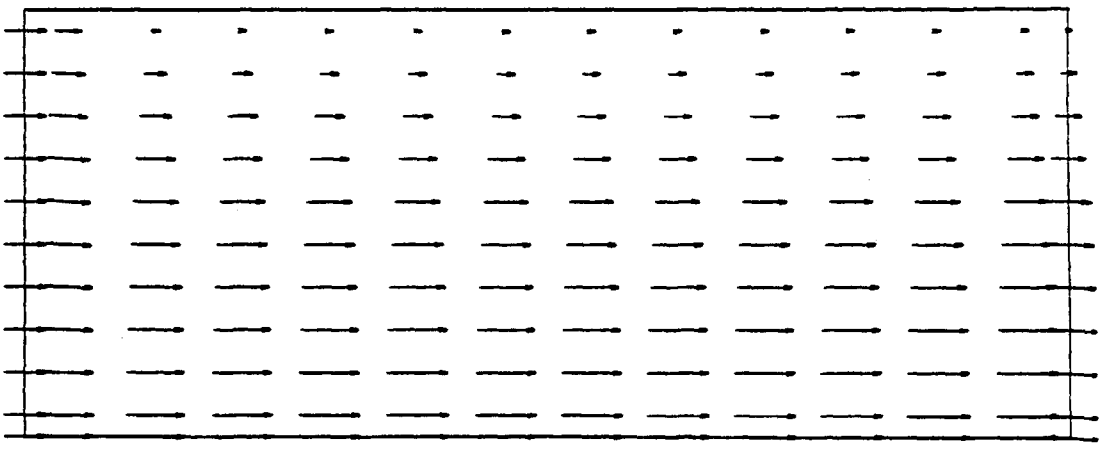


FIGURE 6.2 : VELOCITY-VECTOR PLOT FOR DEVELOPING OPEN-CHANNEL FLOW

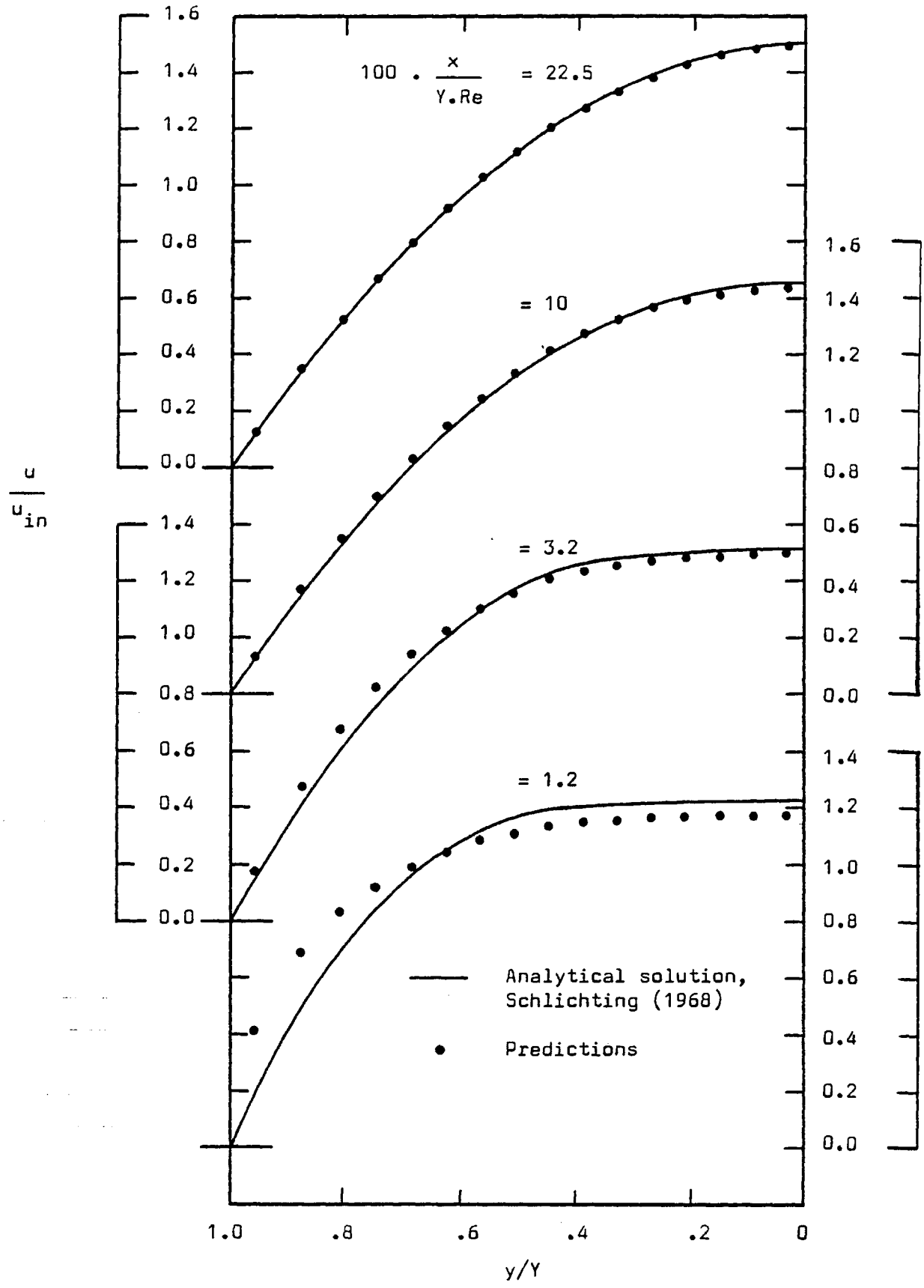
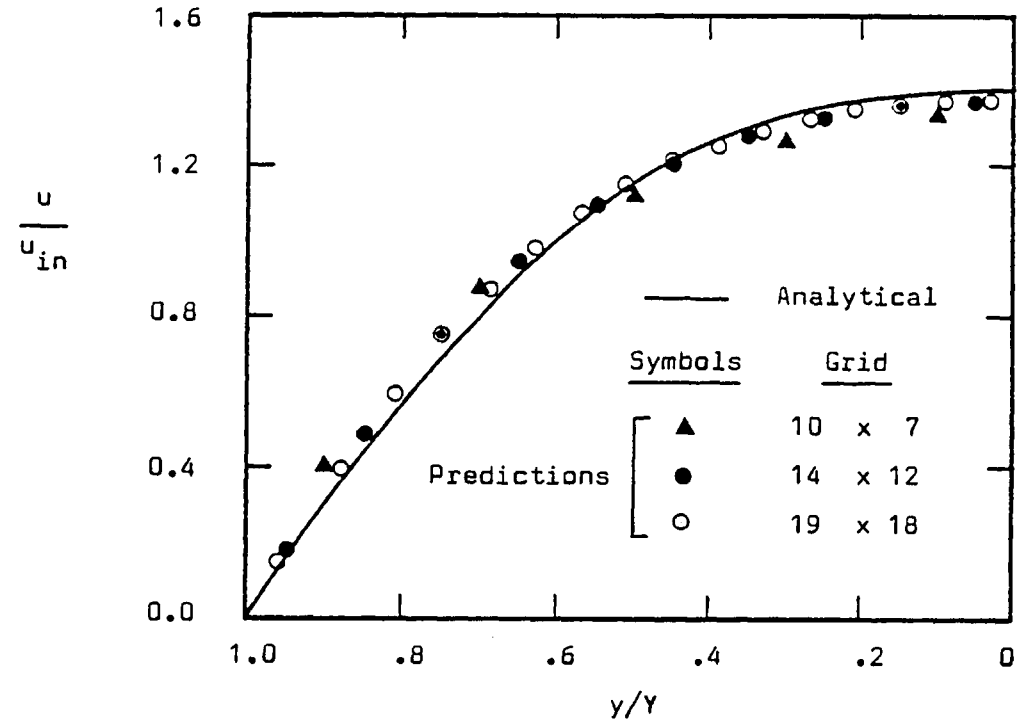


FIGURE 6.3 : VELOCITY DISTRIBUTION OF THE LAMINAR DEVELOPING FLOW IN A STRAIGHT OPEN CHANNEL



(a) Cross-stream velocity profile at 100. $\frac{x}{Y.Re}$ = 6

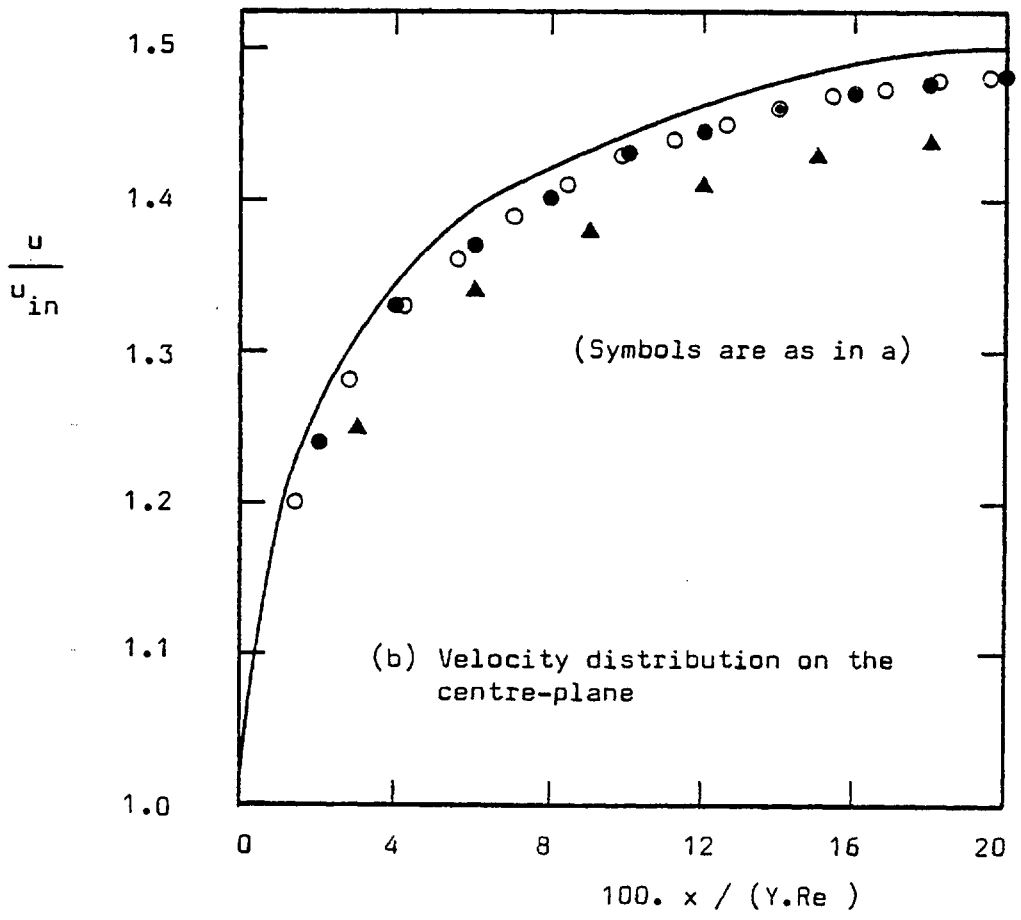


FIGURE 6.4 : GRID-DEPENDENCE CHECK, OPEN-CHANNEL FLOW

6.2.5 Grid-Dependence Check

Figures 6.4 (a) and 6.4 (b) show the comparison between the analytical solution and the predicted results for the three different finite-difference grids used, as specified in Section 6.2.3 (d). It is seen that the two finer grids employed; namely, the 14 x 12 and 19 x 18 grids, give substantially grid-independent results as compared to the 10 x 7 grid. The finer the grid spacing employed, the closer are the results to the analytical solution.

6.3 SUBCRITICAL LAMINAR SQUARE-CAVITY FLOW

6.3.1 Introduction

The objective of this study is to assess the accuracy of the numerical scheme, for another wholly subcritical flow, in the presence of flow recirculation. For a low value of Froude number the depth of flow will remain effectively constant and hence comparison of results can be made with those considered by, amongst many, Burggraf (1966), for confined cavity flows.

6.3.2 Problem Specification

(a) Flow situation

A constant-property fluid inside a square cavity, of side length Y, is set in laminar motion by a steadily moving lid. Figure 6.5 shows the geometry of the flow; the velocity of the lid being U. Owing to

viscous friction, a large recirculation zone will be formed inside the flow. The surface elevation of the fluid is free to change but, because the gravity forces predominate over the inertia forces (low Fr), the flow will have a flat surface.

(b) Flow parameters

The laminar flow inside the square cavity is characterized by the value of Reynolds number (Re) based on the lid velocity and side length, given by: $Re = \rho U Y / \mu$. The reference Froude number (Fr_{ref}) based on the lid velocity and a reference depth (h_{ref}) is defined as : $Fr_{ref} = U / (g\, h_{ref})^{\frac{1}{2}}$.

For this study the flow parameters are chosen to be:

$U = 0.01$ m/s

$Y = 1.0$ m

$h_{ref} = 0.1$ m

$Re = 1.0$

$Fr_{ref} = 0.01$

The task of this study is to compute, for the above parameters, the distribution of the velocity and hence the values of vorticity and coordinates of the vortex centre. These are to be compared with available numerical solutions.

6.3.3 Details of the Computations

(a) Equations solved

The equations solved are the continuity and the two momentum

equations given by the equation set (6.2) to (6.4) in Section 6.2.3.

(b) Boundary conditions

The boundary conditions employed in the computations, for the flow geometry shown in Figure 6.5, are:

(1) Moving lid : $u = U$,

$v = 0$,

$\frac{\partial h}{\partial y} = 0$.(6.9)

(2) Stationary walls : $u = v = \frac{\partial h}{\partial y}$ (or $\frac{\partial h}{\partial x}$) $= 0$.(6.10)

(c) Initial conditions

Starting the solution with appropriate finite values is always advantageous and improves the stability and convergence speed of the solution. Figure 6.6 shows a sketch of the initial field values used for the u- and v-velocities based on overall continuity. The initial field values for the depth of flow were uniform and equal to h_{ref} .

(d) Finite-difference grid

Three different finite-difference grids were used: 7 x 7, 12 x 12 and 18 x 18; all with uniform spacings which produced square main-cells. As will be demonstrated later, the 12 x 12 grid is adequate to ensure grid-independent results for a Reynolds number of unity.

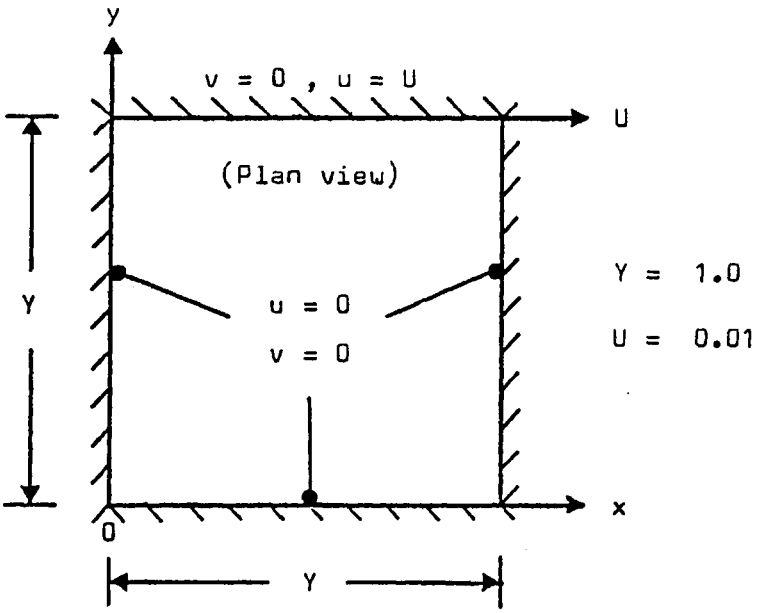
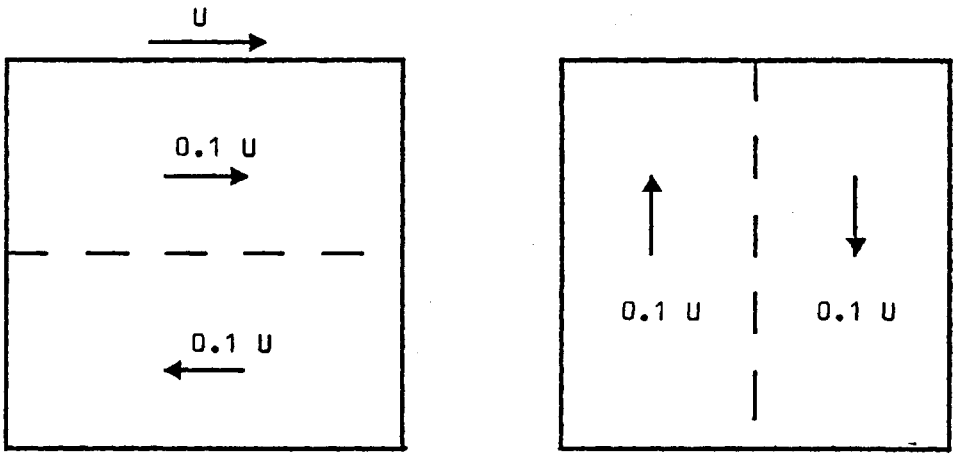


FIGURE 6.5 : CAVITY, SHOWING GEOMETRY, COORDINATES, AND BOUNDARY CONDITIONS



(a) u-velocity (b) v-velocity

FIGURE 6.6 : INITIAL FIELD VALUES FOR THE VELOCITIES

(e) Other details

Normal depth gradients at all the boundaries were set to zero; unlike pressure, the depth is not a relative quantity and hence a reference value of depth was required to be set in the field. A grid point (arbitrarily chosen) was, accordingly, fixed at the reference depth (h_{ref}) which helped to keep the total volume of the liquid inside the cavity constant.

Residuals for u and v were normalized by a momentum flow-rate arbitrarily chosen as $Y\, h_{ref}\, \bar{u}^2$, where $\bar{u}$ is an average velocity taken as half of the lid velocity. The mass residuals were similarly normalized by $Y\, h_{ref}\, \bar{u}$. The solution was found to be converged at 40 iterations of the flow field. The residuals and selected field values were monitored at every iteration. The field values were printed out at intervals. The computational details are listed in Table 6.2.

VARIABLE	VALUE
Re	1.0
Fr_{ref}	0.01
Grid	12 x 12
Type of grid spacing	Uniform
Number of iterations	40
RELAXU, RELAXV, RELAXH, RELAXP	1.0, 1.0, 1.0, 1.0
Overall normalized continuity error	2.7 E-4
Max. h' normalized to h_{ref}	6.3 E-8
Computer time in CDC 6600 seconds	4.3

TABLE 6.2 : COMPUTATIONAL DETAILS FOR SUBCRITICAL LAMINAR CAVITY FLOW

6.3.4 Results and Disussion

The velocity-vector plot is displayed in Figure 6.7 and the stream-function contours, deduced from the calculated velocity distribution, in Figure 6.8. These results illustrate the features of the vortical flow which occurs for the cavity problem.

The coordinates (x,y) of the vortex centre are found to be (0.5, 0.76); these can be compared with those reported by Burggraf: (0.5, 0.77) for Reynolds number approaching zero and obtained from a 51 x 51 finite-difference grid. The value of vorticity, defined as $(\partial u / \partial y - \partial v / \partial x) / U$, at the vortex centre is found to be 3.5; the corresponding value from Burggraf is 3.2.

The u-velocity profile along the central vertical plane is shown in Figure 6.9 along with that presented by Burggraf. The solid line represents the present predictions for the 12 x 12 grid and it can be seen that the agreement is good.

Owing to very low Froude number values prevailing in the flow, the depth remains effectively uniform at the value of h_{ref} .

6.3.5 Grid-Dependence Check

The u-velocity profiles plotted in Figure 6.9 have been obtained with different grids. It can be seen that the two finer grids employed; namely, the 12 x 12 and 18 x 18 grids, give substantially grid-independent results as compared to the 7 x 7 grid. As the grid is successively refined, the profile asymptotically approaches the correct one.

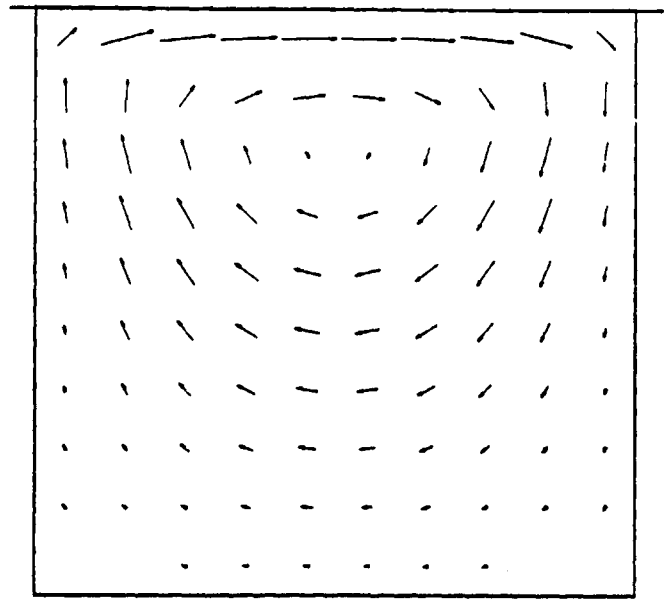


FIGURE 6.7 : VELOCITY-VECTOR PLOT FOR FREE-SURFACE CAVITY FLOW. (Re = 1, Fr_{ref} = 0.01)

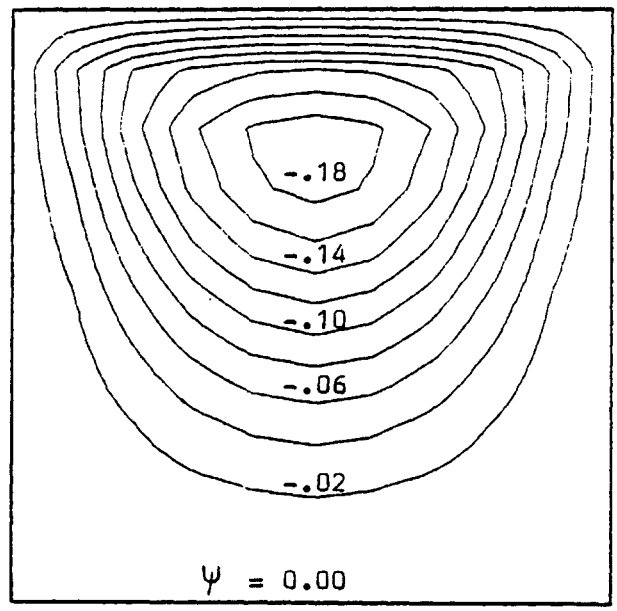


FIGURE 6.8 : STREAM-FUNCTION CONTOURS FOR FREE-SURFACE CAVITY FLOW. (Re = 1, Fr_{ref} = 0.01)

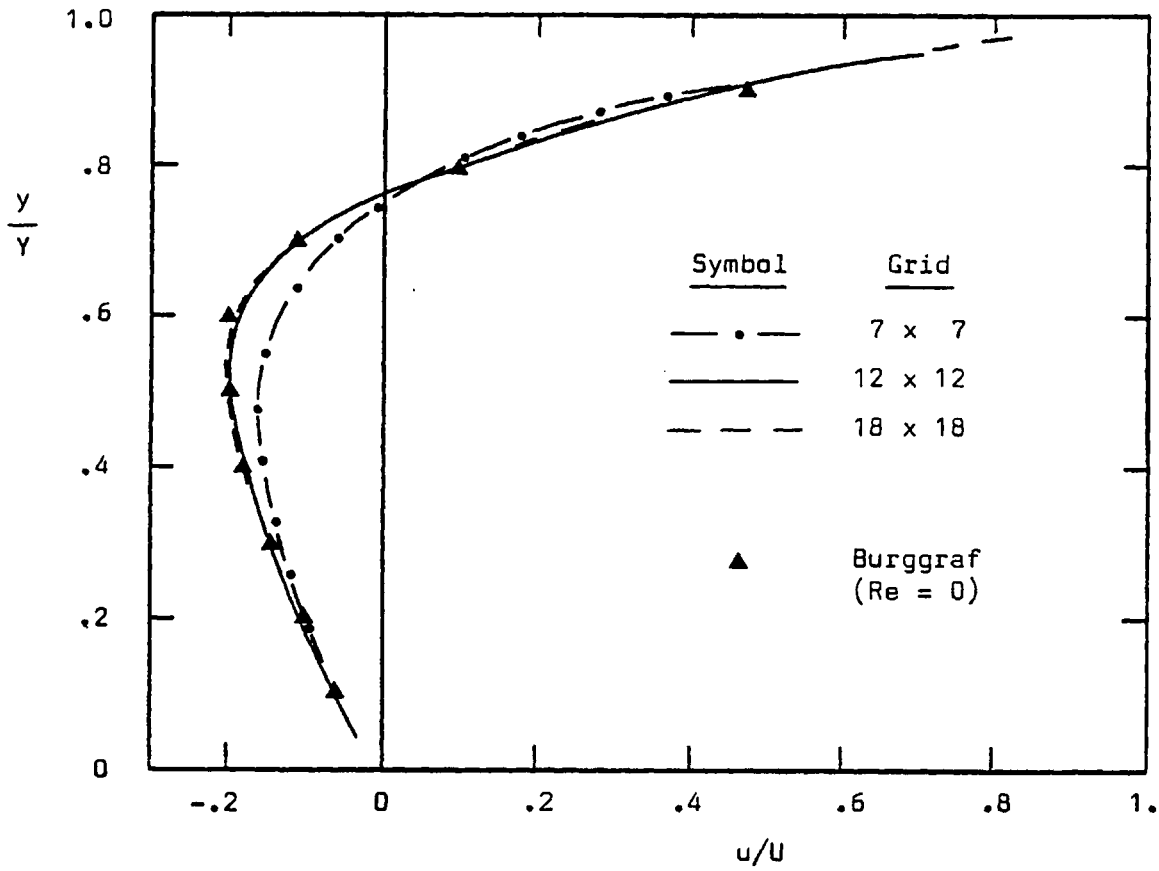


FIGURE 6.9 : u-VELOCITY PROFILES ACROSS THE VERTICAL CENTRE-PLANE, FREE-SURFACE CAVITY FLOW. (Re = 1, Fr_{ref} = 0.01)

6.4 SPREAD OF DEPTH DISCONTINUITY IN SUPERCRITICAL FLOWS

6.4.1 Introduction

The objectives of this study are to validate the model and assess the accuracy of the numerical solution procedure for a simple flow situation in which the flow is wholly supercritical. The study is motivated by the existence of an analytical solution which determines the angle of spread of a small, sharp depth discontinuity, i.e. an infinitesimal disturbance in the flow, as a function of Froude number.

6.4.2 Problem Specification

(a) Flow situation

Figure 6.10 shows the geometry of the flow which simulates the spread of a small, sharp discontinuity in depth introduced at the inlet of a straight, rectangular, horizontal channel of length L and width Y. Uniform velocity (U) is prescribed at the channel inlet. As long as the flow remains supercritical, the depth discontinuity will develop into two waves which spread in the downstream direction at the same angle to the main flow direction. This angle of spread, its counterpart in compressible-gas flows is known as the "Mach angle", is uniquely determined by the local value of Froude number. For an infinitesimal disturbance, the value of Froude number remains practically the same everywhere in the flow; the two waves will spread out, accordingly, at equal characteristic angles. A complicated, but regular, flow

pattern results when the two waves interfere with each other after meeting and reflecting from the channel side walls.

(b) Theoretical consideration

In the vicinity of such a depth discontinuity, i.e. far away from walls and planes of symmetry, two waves form and travel downstream at an angle (α), to the main direction of flow, given by the theoretical analysis for inviscid flows as:

$$\alpha = \sin^{-1} \frac{1}{Fr} \qquad ,(6.11)$$

where Fr is the mean value of Froude number based on U and $\bar{h}$ ($= \frac{h_1 + h_2}{2}$) and given by:

$$Fr = U / (g \bar{h})^{\frac{1}{2}} \qquad ,(6.12)$$

h_1 and h_2 are the depths of flow at the inlet plane to the channel which constitute the discontinuity as seen in Figure 6.10. For $h_1 / h_2 \approx 1$, the value Fr will effectively prevail everywhere in the flow domain.

The angle (α) given by equation (6.11) is simply arrived at by theoretical analysis. A body, small enough to be considered as a single point, travels in a straight line through a stationary fluid with a speed u greater than the wave speed c. The movement of the body generates surface waves in the fluid which are transmitted with speed c radially in all directions. If the body is at point A (see

Figure 6.11) at time $t = 0$, then at a time t later the waves which originated from the body when it was at A will have grown into a circle of radius ct . During that time the body itself moves a distance $AB = ut$. Since $u > c$, the body is able to travel ahead of the surface waves and arrives at point B which is outside the circle of radius ct (and also outside other circles formed by surface waves started at intermediate times). The line CB is a common tangent to all these circles formed and makes an angle α to the direction of motion given by: $\sin \alpha = \frac{ct}{ut} = \frac{1}{Fr}$. This is equation (6.11) given above.

(c) Flow parameters

The angle of spread of a depth discontinuity is uniquely determined by the Froude number of the flow. For this study the flow parameters are chosen as follows:

$L = 0.3$ m (channel length)

$Y = 0.1$ m (channel width)

$h_1 = 0.99$ cm

$h_2 = 1.01$ cm

These have given a depth discontinuity of 0.02 cm in a mean depth ($\bar{h}$) of 1.0 cm, i.e. a 2% discontinuity in depth.

The inlet velocity (U) is prescribed as uniform and is chosen to vary between 0.47 and 2.04 m/s; this gives a range of Froude number values between 1.5 and 6.5.

The task of this study is to compute, for the above parameters, the velocity distributions and surface elevations, and hence the wave angles (α). These are to be compared with theoretical values.

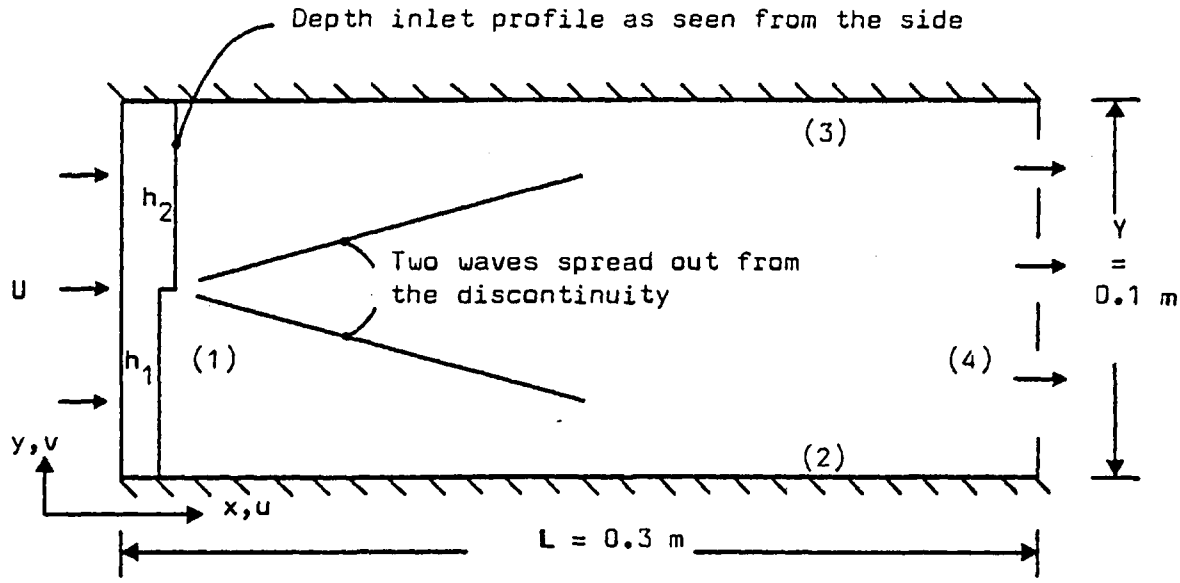


FIGURE 6.10 : SPREAD OF DEPTH DISCONTINUITY, SHOWING GEOMETRY, COORDINATES AND BOUNDARY CONDITIONS

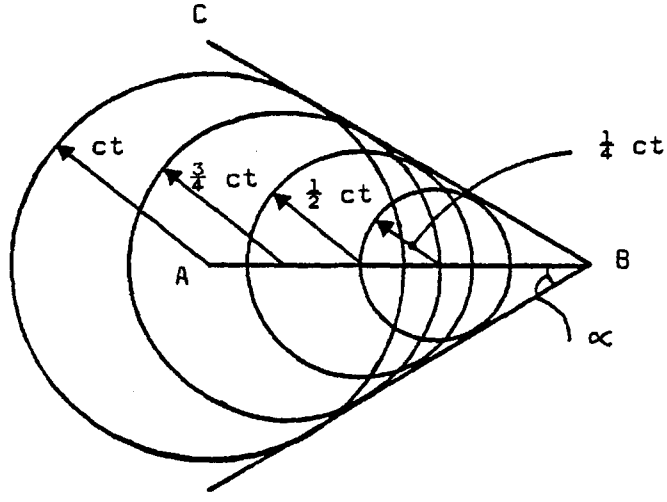


FIGURE 6.11 : THEORETICAL ANALYSIS OF THE ANGLE OF SPREAD OF A POINT DISTURBANCE

6.4.3 Details of the Computations

(a) Equations solved

The equations solved are the continuity and the two momentum equations with the viscous terms and wall friction put to zero. These are:

continuity

$$\frac{\partial}{\partial x}(hu) + \frac{\partial}{\partial y}(hv) = 0 \qquad .(6.13)$$

u-momentum

$$\frac{\partial}{\partial x}(h u^2) + \frac{\partial}{\partial y}(huv) = -g h \frac{\partial h}{\partial x} \qquad .(6.14)$$

v-momentum

$$\frac{\partial}{\partial x}(huv) + \frac{\partial}{\partial y}(h v^2) = -g h \frac{\partial h}{\partial y} \qquad .(6.15)$$

(b) Boundary conditions

The boundary conditions employed in the computations, for the flow geometry shown in Figure 6.10, are:

(1) Inlet plane : $u = U$,
$v = 0.0$,
$h = h_1$ (upper half) ,
$h = h_2$ (lower half) .(6.16)

(2) and (3) Side walls : $u = v = \partial h / \partial y = 0$.(6.17)

(4) Exit plane : $\frac{\partial u}{\partial x} = \frac{\partial v}{\partial x} = \frac{\partial h}{\partial x} = 0$.(6.18)

(c) Initial conditions

The u-velocity, v-velocity and depth fields were filled initially with U, 0 and $\bar{h}$ values respectively, where $\bar{h}$ is the mean depth at the inlet.

(d) Finite-difference grid

Four different finite-difference grids were used: 10 x 10, 18 x 18, 28 x 28 and 40 x 40; all with uniform spacings in both the x- and y-directions. As will be demonstrated later, the 28 x 28 grid is adequate to ensure grid-independent results.

(e) Other details

Typical computational details for a converged run are listed in Table 6.3.

VARIABLE	VALUE
Fr	3.19
Grid	28 x 28
Type of grid spacing	Uniform
Number of iterations	30
RELAXU, RELAXV, RELAXH, RELAXP	1.0, 1.0, 1.0, 1.0
Overall continuity error normalized to inlet flow-rate	2.3 E-6
Max. h' normalized to $\bar{h}$	5.8 E-5
Computer time in CDC 6600 seconds	14

TABLE 6.3 : COMPUTATIONAL DETAILS FOR SPREAD OF DEPTH DISCONTINUITY IN SUPERCRITICAL FLOWS

6.4.4 Results and Discussion

Figure 6.12 shows perspective views of the water surface for three cases; namely, Case 1, Case 2 and Case 3 with Froude numbers of 5.43, 3.19 and 1.92 respectively. The surface elevations are exaggerated to enhance clarity. It is clearly seen that the higher the Froude number, the sharper the angle of spread. Figure 6.13 displays the corresponding contour plots of depth. The lines of constant depth, called wavelets, start spreading near the vicinity of the discontinuities as straight lines at angles theoretically given by $\alpha = \sin^{-1} 1/Fr$. However, near the side walls and where the waves interfere with each other, it is seen that the resulting pattern of interference yields a rather complex variation in depth of flow. This is shown clearly in Case 3 of Figure 6.13. (Near the channel entrance and outside the depth levels marked (1) and (10), 0.991 cm and 1.009 cm respectively, the water surface remains undisturbed).

The wave angles are obtained from the calculated results in the region near the discontinuities by evaluating the angles of depth levels (1) and (10) and taking their average value. These wave angles are plotted and compared with the theoretical values for a range of Froude number between 1.5 and 6.5 in Figure 6.14 and show good agreement.

6.4.5 Ggid-Dependence Check

Figure 6.15 presents the results of a grid-dependence check for a typical run (Case 2, Fr= 3.19). Four different grid sizes were tested as specified in Section 6.4.3 (d). Figure 6.15(a) shows a cross-stream depth profile at $x/Y = 1.0$, whereas Figure 6.15(b) represents the depth profile along the bottom wall of the channel. It is seen that

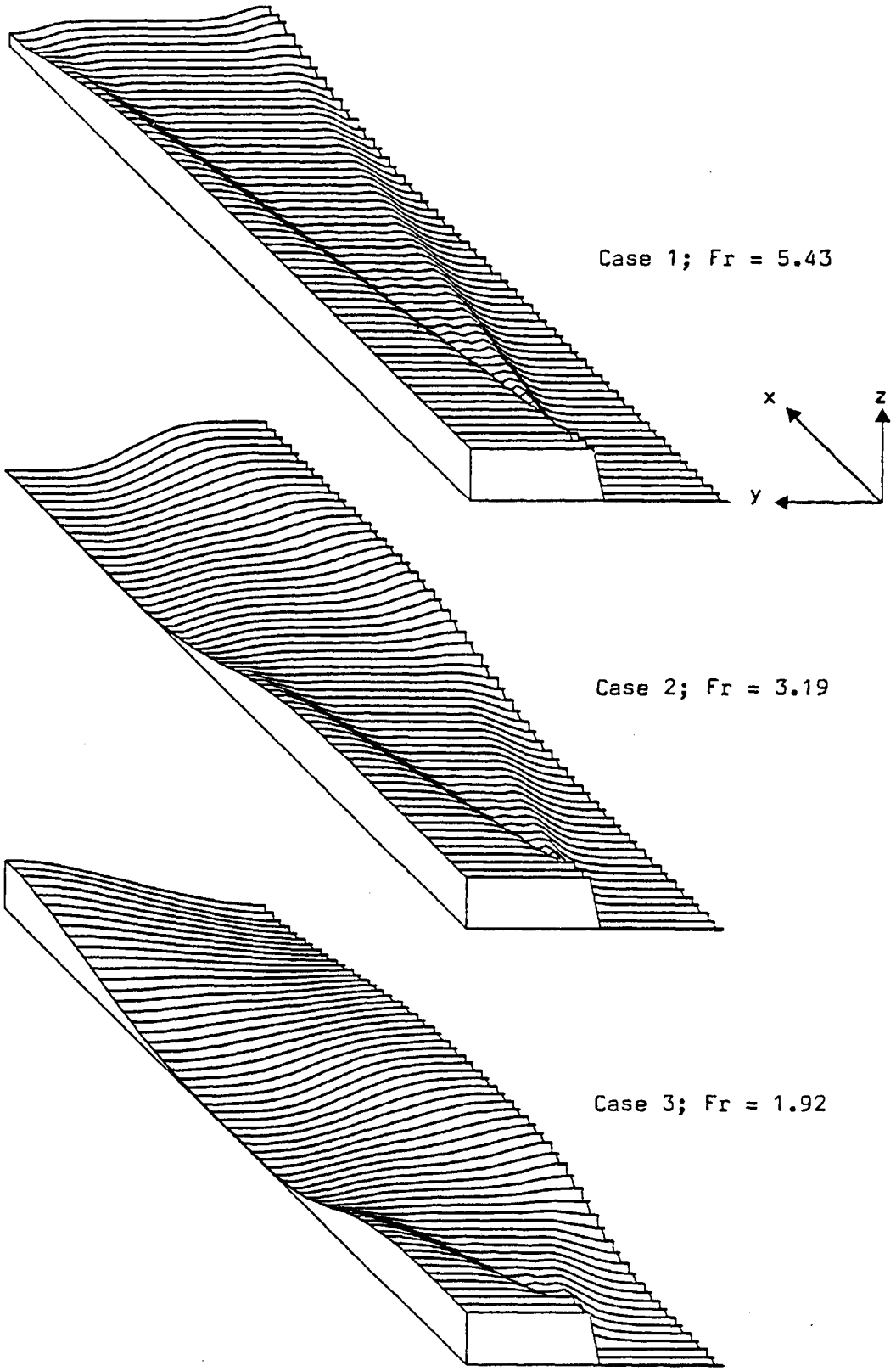
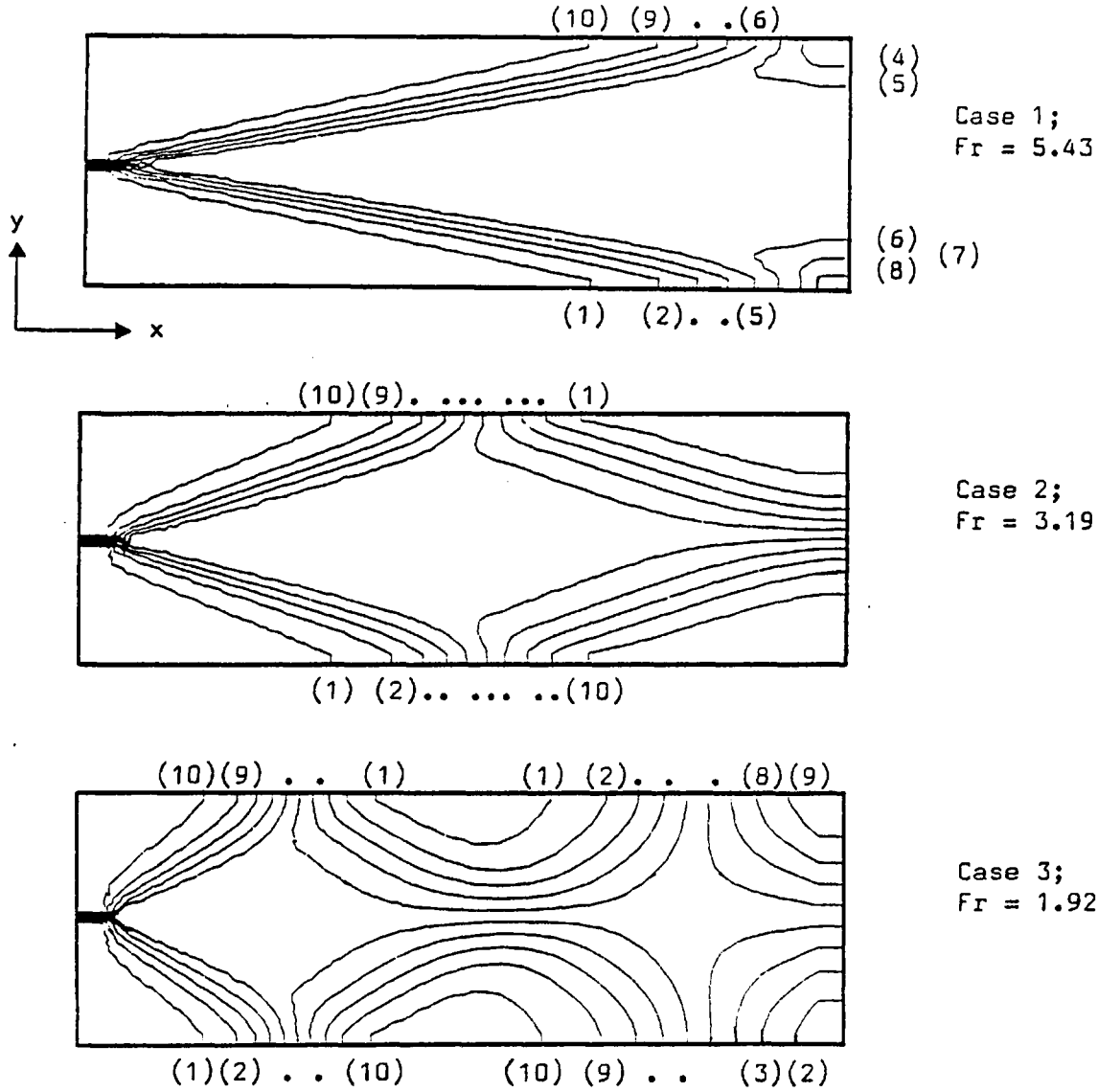


FIGURE 6.12 : PERSPECTIVE VIEWS OF SURFACE ELEVATION;
SPREAD OF DEPTH DISCONTINUITY, CASES 1,2 AND 3



Contour No.	Value (cm)	Contour No.	Value (cm)
(1)	0.991	(6)	1.001
(2)	0.993	(7)	1.003
(3)	0.995	(8)	1.005
(4)	0.997	(9)	1.007
(5)	0.999	(10)	1.009

FIGURE 6.13 : CONTOUR PLOTS OF DEPTH; SPREAD OF DEPTH DISCONTINUITY, CASES 1,2 AND 3

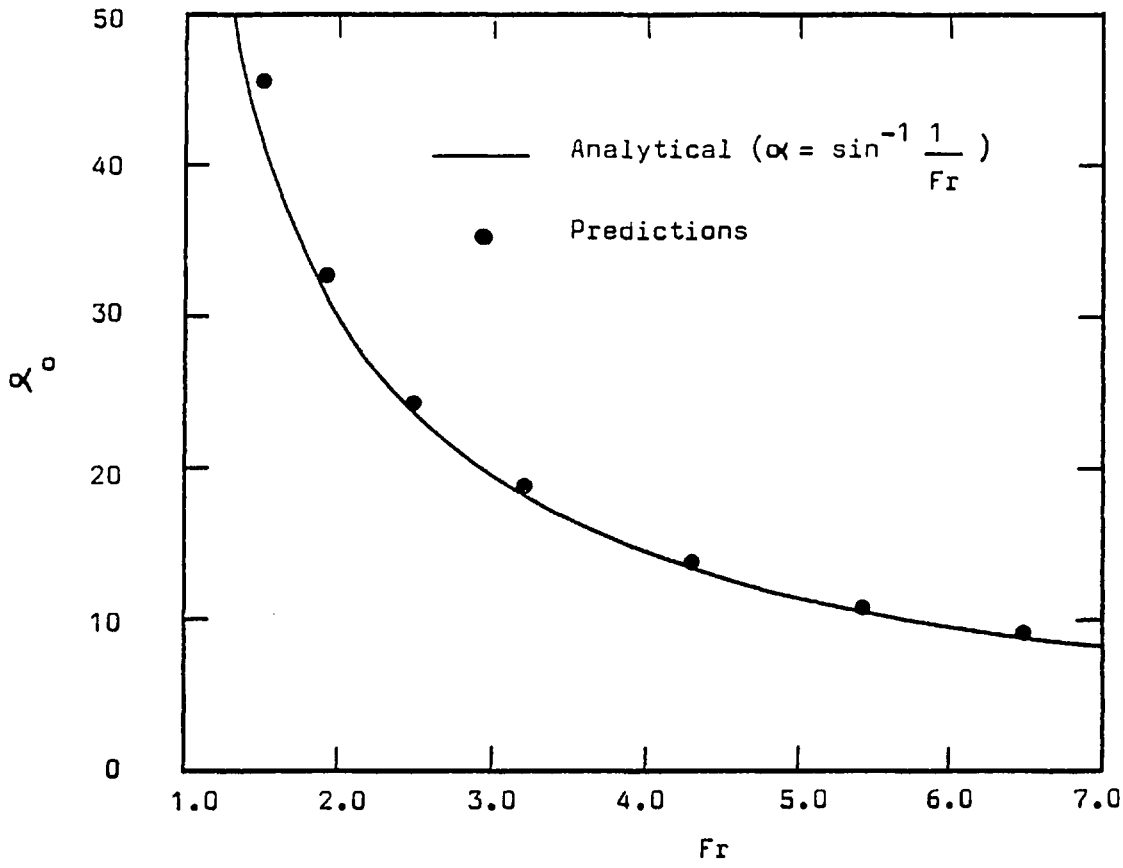
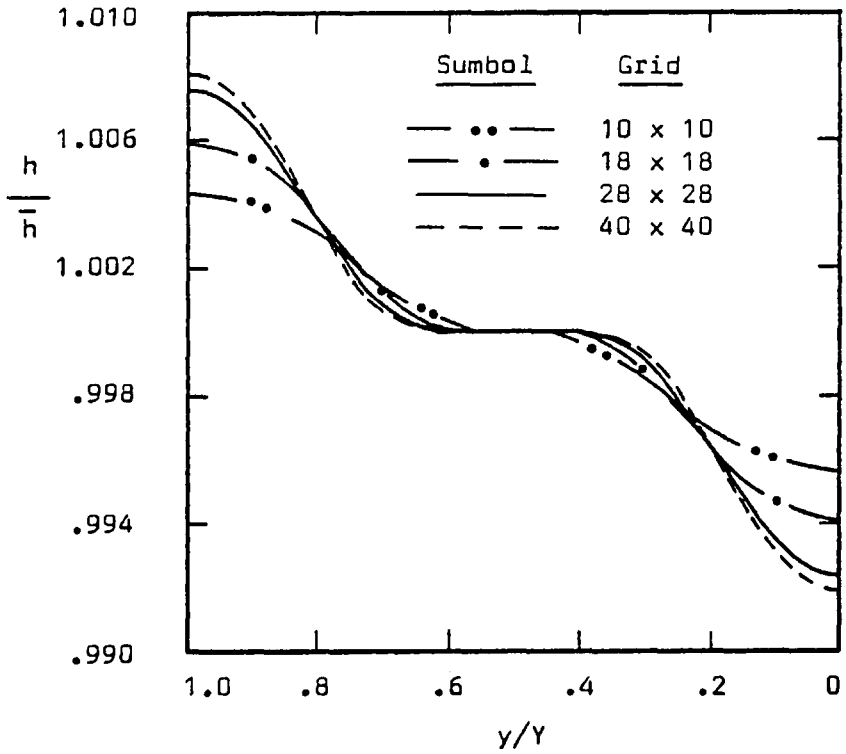
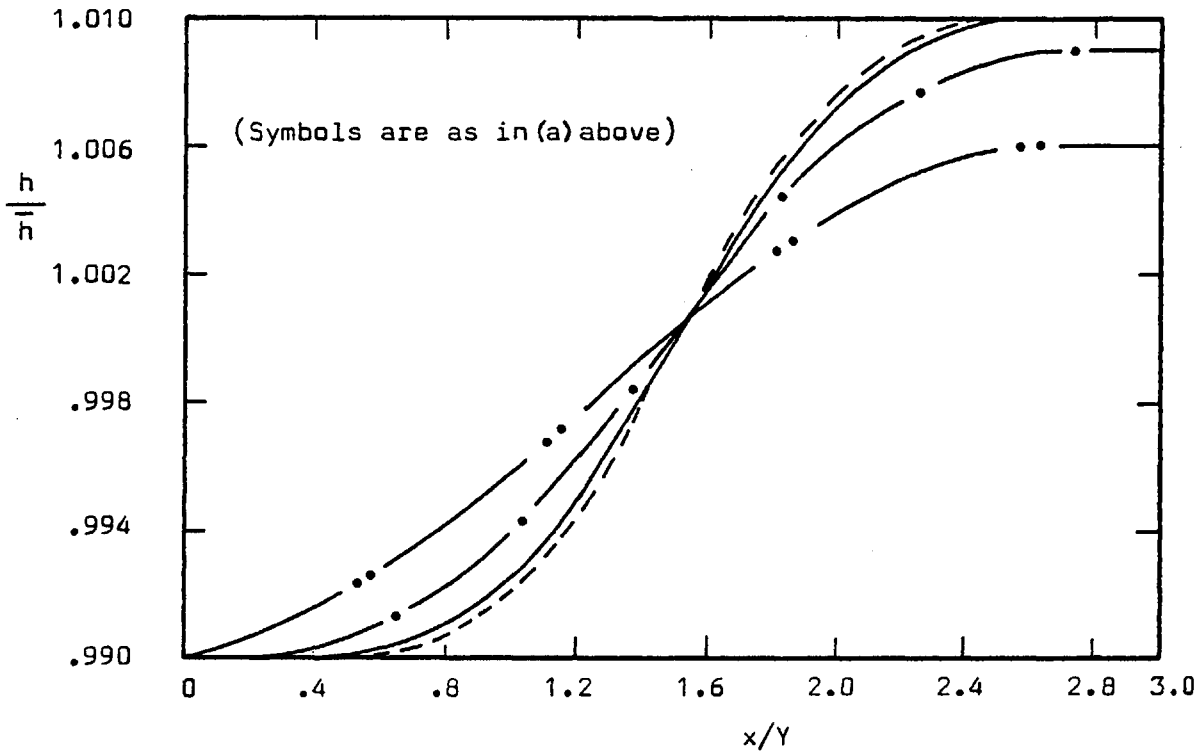


FIGURE 6.14 : DEPTH DISCONTINUITY; WAVE ANGLE VERSUS FROUDE NUMBER



(a) Cross-stream depth profile at x/Y = 1.0



(b) Depth profile along the bottom wall

FIGURE 6.15 : GRID-DEPENDENCE CHECK; SPREAD OF DEPTH DISCONTINUITY (Case 2, Fr = 3.19)

the two finer grids employed; namely, the 28 x 28 and 40 x 40 grids, give substantially grid-independent results as compared to the 18 x 18 and 10 x 10 grids.

6.4.6 Concluding Remarks

The agreement between computed and analytical solutions for the angles of spread of infinitesimal depth discontinuities is shown to be excellent. With reference to the objectives laid down in Section 6.4.1, it can be concluded that the numerical solution procedure is accurate when compared with analytical solutions for such simple and wholly supercritical flows.

6.5 SUPERCRITICAL FLOW PAST ABRUPT CHANNEL EXPANSIONS

6.5.1 Introduction

The objectives of this study are to validate the model and assess the accuracy of the numerical solution procedure for another wholly supercritical flow situation. The study is motivated by its importance in the design of hydraulic structures, and the availability of experimental data and solutions by the method of characteristics.

6.5.2 Problem Specification

(a) Flow situation

Figure 6.16(a) shows the geometry of the flow which simulates an

extreme case of a channel expansion represented by the abrupt expansion of the side walls. The channel is horizontal, straight and of rectangular cross-section. The overall length of the expansion is L; the expansion width is Y. A uniform stream, of velocity u_{in} and depth h_{in}, approaches the expansion from a channel of width b. Only one half of the physical domain is shown and solved for, due to symmetry of flow on either side of the centre-plane of the channel.

The variation in velocity and depth through such an expansion, i.e. abrupt and horizontal, will depend on the surface roughness of the channel floor and walls, the rate of flow, and the fluid properties. Under fluid properties, one should consider the density, specific weight, viscosity, and surface tension. Except in small channels, however, both viscosity and surface tension are of very minor importance, and the fluid properties then reduce to g, the gravitational acceleration. Accordingly, for given boundary conditions, the flow will depend solely upon the magnitude of the Froude number of the approaching stream ($Fr_{in} = u_{in} / (g\, h_{in})^{\frac{1}{2}}$).

For Froude number greater than unity, the depth then being less than the critical, an enlargement of the cross section will result in a reduction in mean surface elevation and a corresponding increase in mean velocity (this is in complete contrast to subcritical flows); the flow will also fail to follow the boundaries, leaving what is termed a "dry region" behind the expanding stream.

(b) Further analysis and relevant studies

The two expansion corners produce disturbances (wavelets) which cross the stream at characteristic angles, referred to as the wave

angles α, determined by the local values of Froude number ($\alpha = \sin^{-1}\frac{1}{Fr}$). The resulting pattern of interference, in the zone in which these wavelets intersect, will yield a rather complex variation in depth and velocity of flow.

If x and y are the longitudinal and lateral coordinates (measured from the expansion plane and the plane of symmetry, respectively, see Figure 6.16(a)) of a point of depth h, and if no other factors than the acceleration of gravity and boundary resistance are assumed to influence the flow, the depth of flow can then be described by the following dimensionless relationship:

$$\frac{h}{h_{in}} = f_1\left(\frac{x}{h_{in}}, \frac{y}{h_{in}}, \frac{b}{h_{in}}, Fr_{in}, C_f\right) \qquad .(6.19)$$

The depth of flow (h/h_{in}) may be determined, under certain conditions, by a rather laborious analysis of each element of the resulting pattern of interference in accordance with elementry wave theory (based on the continuity and momentum conditions applied to a unit length of the disturbance line, together with geometric relations obtained from a corresponding vector diagram), see for example Ippen (1950). The conditions that must be satisfied are:

(i) Constant specific head, regardless of the total number of differential wavelets traversed, this implies that the energy loss due to boundary resistance is negligible.

(ii) The channel walls are vertical and the floor is horizontal.

(iii) A wave angle α is equal everywhere to the local value of $\sin^{-1}\frac{1}{Fr}$.

(iv) Conditions of hydrostatic pressure distribution must be assumed at all points.

Rouse, et al (1951) have made the above assumptions for mapping the surface contours of the flow near the expansion point by means of a systematic graphical approach known as the method of characteristics. They have also conducted experimental measurements for such abrupt expansions, and the results were presented in the form of generalized surface contours. A small discrepancy was found between the measured contours and those obtained by the method of characteristics. This was attributed to the failure of the characteristics method to provide for any variation of the total head due to boundary resistance. (It should be emphasized here that the solution procedure presented in this thesis is not restricted to assumptions (i) and (ii) specified above. Furthermore, if a hydraulic jump is to form downstream, as a result of boundary curvature or by an increase in tailwater depth, the characteristics method would fail to predict such a situation).

(c) Available experimental data

Rouse, et al (1951) presented experimental measurements of the surface configuration at abrupt expansions. The expansion, 5 ft wide and 16 ft long, was covered with oiled hardboard and paved with finished concrete throughout. The plane of symmetry of the transition was assumed to be a channel side wall; this was made of glass for the purposes of exerting minimum resistance to the flow and to enhance observation. The flow entered the expansion through interchangeable nozzles yielding rectangular jets 0.4 ft by 0.4 ft, 0.3 ft by 0.6 ft, and 0.25 ft by 1.0 ft in cross section - that is, having width-depth ratios of 1, 2 and 4. Rates of discharge were such that flow at any inlet Froude number (Fr_{in}) from 1 to 8 could be established.

A functional relationship similar to that given by equation (6.19)

was reduced to the form:

$$\frac{h}{h_{in}} = f_2 \left(\frac{x}{b}, \frac{y}{b}, Fr_{in}, C_f \right) \qquad ,(6.20)$$

by combining the relative coordinate terms x/h_{in} and y/h_{in} with the initial width-depth ratio, b/h_{in} .

The above relationship assumes a hydrostatic-pressure distribution at all points. The fact that the flow near the corners of expansion fails to satisfy this condition is of minimal importance as long as the width to depth ratio (b/h_{in}) is large, e.g. in wide, shallow channels.

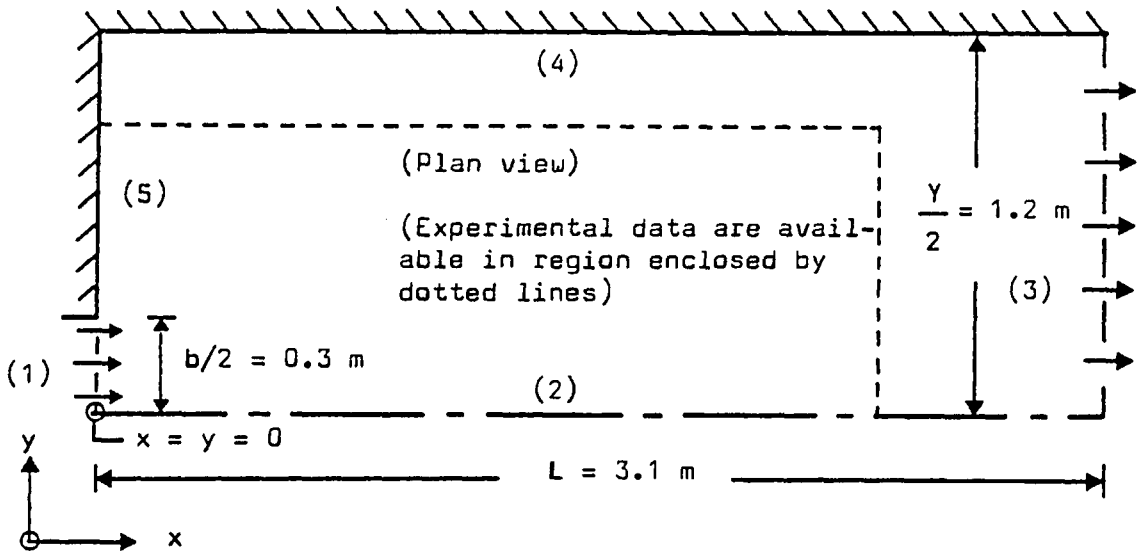
From their experimental results, the authors indicated that the axial locations of the surface contours were essentially a linear function of Fr_{in} . In other words, dividing all values of x/b by Fr_{in} should tend to superpose all equivalent contours for all Froude numbers. Equation (6.20) was thereby reduced to:

$$\frac{h}{h_{in}} = f_3 \left(\frac{x}{b\ Fr_{in}}, \frac{y}{b}, C_f \right) \qquad ,(6.21)$$

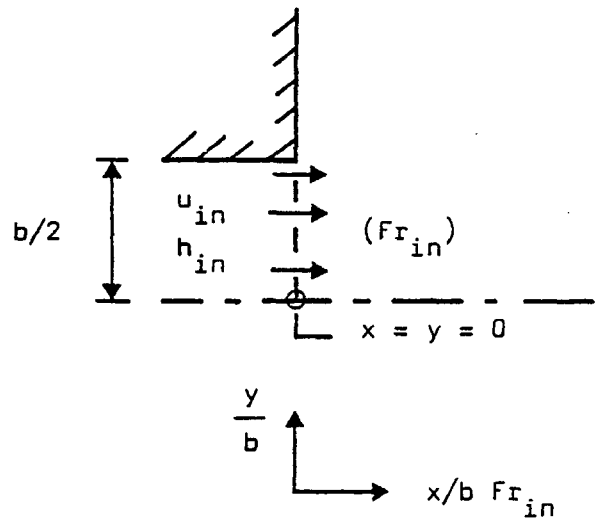
the generalized dimensionless coordinates are shown in Figure 6.16(b).

It was also established that the variation in specific head due to boundary resistance did not materially affect the results. This was also found in the present study when results obtained with different values of C_f were compared.

The experimental measurements of Rouse, et al were presented in the generalized diagram of dimensionless depth contours near the expan-



(a) Showing geometry, coordinates, and boundary conditions



(b) Generalized dimensionless coordinates

FIGURE 6.16 : FLOW SITUATION; SUPERCRITICAL FLOW PAST ABRUPT EXPANSION

sion corner and up to $x/b\ Fr_{in}$ = 2.0 and y/b = 1.5 (this area is enclosed within dotted lines in Figure 6.16(a)). These results will be presented along with the currently computed ones in Section 6.5.4.

(d) Flow parameters

The surface contours for the flow situation specified above are described by the functional relationship given by equation (6.21). The flow parameters for this study are chosen as follows (see Figure 6.16 a):

L = 3.1 m

$Y/2$ = 1.2 m

$b/2$ = 0.3 m

u_{in} = 1.72 m/s

h_{in} = 0.075 m

C_f = 0.001

The derived quantities are:

Fr_{in} = 2.0

$x/b\ Fr_{in}$ = 0.0 to 2.58

y/b = 0.0 to 2.00

b/h_{in} = 8.0 (width to depth ratio of approaching stream)

The value of C_f was chosen to correspond to the experimental smooth surfaces.

The task of this study is to compute, for the above parameters, the distribution of velocities and depth. These are to be compared with available experimental data of the dimensionless depth contours. A grid-dependence check is to be conducted together with a study of the effect of the empirical friction-factor employed.

6.5.3 Details of the Computations

(a) Equations solved

The equations solved are the continuity and the two momentum equations given by:

continuity

$$\frac{\partial}{\partial x}(hu) + \frac{\partial}{\partial y}(hv) = 0 \qquad .(6.22)$$

u-momentum

$$\frac{\partial}{\partial x}(h\,u^2) + \frac{\partial}{\partial y}(huv) = -gh\frac{\partial h}{\partial x} - C_f\,u\,(u^2+v^2)^{\frac{1}{2}} \qquad .(6.23)$$

v-momentum

$$\frac{\partial}{\partial x}(huv) + \frac{\partial}{\partial y}(h\,v^2) = -gh\frac{\partial h}{\partial y} - C_f\,v\,(u^2+v^2)^{\frac{1}{2}} \qquad .(6.24)$$

(b) Boundary conditions

The boundary conditions employed in the computations, for the flow geometry shown in Figure 6.16(a), are:

(1) Inlet plane : $u = u_{in}$ (uniformly distributed),
$v = 0.0$,
$h = h_{in}$ (uniformly distributed) .(6.25)

(2) Plane of symmetry : $\partial u/\partial y = v = \partial h/\partial y = 0$.(6.26)

(3) Exit plane : $\partial u/\partial x = \partial v/\partial x = 0$,
h is fixed at $h_{in}/10.0$.(6.27)

(4) Top wall : $u = v = \partial h/\partial y = 0$.(6.28)

(5) Side wall : $u = v = \partial h/\partial x = 0$.(6.29)

The top wall is located far away from the expansion point region, thus a fair comparison with the experimental data can be made. This also applies to the exit plane at which different values of depth were investigated and found to have no effect on the upstream region as long as the outlet conditions remain supercritical.

(c) Initial conditions

The depth field was filled initially with uniform values equal to h_{in} and appropriate average values were used for the u-velocity field. It was advantageous to start the solution with a non-zero v-velocity field; uniform arbitrary values of $0.01\ u_{in}$ were used.

(d) Finite-difference grid

Three different grids were used: 10 x 8 , 14 x 11 and 18 x 14 (in the x- and y-directions respectively). The grid lines were non-uniformly distributed in both directions. Generally, x-constant lines were more densely packed in the region just downstream from the inlet plane; the y-constant lines were less densely packed in the region near the top wall. As will be demonstrated, the 14 x 11 grid is adequate to ensure grid-independent results; this grid distribution is presented later.

(e) Other details

Typical computational details for a converged run are listed in Table 6.4.

VARIABLE	VALUE
Fr_{in}	2.00
C_f	0.001
Grid	14 x 11
Type of grid spacing	Non-uniform
Number of iterations	40
RELAXU, RELAXV, RELAXH, RELAXP	0.8, 0.8, 0.8, 1.0
Overall normalized continuity error	2.7 E-5
Max. h' normalized to h_{in}	7.5 E-5
Computer time in CDC 6600 seconds	3.4

TABLE 6.4 : COMPUTATIONAL DETAILS FOR SUPERCRITICAL FLOW PAST ABRUPT EXPANSION

6.5.4 Results and Discussion

All the results presented below are for the 14 x 11 grid and for a C_f value of 0.001, unless otherwise specified.

Figures 6.17 and 6.18 show the perspective views of surface elevation and the velocity-vector plot respectively. These figures display, very clearly, the overall features of a supercritical flow expanding past abrupt expansions. As the supercritical stream enters the expansion plane, it undergoes a gradual decrease in depth in both the x- and y-directions as evident in Figure 6.17. Corresponding changes in flow direction and velocity magnitudes are described qualitatively by the velocity-vector plot of Figure 6.18.

The top boundary of the calculation domain, which simulates a wall, was placed far away from the expansion corner; however, the computations were carried out for a distance downstream sufficient for the

expanding stream to meet this wall, and in doing so, the depth increases in this region as can be seen in Figure 6.17. This impingement would have created a reflected wave across the flow had the computations been carried out for a still longer channel. The depression in depth seen in the region near the top wall and the exit boundary is due to the prescription of a uniform exit depth there as a boundary condition. However, the magnitude of this boundary condition does not materially affect the upstream flow as long as conditions at the exit plane remain supercritical. Furthermore, the region of interest is well inside the flow boundaries and in which the experimental data are available (this is the region enclosed by dotted lines in Figure 6.16(a)).

Figure 6.19 shows the comparison between the predictions and experimental results of Rouse, et al for the dimensionless depth contours. The agreement is seen to be generally good. Figure 6.20 shows the computed stream-function contours, normalized to the inlet flow-rate, and contours of Fr_x. These contours represent clearly the expanding nature of the flow.

One of the interesting features of the flow is the presence of a "dry region" stretching behind the expanding stream; the computed values of velocities and depth are practically zero as compared to their mean values in the flow. This is realized by examining the previous figures discussed above.

6.5.5 Grid-Dependence Check

Figure 6.21 presents some results of a grid-dependence check for the three different finite-difference grids specified in Section 6.5.3(d). Figure 6.21(a) represents the depth distribution on two

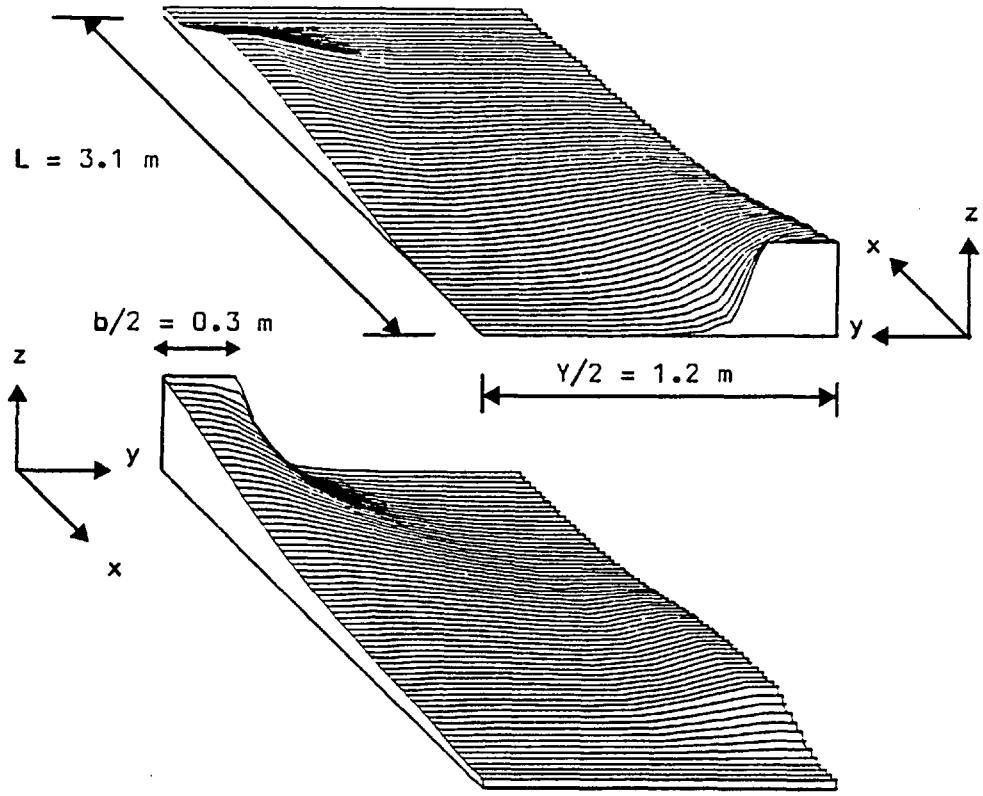


FIGURE 6.17 : PERSPECTIVE VIEWS OF SURFACE ELEVATION; SUPER-CRITICAL FLOW PAST ABRUPT EXPANSION, Fr_{in} = 2.0

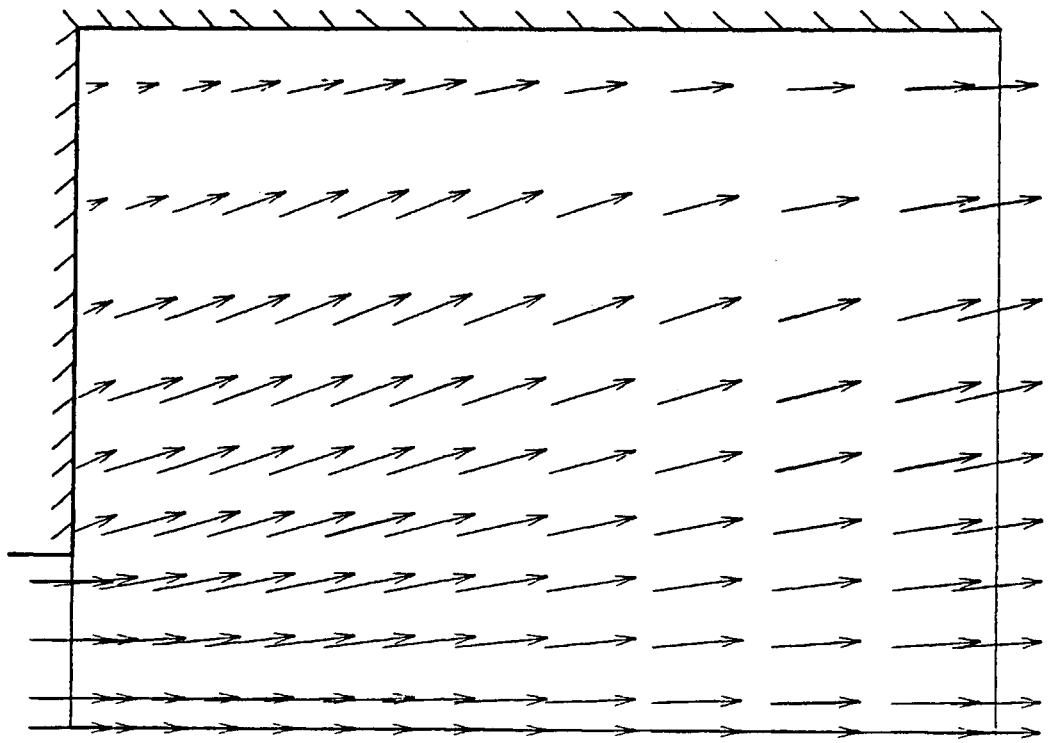


FIGURE 6.18 : VELOCITY-VECTOR PLOT FOR ABRUPT EXPANSION, Fr_{in} = 2.0

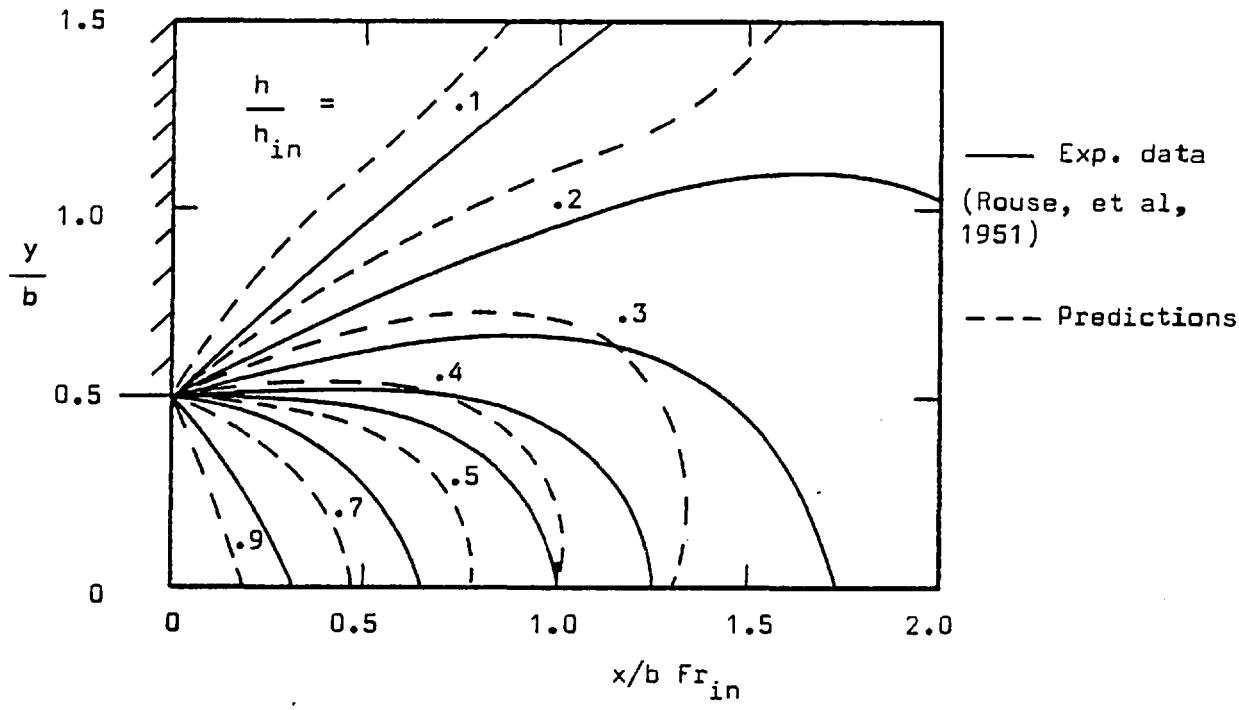


FIGURE 6.19 : DIMENSIONLESS DEPTH CONTOURS FOR ABRUPT EXPANSION; COMPARISON WITH EXPERIMENTAL DATA, Fr_{in} = 2.0

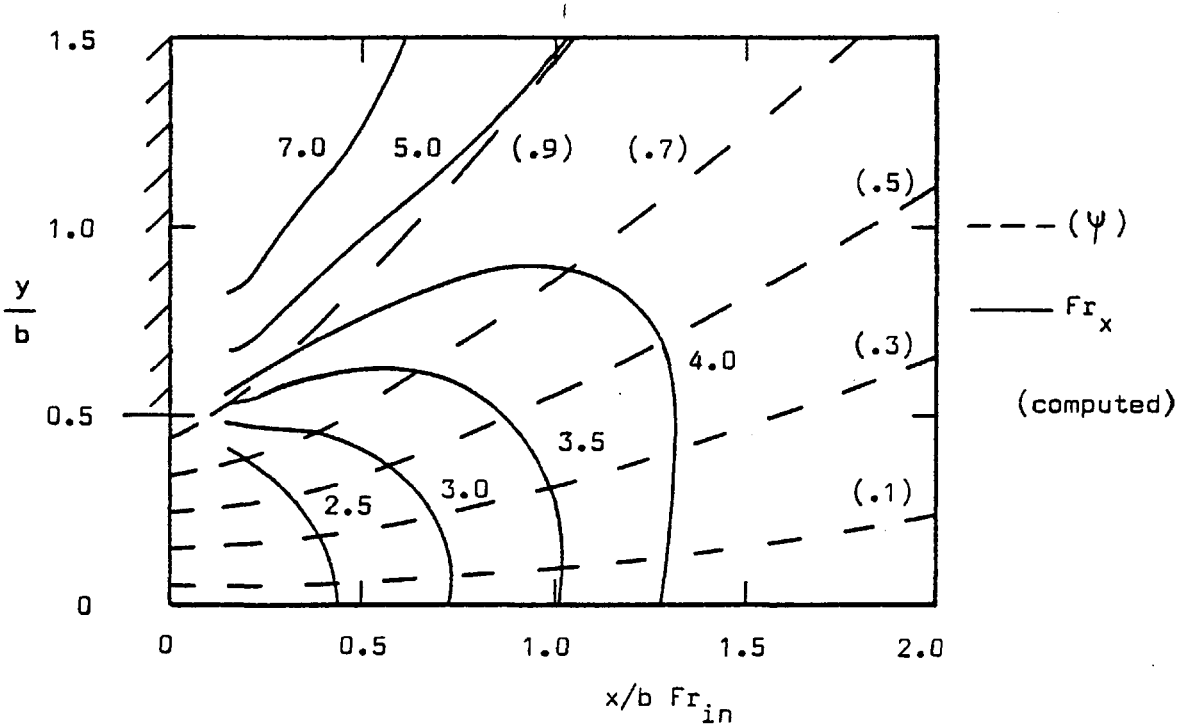
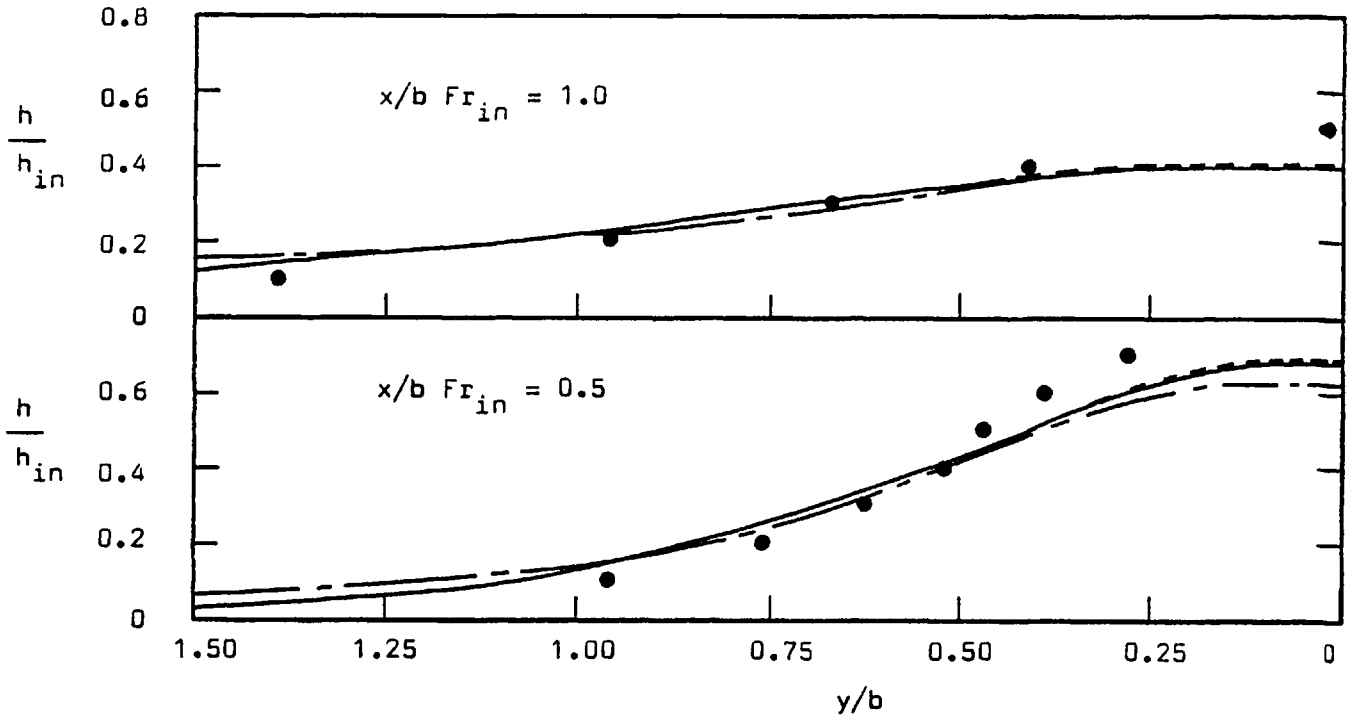
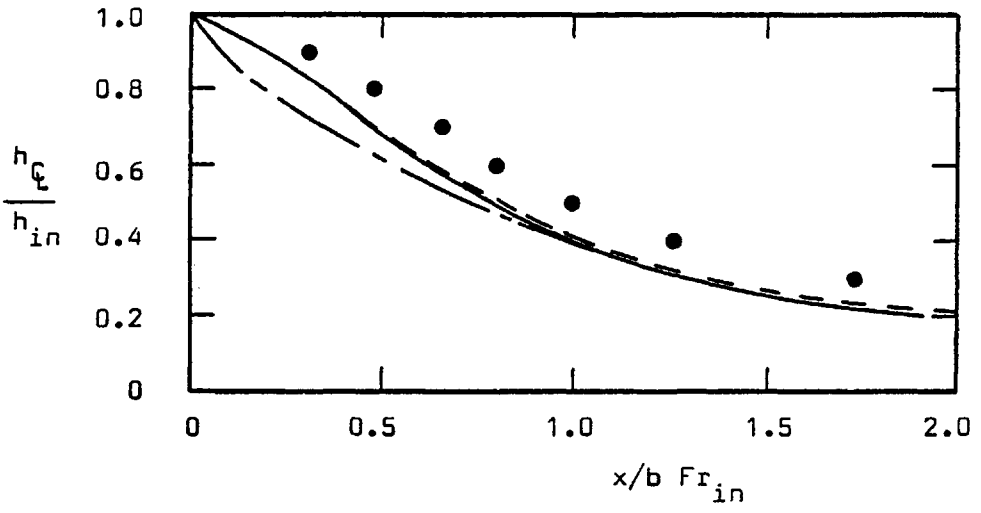


FIGURE 6.20 : NORMALIZED STREAM-FUNCTION CONTOURS AND Fr_x CONTOURS FOR ABRUPT EXPANSION, Fr_{in} = 2.0



(a) Depth distribution along two cross-stream stations



(b) Depth distribution along plane of symmetry

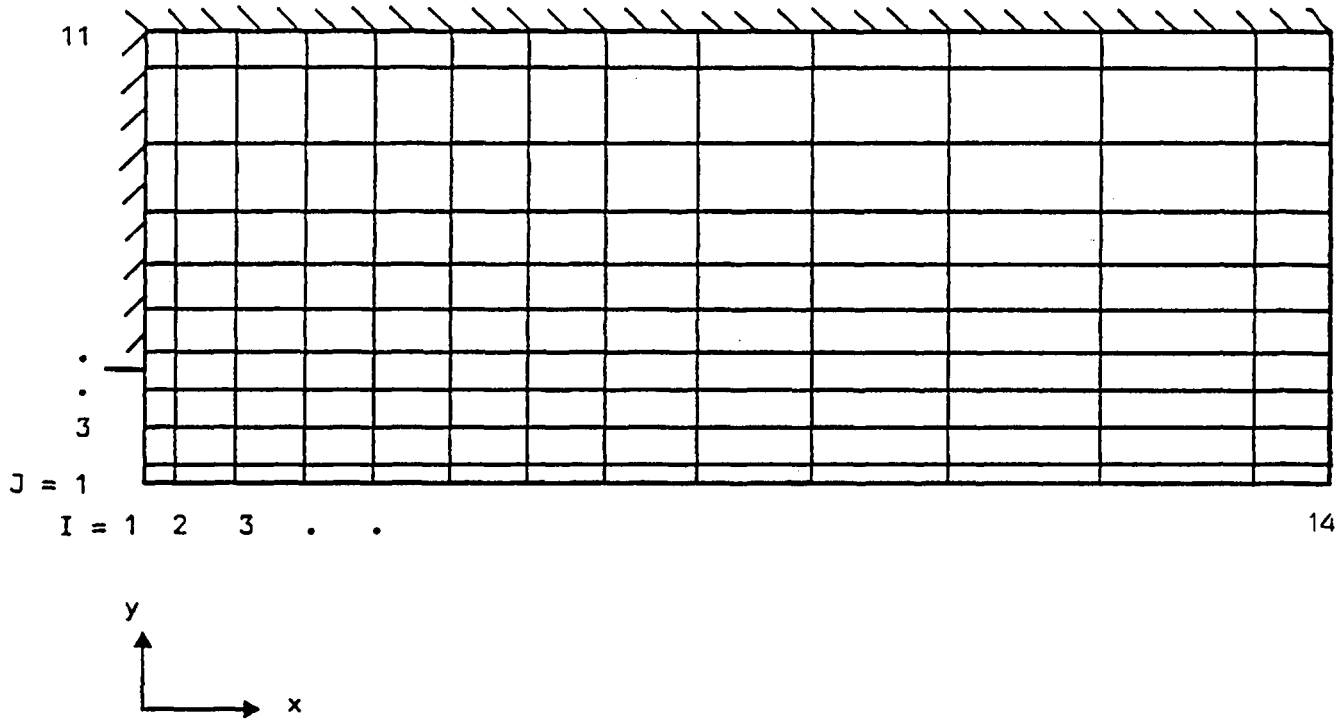
● Exp. data (Rouse, et al, 1951)

——— - ——— Predictions; Grid 10 x 8

——————— // ; Grid 14 x 11

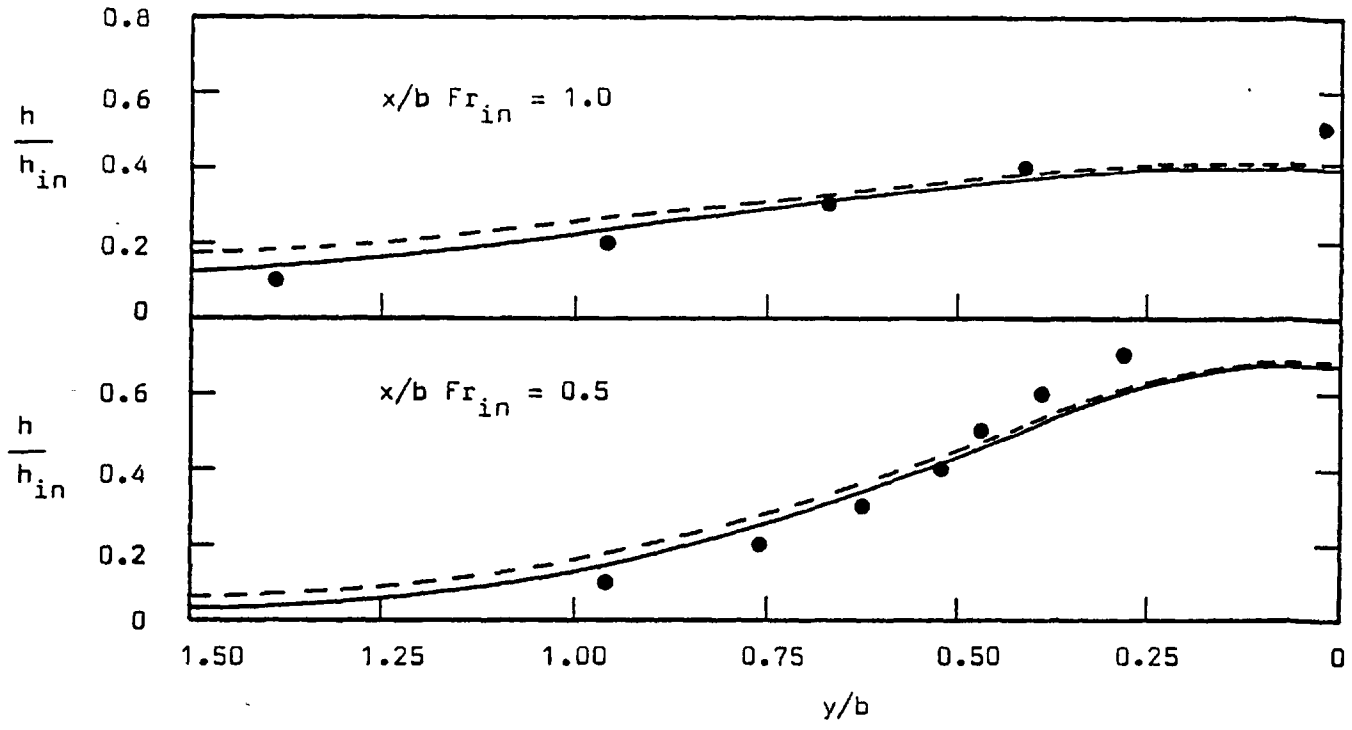
– – – – – – // ; Grid 18 x 14

FIGURE 6.21 : GRID-DEPENDENCE CHECK; ABRUPT EXPANSION

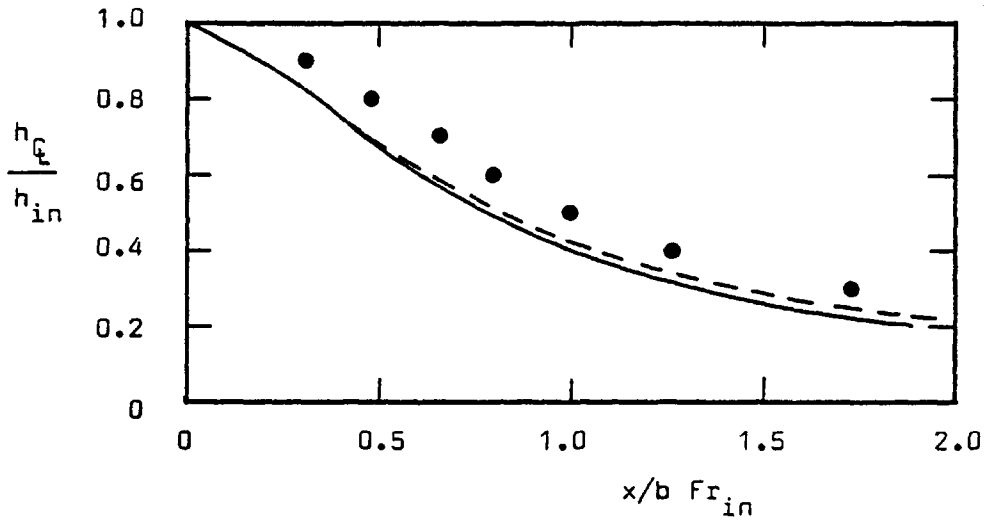


I	x	I	x	J	y	J	y
1	0.00	8	1.20	1	0.00	8	0.72
2	0.08	9	1.44	2	0.05	9	0.90
3	0.24	10	1.74	3	0.15	10	1.10
4	0.42	11	2.10	4	0.25	11	1.20
5	0.60	12	2.50	5	0.35		
6	0.80	13	2.90	6	0.46		
7	1.00	14	3.10	7	0.58		

FIGURE 6.22 : GRID USED TO PREDICT SUPERCRITICAL FLOW PAST ABRUPT EXPANSION



(a) Depth distribution along two cross-stream stations



(b) Depth distribution along plane of symmetry

● Exp. data (Rouse, et al, 1951)

——— Predictions; C_f = 0.001

– – – // ; C_f = 0.003

FIGURE 6.23 : FRICTION-FACTOR INVESTIGATION; ABRUPT EXPANSION

cross-stream stations together with the experimental data, whereas Figure 6.21(b) represents the depth distribution along the plane of symmetry. It is seen that the two finer grids employed; namely, the 14 x 11 and 18 x 14 grids, give substantially grid-independent results as compared to the coarser grid of 10 x 8.

Figure 6.22 shows the distribution of grid lines for the 14 x 11 grid.

6.5.6 Friction-Factor Investigation

The value of the friction factor (C_f), employed in the computations presented above, was 0.001; this corresponded to the smooth surfaces of the experiments conducted by Rouse, et al. These authors reported that the boundary resistance did not materially affect the results. This was proved to be correct by the present computed results, shown in Figures 6.23(a) and 6.23(b), which represent typical depth profiles for C_f of 0.001 and 0.003. The latter value corresponds to rough surfaces and has given, as expected, a slight increase in depth. It is interesting to note that the surface resistance is more effective on the flow in shallower regions and is shown by the slightly larger deviations of the dotted lines from the solid ones in such regions.

6.5.7 Concluding Remarks

The agreement between computed and experimental data for the supercritical flow past abrupt expansions is shown to be good. The surface resistance of the channel was shown to be an insignificant factor for such flow situations.

With reference to the objectives laid down in Section 6.5.1, it can be concluded that the numerical solution procedure is accurate in simulating such supercritical flows.

6.6 CLOSURE

In this chapter the numerical accuracy of the solution procedure and the physical realism of the predictions were examined for continuous flows and shown to be good. Four cases in all were considered; two cases were for wholly subcritical flows and the other two simulated wholly supercritical flows. Regarding the economy of the procedure, the computer time required for each case was very modest. These findings have lent confidence to the application of the model to more physically complex flow situations including hydraulic jumps.

C H A P T E R 7

PREDICTIONS TO COMPARE WITH EXPERIMENTAL RESULTS

7.1 INTRODUCTION

In Chapter 6, the numerical model was validated for a number of continuous flows. Further testing and application of the procedure to other continuous flow situations are considered here. However, the main purpose of this chapter (and the following one) is to validate the model and assess the accuracy of the numerical solution procedure applied to discontinuous flows, i.e. flows with hydraulic jumps.

The predictions presented in this chapter are compared to the results obtained from the experimental investigations described in Chapter 5. This helps to assess the physical realism of the model. Theoretical results also exist for the one-dimensional flow situation considered, and this further examines the accuracy of the procedure.

The present chapter consists of two main sections in which the computed results are presented and discussed. The first main section presents a study of the one-dimensional flow with hydraulic jumps, whereas the second main section considers the study of the two-dimensional supercritical flows and those with hydraulic jumps. The experimental results of Chapter 5 are further analysed here, and presented together with the predictions for comparison. The chapter finally closes with a summary of the main findings.

7.2 ONE-DIMENSIONAL STUDY

7.2.1 Introduction

The main objectives of this study are to apply and test the validity of the numerical model for solving one-dimensional flows with hydraulic jumps. The predictions are to be compared with the experimental data given in Section 5.2 and with some simple analytical relations considered in Section 7.2.2 (b).

7.2.2 Problem Specification

(a) Flow situation

The physical situation considered represents a one-dimensional supercritical flow entering from below a sluice gate and flowing along a straight, rectangular and horizontal channel (the geometry of the flow has been fully described in Section 5.2.2 and shown in Figure 5.1; the symbols are as used before). The flow then undergoes a hydraulic jump due to subcritical conditions prevailing at the exit boundary. The location and strength of this jump depend upon the flow parameters and the channel-surface resistance. The flow is, therefore, controlled by both upstream and downstream conditions. The upstream conditions are determined by the headwater depth (h_4 ; the depth on the upstream side of the sluice gate) and the height of the opening below the sluice (h_5), whereas the downstream conditions are determined by the tailwater depth (h_t).

In the supercritical flow region, the depth increases with distance along the channel (due to wall friction) and this is accompanied by a corresponding decrease in velocity and hence a decrease in Froude number.

The opposite flow behaviour is true in the subcritical region but with smaller changes since the friction effect is much less pronounced there. This flow behaviour is similar to that of compressible-gas flows with friction in a constant-area duct, or to isentropic flow in converging ducts, i.e. :

$$\partial h/\partial x > 0 \quad \text{and} \quad \partial u/\partial x < 0 \quad \text{for} \quad Fr > 1 \quad ,$$
$$\partial h/\partial x < 0 \quad \text{and} \quad \partial u/\partial x > 0 \quad \text{for} \quad Fr < 1 \qquad .(7.1)$$

The flow at a short distance from the sluice gate is characterized by the presence of the so called "vena contracra". As stated in Section 5.2.5, the depth below the gate (h_5) would not give a true representation of the inlet flow depth to the test section. A station was therefore chosen at 15 cm from the sluice and will be referred to as the inlet boundary. Variables, at this station, have been given subscript 3.

(b) Theoretical consideration

Analytical relationships can be derived to describe the basic physical characteristics of the hydraulic jumps, see for example Chow (1959, p. 393) or Sellin (1969, p. 55). Simple control-volume analysis across the jump, based on continuity and momentum equations, gives the following relation:

$$h_2 / h_1 = -0.5 + (0.25 + 2 (Fr_1)^2)^{\frac{1}{2}} \qquad ,(7.2)$$

where subscripts 1 and 2 represent the variable concerned before and after the jump respectively. The depths h_1 and h_2 are called the "conjugate" or "sequent" depths.

In the above analysis, the energy loss due to the shear force at

the channel walls is neglected since the channel length occupied by the jump is short in relation to the overall length. However, the energy lost in the jump using Bernoulli's theorem (given by the difference in the energies on either side) is:

$$\Delta E = E_1 - E_2 = h_1 + \frac{q^2}{2g\,h_1^2} - h_2 - \frac{q^2}{2g\,h_2^2} \qquad ,(7.3)$$

in which ΔE is the eddy loss and q is the discharge per unit width.

Equation (7.3) can be put in a simpler form, by substituting $(Fr_1)^2 = q^2/\,g\,h_1^3$ and using equations (7.2) and (7.3), as:

$$\Delta E = (\,h_2 - h_1\,)^3 \,/\, 4\,h_1\,h_2 \qquad .(7.4)$$

The height of the jump (h_j) is defined as:

$$h_j = h_2 - h_1 \qquad ,(7.5)$$

This can be put in a dimensionless function of Fr_1 as:

$$\frac{h_j}{E_1} = \frac{(\,1 + 8\,(Fr_1)^2\,)^{\frac{1}{2}} - 3}{(Fr_1)^2 + 2} \qquad .(7.6)$$

Remarks

- Since the physical characteristics of the jumps are functions of Fr_1, they can all be plotted against Fr_1, resulting in a set of characteristics curves. These will be presented later together with the experimental and computed results.
- It is to be emphasized that this simple analysis considers neither

the length of the jump nor the actual surface profile of the jump (the present numerical model, being a depth-averaged one, also suffers from such limitations as discussed in Chapter 4). For a detailed experimental study of these particular jump characteristics, see Bakhmeteff and Matzke (1936). It suffices to mention here that the length of the jump (L) lies within the limits $5 < L/h_2 < 6.5$ based on experimental results.

- These analyses provide the physical characteristics of the flow across the jump and hence can be used with methods of computing the surface profiles of different types to locate the position of a jump. These methods are based on empirical input and are tedious to conduct, see for example Chow (1959, Chapter 10). However, in the present study, the analytical locations of jumps are obtained by the jump relations and the computed supercritical surface profile.

(c) Experimental information

The experimental investigation described in Section 5.2 provided measurements of the surface profiles and locations of the hydraulic jumps for different tailwater depths and for different discharges. These were shown in Figure 5.2 and will be further analysed in Section 7.2.4 together with the computed results.

(d) Flow parameters

For a fixed opening height below the sluice gate (h_5), the flow is influenced by the tailwater depth (h_t), the headwater depth (h_4) and the channel-wall resistance factor (C_f). The flow parameters chosen are the same as the experimental ones and were listed in Table 5.1.

The values of C_f used in the present study are:

C_f = 0.003 for the channel bed (rough timber finish) ,

C_f = 0.001 for the side walls (glass).

A study of the effect of friction factor on the flow will be conducted.

The task of this study is to compute, for the above parameters, the elevations of the water surface and the distribution of velocities. The hydraulic-jump locations and the physical characteristics across the jumps are to be calculated from these predictions. These are to be compared with experimental and analytical results.

7.2.3 Details of the Computations

(a) Equations solved

The equations solved are the continuity and the u-momentum equations given by equations (6.22) and (6.23) in Section 6.5.3 (a). (The v-momentum equation is, of course, not solved, and the v's appearing in the continuity and u-momentum equations are set to zero).

(b) Boundary conditions

(i) Supercritical inlet : $u = u_3$,
$h = h_3$.(7.7)

(ii) Subcritical outlet : $h = h_t$.(7.8)

Remark

It is to be emphasized that the inlet for the computations is taken at 15 cm downstream from the sluice gate, so as to avoid the contraction in depth due to the presence of the "vena contracta".

(c) Initial conditions

The solution was started with the field variables filled with uniform values corresponding to those prevailing at the inlet, i.e. u_3 and h_3 for the u and h fields respectively.

(d) Finite-difference grid

In order to examine the effects of grid size on the solution, three different finite-difference grids were used for this investigation: 24, 46 and 72; all with uniform spacings. As will be demonstrated later, the 46 grid is adequate to ensure grid-independent results and give good resolution of the hydraulic jumps.

(e) Other details

No under-relaxation factors were needed; this is because the flow is simple and one-dimensional. However, the effect of the exit boundary conditions on the solution was "under-relaxed". Such a technique is discussed in Section 4.4.5 in which the final value of the tailwater depth (h_t) is reached after adding moderate successive increments (at the end of intervals of iterations) to the initial value of depth specified at the exit. For a typical study in which the maximum h_t was 5.9 cm, an increment of about 0.5 cm was used. This provided a parametric study in which converged solutions at different h_t were obtained in one single computer run.

In such computations, the hydraulic jump is initially found at the exit and then moves upstream as the solution progresses with further increase in h_t. Typical run information is presented in Table 7.1.

VARIABLE	VALUE
h_3	1.31 cm
q	1.823 E-2 m^2/s
$Fr_3 = q / (g\ h_3^3)^{\frac{1}{2}}$	3.88
h_t	4.46 cm
Grid	46 (uniformly spaced)
Number of iterations	100
RELAXU, RELAXH and RELAXP	1.0, 1.0 and 1.0
Overall continuity error normalized to inlet flow-rate	1.0 E-6
Max. h' normalized to h_3	2.3 E-3
Computer time in CDC 6600 seconds	8

TABLE 7.1 : COMPUTATIONAL DETAILS FOR ONE-DIMENSIONAL HYDRAULIC JUMPS

7.2.4 Presentation of the Results

All the results presented below are for the grid of 46 nodes and for C_f values of 0.003 and 0.001 (for the bed and side walls respectively), unless otherwise specified.

The results are presented in terms of elevations of the water surface and the characteristic curves of hydraulic jumps. Figure 7.1 shows the experimental points and the computed profiles of the water surface at varying tailwater depths and for a fixed discharge. The critical-depth line is shown as a dotted line (evaluated from $h_c \equiv (q^2/g)^{\frac{1}{3}}$). Figure 7.2 represents the physical characteristic curves of the jumps versus Fr_1 (Froude number at the toe of jumps) for the theoretical, experimental, and computed results. Figure 7.3 is constructed to show the variation of jump location with tailwater depth for

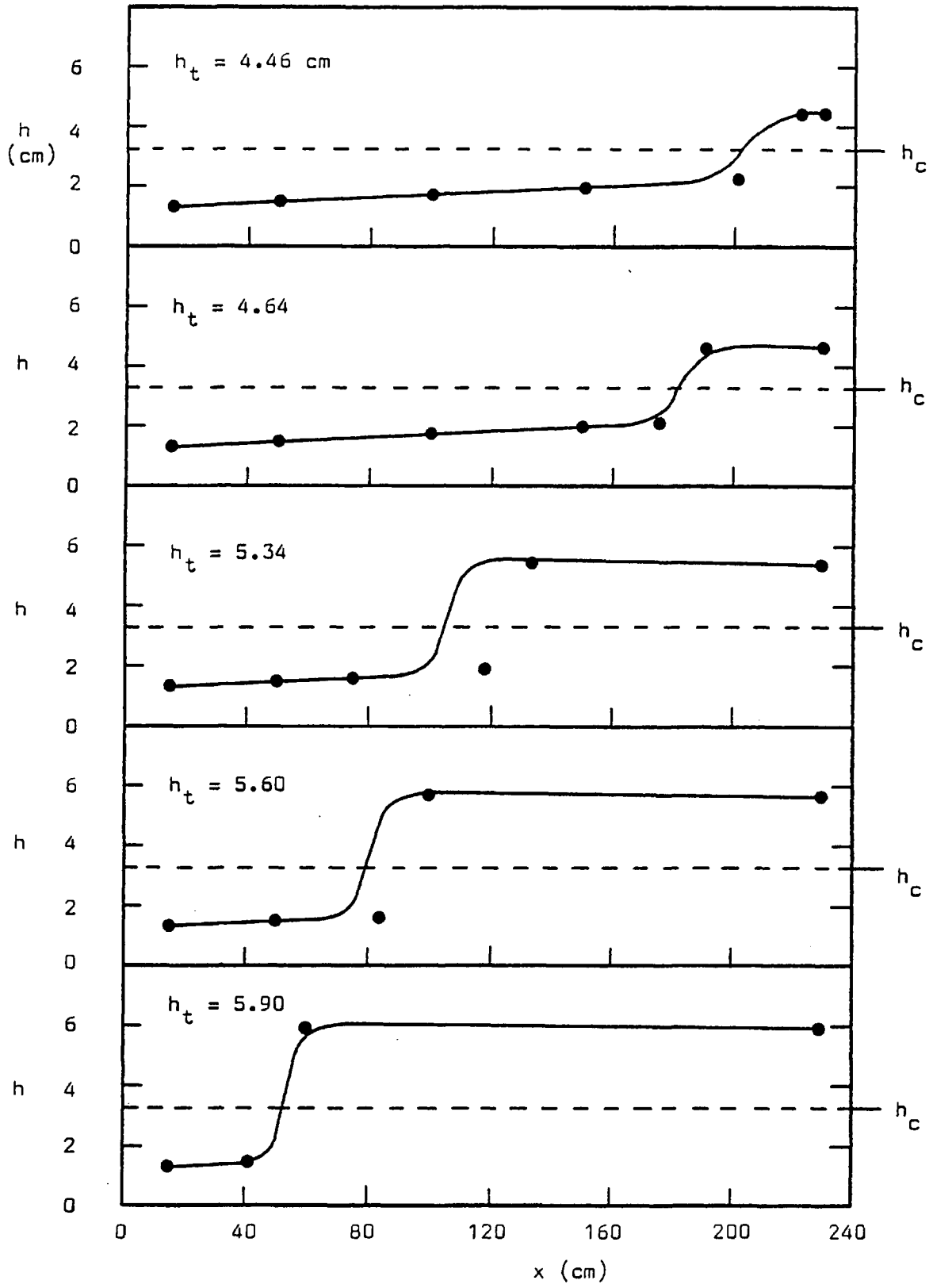
the fixed discharge problem.

The above results comprise Set 1 of the experimental investigation. Figure 7.4 presents the results for Set 2 in terms of the experimental points and the computed profiles of the water surface at varying discharges and for a fixed h_t . The critical-depth lines are also shown as dotted lines.

7.2.5 Discussion of the Results

The grid size and friction factors employed for this study have given good results as compared to both the experimental and analytical ones. In all the computed runs, the jumps were smeared over two or three grid nodes (as expected from any numerical scheme applied to discontinuous flows). However, for a sufficiently fine grid, as used here, the smearing will be much less and will only occupy a short length as compared to the overall length of the channel as evident in Figures 7.1 and 7.4. The computed surface profiles nearly coincide with the measured depth points in both the supercritical and subcritical regions. The surface-resistance effect on the flow is less pronounced in deeper regions than in shallower ones. Thus, in situations like the ones depicted in Figures 7.1 and 7.4, the depth of flow in a subcritical region decreases very little in the downstream direction, and can be considered to be practically uniform. The tailwater depth, therefore, can be considered to prevail over the whole of the subcritical flow region.

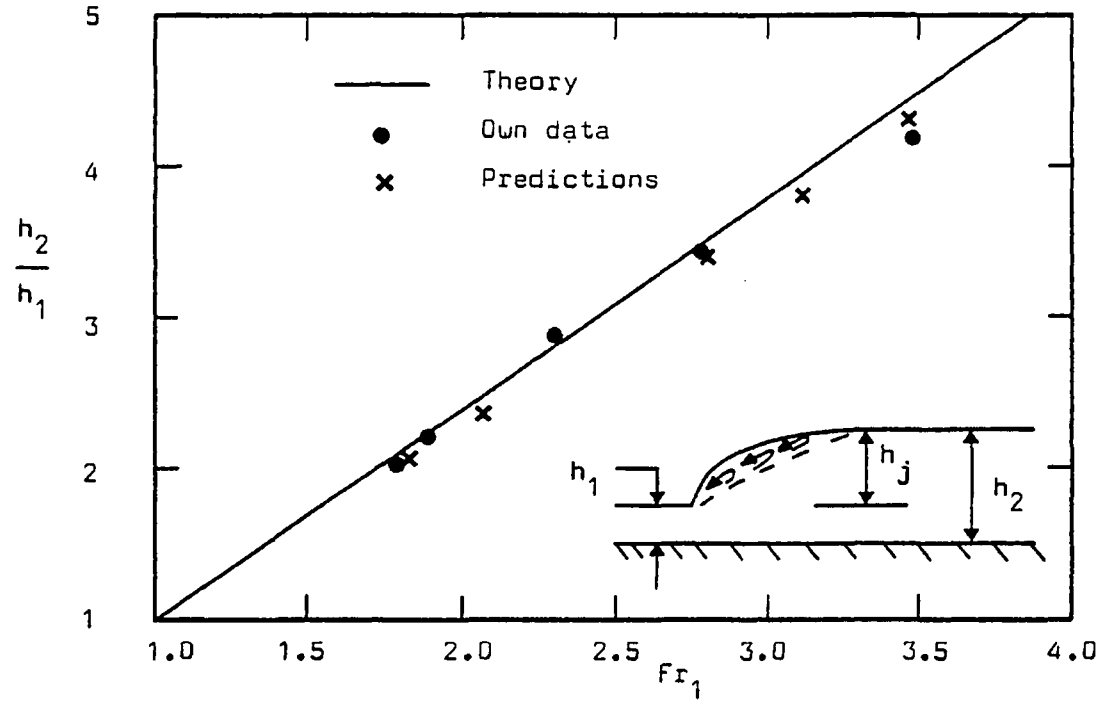
As far as the locations of hydraulic jumps are concerned, the computed results generally give good agreement with both the theoretical and measured ones. Figure 7.3 shows such comparisons for the fixed discharge problems. The computed locations seem to lie on the upstream side of the measured ones. It may be expected, therefore, that the



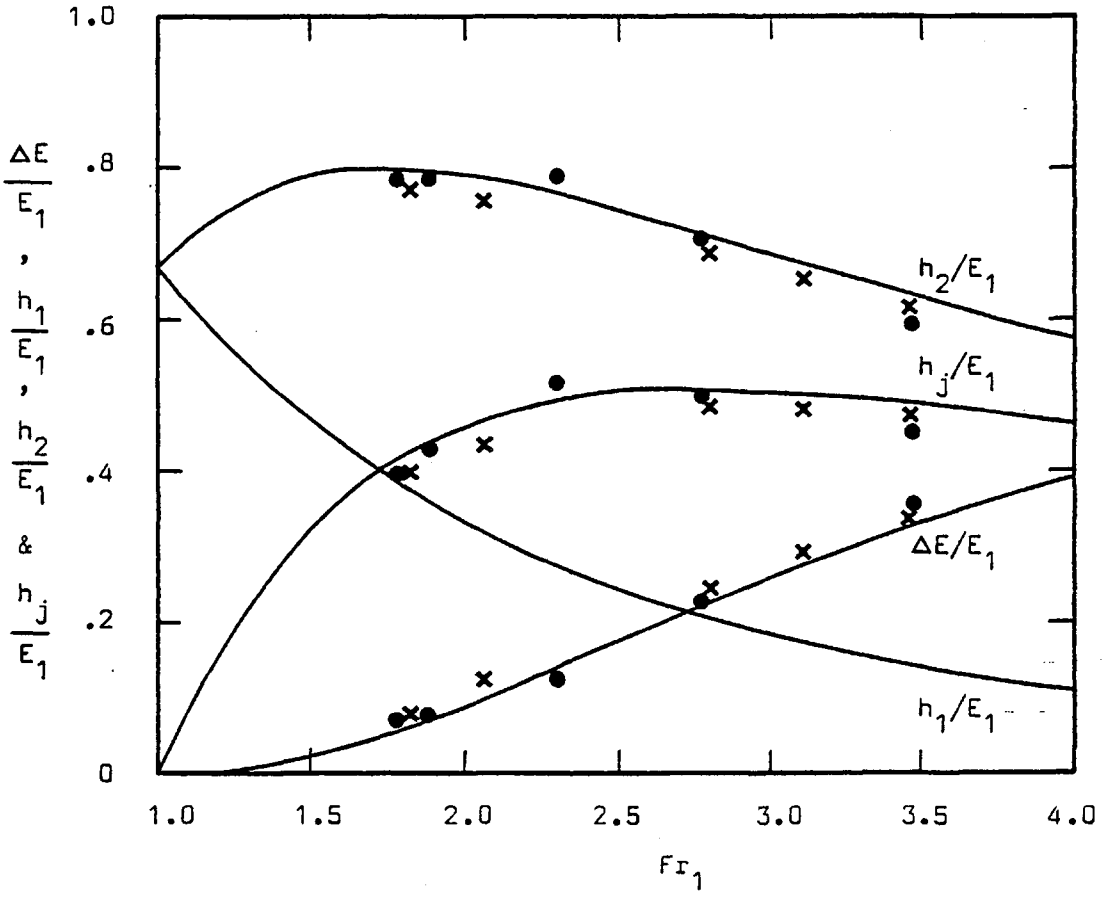
(h_3 = 1.31 cm, q = 1.823 E-2 m^2/s, Fr_3 = 3.88, C_f (bed) = 0.003)

● Own data
——— Predictions
– – – Critical-depth line

FIGURE 7.1 : WATER-SURFACE PROFILES OF 1D HYDRAULIC JUMPS AT DIFFERENT h_t AND FOR FIXED q

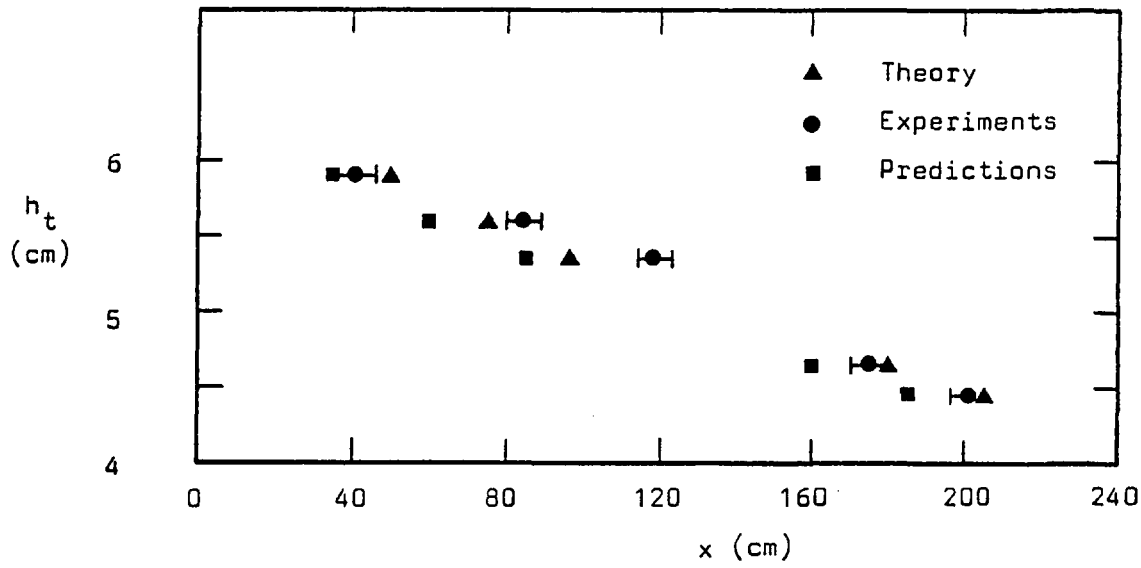


(a) Conjugate depths ratio versus Froude number



(b) Relative energy loss, initial depth, conjugate depth and height of jump versus Froude number

FIGURE 7.2 : CHARACTERISTIC CURVES OF HYDRAULIC JUMPS



h_3 = 1.31 cm (measured at x = 15 cm from sluice gate)

q = 1.823 E-2 m^2/s

Fr_3 = 3.88

C_f = 0.003 and 0.001 for bottom and side walls respectively

FIGURE 7.3 : LOCATIONS OF THE BEGINNING OF THE HYDRAULIC JUMPS VERSUS TAILWATER DEPTH

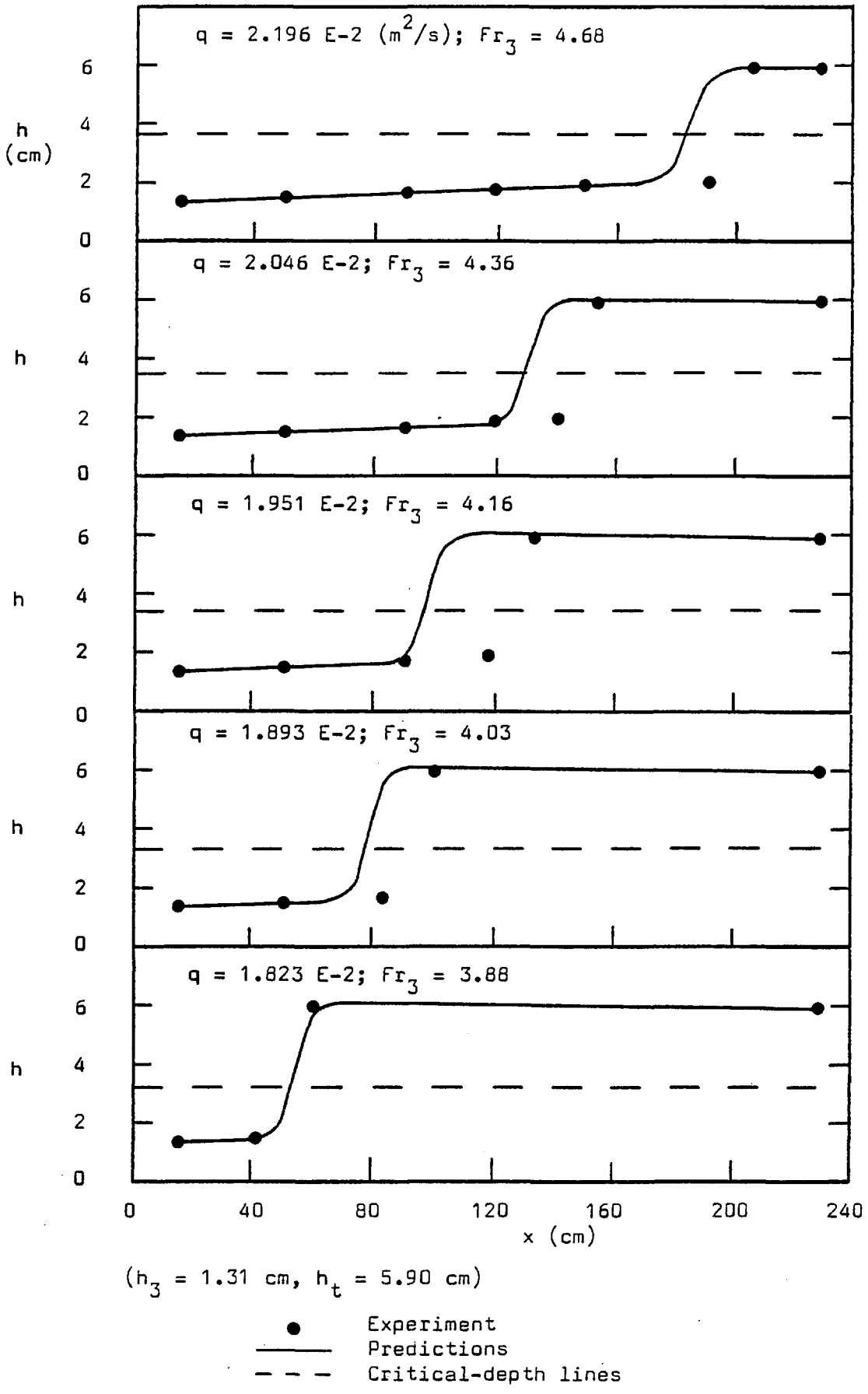


FIGURE 7.4 : WATER-SURFACE PROFILES OF 1D HYDRAULIC JUMPS AT DIFFERENT q AND FOR FIXED h_t

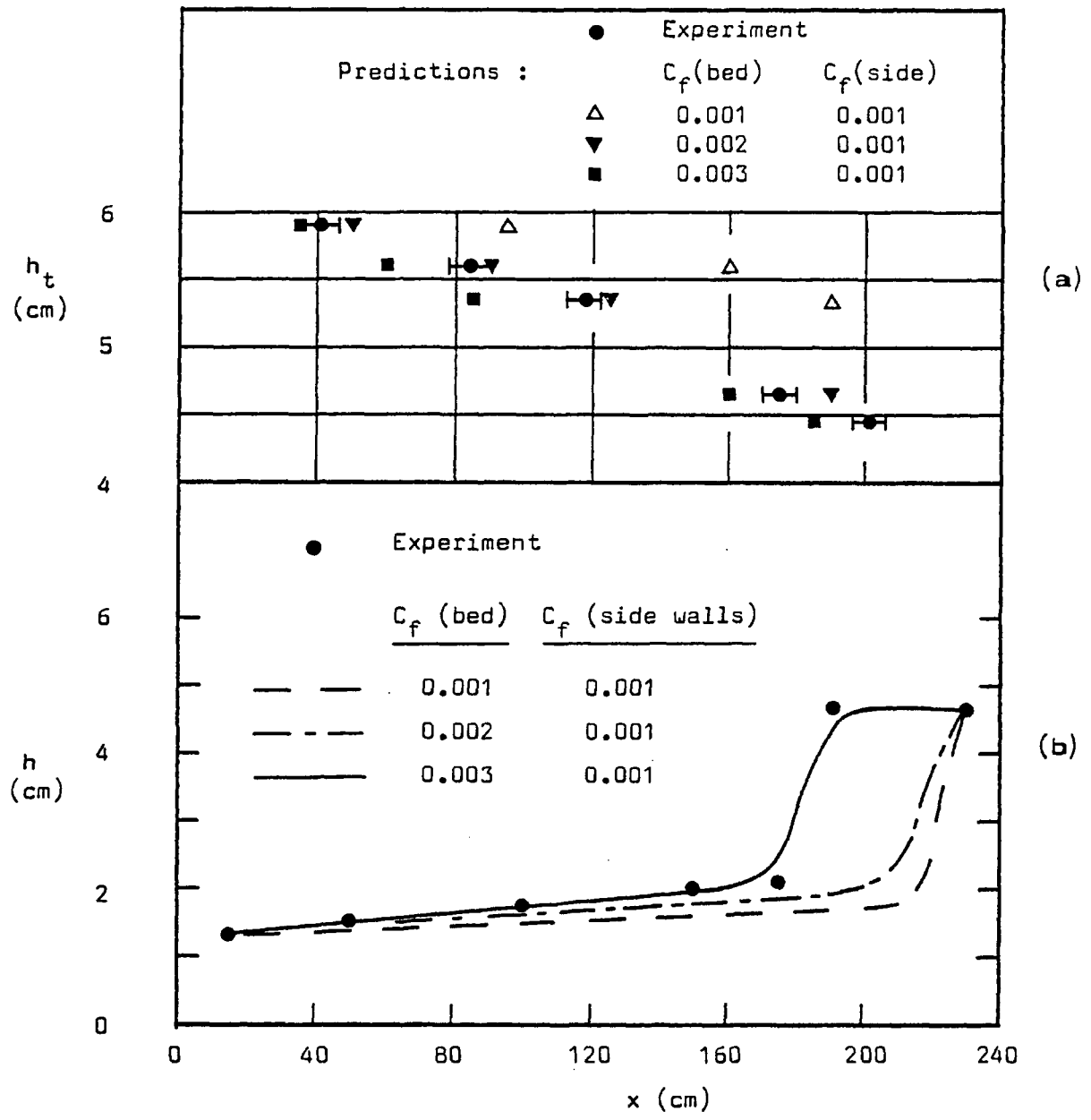
friction factors (C_f) used are a little overestimated. A study of this is conducted in Section 7.2.6. The discrepancy of the computed jump locations as compared to the theoretical ones may be due to the fact that both do not consider the length of the jump (strictly speaking, the theoretical locations shown in Figure 7.3 would have been pushed to the left (upstream side) had the jump lengths been considered). The figure emphasises the trend of all results in that as the tailwater depth increases, the jump moves towards the channel inlet.

The agreement of the results shown in Figure 7.2 (a) and 7.2 (b) of the computed, theoretical, and measured results for the characteristics of the jumps is good. The slight discrepancy in the theoretical curves is attributed to the fact that the theory does not include the surface-frictional losses in the analysis.

7.2.6 Friction-Factor Investigation

The values of C_f employed in the computations presented above, were 0.003 and 0.001 for the channel bed and side walls respectively. These values corresponded to the type of surfaces in the experimental flume. These values also proved to be correctly chosen since the computed results are in good agreement with the measurements. However, the frictional forces are the only forces present that affect the flow apart from, of course, the boundary conditions. It is, therefore, interesting to study the extent to which these factors would affect the surface profiles and the hydraulic-jump locations.

Figure 7.5 presents a typical study in which C_f for the side walls was kept fixed at 0.001 whilst for the channel bed was varied in the range 0.001 to 0.003. The investigations were carried out for Set 1 of the results, i.e. fixed discharge and for varying tailwater depths.



(h_3 = 1.31 cm, q = 1.823 E-2 m^2/s, Fr_3 = 3.88)

(a) Locations of the beginning of the hydraulic jumps versus tailwater depth

(b) Water-surface profile; h_t = 4.64 cm

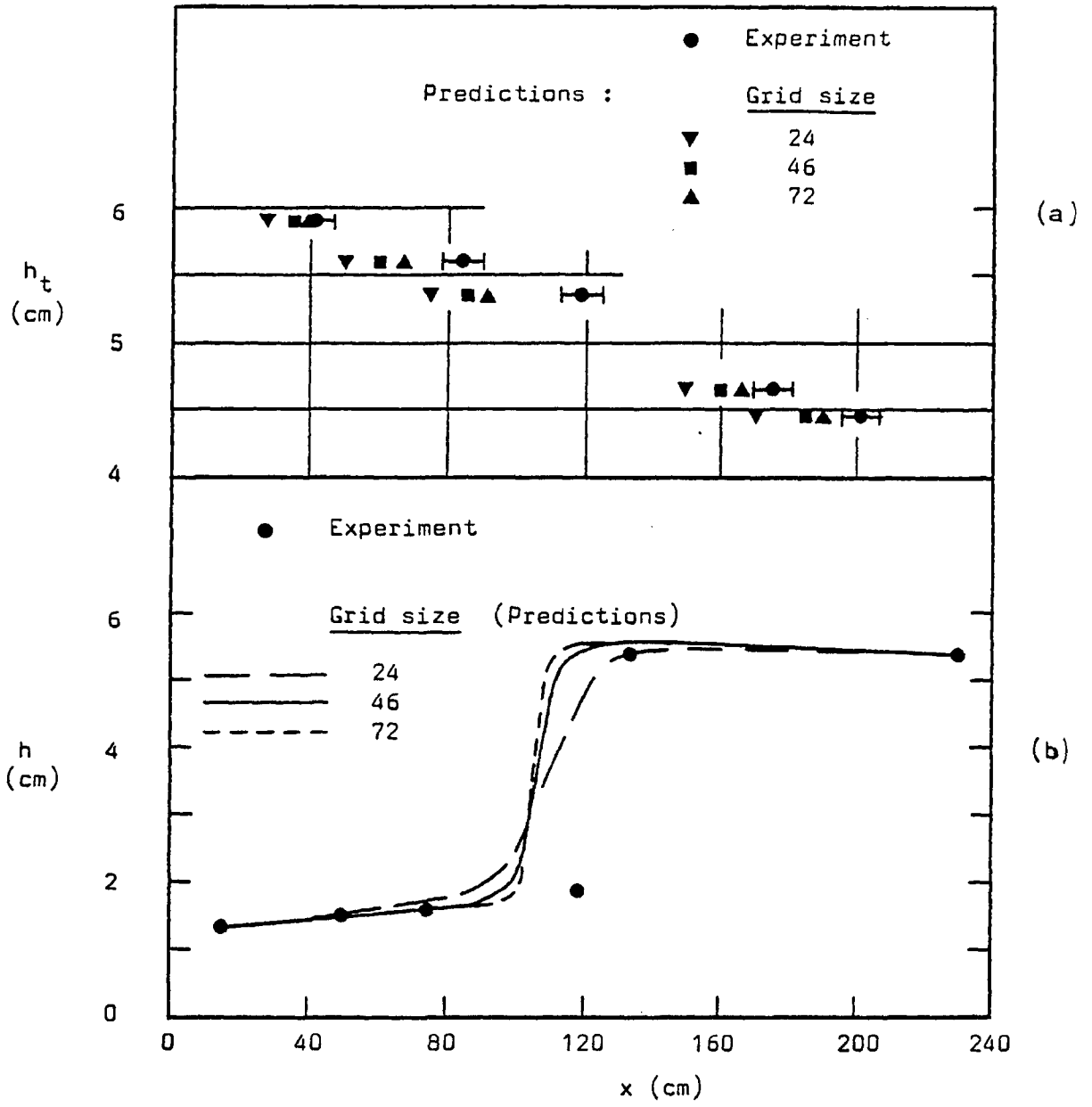
FIGURE 7.5 : FRICTION-FACTOR INFLUENCE FOR 1D HYDRAULIC JUMPS

It is expected that an increase in frictional resistance would increase the depth in the supercritical flow region and would push the jump locations upstream. Figure 7.5 (a) shows the influence of C_f (bed) on the locations of the beginning of the jumps for different h_t . It is seen that the C_f value of 0.001 has pushed the jumps downstream; for h_t less than about 5 cm, the jumps did not exist. The value of 0.002 has pushed the jumps slightly downstream, as compared to the value of 0.003, but has given as good agreement with the measured locations as the value of 0.003. However, the value of 0.003 has given the best resolution for the measured surface profiles as can be seen in Figure 7.5 (b).

It can be concluded from this study, that the friction factor plays an important role in the study of supercritical shallow and one-dimensional flows in channels. Correct estimation of the value of C_f employed, corresponding to the type of surface used, is important.

7.2.7 Grid-Dependence Check

Figure 7.6 presents some results of a grid-dependence check for the three different grids specified in Section 7.2.3 (d). Figure 7.6 (a) shows the locations of the beginning of the jumps for varying h_t , whereas Figure 7.6 (b) shows a typical surface profile for h_t = 5.34 cm. All these results belong to the constant discharge problems; the experimental measurements are shown for comparison. The two finer grids employed; namely, the 46 and 72 grids, give substantially grid-independent results as compared to the coarser grid of 24. This is clearly seen in Figure 7.6 (a) in which the computed results approach asymptotically the measured ones as the grid gets finer. The hydraulic jump will normally be smeared across two or three grid nodes; this smearing is substantially reduced by refining the grid as seen in Figure 7.6 (b). It is interesting to note



(h_3 = 1.31 cm, q = 1.823 E-2 m^2/s, Fr_3 = 3.88)

(a) Locations of the beginning of the hydraulic jumps versus tailwater depth

(b) Water-surface profile; h_t = 5.34 cm

FIGURE 7.6 : GRID-DEPENDENCE CHECK FOR 1D HYDRAULIC JUMPS

that the jump moves, through grid refinement, by a distance that lies within about twice the length of the finite-difference cells of the coarse grid. This length is the distance over which the jump is smeared.

No attempts have been made to refine the grid at the jump location only, since the same grid is used, in one single run, to compute for the different values of h_t . If, on the other hand, a single investigation is required in which the location of the jump is known roughly *beforehand, a rather coarse* grid but with a refined region at the jump location may be advantageous. Moreover, in such situations, a more accurate guess for the initial field values could probably be made.

7.2.8 Concluding Remarks

The agreement between computed, experimental and analytical results for one-dimensional flows with hydraulic jumps has been shown to be good. The surface resistance of the channel was shown to be a significant factor in affecting the flow. With reference to the objectives laid down in Section 7.2.1, it can be concluded that the numerical solution procedure is accurate in simulating such flow situations.

7.3 TWO-DIMENSIONAL STUDY

7.3.1 Introduction

The main objective of this study is to predict the experimental flow situation described in Section 5.3. The first part of the study involves calculations with supercritical conditions at the outlet; this further tests the accuracy of the numerical solution procedure to solve for wholly supercritical flows. The second part of the study then follows which involves calculations with subcritical conditions at the outlet; this tests the validity of the numerical model for solving two-dimensional flows with hydraulic jumps.

7.3.2 Problem Specification

(a) Flow situation

The physical situation simulates the merging of two supercritical streams entering from below sluice gates and flowing along a straight, rectangular and horizontal channel. The two streams are initially parallel to each other, flowing in the same direction and separated at the inlet by a thick wall. Conditions at the outlet boundary can be either supercritical or subcritical. The flow in either case is controlled by upstream conditions determined by the headwater depths ($h_{0,1}$ and $h_{0,2}$) and the height of openings below the gates (d_1 and d_2); it is also controlled, in the latter case, by downstream conditions determined by the tailwater depth (h_t).

The geometry of the flow has been described in Section 5.3.2 and shown in Figure 5.3. The flow characteristics have been discussed in Section 5.3.7.

(b) Experimental information

The experimental investigation described in Section 5.3 provided measurements of the water-surface elevations and locations of the hydraulic jumps for different tailwater depths and for different discharges. These were shown in photographs and perspective views in Figures 5.4 to 5.8, and will be further analysed and compared with the computed results in this section.

(c) Flow parameters

For fixed opening heights below the sluice gates (d_1 and d_2), the flow is influenced by the headwater depths ($h_{0,1}$ and $h_{0,2}$), the tailwater depth (h_t, for subcritical outlet conditions only) and the channel-wall resistance factor (C_f). The flow parameters chosen are the same as the experimental ones belonging to Runs 1 and 2 and were listed in Table 5.2. The value of C_f used in the present study is 0.001 which corresponds to the smooth surface of the flume. A study of the effect of friction factor on the flow will be conducted.

The task of this study is to compute, for the above parameters, the distribution of velocities and elevations of the water surface. The hydraulic-jump locations, if present, are to be calculated from these predictions. These are to be compared with the experimental results.

7.3.3 Calculations with Supercritical Outlet Conditions

7.3.3.1 Details of the Computations

(a) Equations solved

The equations solved are the continuity and the two momentum equations. These equations are identical to the equation set given by equations (6.22) to (6.24).

(b) Boundary conditions

The boundary conditions employed in the computations, for the flow geometry shown in Figure 5.3 (b), are:

(1) Inlet planes (Streams 1 & 2) : h's prescribed the measured values for each stream,
u's uniform, calculated to give the measured flow rate for each stream,
v's are zero.

(2) Side walls and separating wall : u's = v's = 0 ,
$\partial h/\partial y$ or $\partial h/\partial x = 0$.

(3) Exit plane : $\partial u/\partial x = \partial v/\partial x = 0$,
h's prescribed the measured values.

Remark

The inlet planes for the computations (i.e. x = 0) are where the separating wall terminates.

(c) Initial conditions

The depth and pressure fields were filled initially with uniform values equal to $(\bar{h}_{in,1} + \bar{h}_{in,2})/ 2$. Appropriate average values were used for the u-velocity field based on continuity. It was advantageous to start the solution with a non-zero v-velocity field; uniform values of $0.001\ \bar{u}_{in}$ were used.

(d) Finite-difference grid

Three different finite-difference grids were used to predict the experimental results of Run 1. The grid sizes were: 14 x 12, 22 x 20 and 48 x 29 (in the x- and y-directions respectively). The grid lines were uniformly distributed in the y-direction but were slightly expanding in the x-direction near the channel outlet. As will be demonstrated, the 22 x 20 grid is adequate to ensure grid-independent results; this grid distribution is presented later. A slightly longer channel length is considered when predicting the experimental results of Run 2. A grid of 30 x 20 with roughly the same distribution was employed.

(e) Other details

The full length of the experimental test section (3 m long) was not considered. The calculation domain extended a distance of 2.3 m for Run 1. This optimized the size of the finite-difference grids employed since there was no definite need to consider any further part of channel.

Typical computational details for a converged run are listed in Table 7.2.

7.3.3.2 Presentation of the Results

All the results presented below are for a grid of 22 x 20 and for a C_f value of 0.001, unless otherwise stated.

The results are presented in terms of depth profiles at various cross-stream stations together with the experimental measurements, for both Runs 1 and 2. Figure 7.7 shows such profiles for Run 1; whereas

VARIABLE	VALUE
$\bar{h}_{in,1}$ and $\bar{h}_{in,2}$ (cm)	3.09 and 5.52
$\bar{u}_{in,1}$ and $\bar{u}_{in,2}$ (m/s)	1.48 and 1.50
q_1 and q_2 (m^2/s) x 100	4.57 and 8.28
$\overline{Fr}_{in,1}$ and $\overline{Fr}_{in,2}$	2.68 and 2.04
C_f	0.001
Grid	22 x 20 (nearly uniformly spaced)
Number of iterations	120
RELAXU, RELAXV, RELAXH and RELAXP	0.5, 0.5, 0.5 and 0.5
Overall continuity error normalized to inlet flow-rate	5.9 E-5
Max. h' normalized to $\bar{h}_{in,1}$	1.5 E-4
Computer time in CDC 6600 seconds	33

TABLE 7.2 : COMPUTATIONAL DETAILS FOR PREDICTING RUN 1 OF THE 2D EXPERIMENTS WITH SUPERCRITICAL OUTLET CONDITIONS

Figure 7.8 presents, for the same run, both the computed and measured depth distribution along the channel side walls. The computed velocity-vector plot and the stream-function contours (normalized to the overall inlet flow-rate) are displayed in Figures 7.9 (a) and 7.9 (b). The cross-stream depth profiles for Run 2 are shown in Figure 7.10; the corresponding depth distribution along the channel side walls are presented in Figure 7.11.

7.3.3.3 Discussion of the Results

The results presented above clearly display the features of the flow behaviour. At the end of the separating wall, the two supercritical

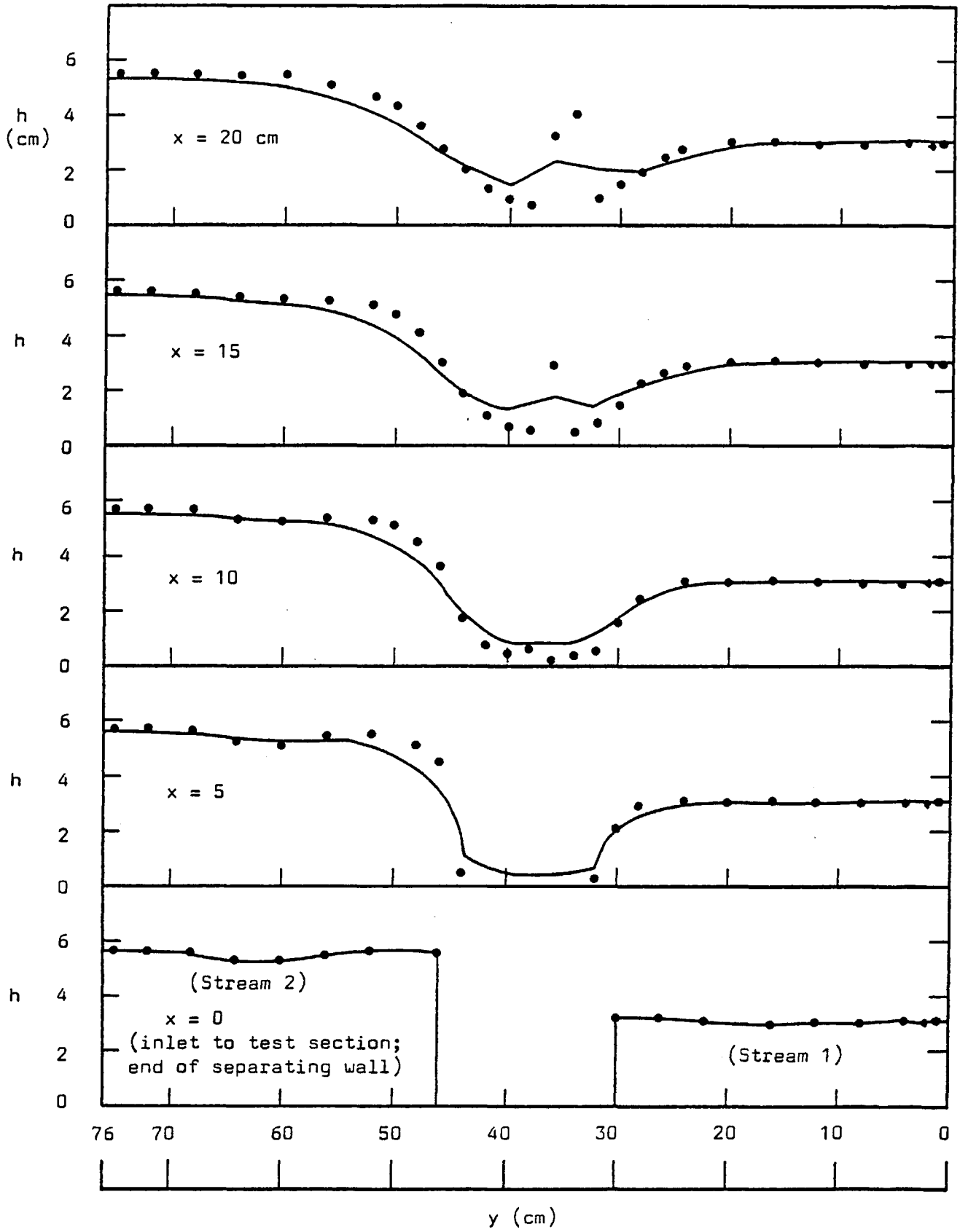


FIGURE 7.7 : CROSS-STREAM DEPTH PROFILES FOR RUN 1

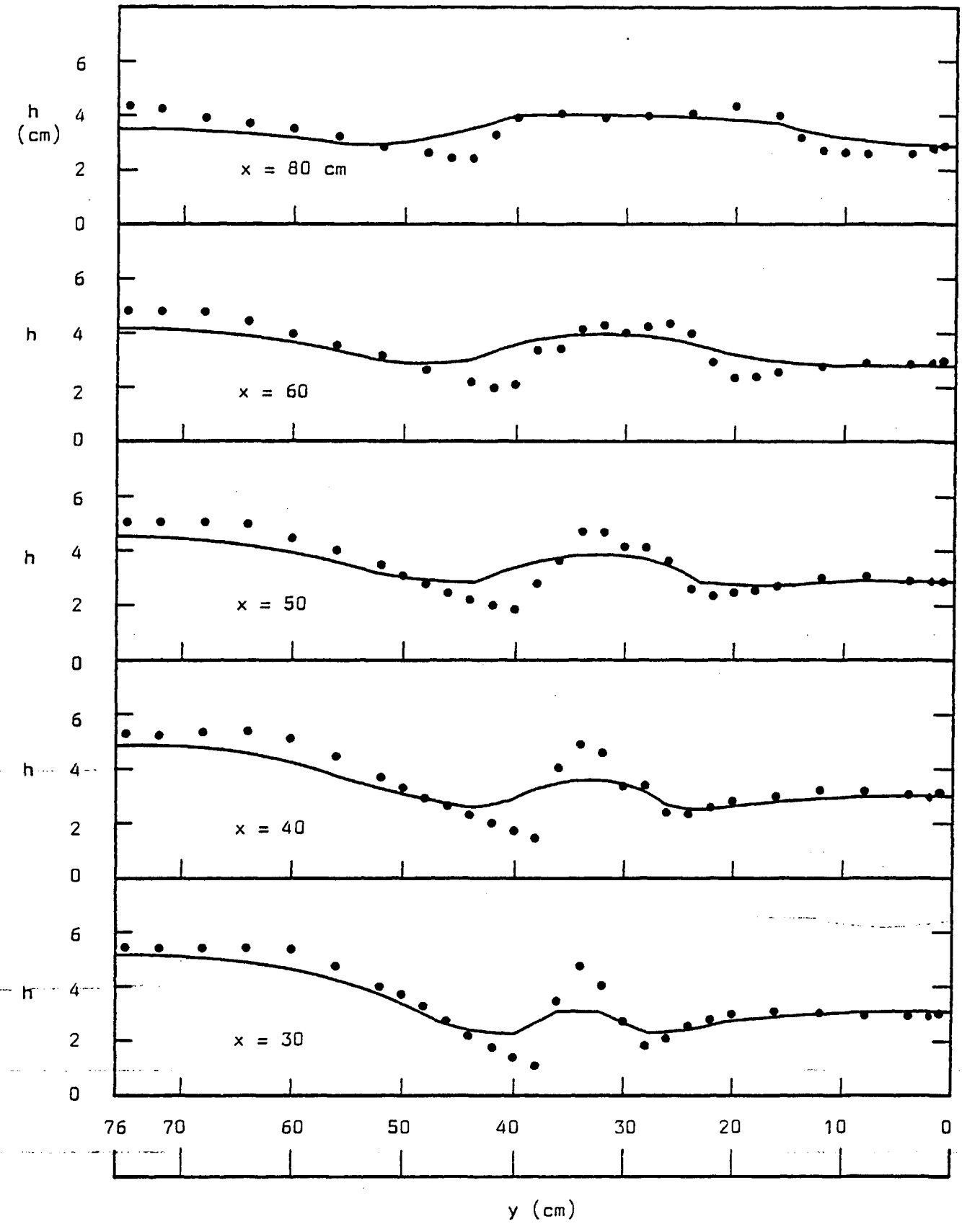


FIGURE 7.7 : (Continued)

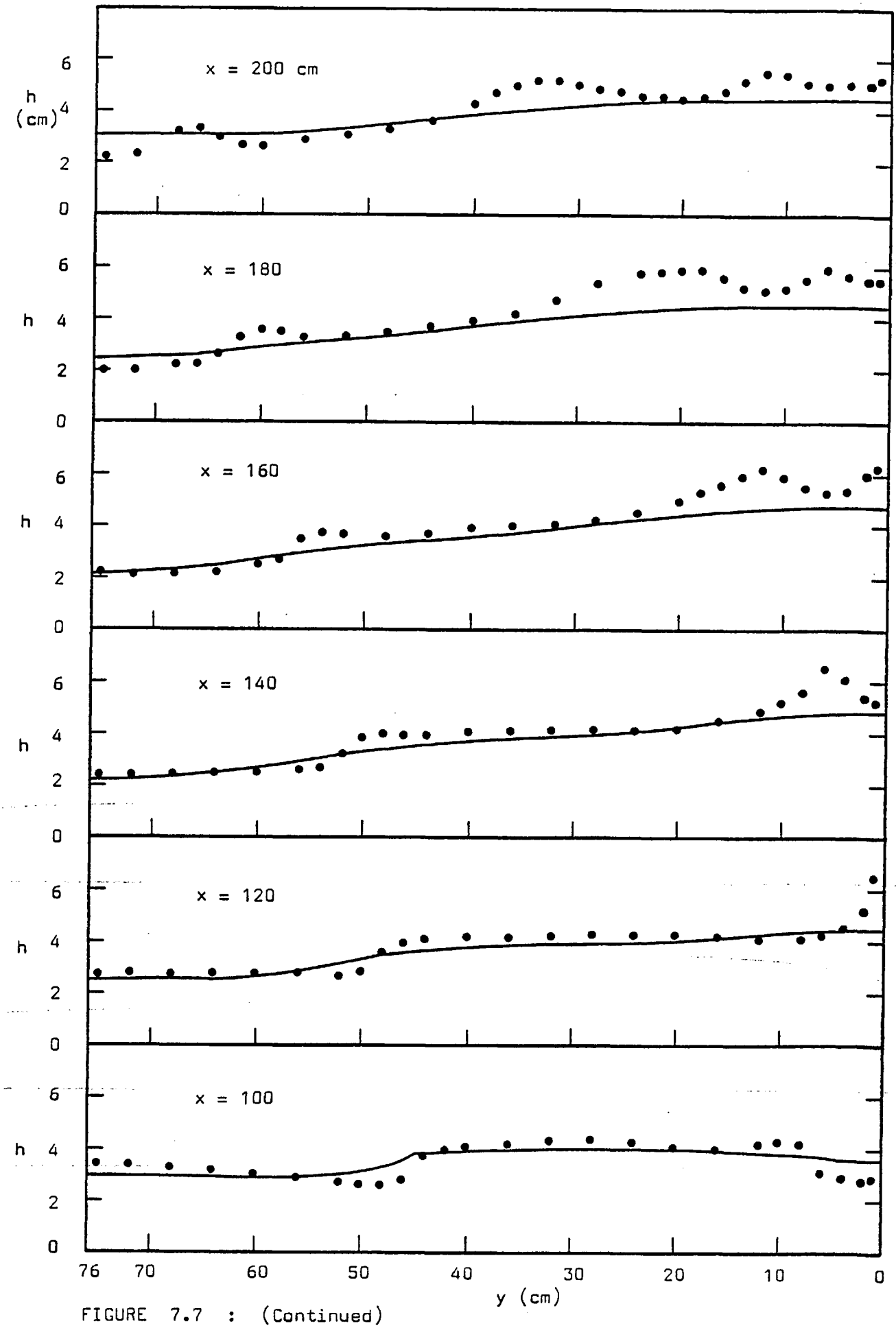


FIGURE 7.7 : (Continued)

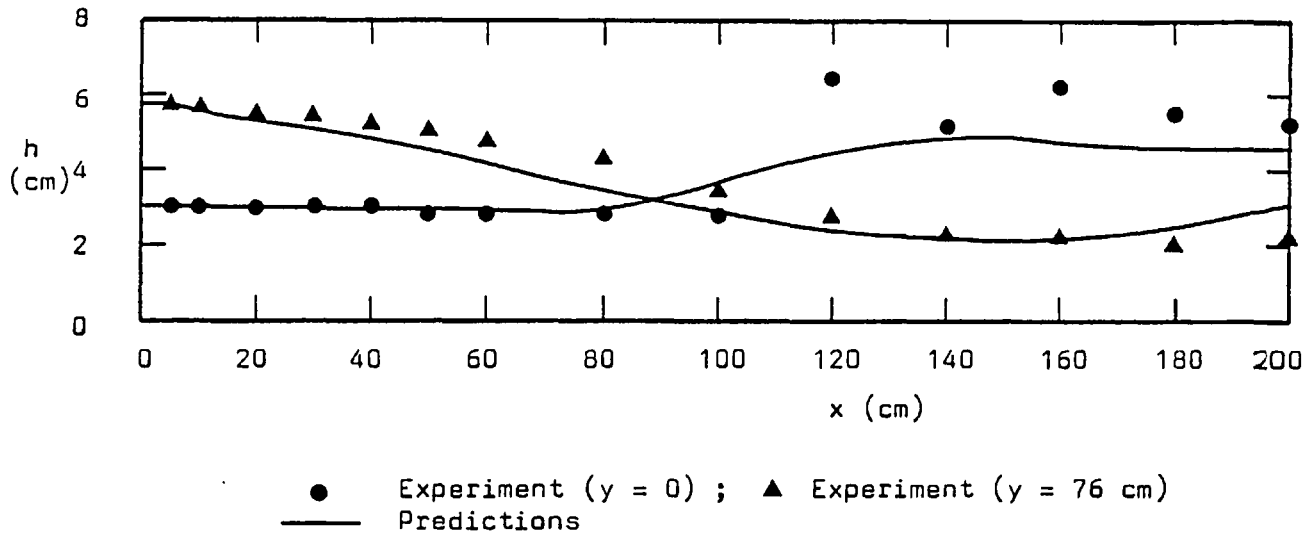
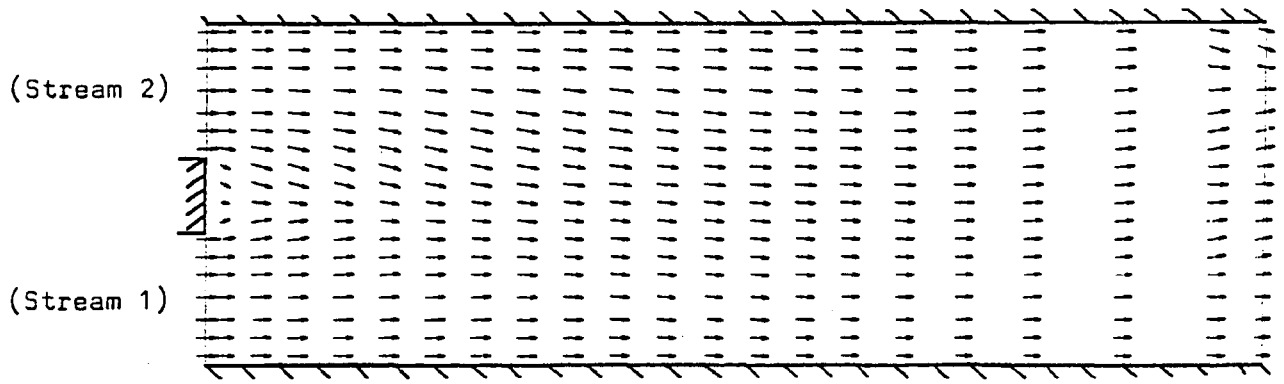
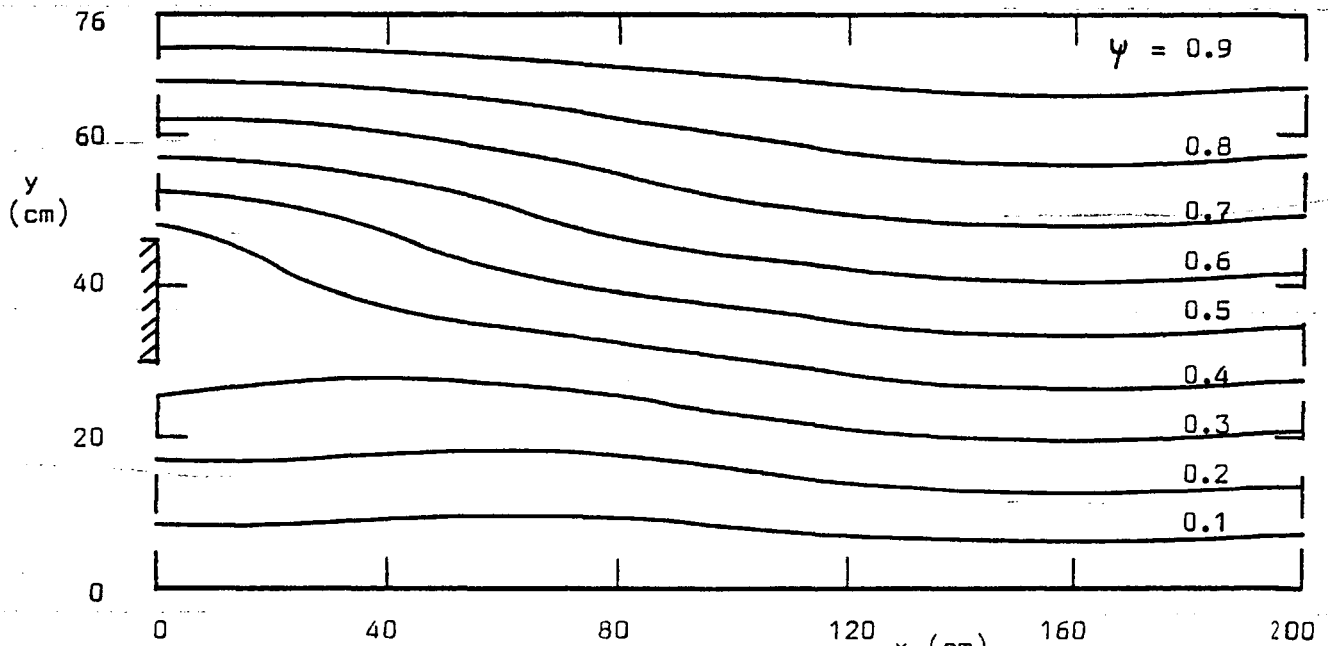


FIGURE 7.8 : DEPTH DISTRIBUTION ALONG THE SIDE WALLS FOR RUN 1



(a) Velocity-vector plot

(b) Stream-function contours



$(\overline{Fr}_{in,1} = 2.68 \ , \ \overline{Fr}_{in,2} = 2.04)$

FIGURE 7.9 : COMPUTED VELOCITY-VECTOR PLOT AND STREAMLINES FOR RUN 1

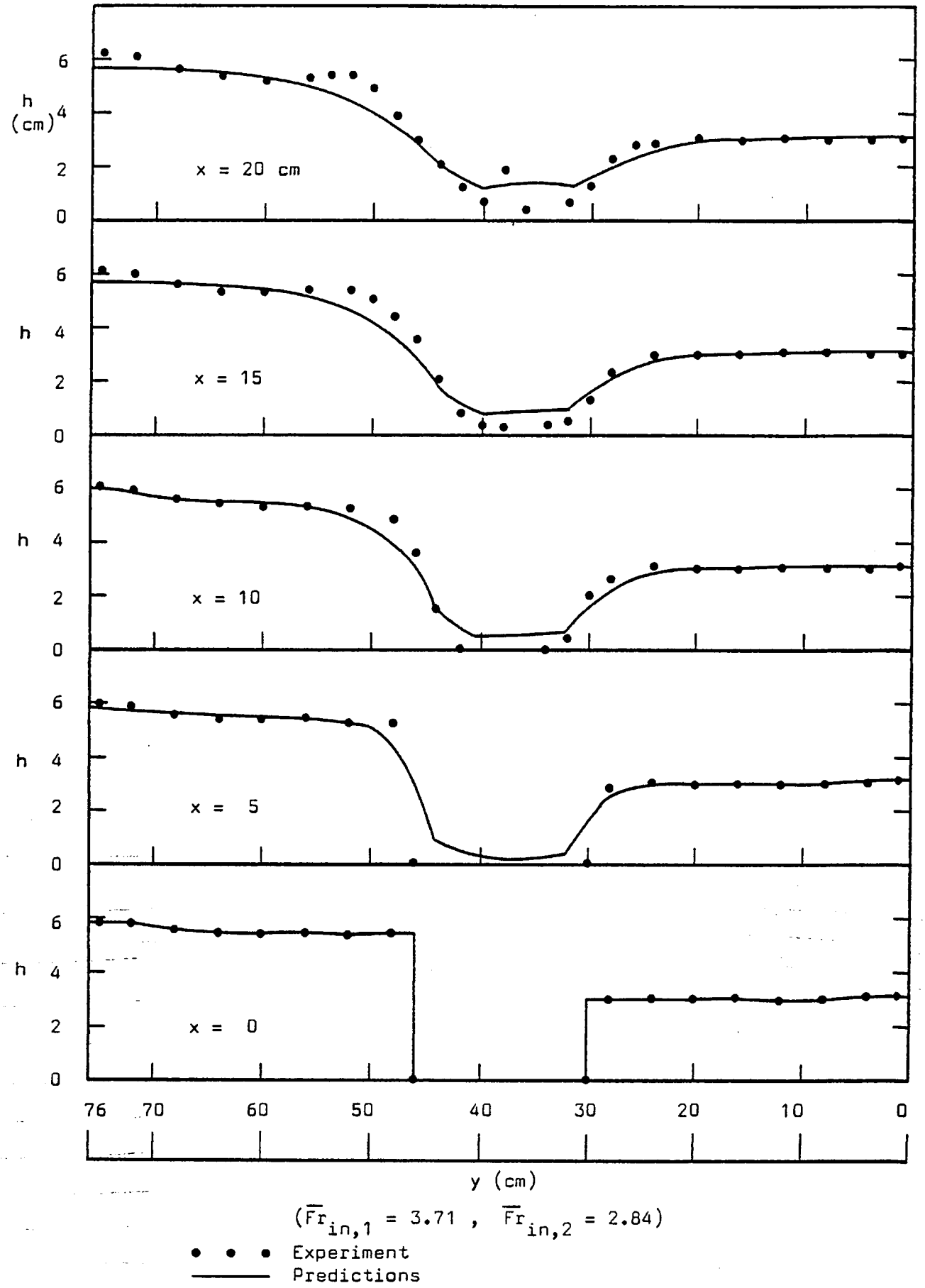


FIGURE 7.10 : CROSS-STREAM DEPTH PROFILES FOR RUN 2

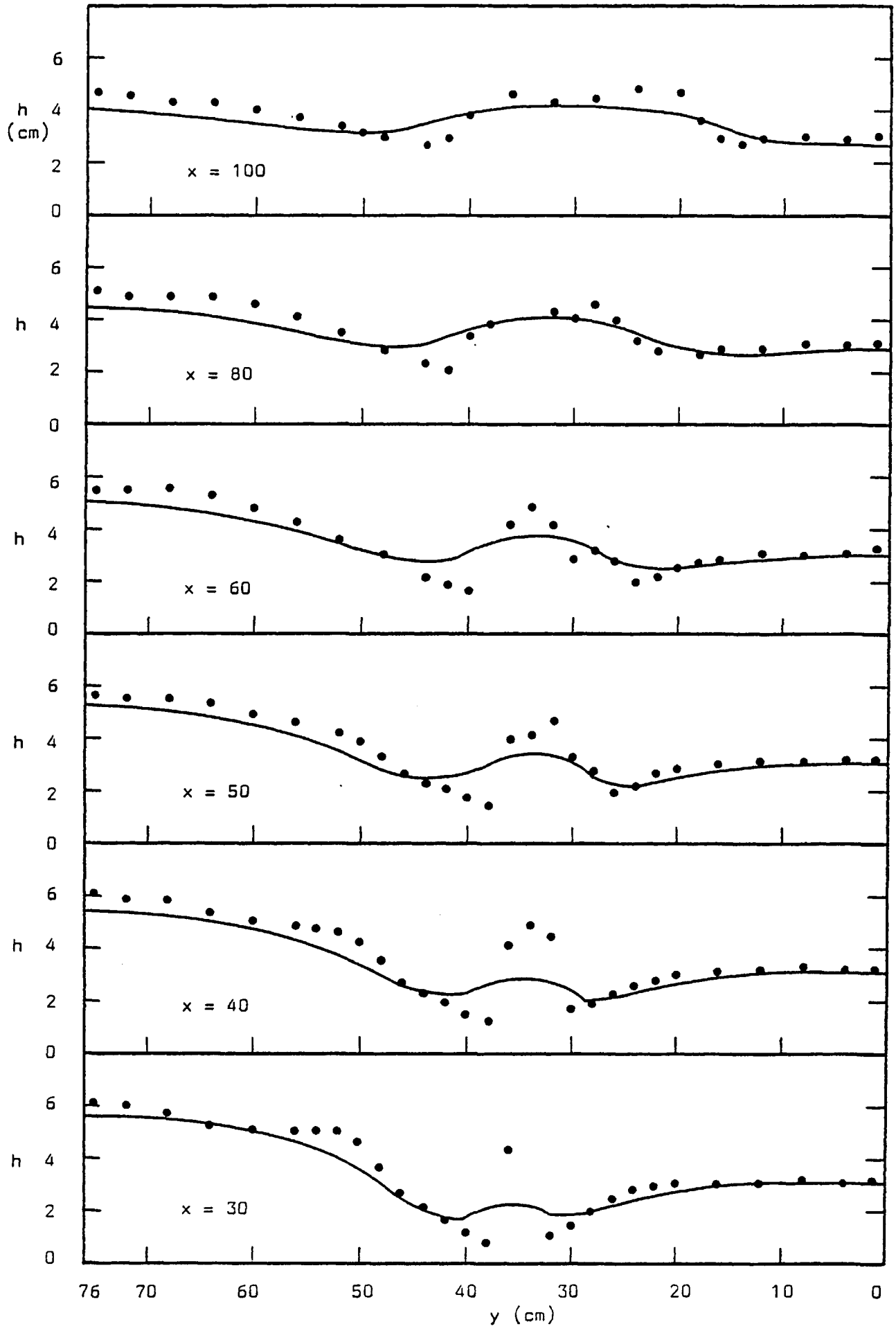


FIGURE 7.10 : (Continued)

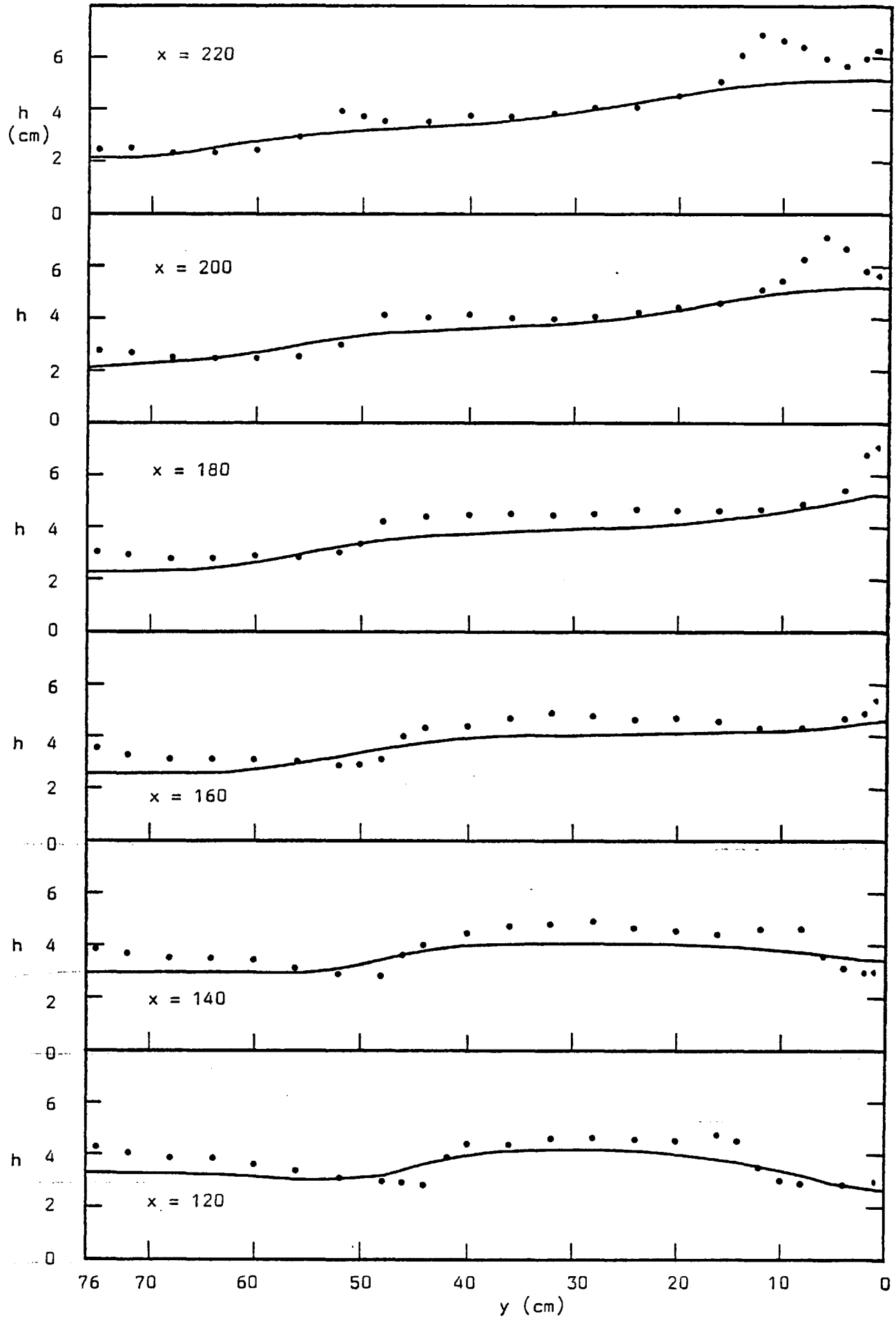


FIGURE 7.10 : (Continued)

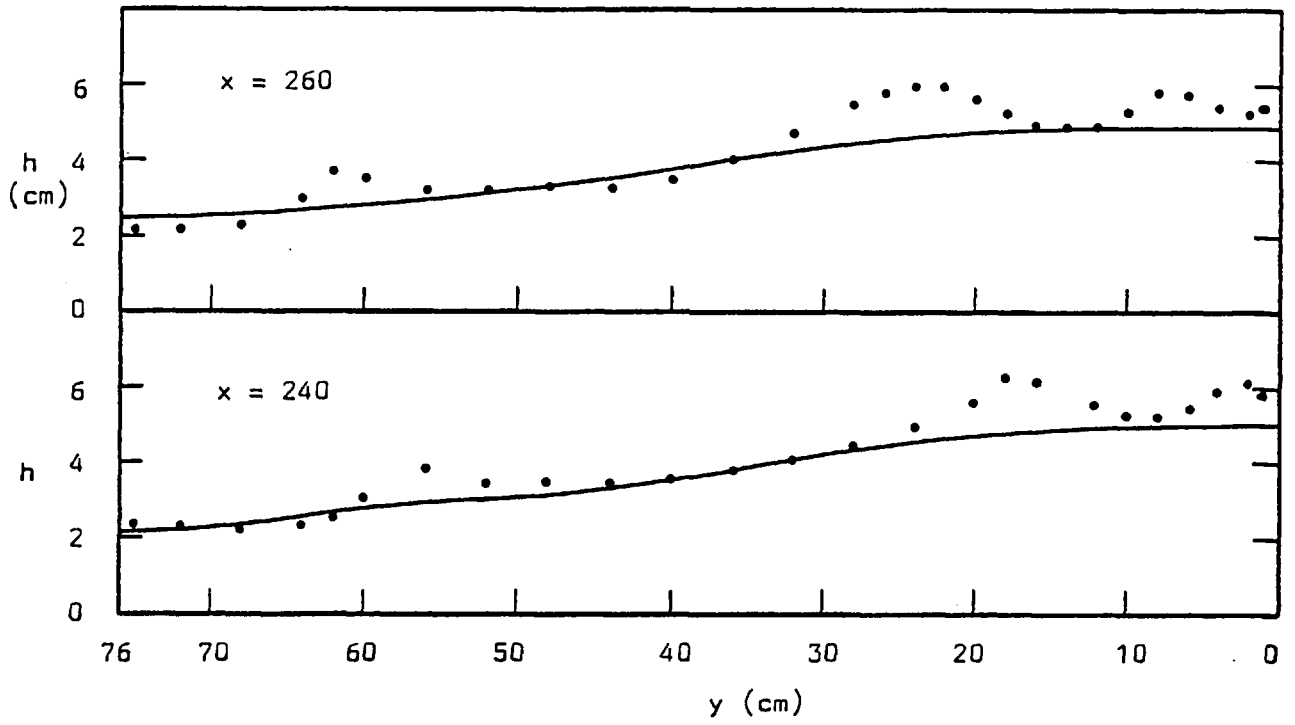
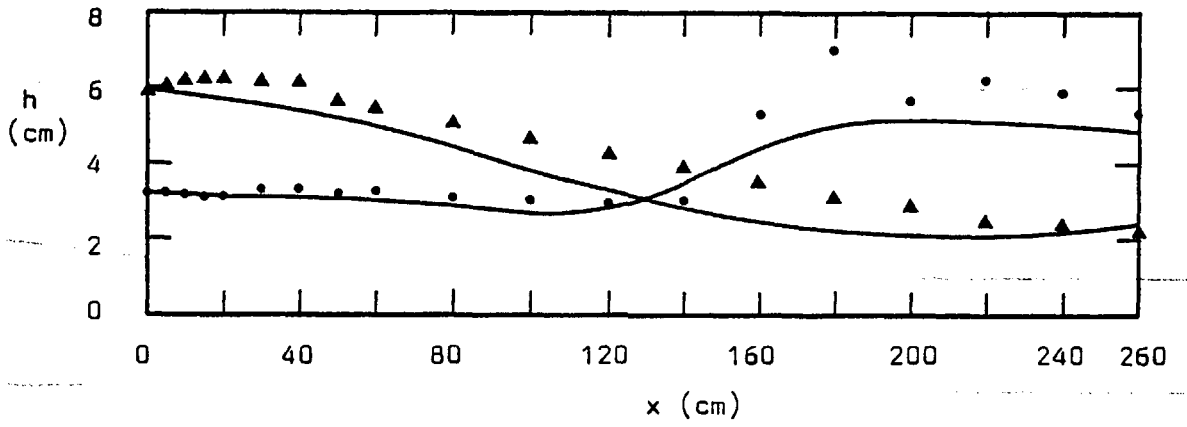


FIGURE 7.10 : (Continued)



● Experiment (y = 0)

▲ // (y = 76 cm)

——— Predictions

FIGURE 7.11 : DEPTH DISTRIBUTION ALONG THE SIDE WALLS FOR RUN 2

streams expand towards the middle of the channel creating, just downstream of the separating wall, what is termed a "dry region". The velocity-vector plot and the stream-function contours depicted in Figures 7.9 (a) and 7.9 (b) show clearly the initial expanding nature of the flow. Both the computed and measured depths in the "dry region" are practically zero and the flow remains very shallow over a distance of roughly one width of the separating wall (see Figures 7.7 and 7.10). The depth suddenly rises at the region where the two streams meet forming a deep main wave which travels downstream slightly shifted from the centre of the channel towards the lower momentum stream (Stream 1). This wave then expands and in doing so breaks down, under the action of gravity, to form two waves which part from each other and approach the channel side walls. As each wave meets a side wall, the depth starts to increase rather rapidly (see Figures 7.8 and 7.11) and then reflects away from the wall, across the main stream, as a series of waves.

The computed depth profiles compare well with the experimental results of Runs 1 and 2. However, the computed variations in depth appear to be underpredicted as compared to the measurements, especially in regions of high depth gradients. This may be attributed to the fact that the numerical model, being a depth-averaged one, neglects the vertical acceleration. This is indeed true since the pressure in such regions is far from being hydrostatically distributed. Nevertheless, the general trend and the positions of the peaks and troughs of the surface are well predicted.

7.3.3.4 Friction-Factor Investigation

The value of C_f employed in the computations presented above, was 0.001 and corresponded to the smooth surface of the flume. However,

it is interesting to study the extent to which the surface resistance affects the flow. Results corresponding to a C_f value of 0.003 (rough surfaces) were obtained and compared to those already presented with a C_f value of 0.001.

Figure 7.12 presents typical results of computed depth profiles as compared to the experimental results of Run 1. Figures 7.12 (a) and (b) compare the results of the depth distribution along two cross-stream stations and along the channel side walls respectively. A slight increase in depth has resulted, as expected, by increasing the C_f value, however, the level of agreement of both computed results with the data is the same.

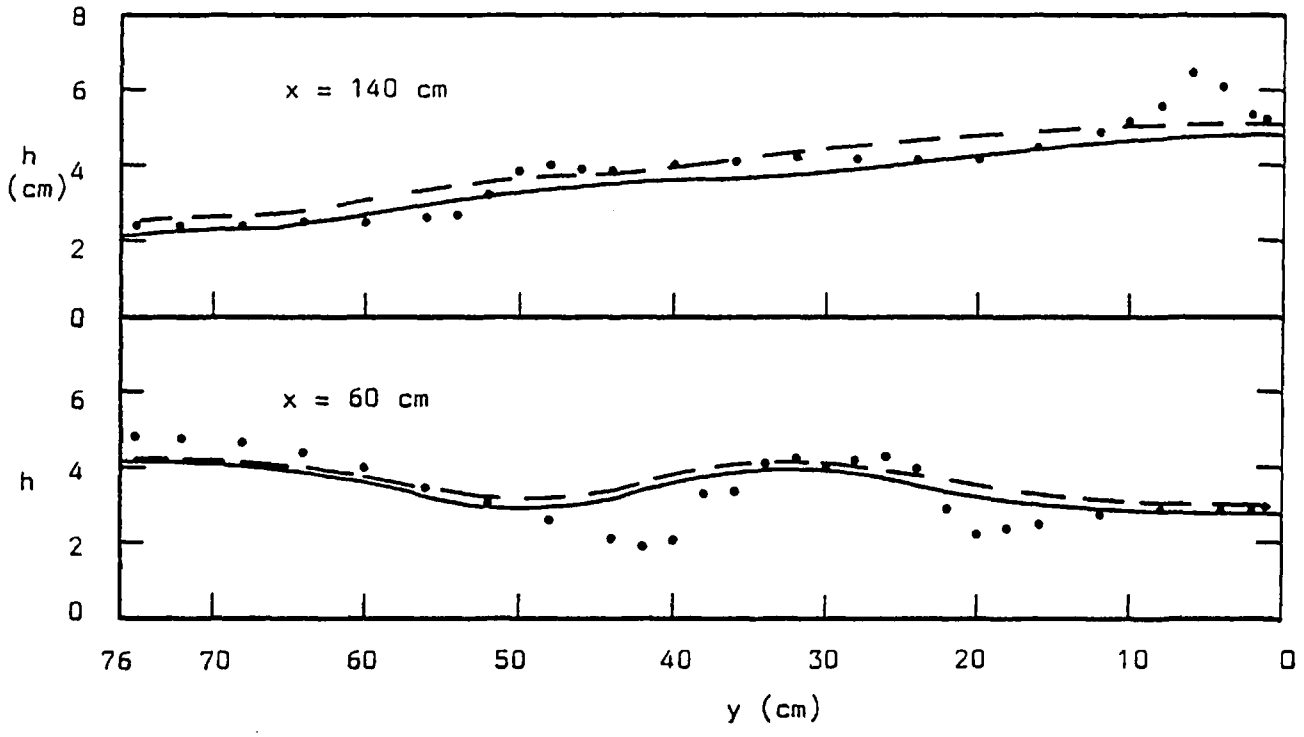
7.3.3.5 Grid-Dependence Check

Figure 7.13 presents some results of a grid-dependence check for the three different grids specified in Section 7.3.3.1 (d). The computed results of Run 1 are plotted for the depth distribution at four different cross-stream stations together with the measured depth points for comparison. It is seen that the two finer grids employed; namely, the 22 x 20 and 48 x 29 grids, give substantially grid-independent results, as compared to the coarser grid of 14 x 12, and produce better resolution of the surface elevations in regions of high depth gradients.

Figure 7.14 shows the distribution of grid lines for the 22 x 20 grid used for Run 1.

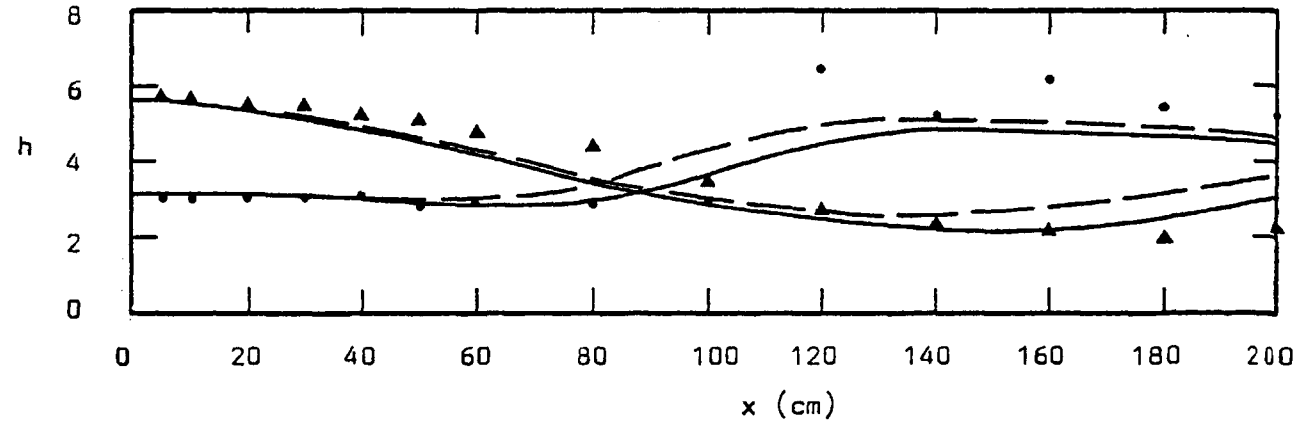
7.3.3.6 Concluding Remarks

The agreement between computed and experimental results, for the merging of two supercritical streams in a rectangular channel with



(a) Depth distribution along two cross-stream stations

(• • Measurements)



(b) Depth distribution along channel side walls

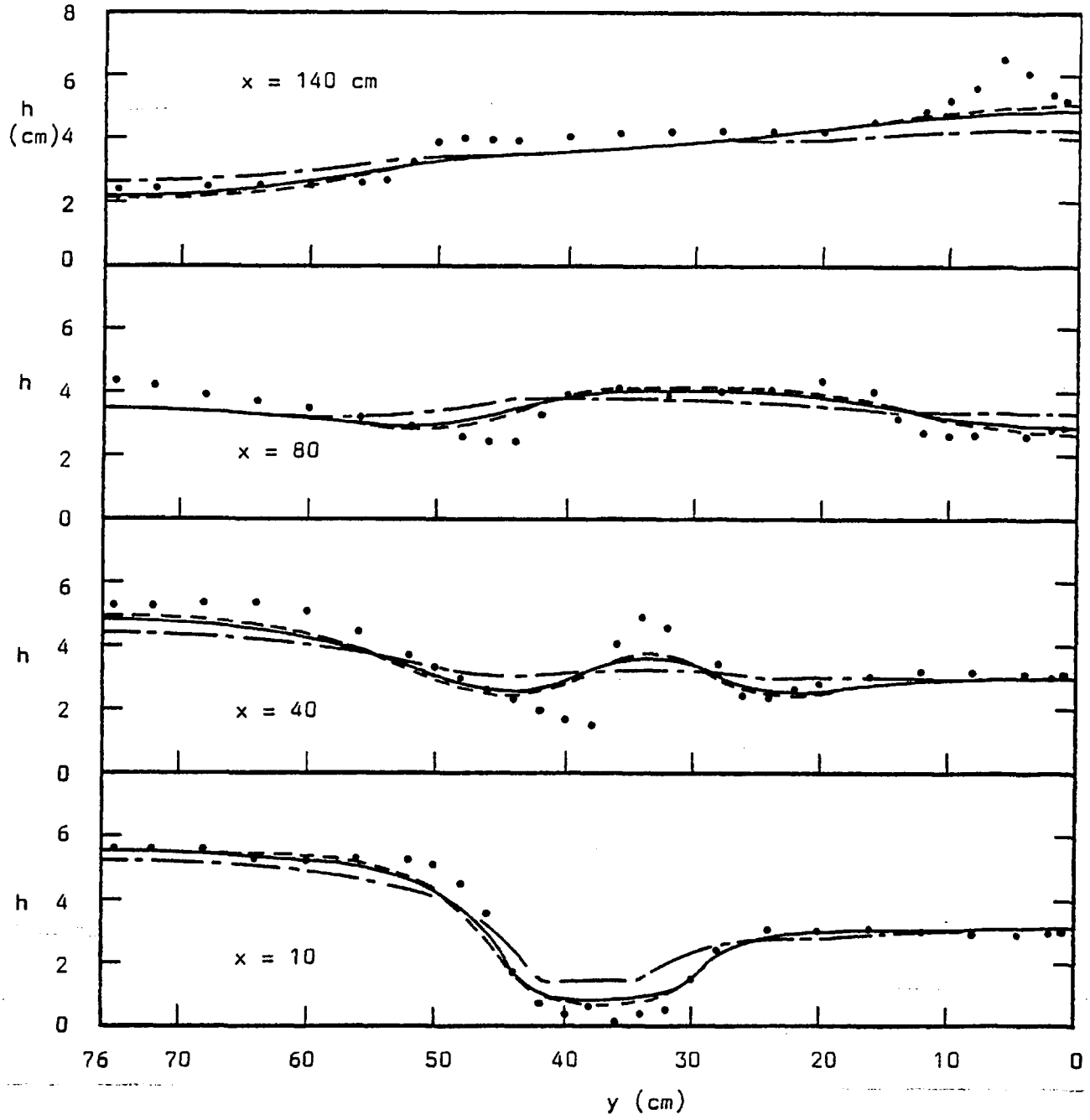
(• • Measurements at y = 0 ,

▲ ▲ // at y = 76 cm)

FIGURE 7.12 : FRICTION-FACTOR INVESTIGATION FOR RUN 1

——— Predictions ; C_f = 0.001

— — // C_f = 0.003



(Depth distribution along four cross-stream stations)

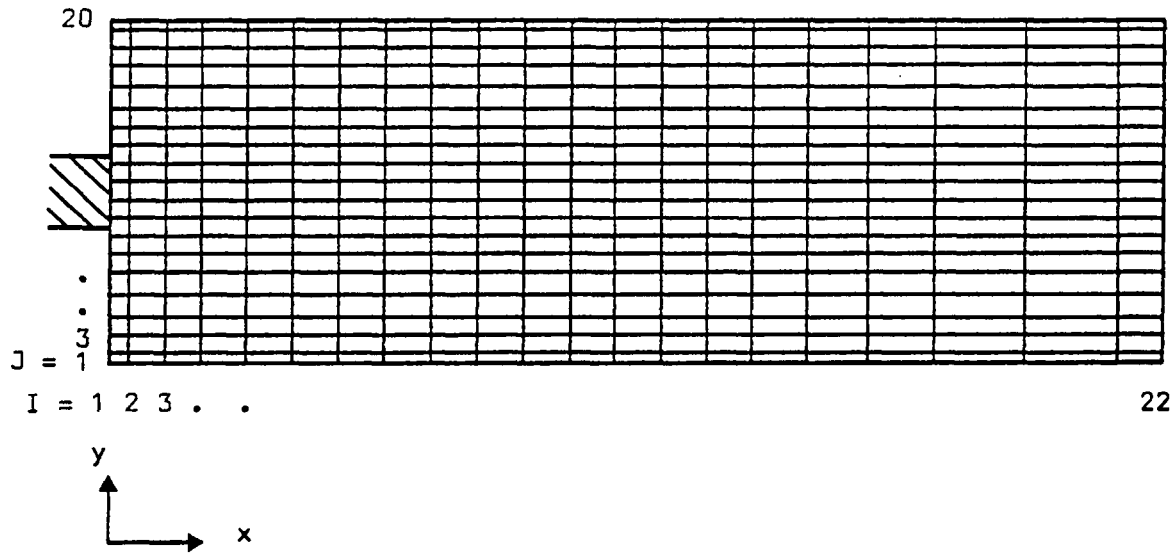
● Measurements

——— - ——— Predictions ; Grid 14 x 12

——————— // ; Grid 22 x 20

- - - - - - - // ; Grid 48 x 29

FIGURE 7.13 : GRID-DEPENDENCE CHECK FOR RUN 1



I	x	I	x	J	y	J	y
1	0.00	12	1.00	1	0.00	12	0.44
2	0.04	13	1.10	2	0.02	13	0.48
3	0.12	14	1.20	3	0.06	14	0.52
4	0.20	15	1.30	4	0.10	15	0.56
5	0.30	16	1.40	5	0.15	16	0.61
6	0.40	17	1.52	6	0.20	17	0.66
7	0.50	18	1.65	7	0.24	18	0.70
8	0.60	19	1.80	8	0.28	19	0.74
9	0.70	20	2.00	9	0.32	20	0.76
10	0.80	21	2.20	10	0.36		
11	0.90	22	2.30	11	0.40		

FIGURE 7.14 : GRID USED TO PREDICT MERGING OF TWO SUPERCRITICAL STREAMS FOR RUN 1

supercritical outlet conditions, is shown to be good. The agreement is only fair in regions of high depth gradients and was attributed to the neglect of vertical acceleration in the numerical model. The channel-surface resistance to the flow in such a situation was shown to be of secondary importance.

With reference to the objectives laid down in Section 7.3.1, it can be concluded that the accuracy of the numerical solution procedure has been further validated for wholly supercritical flows.

7.3.4 Calculations with Subcritical Outlet Conditions

7.3.4.1 Background and General Concept

The objectives of this study and the problem specification have been given in Sections 7.3.1 and 7.3.2. The computed results of Section 7.3.3, for the supercritical outlet conditions for both Runs 1 and 2, were stored for subsequent use in the present study. All that is required is to impose the experimental subcritical conditions at the outlet boundary of the computational domain. The flow is controlled by downstream conditions determined by the tailwater depth (h_t). The upstream conditions are unchanged. The high values of h_t induce hydraulic jumps inside the flow, the positions of which are to be determined computationally and compared to the measured locations. It is expected that the flow upstream of the jump (being supercritical) would be unaffected by the presence of the jump; downstream of the jump, the depth of flow would be roughly equal to h_t imposed at the outlet.

As with any other numerical scheme, the jump will be smeared, as in the one-dimensional case, over two or three grid lines. It is,

therefore, expected that refining the finite-difference grid would not affect the results in either of the supercritical or subcritical regions, since the results proved to be substantially grid independent. However, by refining the grid a more accurate resolution of the jump region is to be expected. The friction factor (C_f) employed in this study has the same value as in the previous case (0.001). A study of the effect of C_f on the jump location is conducted.

7.3.4.2 Details of the Computations

(a) Equations solved and boundary conditions

There is no change to the equations solved and the boundary conditions used. These are given in Section 7.3.3.1 (a) and (b). However, the depth at the exit plane is prescribed the experimental values for the tailwater depth (h_t).

(b) Initial conditions

All the computations were started from the "in store" values of the variables of the converged solutions to the previous case with supercritical outlet conditions. This practice is used to save computer time.

(c) Finite-difference grid

The grids employed for this study were the same as those used in Section 7.3.3.1 (d).

(d) Other details

As with the one-dimensional computations, the depth specified at

the exit boundary was "under-relaxed", i.e. the final (maximum) value of h_t was reached by adding successive small increments to the initial value of the depth. The process was carried out by iterating for an interval until convergence, before adding the next depth increment. Large depth increments were used at the beginning (about 2 cm), then these were reduced to about 2 mm after the hydraulic jump had started to form in the flow. Each iteration interval lasted for about 350 iterations, with a converged solution obtained and printed out at the end. This practice enabled the whole range of values of h_t to be investigated in a single computer run. In such computations, the jump was initially found at the exit plane and then moved upstream with further increases in h_t.

Rather heavy under-relaxation factors were needed (0.1 for all variables) to secure convergence. This may be due to the "zero-gradient" depth boundary conditions used at the channel side walls which made the jump position rather unstable. Typical run information is presented in Table 7.3.

VARIABLE	VALUE
(for upstream conditions, see Table 7.2)	
h_t	10.2 cm
C_f	0.001
Grid	22 x 20 (nearly uniformly spaced)
Number of iterations	350
RELAXU, RELAXV, RELAXH and RELAXP	0.1, 0.1, 0.1 and 1.0
Overall continuity error normalized to inlet flow-rate	1.8 E-3
Max. h' normalized to $\bar{h}_{in,1}$	3.2 E-3
Computer time in CDC seconds	98

TABLE 7.3 : COMPUTATIONAL DETAILS FOR PREDICTING RUN 1 OF THE 2D EXPERIMENTS WITH SUBCRITICAL OUTLET CONDITIONS

7.3.4.3 Presentation of the Results

All the results presented below are for the grids of 22 x 20 and 30 x 20 for Runs 1 and 2 respectively, and for a C_f value of 0.001 unless otherwise stated.

Some of the results are presented in Figure 7.15 in terms of perspective views of the surface elevations for various tailwater depths (Run 1). The values of h_t increase from 9.8 cm in Figue 7.15 (a) to 10.4 cm in (c). The views are exaggerated in the vertical direction for clarity. A typical computed velocity-vector plot is displayed in Figure 7.16 for Run 1 and for h_t equal to 10.4 cm. The computed results for the same run are presented in Figures 7.17 and 7.18 in terms of contour plots; Figure 7.17 shows the depth contours, whereas Figure 7.18 shows the streamlines and Froude-number contours.

The comparison between the computed and measured jump locations are shown in Figures 7.19 and 7.20 for Runs 1 and 2 respectively. The results are presented and compared in terms of the hydraulic-jump movement with various tailwater depths. The symbols represent the measured locations at the toe of the jumps, whereas the lines represent the computed locations at which Froude number is unity.

7.3.4.4 Discussion of the Results

The computed surface-elevation views shown in Figure 7.15 represent the overall features of the flow as it is influenced by increasing the tailwater depth. The flow upstream of the jump does not feel the presence of the jump; on the downstream side of the jump, the predictions show a practically uniform depth equal to the value of h_t prescribed at the outlet. Figure 7.16 shows, very clearly, a significant reduction in

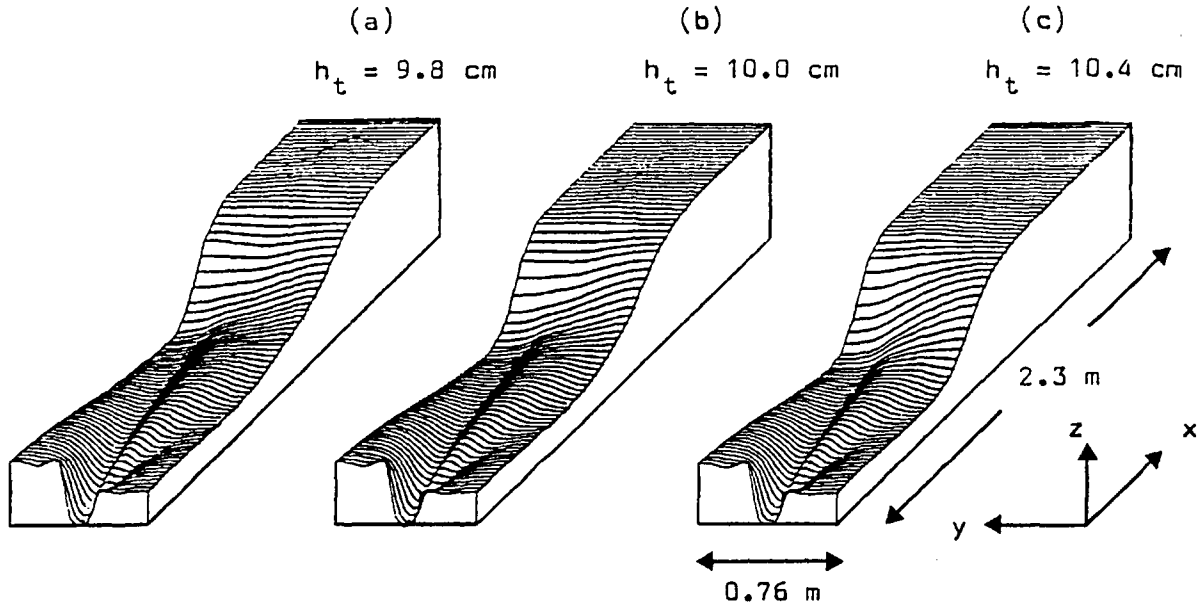


FIGURE 7.15 : PERSPECTIVE VIEWS OF THE SURFACE ELEVATIONS FOR VARIOUS TAILWATER DEPTHS (RUN 1)

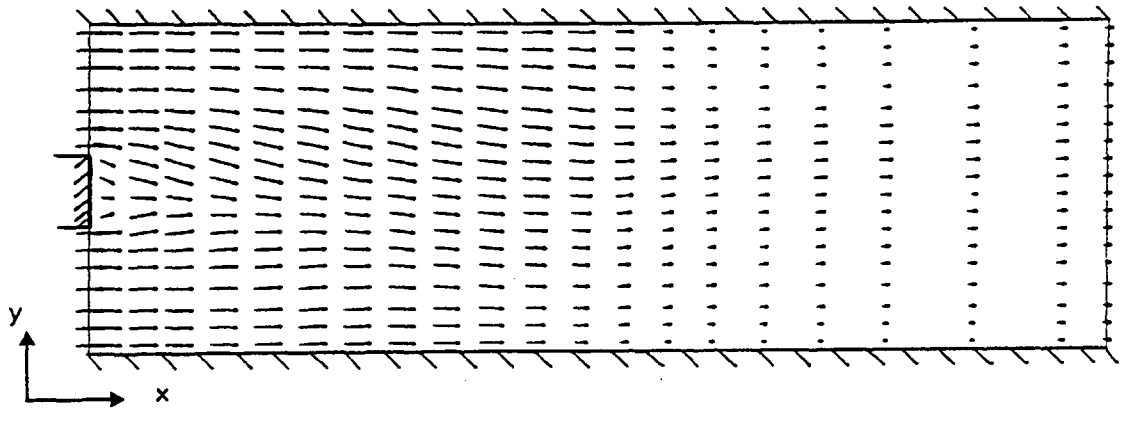


FIGURE 7.16 : VELOCITY-VECTOR PLOT FOR RUN 1 AND h_t = 10.4 cm

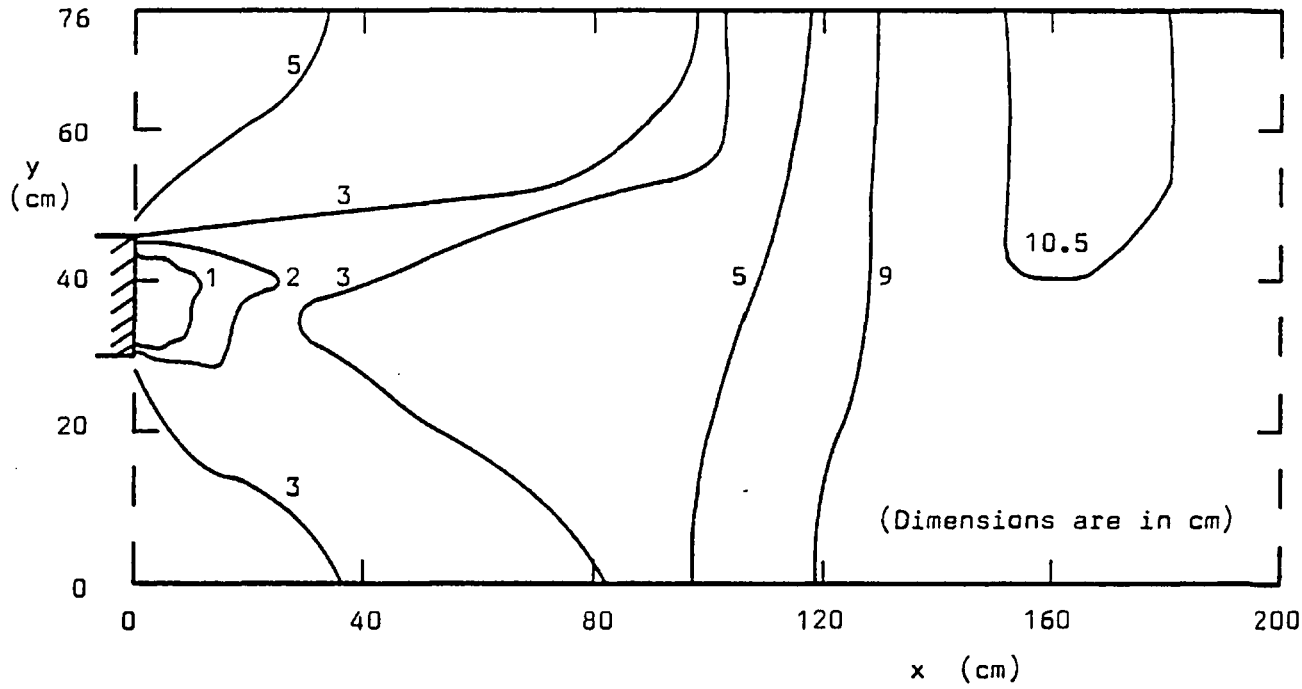


FIGURE 7.17 : COMPUTED DEPTH CONTOURS FOR RUN 1 AND h_t = 10.4 cm

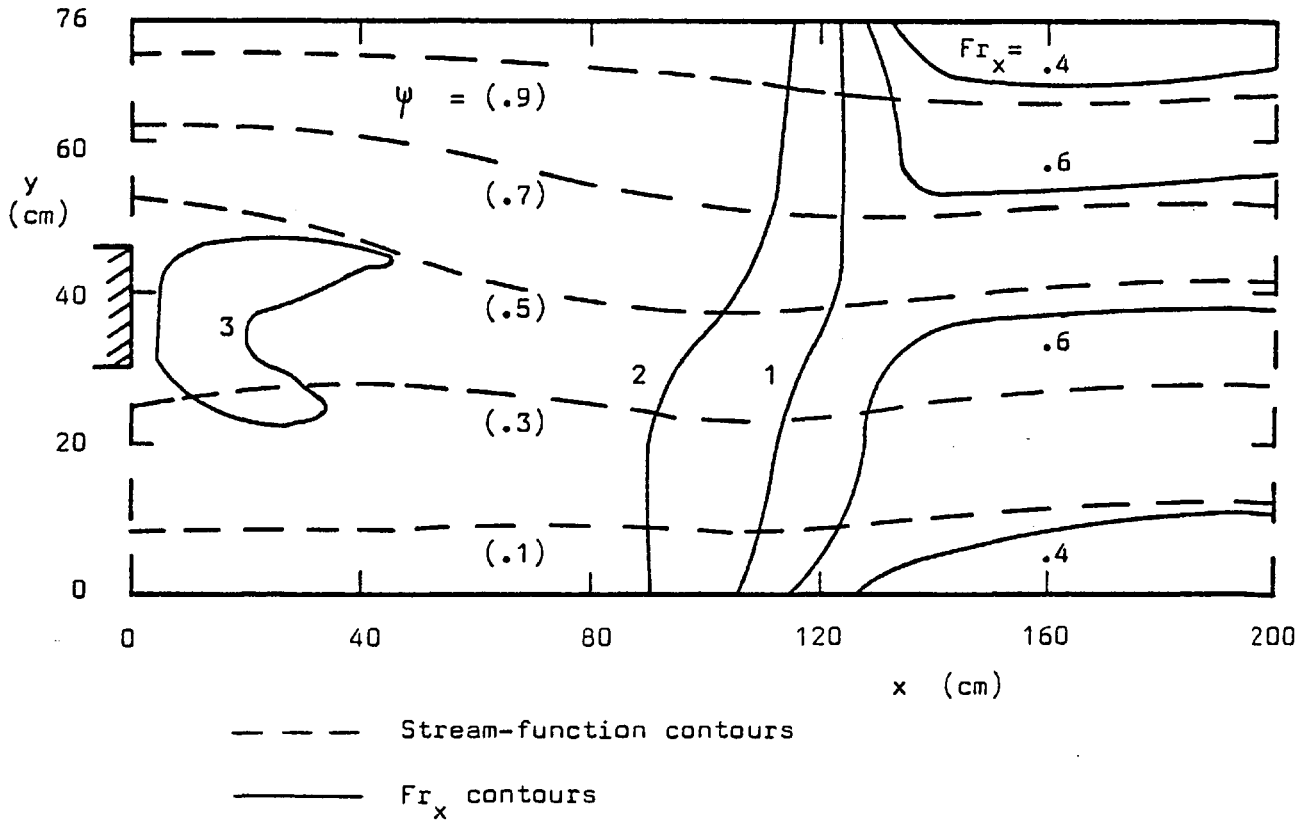


FIGURE 7.18 : COMPUTED STREAMLINES AND FROUDE-NUMBER CONTOURS FOR RUN 1 AND h_t = 10.4 cm

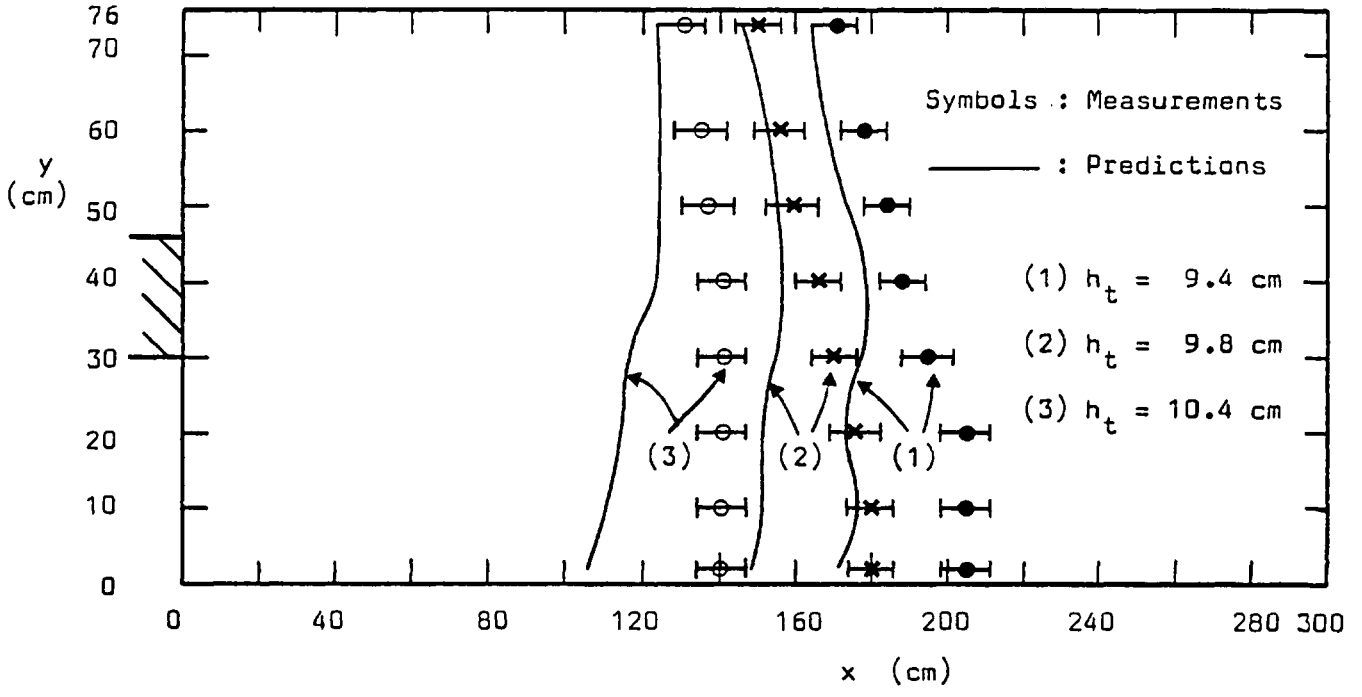


FIGURE 7.19 : HYDRAULIC-JUMP MOVEMENT WITH VARIOUS TAILWATER DEPTHS (RUN 1)

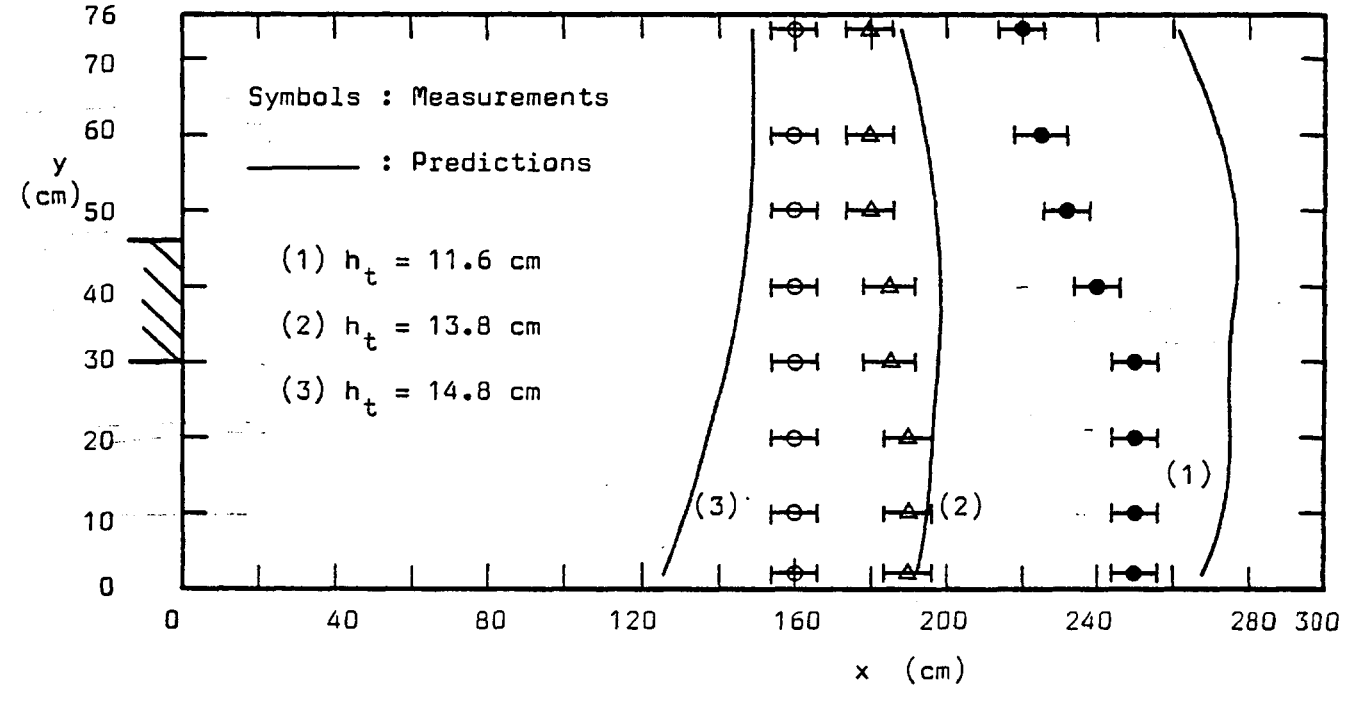


FIGURE 7.20 : HYDRAULIC-JUMP MOVEMENT WITH VARIOUS TAILWATER DEPTHS (RUN 2)

the magnitude of the velocity vectors as the flow changes from supercritical to subcritical. A corresponding increase in depth is evident as seen in Figure 7.15 or by studying the depth contours in Figure 7.17. To further analyse the results, the stream-function contours (normalized to the total flow-rate) and the Froude-number contours, which are both obtained from the computed velocities and depths, are plotted in Figure 7.18.

The jump locations were found to be sensitive to small changes in the tailwater depth (h_t). It is suspected, therefore, that the experimental inaccuracy in measuring the values of h_t (errors of the order of $\pm$ 2 mm), is a major contribution to discrepancies between the computed and measured jump locations. Bearing this, and other experimental inaccuracies (see Section 5.3.6) in mind, the comparisons shown in Figures 7.19 and 7.20 are generally good. Part of the discrepancy is also due to the numerical model being unable to predict accurately the high depth gradients in the supercritical region, for reasons given earlier. The measured locations are subject to slight oscillations and are, therefore, shown with an error margin.

7.3.4.5 Friction-Factor Investigation

The friction factor (C_f) employed in the computations presented above, was 0.001 and corresponded to the smooth surface of the flume. Figure 7.21 shows a typical study of the effect of increasing C_f to the values of 0.002 and 0.003 (the latter corresponds to rough surfaces) on the jump location of Run 1 and for h_t equal to 9.4 cm. The effect of increasing C_f on the results is seen to be significant(this was shown to be of secondary importance for the same flow solved earlier with supercritical outlet conditions).

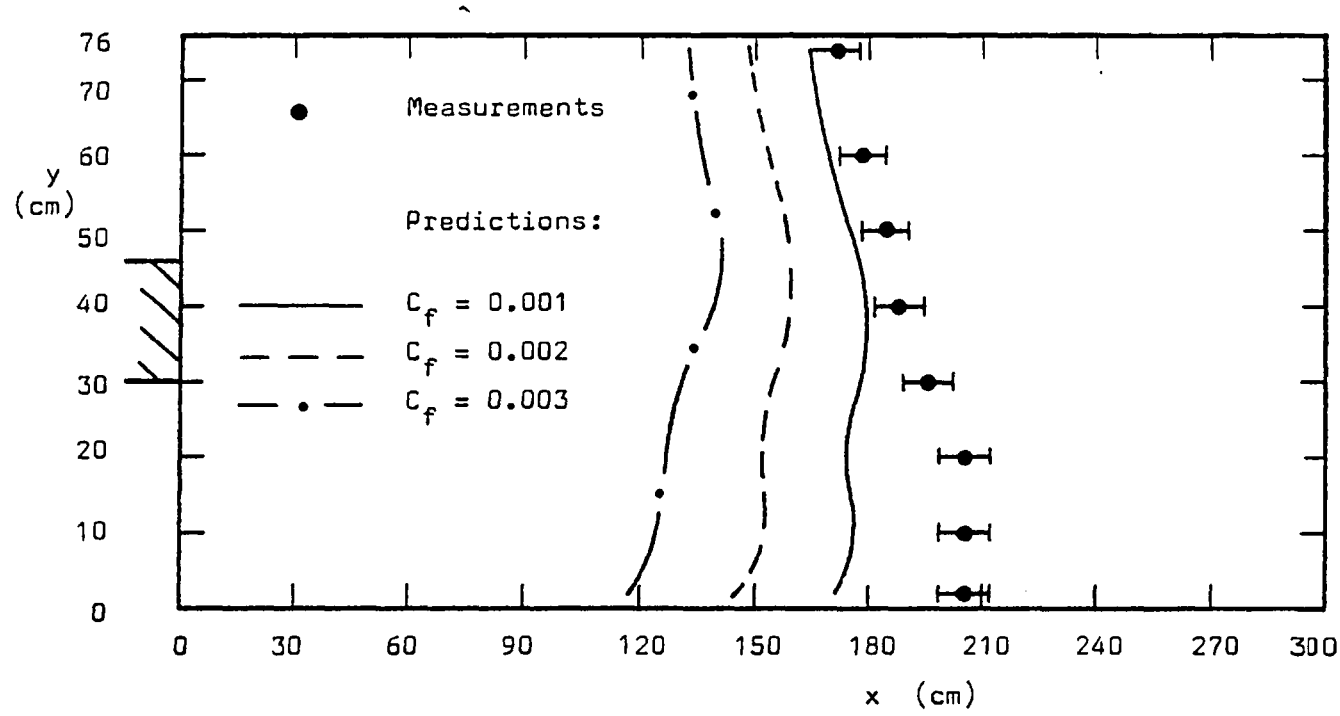


FIGURE 7.21 : FRICTION-FACTOR INVESTIGATION FOR RUN 1 WITH SUBCRITICAL OUTLET CONDITIONS: SHOWING HYDRAULIC-JUMP LOCATION FOR h_t = 9.4 cm

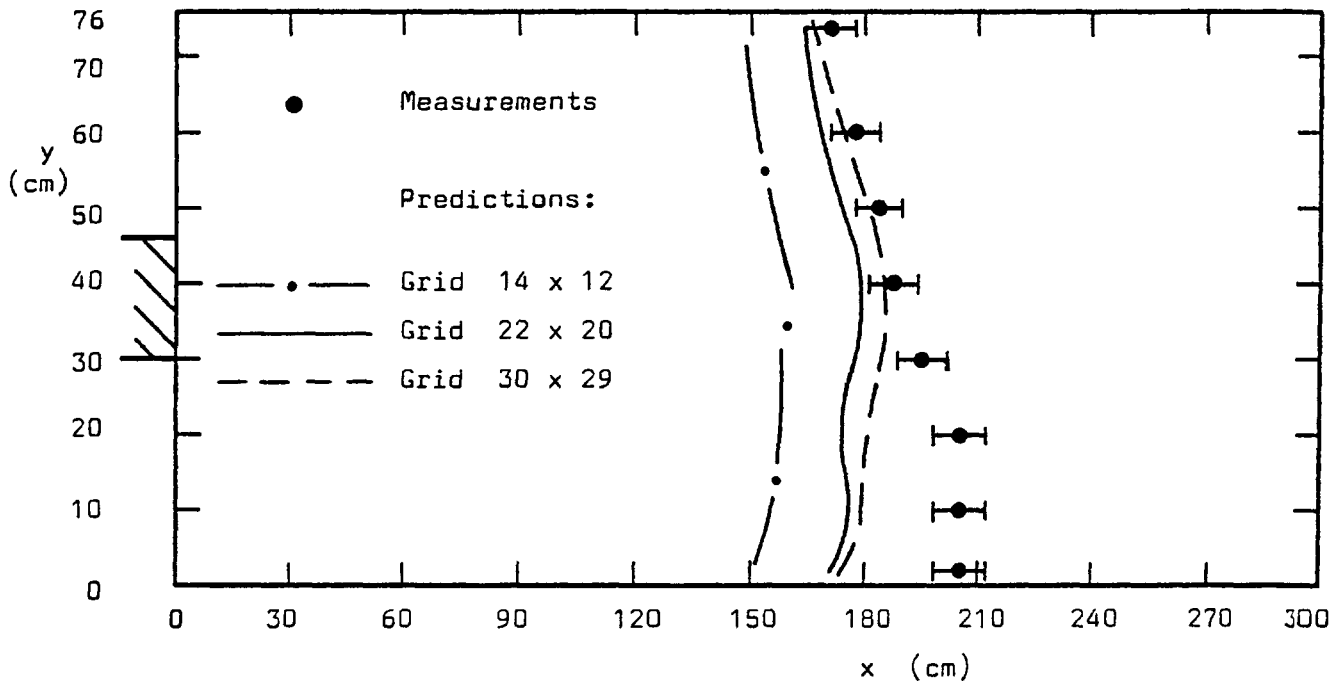


FIGURE 7.22 : GRID-DEPENDENCE CHECK FOR RUN 1 WITH SUBCRITICAL OUTLET CONDITIONS: SHOWING HYDRAULIC-JUMP LOCATION FOR h_t = 9.4 cm

It can be concluded from this study, that the friction factor plays an important role in the study of flows with hydraulic jumps. Correct estimation of the value of C_f for the channel surface in question is important.

7.3.4.6 Grid-Dependence Check

Following the argument presented in Section 7.3.4.1, Figure 7.22 shows the results of a grid-dependence check for three different grids used. The coarse grid of 14 x 12 fails to produce the accurate jump location for the main reason that it has not produced sufficiently grid-independent results for the wholly supercritical flow. However, the improvement in accuracy achieved for the jump location by using a grid of 30 x 29, as compared to the grid of 22 x 20, lies within the length of a finite-difference cell of the 22 x 20 grid. This suggests that smearing is reduced, by grid refinement, by only a small amount and does not justify the cost of using finer grids. It is concluded, therefore, that the grid of 22 x 20 (which proved to give sufficiently grid-independent results for the supercritical flow of Run 1) is an optimum grid to use in this case as far as accuracy and economy are concerned.

7.3.4.7 Concluding Remarks

The agreement between computed and measured jump locations, for the two-dimensional experimental flow situation, has been shown to be generally good. The jump location was shown to be sensitive to even small changes in the tailwater depth. The surface resistance of the channel was shown to be a significant factor in affecting the transition location. The jump location was also found to be sensitive to the size

of finite-difference grids used; however, for sufficiently fine grids, as the one used here, the jump was smeared over only a short distance. No significant improvement was achieved by further grid refinement. The convergence rate was rather slow because of the heavier under-relaxation factors employed since the "zero-gradient" depth boundary conditions used at the side walls are the most unstable type of boundary condition especially in such a flow situation.

With reference to the objectives laid down in Section 7.3.1, it can be concluded that the accuracy of the numerical solution procedure has been validated for two-dimensional flows with hydraulic jumps.

7.4 CLOSURE

In this chapter the numerical accuracy of the solution procedure and the physical realism of the predictions were examined for discontinuous flows and shown to be good. The predictions were compared to the one- and two-dimensional results obtained from experimental investigations. Regarding the economy of the procedure, the computer time was modest for the solution of such complicated flow situations.

Further testing and application of the model to flows with hydraulic jumps will be considered in the next chapter, where the model is applied to simulation of compressible-gas flows including shock waves.

CHAPTER 8

CALCULATION OF TRANSONIC FLOWS USING THE HYDRAULIC ANALOGY

8.1 INTRODUCTION

In the previous two chapters, the numerical model was validated for a number of continuous and discontinuous shallow-water flows. The purpose of this chapter is two fold: firstly, to further apply and test the accuracy of the numerical solution procedure to other discontinuous flow situations and, secondly, to study and highlight the analogy between free-surface and two-dimensional (plane) compressible-gas flows.

The predictions presented in this chapter are compared to experimental data and various solutions by others, of compressible-gas flows including shock waves.

The present chapter consists of three main sections, the first of which considers the details of the analogy. The other two main sections contain the study, using the analogy, applied to two compressible-gas flow situations which include shock waves. The first case simulates the Mach-stem flow of overexpanded free jets, while the second case simulates the impingement of supersonic flows on a blunt body. The chapter closes with a summary of the main findings and an overall look at the performance of the present solution technique.

8.2 THE ANALOGY BETWEEN FREE-SURFACE AND COMPRESSIBLE-GAS FLOWS

8.2.1 Background and General Concept

The normal shock wave in gas flow is analogous to the hydraulic

jump in shallow-water flow. Analogous to the oblique shock and rarefaction waves in gas flow are the oblique liquid waves produced in a channel by changes in the direction of the channel walls or by changes in floor elevation. A body placed in an open channel with flow at a Froude number greater than unity causes waves on the surface that are analogous to shock and rarefaction waves on a similar two-dimensional body in a supersonic wind-tunnel.

It has long been realized that a close analogy exists between frictionless shallow-water flows and two-dimensional compressible-gas flows in adiabatic processes. Nevertheless, this analogy was restricted, in the past, to experimental measurements in water tables in order to demonstrate and study the behaviour of a compressible gas in similar flow situations. Those studies were, however, only valid for a fictitious gas of a specific-heat ratio (γ) equal to 2 and, thus, could represent only a qualitative analogy between the two flows. In Section 1.2.3, such an analogy was discussed to a certain extent and summarized in Table 1.2.

In the following section it is shown that only minor adjustments to the shallow-water equations are needed to achieve an exact analogy to those of compressible-gas flow for any value of γ. It is expected, therefore, that good quantitative results for a compressible-gas flow should be forthcoming when the "modified" hydraulic analogy is applied.

8.2.2 Mathematical Analysis

(a) Shallow-water flow equations

The frictionless shallow-water flow equations are repeated here for comparison, these are:

continuity

$$\frac{\partial}{\partial x}\ (\ hu\ )\ +\ \frac{\partial}{\partial y}\ (\ hv\ )\ =\ 0 \qquad ,(8.1)$$

x-momentum

$$\frac{\partial}{\partial x}\ (\ hu^2\ )\ +\ \frac{\partial}{\partial y}\ (\ huv\ )\ =\ -\ g\ h\ \frac{\partial h}{\partial x} \qquad ,(8.2)$$

y-momentum

$$\frac{\partial}{\partial x}\ (\ huv\ )\ +\ \frac{\partial}{\partial y}\ (\ hv^2\ )\ =\ -\ g\ h\ \frac{\partial h}{\partial y} \qquad ,(8.3)$$

By splitting the derivatives in equations (8.2) and (8.3), and using the continuity equation (8.1), one gets:

x-momentum

$$u\ \frac{\partial u}{\partial x}\ +\ v\ \frac{\partial u}{\partial y}\ =\ -\ g\ \frac{\partial h}{\partial x} \qquad ,(8.4)$$

y-momentum

$$u\ \frac{\partial v}{\partial x}\ +\ v\ \frac{\partial v}{\partial y}\ =\ -\ g\ \frac{\partial h}{\partial y} \qquad .(8.5)$$

(b) Compressible-gas flow equations

The equations, appropriate to inviscid two-dimensional flow of a compressible gas, are:

continuity

$$\frac{\partial}{\partial x}(\rho u) + \frac{\partial}{\partial y}(\rho v) = 0 \qquad ,(8.6)$$

x-momentum

$$u\frac{\partial u}{\partial x} + v\frac{\partial u}{\partial y} = -\frac{1}{\rho}\frac{\partial p}{\partial x} \qquad ,(8.7)$$

y-momentum

$$u\frac{\partial v}{\partial x} + v\frac{\partial v}{\partial y} = -\frac{1}{\rho}\frac{\partial p}{\partial y} \qquad ,(8.8)$$

The pressure (p) appearing in equations (8.7) and (8.8) can be put in terms of the density (ρ) via the isentropic relationship for a perfect gas, namely:

$$\frac{p}{p_0} = \left(\frac{\rho}{\rho_0}\right)^{\gamma} \qquad ,(8.9)$$

where subscript 0 designates the stagnation value of the variable and γ is the specific-heat ratio of the gas, hence:

$$\frac{\partial p}{\partial x} = \frac{p_0}{\rho_0^{\gamma}}\,\gamma\,\rho^{\gamma-1}\,\frac{\partial \rho}{\partial x} \qquad ,(8.10)$$

$$\frac{\partial p}{\partial y} = \frac{p_0}{\rho_0^{\gamma}}\,\gamma\,\rho^{\gamma-1}\,\frac{\partial \rho}{\partial y} \qquad .(8.11)$$

Substituting equations (8.10) and (8.11) into equations (8.7) and (8.8), one gets:

x-momentum

$$u \frac{\partial u}{\partial x} + v \frac{\partial u}{\partial y} = - \frac{p_0}{\varrho_0^{\gamma}} \gamma \varrho^{\gamma-2} \frac{\partial \varrho}{\partial x} \qquad ,(8.12)$$

y-momentum

$$u \frac{\partial v}{\partial x} + v \frac{\partial v}{\partial y} = - \frac{p_0}{\varrho_0^{\gamma}} \gamma \varrho^{\gamma-2} \frac{\partial \varrho}{\partial y} \qquad .(8.13)$$

(c) Analogy between the two sets of equations

The final form of the two sets of equations are given in Table 8.1 for comparison.

SHALLOW-WATER EQUATIONS	COMPRESSIBLE-GAS FLOW EQUATIONS
continuity	continuity
$\frac{\partial}{\partial x}(h u) + \frac{\partial}{\partial y}(h v) = 0$	$\frac{\partial}{\partial x}(\varrho u) + \frac{\partial}{\partial y}(\varrho v) = 0$
x-momentum	x-momentum
$u \frac{\partial u}{\partial x} + v \frac{\partial u}{\partial y} = - g \frac{\partial h}{\partial x}$	$u \frac{\partial u}{\partial x} + v \frac{\partial u}{\partial y} = - \frac{p_0}{\varrho_0^{\gamma}} \gamma \varrho^{\gamma-2} \frac{\partial \varrho}{\partial x}$
y-momentum	y-momentum
$u \frac{\partial v}{\partial x} + v \frac{\partial v}{\partial y} = - g \frac{\partial h}{\partial y}$	$u \frac{\partial v}{\partial x} + v \frac{\partial v}{\partial y} = - \frac{p_0}{\varrho_0^{\gamma}} \gamma \varrho^{\gamma-2} \frac{\partial \varrho}{\partial y}$

TABLE 8.1 : COMPARISON BETWEEN SHALLOW-WATER AND COMPRESSIBLE-GAS FLOW EQUATIONS

By studying the table, it will be evident that the corresponding equations become identical if:

- the height (h) is analogous ($\sim$) to density (ϱ) in the compressible flow:

$$\boxed{h \sim \varrho} \quad , \tag{8.14}$$

- the gravitational acceleration (g) is analogous to $\frac{p_0}{\varrho_0^{\gamma}} \gamma \varrho^{\gamma-2}$ in the compressible flow:

$$g \sim \frac{p_0}{\varrho_0^{\gamma}} \gamma \varrho^{\gamma-2} \quad , \tag{8.15}$$

The analogous relation given by equation (8.15) can be simplified, using equation (8.9), as follows:

$$g \sim \frac{p}{\varrho^{\gamma}} \gamma \varrho^{\gamma-2} \quad , \text{i.e.} \quad g \sim \frac{p}{\varrho^2} \gamma \tag{8.16}$$

Now, by replacing ϱ by h, and p by the hydrostatic pressure force (per unit density) $g h^2/2$, relation (8.16) gives:

$$\boxed{g \sim \frac{\gamma}{2} g} \quad . \tag{8.17}$$

If γ is equal to 2, then $g \sim g$ and this achieves the hydraulic analogy to a fictitious gas of $\gamma = 2$. But there is no necessity for the "analogous gas" to have a specific-heat ratio of 2, as g in the numerical model can be replaced by $\frac{\gamma}{2} g$ for any value of γ.

8.3 SIMULATION OF OVEREXPANDED TRANSONIC FREE JETS

8.3.1 Introduction

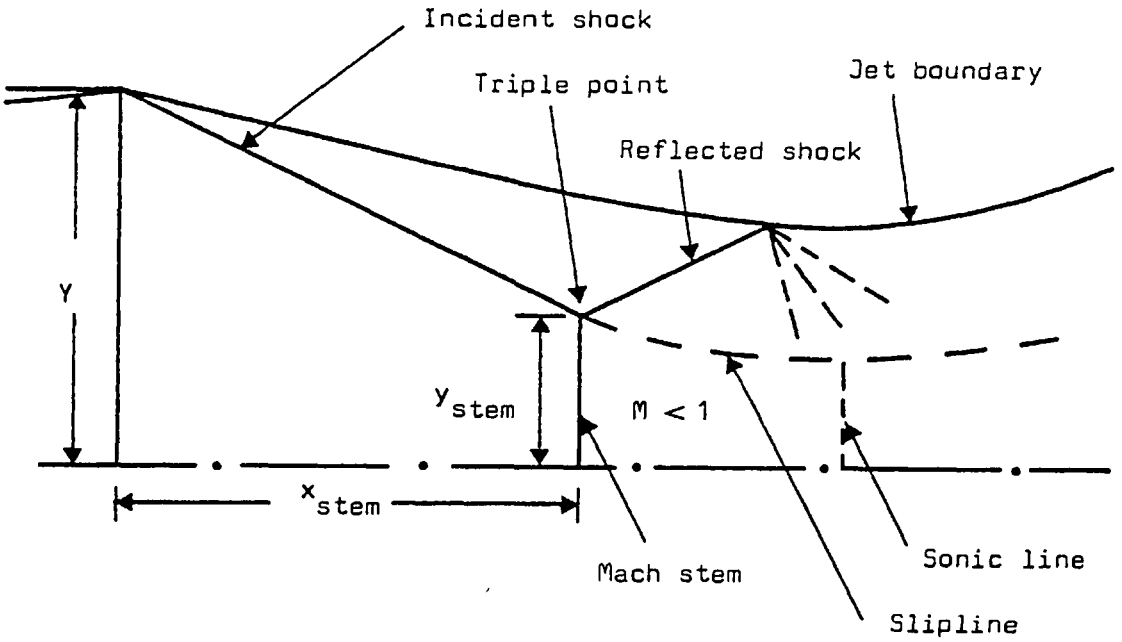
The main objectives of this study are to test the validity of the hydraulic analogy ($\gamma = 2$) and the modified analogy (γ equals the value appropriate to the gas simulated; e.g. $\gamma_{air} = 1.4$) to 2-D compressible-gas flows. The study investigates the stability of the numerical scheme for fixed free-stream boundary conditions, and further investigates the sensitivity of the procedure to grid refinement for discontinuous flows.

8.3.2 Problem Specification

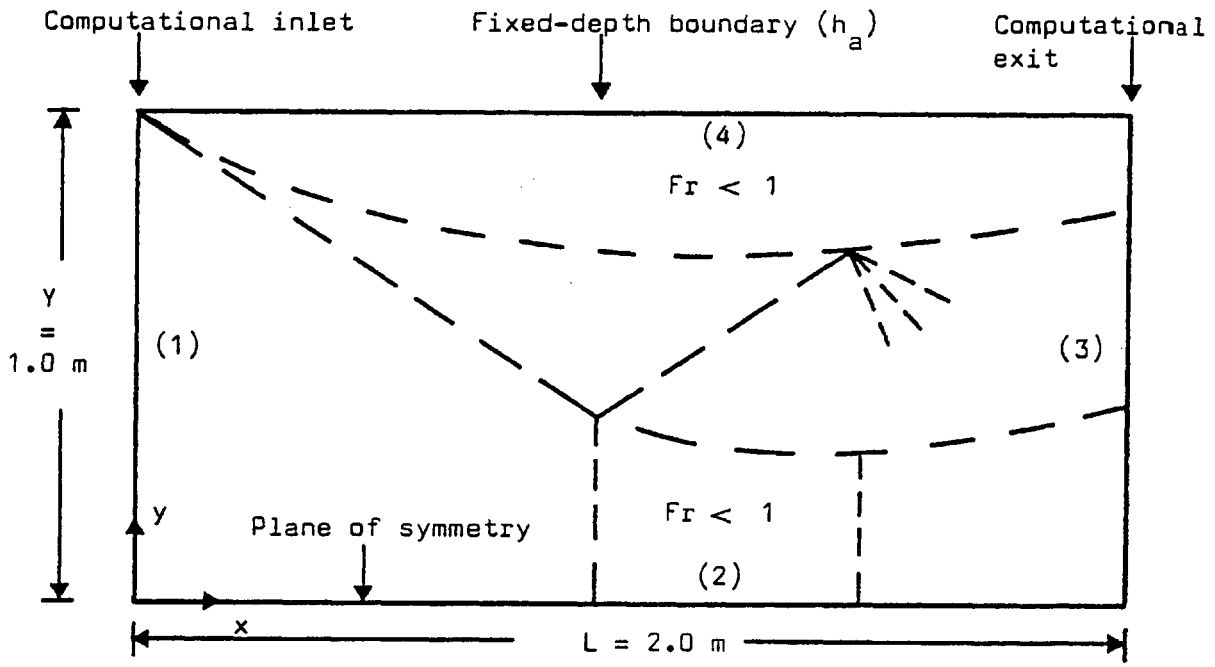
(a) Flow situation and shock structure

The physical situation simulates a supersonic jet exhausting into a stagnant ambient from a two-dimensional nozzle at a pressure less than the ambient pressure. In adjusting to the high pressure surroundings, the jet boundary collapses producing a jet shock which, in a short distance, impinges on the jet centre-plane. The shock may be reflected from the centre-plane (regular reflection), or if strong, generates a Mach stem (Riemann wave) reflection as shown in Figure 8.1 (a). In both cases, reflected shocks are formed which intersect with the jet boundary reflecting as expansion waves, and the whole process is repeated until viscous effects become predominant.

The flowfield pattern is primarily dependent upon the nozzle exit pressure (p_n), Mach number (M_n), ratio of specific heats (γ), ambient pressure (p_a), and the nozzle exit flow direction. As the operating pressure ratio (p_n / p_a) is increased, the standoff distance (x_{stem}) of the Riemann wave from the nozzle exit increases; whereas the width of the



(a) The compressible-gas flow situation (side view)



(b) The analogous situation in free-surface flows (plan view)

FIGURE 8.1 : DIAGRAMATIC VIEWS OF AN OVEREXPANDED FREE JET

Riemann wave (half width being y_{stem}) decreases. Figure 8.1 (b) represents the geometry of the hydraulic model and outlines the boundary conditions employed as detailed in Section 8.3.3 (b). The nozzle exit half-height and the channel half-width being Y.

(b) Theoretical and experimental information

Supersonic jet flow research has centred mainly on axisymmetric free jet flows because of their practical applications in jet engines and rocket technology. Consequently, research on two-dimensional jet flows has lagged, especially in the experimental field. The work published on two-dimensional overexpanded jets is even rarer. Such selected studies are summarized in Table 8.2.

Author (s)	Year	Application
Ferri	1949	Experimental study; overexpanded jets.
Sheeran & Dosanjh	1968	Experimental study; underexpanded jets.
Werle, et al	1970	Theoretical study (method of characteristics) and experimental study; underexpanded jets.
Sinha, et al	1971	Theoretical study (time-marching finite-difference method); underexpanded jets.
Chow & Chang	1975	Theoretical study (method of characteristics); overexpanded jets.
Small	1979	Theoretical study (transonic small-disturbance theory); overexpanded jets.

TABLE 8.2 : STUDIES OF TWO-DIMENSIONAL (PLANE) TRANSONIC FREE JETS

Most of these studies have lacked a detailed description of the plume of the 2-D jets, and the boundary conditions used. Some of the

results were presented with no comparison whatsoever. However, these studies have indicated that mixing and viscous interactions are not crucial in the determination of the overall structure of the plume so far as the region between the jet and the Riemann wave is concerned.

The experimental data of Ferri (1949) are used in the present study for comparison. The data available are obtained from Schlieren photographs for the standoff distances and widths of the Riemann waves, appropriately nondimensionalized, for the pressure ratios (p_n / p_a) of 0.53 and 0.51 for air at a nozzle Mach-number of 1.92.

(c) Flow parameters

The study is conducted for an exit Mach-number (Froude number) of 1.92 and a specific-heat ratio of 1.4. The pressure ratios investigated ($p_n / p_a = (h_n / h_a)^{\gamma}$) are between 0.40 and 0.74. The study is also carried out for a value of γ equal to 2; this is in order to investigate the validity of the hydraulic analogy to real gas flows. The detailed flow parameters used are as follows:

L (channel length)	=	2.0 m
Y (channel half-width)	=	1.0 m
u_n (inlet u-velocity)	=	1.12 m/s
v_n (inlet v-velocity)	=	0.0
h_n (inlet depth)	=	0.05 m
h_a (surroundings depth)	=	0.062 to 0.096 m
γ	=	1.4 and 2.0

The task of this study is to compute, for the above parameters, the distribution of velocities and the water surface elevations. The locations and widths of the Riemann waves, if present, are to be

calculated from these predictions using the free-surface flows. These are to be compared with the available experimental data for the compressible-gas flows. Further, for a typical case, runs are performed to assess the effect of the grid size on the solution.

8.3.3 Details of the Computations

(a) Equations solved

The equations solved are the continuity and the two momentum equations given by equations (8.1) to (8.3).

(b) Boundary conditions

The boundary conditions employed in the computations, for the flow geometry shown in Figure 8.1 (b), are:

(1) Inlet plane : The flow is prescribed as uniform and parallel to the jet centre-plane, with:
$u = u_n$, $h = h_n$ and $v = v_n = 0$

(2) Plane of symmetry : $v = \partial u/\partial y = \partial h/\partial y = 0$

(3) Exit plane : The exit boundary is placed sufficiently far downstream for the flow to be supercritical. The depth prescribed there is uniform and equal to the surroundings depth (h_a).

(4) Fixed free-stream boundary : The top boundary of the channel flow domain simulates stagnant and fixed pressure surroundings, with:
$u = 0$, $h = h_a$ and $\partial v/\partial y = 0$.

Remark : The top boundary, therefore, simulates an infinite-capacity reservoir with uniform depth (h_a) prevailing everywhere and with flow crossing the boundary only in the direction normal to the symmetry plane.

(c) Initial conditions

The u-velocity, depth and pressure fields were initialised with uniform values equal to u_n , h_n and h_n respectively. It was advantageous to start the solution with a non-zero v-velocity field; uniform values of $- 0.01\ u_n$ were used.

(d) Finite-difference grid

In order to examine the effects of grid size on the solutions, six separate runs were performed for the pressure ratio = 0.55 jet ($Fr_n = M_n = 2.0$, the channel length and width were 2.4 and 1.0 m respectively). Firstly the grid was refined in the x-direction whilst fixed in the y-direction at 11 nodes; these grids were (12, 22, 35 and 45) x 11. Then the grid was refined in the y-direction whilst fixed in the x-direction at 35 nodes; these grids were 35 x (15, 20). The grid lines were uniformly distributed in both the x- and y-directions. As will be demonstrated later, the 35 x 15 grid gives substantially grid-independent results. The finite-difference grid aspect-ratio for such a grid is roughly unity.

(e) Other details

The width and position of the Riemann wave are an outcome of the calculation. No initial subcritical regions are inserted in the flow, and the wave is captured by the numerical procedure. A single computer run is made to investigate the whole pressure-ratio (PR) range. The solution is started at the highest end of PR and proceeds towards the smallest PR required, with intermediate converged solutions printed out for those PR's wanted. About 200 iterations are required for the convergence of each pressure-ratio solution.

The convergence rate of the solution and stability of the procedure are found to be quite satisfactory at moderate under-relaxation factors and are enhanced by the fixed depth boundary conditions applied at the free-stream boundary. Typical run information is summarized in Table 8.3.

VARIABLE	VALUE
$Fr_n = M_n$	1.92
γ	1.40
Pressure ratio ($P_n/P_a = (h_n/h_a)^{\gamma}$)	0.51
"Nozzle" exit flow angle	0^o
Grid	35 x 15
Type of grid spacing	Uniform
Grid size ($\Delta x / \Delta y$)	0.86
Number of iterations	200
RELAXU, RELAXV, RELAXH and RELAXP	0.5, 0.5, 0.5 and 1.0
Overall continuity error normalized to inlet flow-rate	3.5 E-7
Max. h' normalized to h_n	8.2 E-7
Computer time in CDC 6600 seconds	72

TABLE 8.3 : COMPUTATIONAL DETAILS FOR PREDICTING TWO-DIMENSIONAL OVEREXPANDED FREE JET

8.3.4 Presentation of the Results

The computed general behaviour of the flow is presented in Figures 8.2 and 8.3. This is shown in terms of perspective views of surface elevations and a velocity-vector plot for the pressue ratio of

0.51, and for $\gamma = 1.4$. Figure 8.4 shows the corresponding computed depth contours normalized to the channel-inlet depth (h_n). The Froude-number contours and streamlines (dashed lines) are presented in Figure 8.5.

The computed width and location of the Riemann waves are plotted against the pressure ratio (P_n / P_a) and compared with the experimental values of Ferri (1949) in Figure 8.6. The values corresponding to the hydraulic analogy ($\gamma = 2$) are also shown for comparison.

8.3.5 Discussion of the Results

The computed surface elevation views shown in Figure 8.2 represent the overall features of the flow. The stream boundary collapses, in adjusting to the high depth surroundings, producing an oblique hydraulic-jump which, in a short distance, impinges on the stream centre-plane. In doing so, for the pressure ratio in question, the depth increases rapidly and a normal jump is formed (Riemann wave in analogous compressible-gas flow). A reflected shock is then formed and moves towards the stream boundary. The plot depicted in Figure 8.3, presents the direction and magnitude of the velocity vectors and shows, clearly, a flow crossing the top boundary normal to the main stream due to the high depth-gradient. Downstream, the depth gradient decreases and negligible fluid crosses the top boundary.

The contours presented in Figures 8.4 and 8.5 further analyse the results in a quantitative manner. The depth contours of Figure 8.4 shows different levels of depth condensed in a small region around the shock. The depth gradients downstream of the shock become less steeper and the streamlines straighten out as seen in Figure 8.5. The flow in this region is usually analysed and modelled as being one-dimensional (

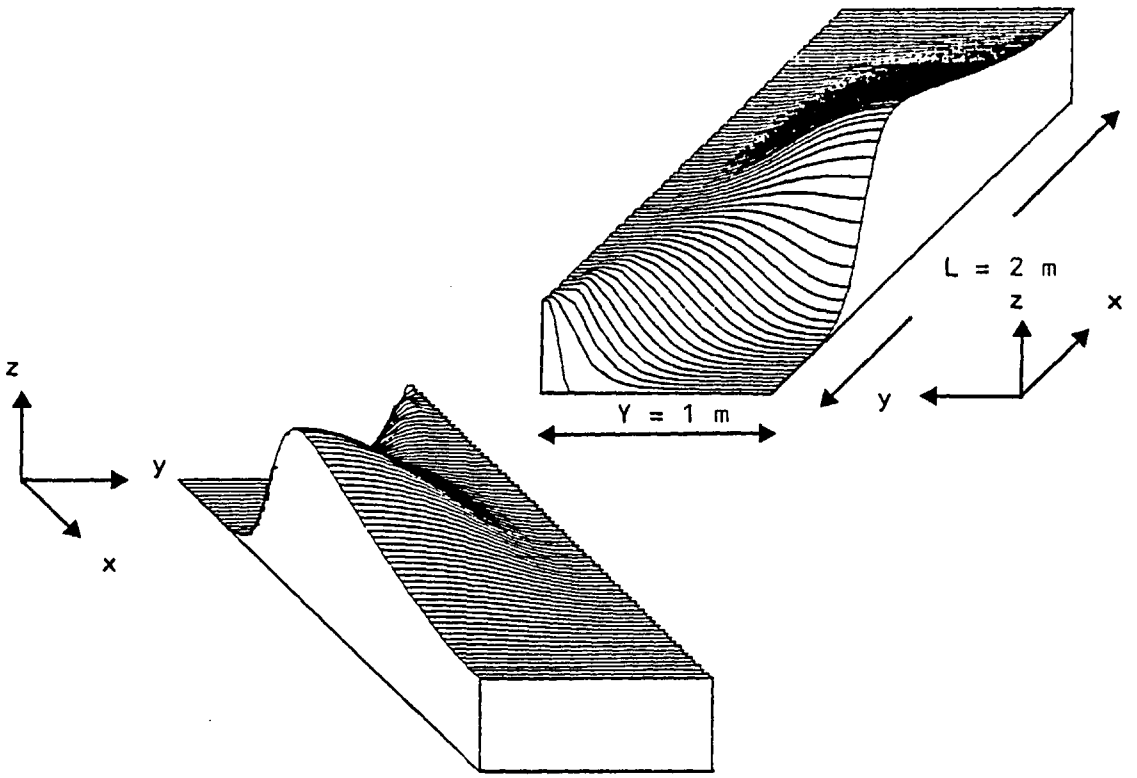


FIGURE 8.2 : PERSPECTIVE VIEWS OF THE SURFACE ELEVATIONS FOR THE SIMULATION OF OVEREXPANDED JETS (M_n = 1.92, PRESSURE RATIO = 0.51, γ = 1.4)

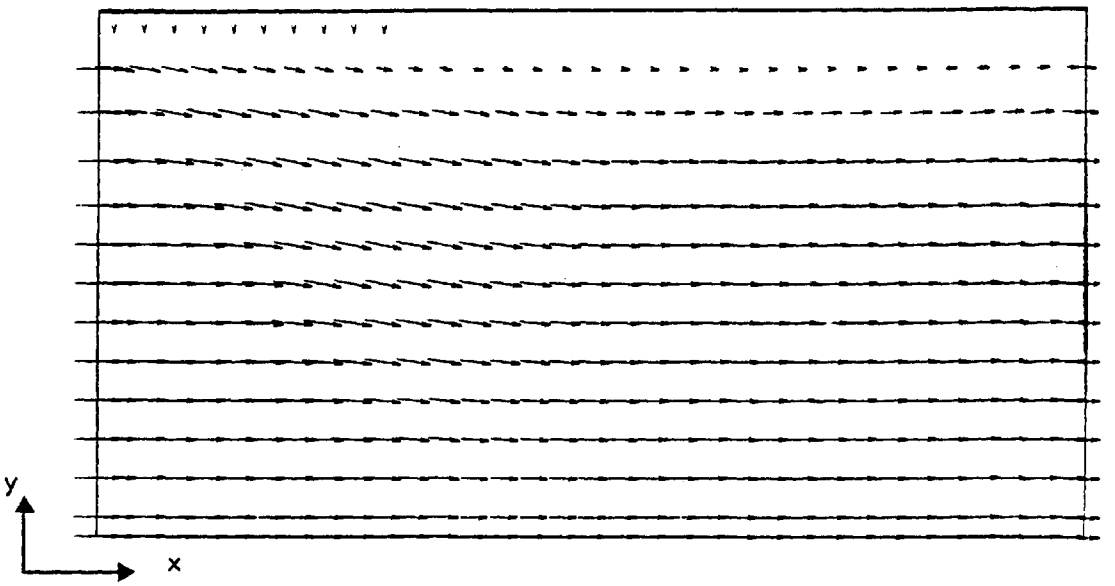


FIGURE 8.3 : VELOCITY-VECTOR PLOT FOR THE SIMULATION OF OVER-EXPANDED JETS (M_n = 1.92, PRESSURE RATIO = 0.51, γ = 1.4)

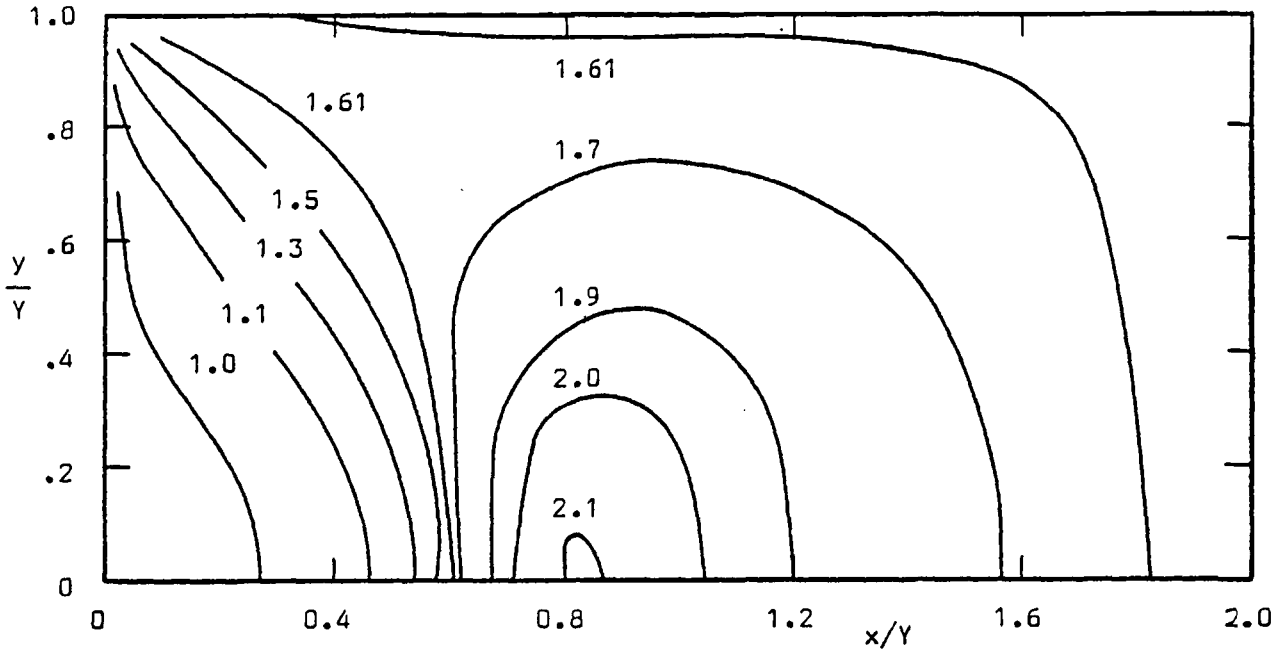
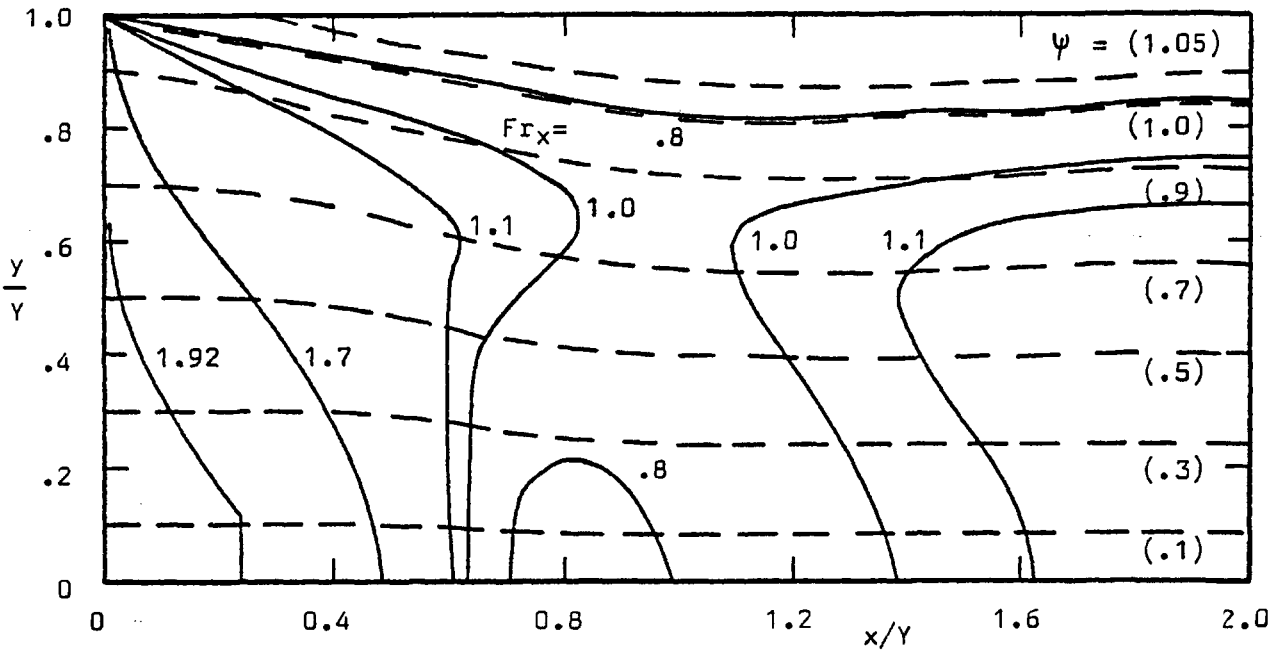


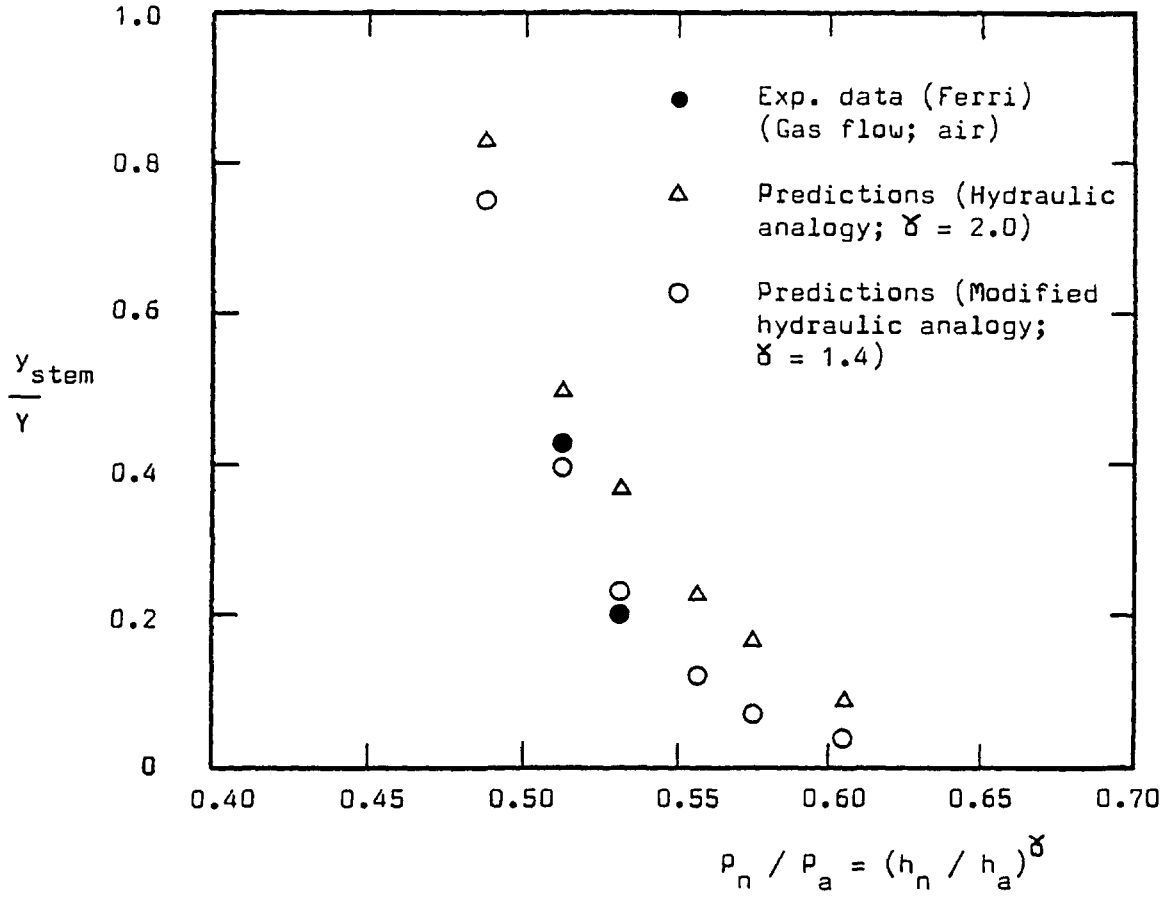
FIGURE 8.4 : COMPUTED DEPTH CONTOURS NORMALIZED TO h_n ;
SIMULATION OF OVEREXPANDED JET
(M_n = 1.92, PRESSURE RATIO = 0.51, γ = 1.4)



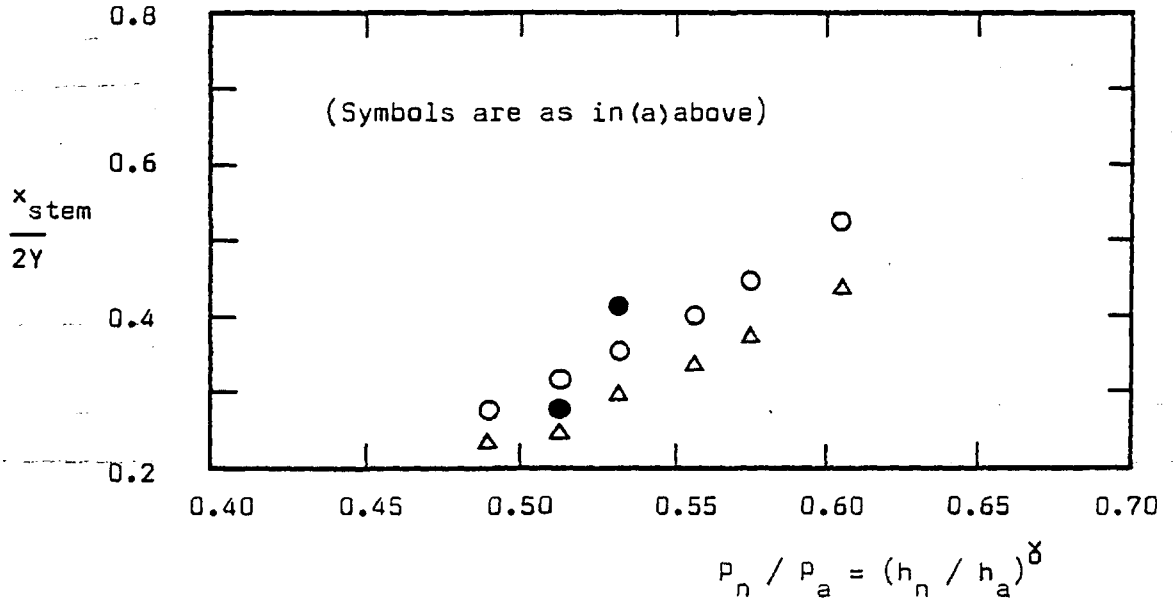
— — — Stream-function contours

——— Fr_x contours

FIGURE 8.5 : COMPUTED STREAMLINES AND FROUDE-NUMBER CONTOURS;
SIMULATION OF OVEREXPANDED JET
(M_n = 1.92, PRESSURE RATIO = 0.51, γ = 1.4)



(a) Height of Riemann wave versus pressure ratio



(b) Location of Riemann wave versus pressure ratio

FIGURE 8.6 : COMPARISON OF RIEMANN WAVE PARAMETERS FOR M_n (= Fr_n) OF 1.92; OVEREXPANDED FREE JETS

this is often used together with the application of the method of characteristics in the "supersonic" region to determine the location of the triple point). It is interesting to note that the stream-function contours, normalized to the inlet-channel flow-rate, have values in excess of 1, this is because of flow crossing the top boundary into the main stream for reasons given earlier.

The computed results shown in Figure 8.6 exhibit the correct trends, with the "Riemann wave" moving away from the channel inlet and decreasing in size as the pressure ratio increases. The experimental points show very good agreement with the computed results of the modified hydraulic analogy for δ = 1.4. Those made with the hydraulic analogy (δ = 2) are qualitatively similar but show only fair quantitative agreement. The average discrepancies between the two computed results, for the pressure-ratio range investigated, are about 40% in the heights of Riemann waves (overpredicted for δ = 2) and about 20% in the locations of Riemann waves (underpredicted for δ = 2).

The pressure-ratio range in which Riemann type reflection occurs is about 0.48 to 0.61. Below a pressure ratio of 0.48, the region downstream of the normal shock, across the whole channel width, becomes subcritical. Above a pressure ratio of 0.61, no subcritical region is captured and regular reflection occurs.

8.3.6 Grid-Dependence Check

Figures 8.7 and 8.8 show the effects of the grid size on the solution. Figure 8.7 shows the effect of refining the grid, in the x-direction, on the depth distribution on the flow centre-plane. While Figure 8.8 shows the effect of grid refinement, in the y-direction, on the depth distribution for three different cross-stream locations.

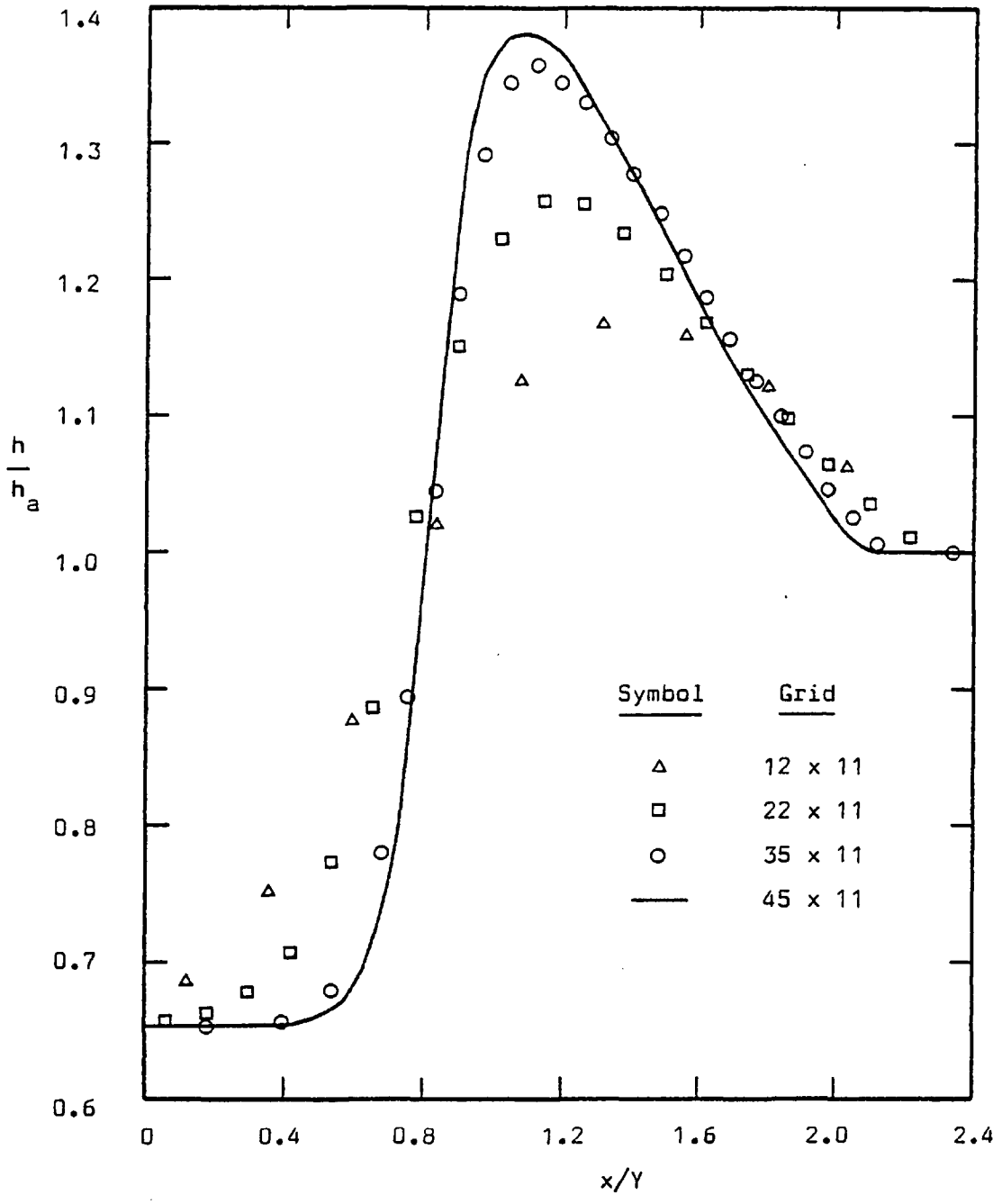


FIGURE 8.7 : COMPUTED CENTRE-PLANE DEPTH VARIATIONS; SIMULATION OF OVEREXPANDED JET (M_n = 2.0, PRESSURE RATIO = 0.55, γ = 1.4)

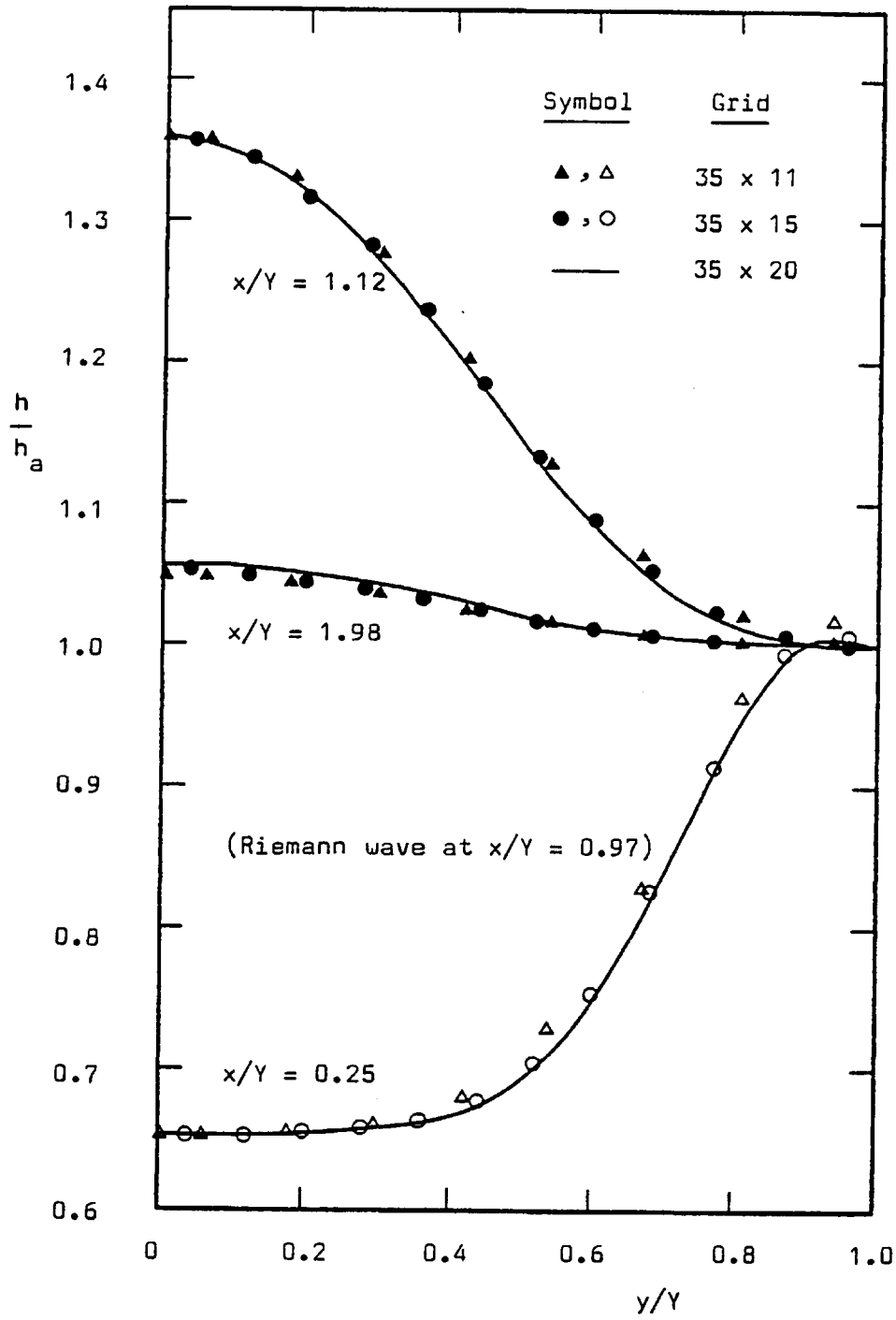


FIGURE 8.8 : COMPUTED DEPTH VARIATIONS AT THREE CROSS-STREAM LOCATIONS; SIMULATION OF OVEREXPANDED JET (M_n = 2.0, PRESSURE RATIO = 0.55, γ = 1.4)

The grid sizes are as specified in Section 8.3.3 (d) and tested on the flow with M_n = 2.0, pressure ratio = 0.55 and γ = 1.4. The centre-plane profile and the cross-stream profile at x/Y = 1.12 present typical depth variations along and across (on the downstream side) the Riemann wave on which high depth gradients prevail.

It is shown in Figure 8.7 that the jump smearing is reduced substantially by refining the grid. No significant change is observed by refining the grid from 35 x 11 to 45 x 11. Increasing the number of nodes in the y-direction, from 11 to 15 and then to 20, produces an insignificant change in the depth profiles as seen in Figure 8.8. The grid of 35 x 15 was chosen and regarded as giving grid-independent results.

8.3.7 Concluding Remarks

With reference to the objectives laid down in Section 8.3.1, the following remarks can be made:

(a) The computed results obtained from the modified hydraulic analogy have shown good agreement with experimental data, for a 2-D compressible-gas flow, by simulating an overexpanded jet. The agreement was only fair when using the hydraulic analogy (γ = 2) and it can only be concluded that qualitative agreement is achieved as generally expected.

(b) The convergence speed and stability of the numerical solution procedure were enhanced by using fixed-depth boundary conditions on the free stream as employed in the present investigation.

(c) The smearing across hydraulic jumps (shocks) was reduced substantially by refining the grid. However, sufficiently grid-independent results were obtained by employing a moderate grid size.

8.4 SIMULATION OF SUPERSONIC FLOW IMPINGEMENT ON A BLUNT BODY

8.4.1 Introduction

The main objectives of this study are to provide further validation and application of the modified analogy of free-surface flows to two-dimensional compressible-gas flows with shock waves. The validity of the hydraulic analogy of free-surface flows, i.e. where $\gamma = 2$, is also tested by comparison to flows of real gases with $\gamma = 1.4$. The stability of the numerical scheme, for simulating such discontinuous flows and the sensitivity of the solution to grid refinement, are investigated. The study is motivated by the availability of experimental data and results from various theoretical approaches, for the locations and shapes of detached shock waves in front of a flat-faced blunt body.

8.4.2 Problem Specification

(a) Flow situation and structure

The physical situation simulates the impingement of uniform and two-dimensional supersonic flows on a blunt body. The blunt body under consideration represents a 180^{o} wedge (referred to as a block) of half width B. The block is placed with its central plane parallel to the approaching flow, i.e. at zero angle of attack, which yields a symmetric flow pattern around the body. Consequently, the flow pattern for the complete block is obtained by studying one symmetric half of the flow domain, see Figure 8.9.

In adjusting to the stagnant conditions which prevail on the block face, the supersonic (supercritical) stream undergoes an oblique shock wave (hydraulic jump); a subsonic (subcritical) region is then

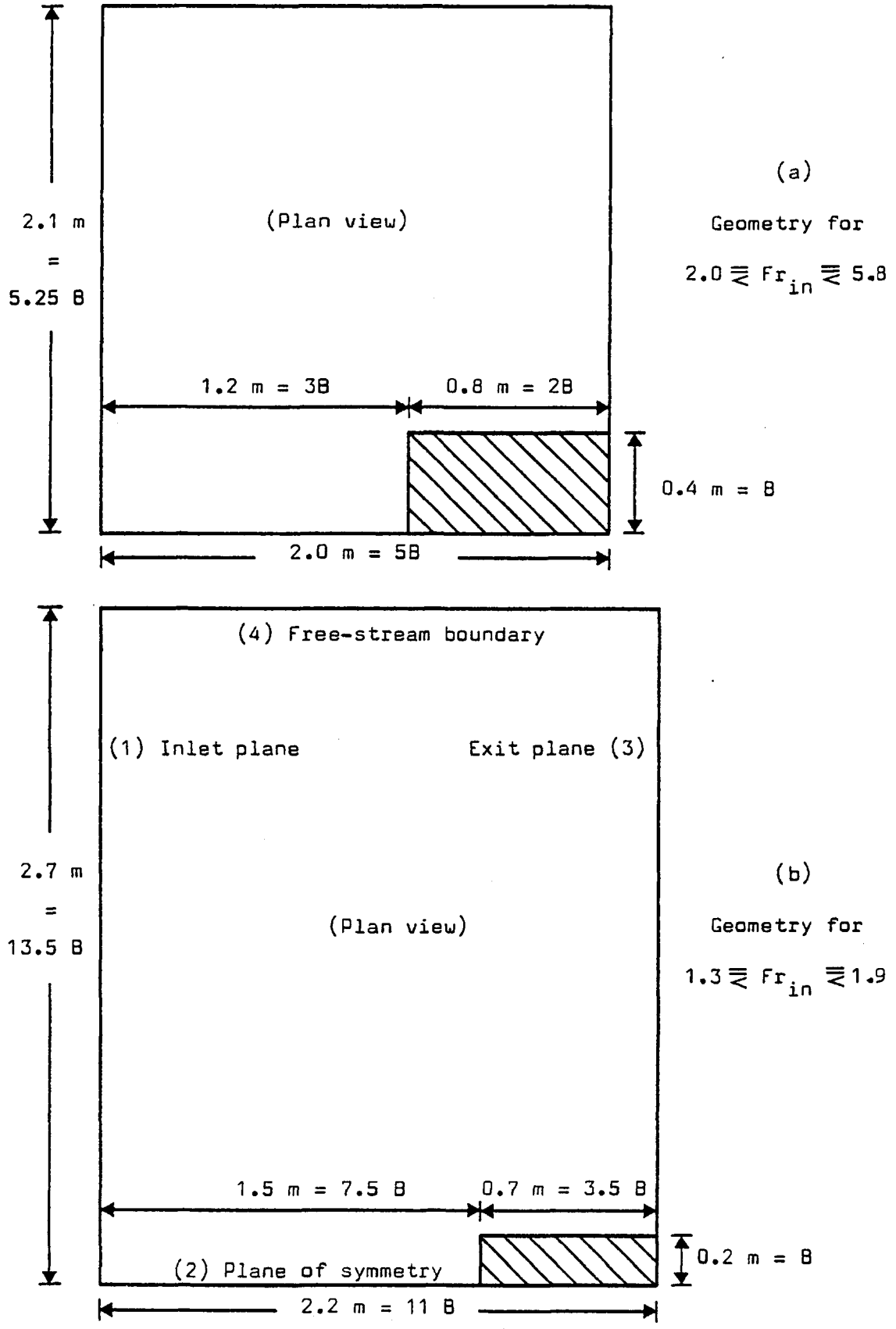


FIGURE 8.9 : FLOW IMPINGEMENT ON A BLUNT BODY SHOWING GEOMETRY AND BOUNDARY CONDITIONS

created between the shock and the body. The subsonic flow is deflected round the body and accelerates, due to expansion, to supersonic flow again passing the sonic (critical) line. The sonic line extends from the tip of the body to a point on the shock.

The shock wave will always be detached, and is called a head or bow wave, due to the large angle of the wedge which is well beyond the critical angle for any free-stream Mach number (the critical half-angle for wedges being about 45^{o} for $\gamma = 1.4$). The portion of the detached shock wave immediately on the central plane is normal to the incoming flow. Thus, the flow characteristics in this small region approximate those for a normal shock wave; on either side, the shock becomes oblique and its strength decreases.

The flowfield pattern is primarily dependent upon the free-stream Mach number (M_{in}) and the width of the body (2B). As M_{in} decreases, the shock wave moves farther away from the body and becomes weaker.

(b) Theoretical and experimental information

Studies of supersonic flow impingement on blunt bodies have centred mainly on axially-symmetric flows. This is because shapes such as discs, spherical caps, blunted cones, etc. assume more practical importance in space technology. However, studies on two-dimensional flat-faced bodies, like the one considered here, are common as typical examples for testing theoretical models. This is because 2-D flows are simpler to analyse and, finite-difference grids of fixed type are easier to fit on flat shapes such as a rectangular body.

A few selected studies on plane supersonic flow impingement on rectangular bodies are summarized in Table 8.4.

Author (s)	Year	Study
(1) Moeckel	1949	Theoretical (continuity and geometric approximate methods); M_{in} = 1.15 to 3.6.
(2) Griffith	1952	Experimental; M_{in} = 1.16 to 1.80.
(3) Xerikos & Anderson	1962	Theoretical (method of integral relations); M_{in} = 5.80.
(4) Burstein	1966	Theoretical (time-marching finite-difference method, 2nd order accuracy); M_{in} = 4.23 (γ = 1.4) & 10.0 (γ = 1.17).
(5) Bazzhin, in Hayes & Probstein	1966	Theoretical (method of integral relations); M_{in} = 5.0 & 20.0.
(6) Palumbo & Rubin	1972	Theoretical (time-marching finite-difference method, 2nd order accuracy); M_{in} = 2.0.
(7) Harten & Zwas	1972	Theoretical (time-marching finite-difference method, hybrid scheme); M_{in} = 4.23.
(8) Srinivas & Gururaja	1977	Theoretical (time-marching finite-difference method, 1st order accuracy); M_{in} = 4.23.

TABLE 8.4 : SELECTED STUDIES OF TWO-DIMENSIONAL (PLANE) SUPERSONIC FLOW IMPINGEMENT ON RECTANGULAR BODIES

(γ = 1.4 unless stated)

The information obtained from most of these studies is limited to shapes and locations of the detached shock waves and the results lack comparison with experimental data. The computed results were validated by comparison with the results of other schemes and, generally, good agreement was found. The computer time required for the solutions obtained using the time-marching techniques was measured in number of

hours. Steady-state solutions were achieved in the region of 2000 time steps. These studies were briefly discussed in Section 2.5.2.

(c) Flow parameters

The study is carried out for a wide range of free-stream Froude (Mach) number. The free-stream depth and velocity are chosen to yield Froude numbers (Fr_{in}) between 1.3 and 5.8. The study simulates a precific-heat ratio of 1.4 (air).

The detached shock-wave location and shape are highly dependent on Fr_{in}. Thus, in order to simulate the flow accurately and economically, two different block and flow domain sizes were found to be necessary depending on whether Fr_{in} is high or low. Figures 8.9 (a) and 8.9 (b) show the block and flow domain sizes which were found to be optimum for $2.0 \leqq Fr_{in} \leqq 5.8$ and $1.3 \leqq Fr_{in} \leqq 1.9$ respectively. The flow domain and block sizes are clearly dimensioned in terms of physical lengths and also in terms of ratios of block half-width (B). The detailed flow parameters used are as follows:

(i) $2.0 \leqq Fr_{in} \leqq 5.8$

Block half-width	=	0.40	m	or	1.00 B
Channel length	=	2.00	m	or	5.00 B
Channel half-width	=	2.10	m	or	5.25 B
h_{in}	=	0.03	m		
u_{in}	=	0.91	m/s	to	2.63 m/s

The block is positioned at a distance equal to 3B from the inlet plane.

(ii) $1.3 \leqq Fr_{in} \leqq 1.9$

Block half-width	=	0.20	m	or	1.0 B
Channel length	=	2.20	m	or	11.0 B
Channel half-width	=	2.70	m	or	13.5 B

h_{in} = 0.01 m

u_{in} = 0.34 m/s to 0.5 m/s

The block face is positioned at a distance equal to 7.5B from the inlet plane.

The study is also carried out to simulate flows with a specific-heat ratio of 2.0 in order to test the validity of the hydraulic analogy.

The task of this study is to compute, for the above parameters, the distribution of velocities and depths. The shape and location of the detached shock waves and sonic lines are to be calculated from these predictions using the free-surface flows. These are to be compared with the available experimental data and solutions by others for the compressible-gas flows. Further, runs are performed to assess the effect of grid size on the solution.

8.4.3 Details of the Computations

(a) Equations solved

The equations solved are given by equations (8.1) to (8.3)

(b) Boundary conditions

The boundary conditions employed in the computations, for the flow geometry shown in Figure 8.9, are:

(1) Inlet plane (free stream) : The variable values specified at the inlet plane assume uniform free-stream conditions with:
$u = u_{in}$, $h = h_{in}$ and $v = v_{in} = 0$.

(2) Plane of symmetry : $v = \partial u / \partial y = \partial h / \partial y = 0$.

(3) Exit plane : Uniform depth equal to the free-stream depth (h_{in}) is prescribed.

(4) Top boundary (free stream) : The top boundary of the flow domain simulates the uniform free-stream conditions with:
$u = u_{in}$, $h = h_{in}$ and $\partial v / \partial y = 0$.

(5) Block : $u = v = 0$.

Remarks

- The location of the exit boundary does not affect the flow upstream provided it is in the supercritical region. Nevertheless, the exit boundary is placed further downstream from the block surface in order to study the flow at a sufficient distance downstream of the sonic line.

- The inlet and top boundaries of the flow domain, which assume free-stream conditions, are located far away from the block. The conditions prevailing there would, then, be the undisturbed free-stream conditions.

(c) Initial conditions

The computations were started by using the free-stream conditions as initial conditions. It was advantageous to start the solution with a non-zero v-velocity field and uniform values of $0.05\ u_{in}$ were used.

(d) Finite-difference grids

In order to examine the effects of grid size on the solutions, seven separate runs were performed for a free-stream Froude number of 2.8 (which lies roughly in the middle range of Fr_{in} studied). Firstly,

the grid was refined in the x-direction whilst fixed in the y-direction at 23 nodes; these grids were (12, 20, 27 and 36) x 23. Then the grid refinement was tested in the y-direction whilst fixed in the x-direction at 36 nodes; these grids were 36 x (12, 17 and 30). The grid lines were non-uniformly distributed in both the x- and y-directions. Constant x-lines were more packed ahead of the block surface, whilst constant y-lines were coarsely distributed away from the block towards the top boundary.

As will be demonstrated later, a grid of 27 x 17 gives substantially grid-independent results. However, an even finer grid of 36 x 30 was employed in this study so as to ensure sufficient grid-independent results for the whole range of Froude numbers ($2.0 \leqq Fr_{in} \leqq 5.8$). Similar grid distribution was used for $1.3 \leqq Fr_{in} \leqq 1.9$ but with a grid of 36 x 35 fitted on a larger physical domain. The distributions of these grids are shown later.

(e) Other details

Preliminary runs were first made in order to decide upon the optimum physical size of the flow domain and also on optimum grid size and distribution for a wide range of Fr_{in} . A single computer run was then made to investigate the whole range of Fr_{in} between 2.0 and 5.8. Another run was also made but for a larger physical domain, to investigate the whole range of Fr_{in} between 1.3 and 1.9.

Due to the initial conditions used the shock was initially produced at the block face; as the solution progressed it became detached. Intermediate converged solutions were obtained and printed out for those values of Fr_{in} selected. About 300 iterations were required for the convergence of each solution. By monitoring the momentum and continuity

errors and the variable changes with iteration, it was found that the numerical scheme was very stable and produced monotonic convergence. Typical run information is summarized in Table 8.5.

VARIABLE	VALUE
$Fr_{in} = M_{in}$	2.80
γ	1.40
Grid	36 x 30
Type of grid spacing	Non-uniform
Number of iterations	300
RELAXU, RELAXV, RELAXH and RELAXP	0.5, 0.5, 0.5 and 1.0
Overall continuity error normalized to inlet flow-rate	3.4 E-4
Max. h' normalized to h_{in}	5.5 E-4
Computer time in CDC 6600 seconds	260

TABLE 8.5 : COMPUTATIONAL DETAILS FOR PREDICTING FLOW IMPINGEMENT ON A RECTANGULAR BODY

8.4.4 Presentation of the Results

All the results presented and discussed below for the impingement on rectangular bodies, i.e. 180^{o} wedges, are for $\gamma = 1.4$ unless specifically stated.

The general behaviour of the computed flow is presented in Figures 8.10 and 8.11. This is shown with perspective views of surface elevations (viewed from different angles) and a velocity-vector plot. The free-stream Froude number is 5.0 and the geometry used is the one depicted in Figure 8.9 (a). The corresponding detailed description of

the flow is presented in Figures 8.12 and 8.13. Figure 8.12 shows the computed depth contours normalized to the free-stream depth; whereas Figure 8.13 presents the computed Froude-number contours (continuous lines) and the stream-function contours (dashed lines), normalized to the inlet flow-rate, up to y/B = 4.2. In the region beyond y/B = 4.2 and up to y/B = 5.25 where the top boundary is located, the free-stream conditions prevail.

Figure 8.14 presents the comparison between theoretical, numerical and experimental shock standoff distances (L), appropriately non-dimensionalized to the block half-width (B). The computed L's using the hydraulic analogy (γ = 2) are also shown for comparison.

Figures 8.15 to 8.17 present the shock shape, shock location and sonic line at different free-stream Mach numbers ($M_{in} = Fr_{in}$). The predicted results are compared to the experimental results of Griffith (1952) and to the results of Bazzhin (in Hayes, W.D. et al, 1966) obtained from the method of integral relations.

Figure 8.18 shows the pressure (or depth) distribution on the block face normal to the free stream. The variable distributions are appropriately normalized to their stagnation values (with subscript 0) at the centre-plane. This normalization enables direct pressure comparison between free-surface and compressible-gas flows through $P / P_0 = (h / h_0)^{\gamma}$. The computed results are compared to the experimental data of Griffith for compressible-air flow.

Figure 8.19 shows a comparison between a one-dimensional analysis for the depth ratio across the jump (normal jump conditions) and the computed depth ratio across the bow shock on the centre-plane. (The shock conditions on the centre-plane very closely resemble normal shock conditions).

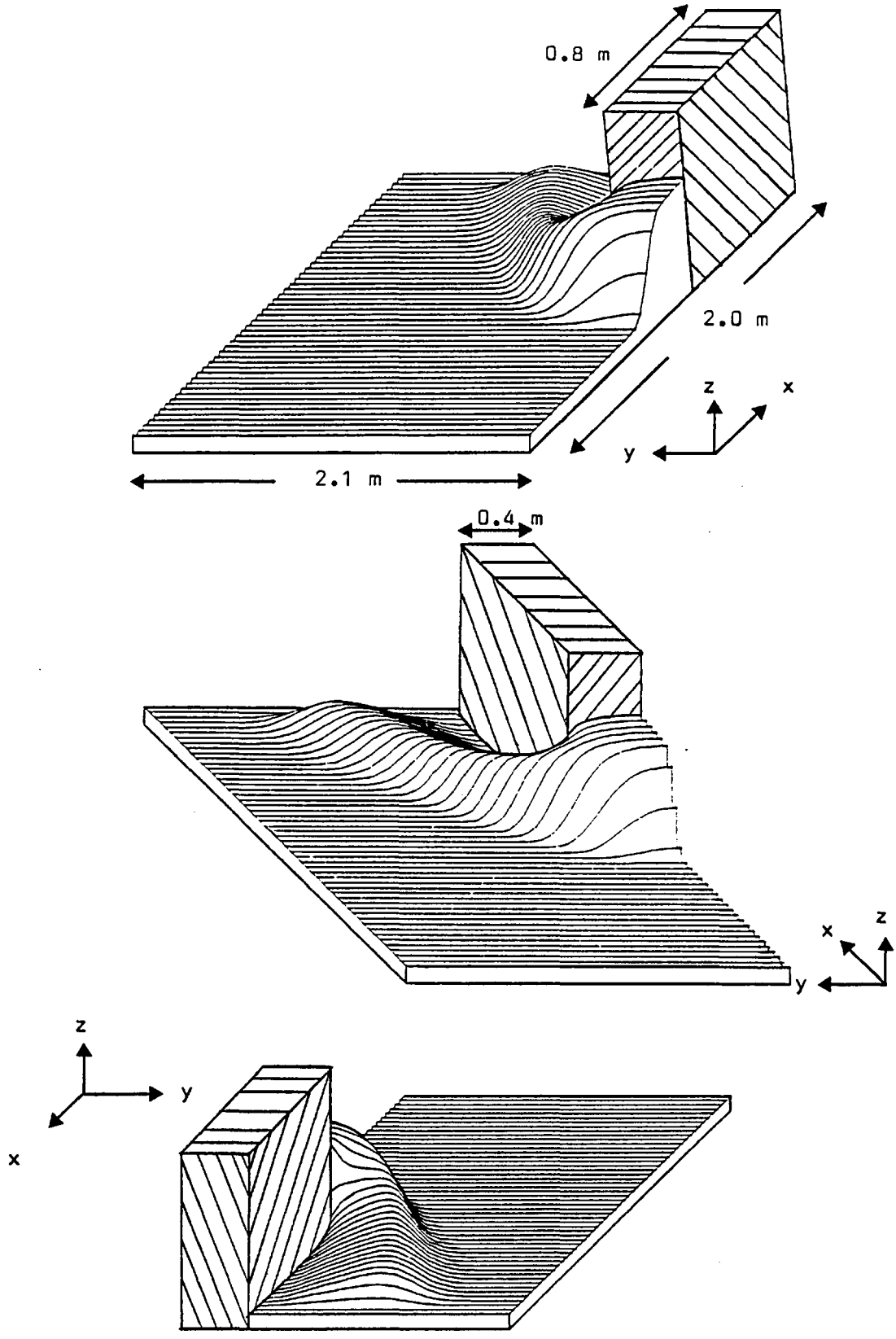


FIGURE 8.10 : PERSPECTIVE VIEWS OF THE SURFACE ELEVATIONS OF FLOW IMPINGEMENT ON A BLUNT BODY ($Fr_{in} = M_{in} = 5.0$, $\gamma = 1.4$)

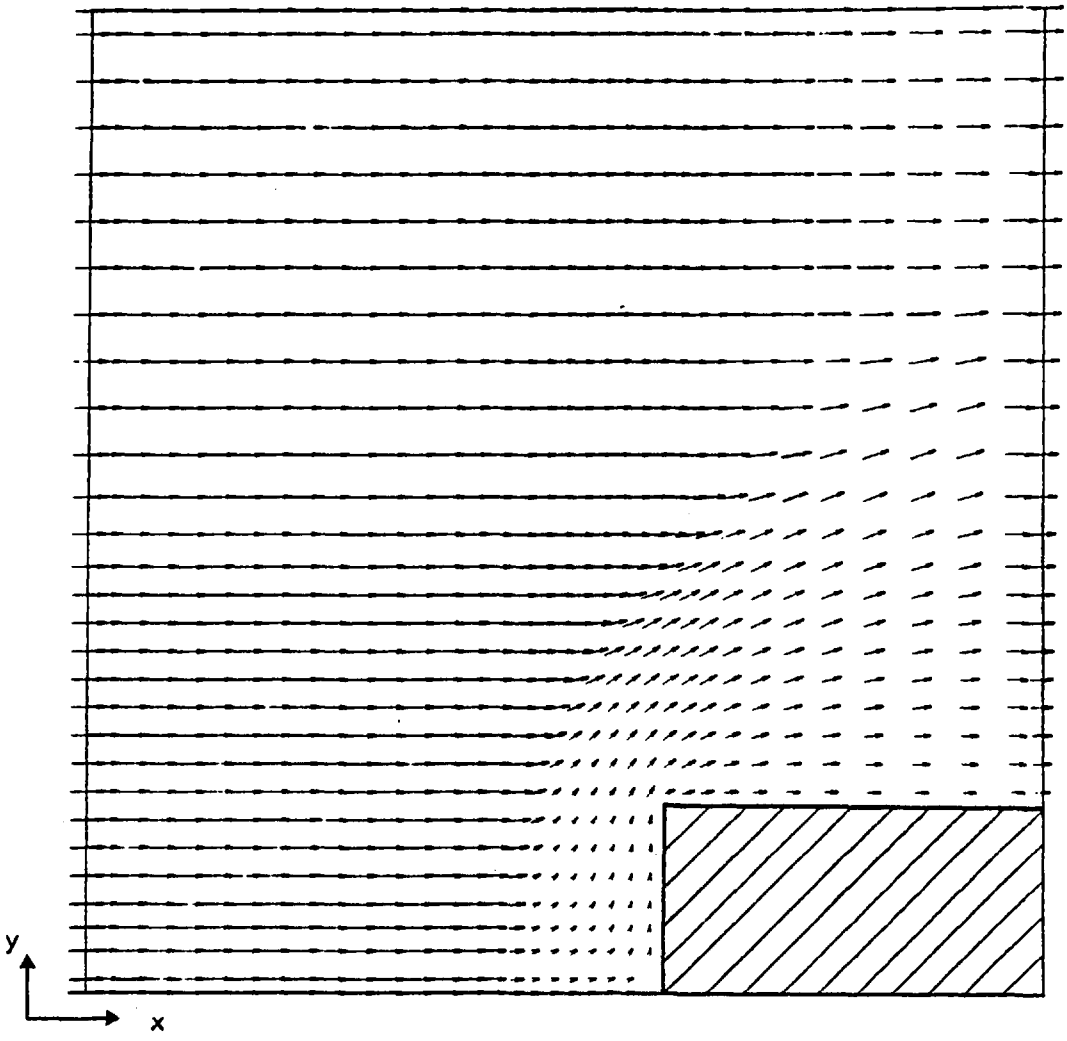


FIGURE 8.11 : VELOCITY-VECTOR PLOT OF FLOW IMPINGEMENT ON A BLUNT BODY ($Fr_{in} = M_{in} = 5.0$, $\gamma = 1.4$)

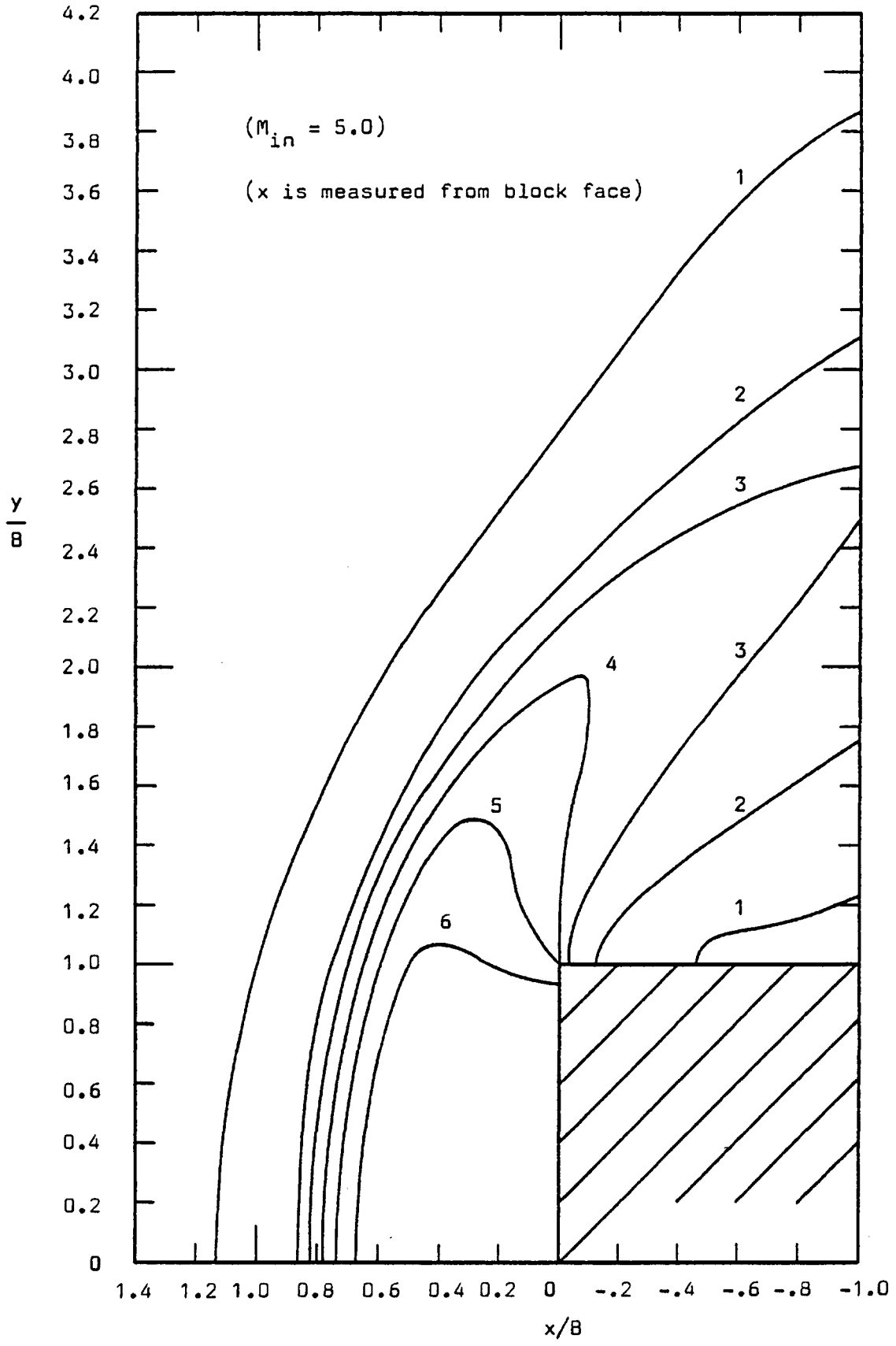
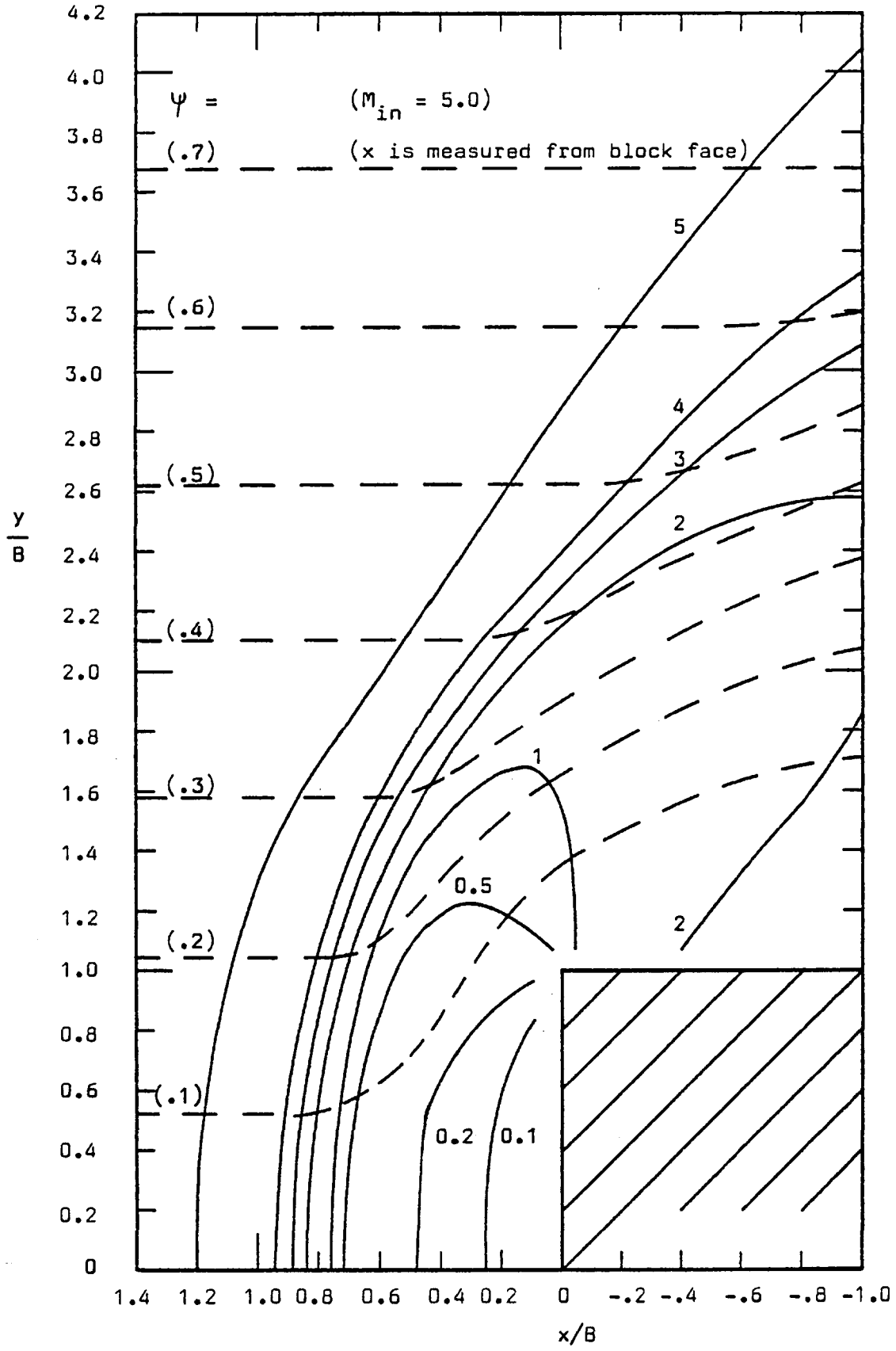


FIGURE 8.12 : COMPUTED DEPTH CONTOURS NORMALIZED TO h_{in} ; SIMULATION OF FLOW IMPINGEMENT ON A BLUNT BODY ($Fr_{in} = M_{in} = 5.0$, $\gamma = 1.4$)



— — — Stream-function contours

——— Fr_x contours

FIGURE 8.13 : COMPUTED STREAMLINES AND FROUDE-NUMBER CONTOURS; SIMULATION OF FLOW IMPINGEMENT ON A BLUNT BODY ($Fr_{in} = M_{in} = 5.0$, $\gamma = 1.4$)

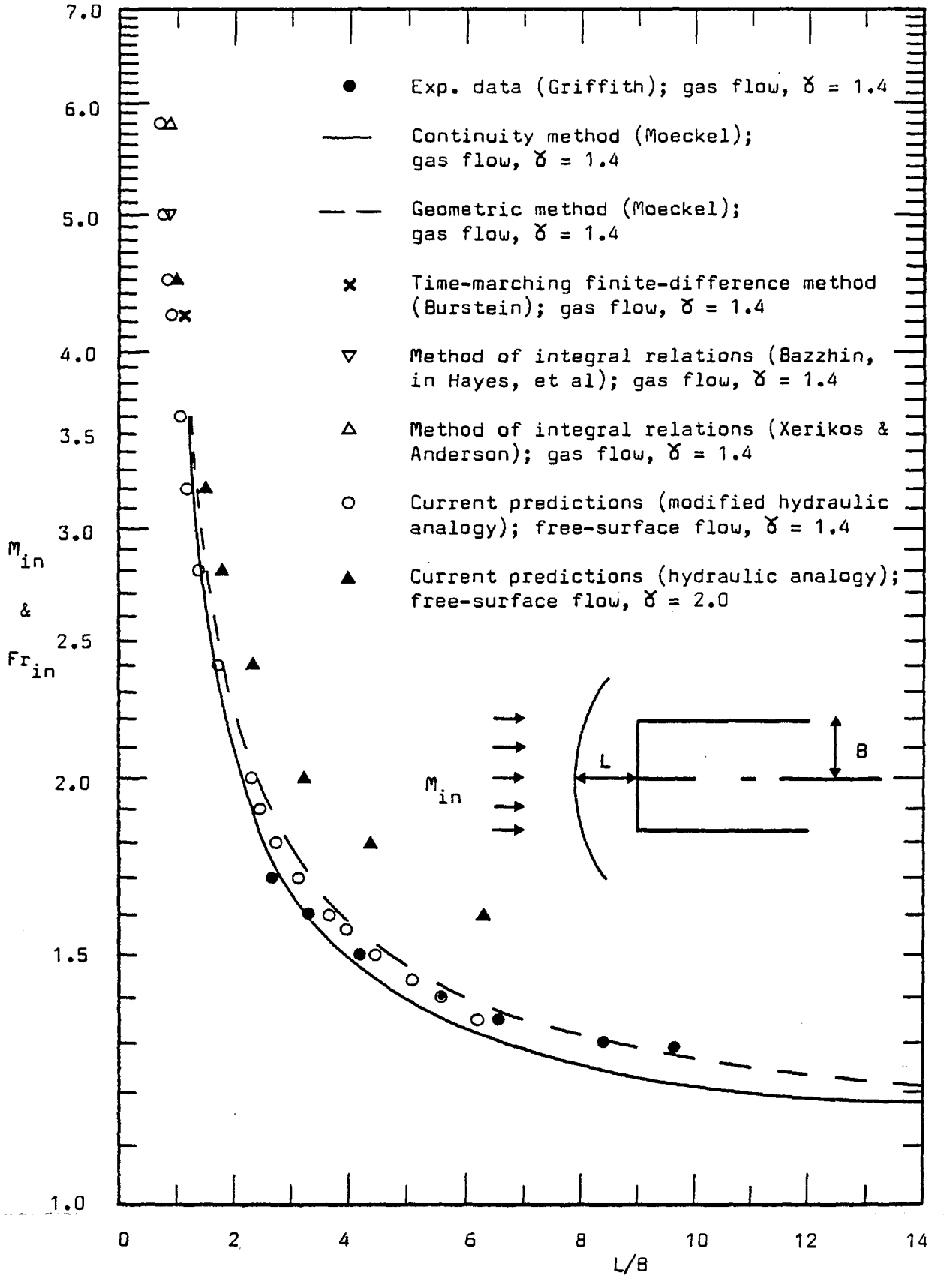
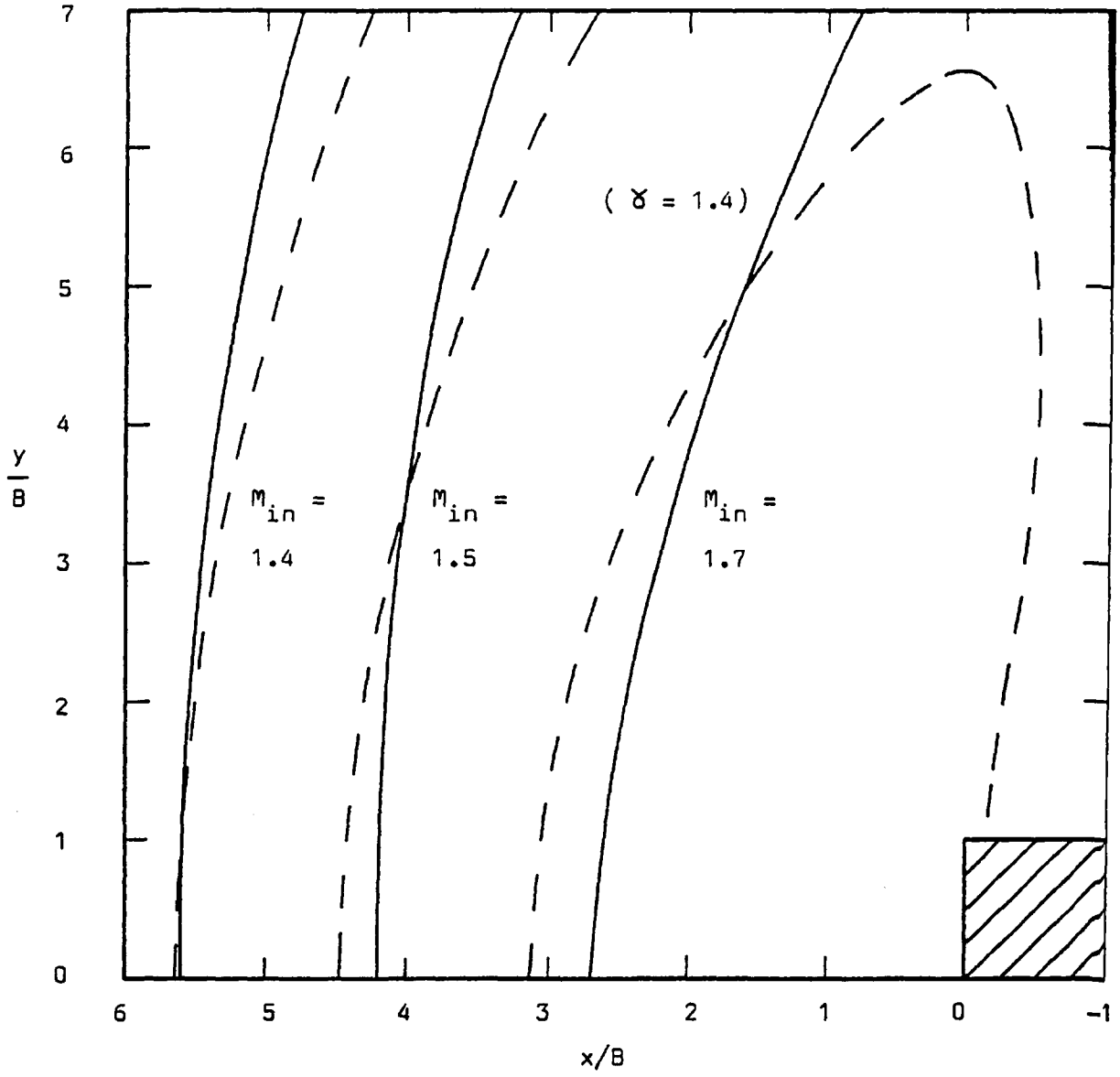


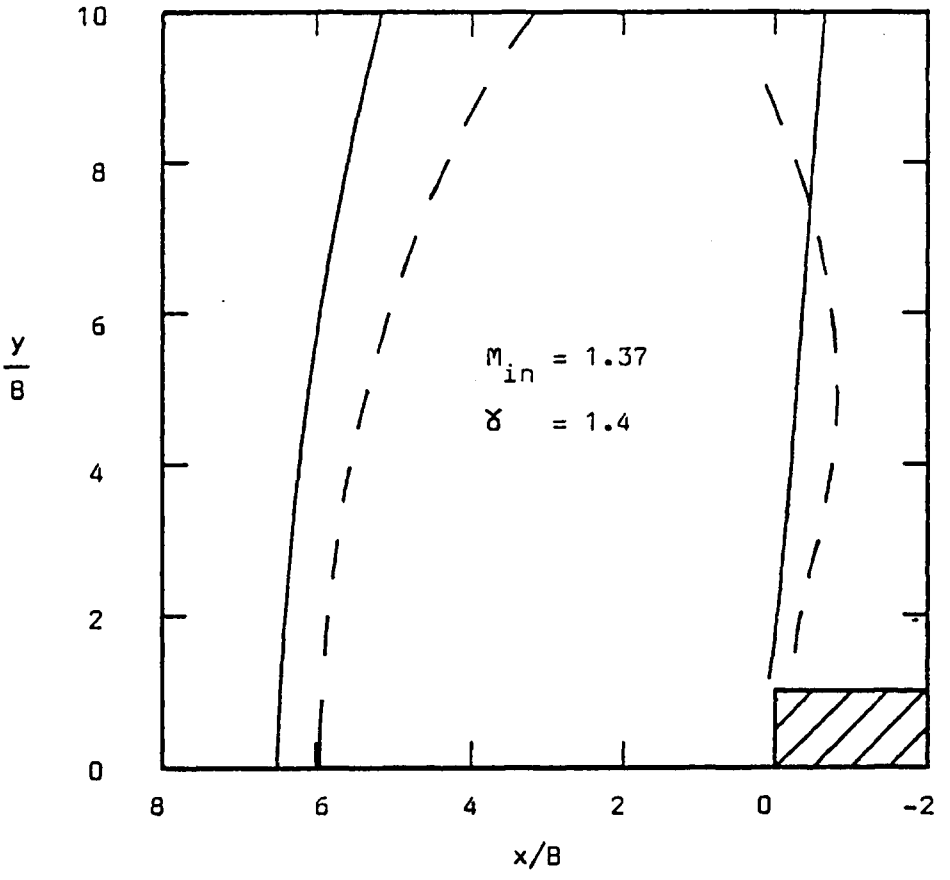
FIGURE 8.14 : COMPARISON OF THEORETICAL, NUMERICAL, AND EXPERIMENTAL SHOCK STANDOFF DISTANCES IN FRONT OF A 180° WEDGE (BLOCK) PLACED NORMAL TO THE FREE STREAM



——— Experiments (Griffith); gas flow, ϑ = 1.4

— — — Predictions; modified hydraulic analogy, ϑ = 1.4

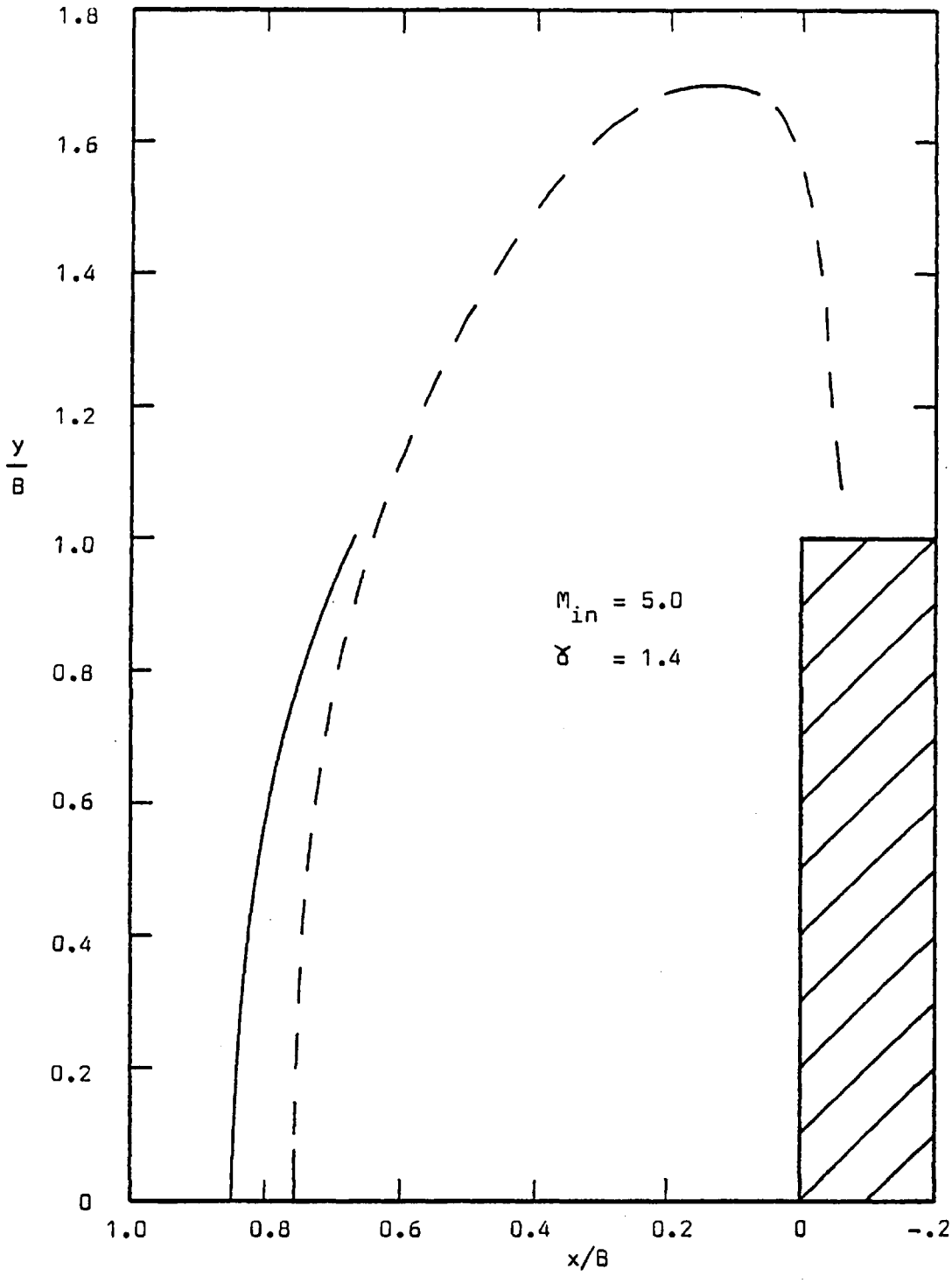
FIGURE 8.15 : SHOCK-WAVE LOCATIONS OF FLOW IMPINGEMENT ON 180° WEDGE AT DIFFERENT FREE-STREAM MACH NUMBERS



——— Experiments (Griffith); gas flow, γ = 1.4

— — — Predictions; modified hydraulic analogy, γ = 1.4

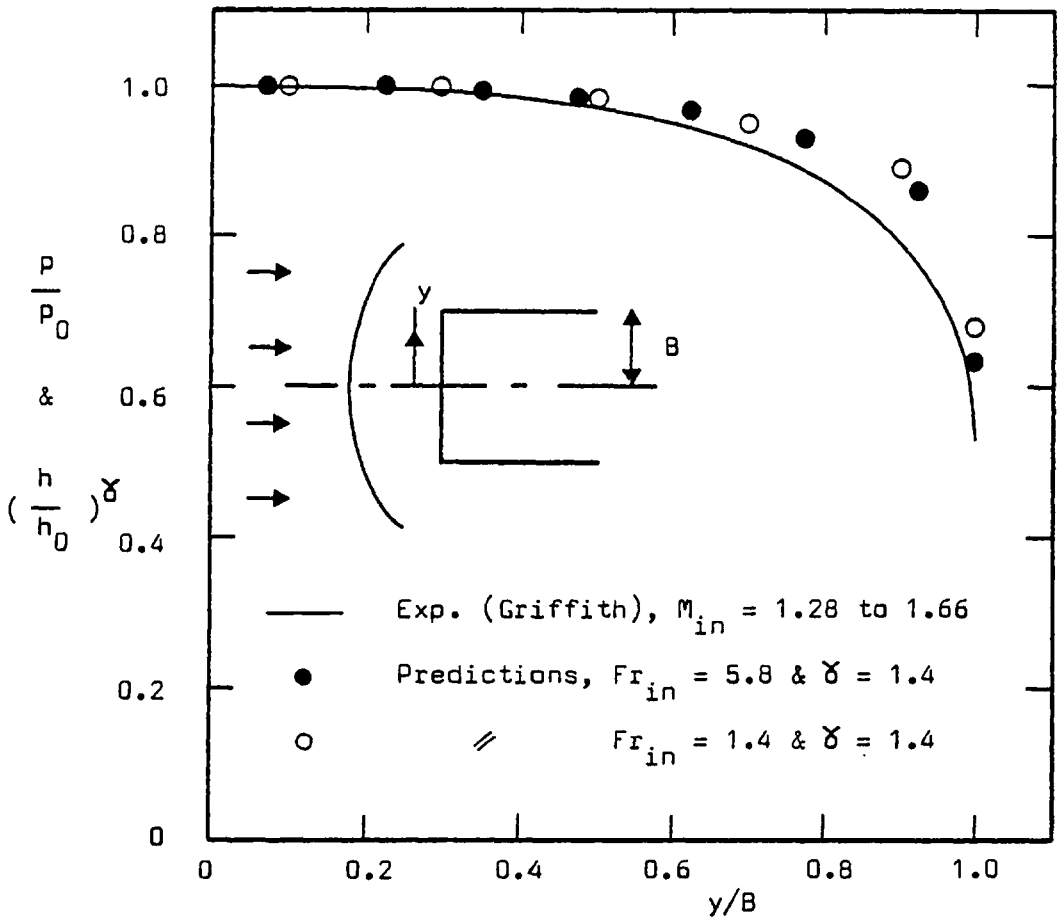
FIGURE 8.16 : SHOCK-WAVE AND SONIC-LINE LOCATIONS OF FLOW IMPINGEMENT ON 180° WEDGE AT FREE-STREAM MACH NUMBER OF 1.37



——— Method of integral relations (Bazzhin, in Hayes, et al); gas flow, ϑ = 1.4

— — — Current predictions; modified hydraulic analogy, ϑ = 1.4

FIGURE 8.17 : SHOCK-WAVE AND SONIC-LINE LOCATIONS OF FLOW IMPINGEMENT ON 180° WEDGE AT FREE-STREAM MACH NUMBER OF 5.0



(Data: compressible-gas flow; air)

(Predictions: free-surface flow; γ = 1.4)

FIGURE 8.18 : PRESSURE DISTRIBUTION ON THE FACE NORMAL TO FREE STREAM OF A 180° WEDGE

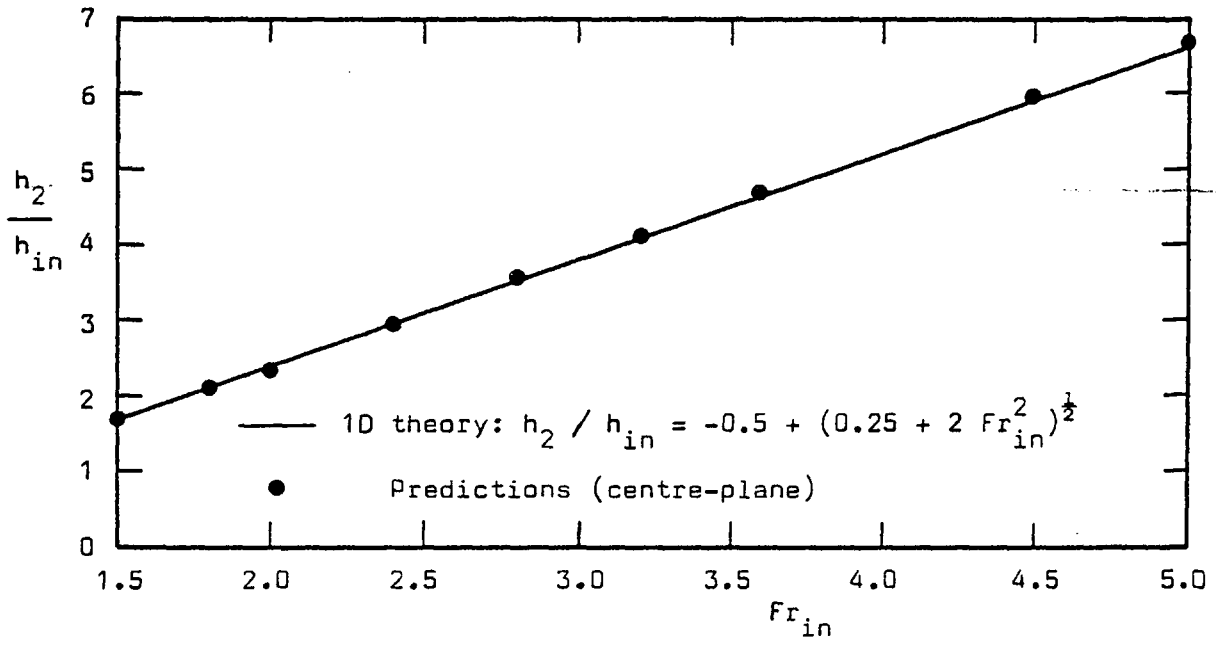


FIGURE 8.19 : CENTRE-PLANE DEPTH RATIO ACROSS THE BOW SHOCK

8.4.5 Discussion of the Results

Figures 8.10 and 8.11 show, very clearly, the overall features of the supercritical flow impingement on a rectangular body as discussed in Section 8.4.2 (a). The depression in depth seen at the exit boundary is due to the prescribed free-stream depth (see Figure 8.10). However, this has no effect on the upstream flow as long as the exit flow remains at supercritical conditions.

The presence of the block in the approaching supercritical flow, induces an oblique hydraulic-jump, across which, there is an abrupt change in the flow properties. This is analogous to a compression wave in compressible-gas flows. Beyond the body corner, the flow expands as depicted by a decrease in depth and an increase in the magnitude of the velocity vectors.

The detailed features of the flow are depicted in Figures 8.12 and 8.13. The compression in the shock region is very well represented by the packed depth contours in front of the block. The depth value, normalized to the free-stream depth, changes from 1 to 6 within two cell lengths. This suggests that the shock is smeared over 2 cells. The flow is then brought to stagnation accompanied by a slight increase in depth; the stagnation depth being 6.83 times h_{in} . The expanding nature of the flow beyond the block corner is again seen by the divergence of the depth contours. The Froude-number contours shown in Figure 8.13 strongly resemble those of the depth contours. The subcritical region is seen very clearly and is enclosed by the shock, the critical line and the body. The present numerical scheme gives the position of the critical (sonic) line on the body correctly, i.e. within a fraction of one cell length of the corner. This is in agreement with the results obtained from the different time-marching finite-difference schemes of

Burstein (1966), Harten and Zwas (1972), and Srinivas and Gururaja (1977). Beyond the corner the Froude number increases rapidly, indicating an expansion wave. The stream-function contours presented on the same figure illustrate how the streamlines are deflected and narrow as they pass through the disturbance created by the block.

The computed shock standoff distance using the modified analogy ($\gamma = 1.4$), plotted against the free-stream Froude (Mach) number in Figure 8.14, shows remarkable agreement with the various theoretical, numerical and experimental values obtained from compressible-air flow. The computed values obtained by using the hydraulic analogy ($\gamma = 2$) show good qualitative agreement. However, for the same free-stream conditions, the shock standoff distance always lies further away from the body as compared to its value using $\gamma = 1.4$. It can, thus, be concluded that an increase in γ (i.e. an increase in the gravitational "constant") pushes the shock upstream. This is identical to the influence of the specific-heat ratio in compressible-gas flows in which the primary effect of an increase in γ is equivalent to a decrease in M_{in}. It is interesting to note that the agreement in shock location, for the two values of γ, becomes closer at higher Fr_{in}. This is because the shock location becomes less sensitive to an increase in Fr_{in} above a value of about 3.0.

The computed shock shapes, drawn in Figures 8.15 to 8.17 for various Fr_{in} (M_{in}), show good agreement with the experimental data of Griffith and the results of Bazzhin obtained from the method of integral relations for compressible-air flows. The discrepancy found at low M_{in}, in the region further away from the symmetry plane, may be attributed to the computational top boundary not being far enough away to simulate real free-stream conditions. It is clearly seen that the shock part close to the symmetry plane resembles a normal shock wave. The experimental sonic line seen in Figure 8.16, attaches itself very near to the body corner;

the computed critical line attaches itself within one cell length of the body corner.

Figure 8.18 shows that nearly identical normalized pressure (or depth) distributions exist on the block face for a considerable range of M_{in} (or Fr_{in}). The comparison between the computed depth ratios to the power γ and the experimental pressure ratios, generally shows good agreement except very close to the corner where the agreement is only fair.

Figure 8.19 shows excellent agreement between the theoretical and computed depth ratio across the shock on the centre-plane. This indicates that the numerical scheme can handle, very efficiently, rapid variations in the flow, such as discontinuities, by giving the correct jump conditions. The shock is, however, smeared over two cells but continuity and momentum have been conserved all the way through the flow domain and across shocks.

8.4.6 Grid-Dependence Check

Figures 8.20 and 8.21 show the effects of the grid size on the solution for a free-stream Froude number value of 2.8. Figure 8.20 shows the effect of refining the grid, in the x-direction, on the depth distribution at the flow centre-plane. Figure 8.21 shows the effect of grid refinement, in the y-direction, on the depth distribution at a cross-stream location of $x/B = 1.0$ (x is measured from the block). The grid sizes are as specified in Section 8.4.3 (d). The centre-plane profile and the cross-stream profile at $x/B = 1.0$ present typical depth variations along and across the bow shock (bow shock at $x/B = 1.4$) at which the highest depth gradients in the flow prevail.

It is shown in Figure 8.20 that the jump smearing is reduced

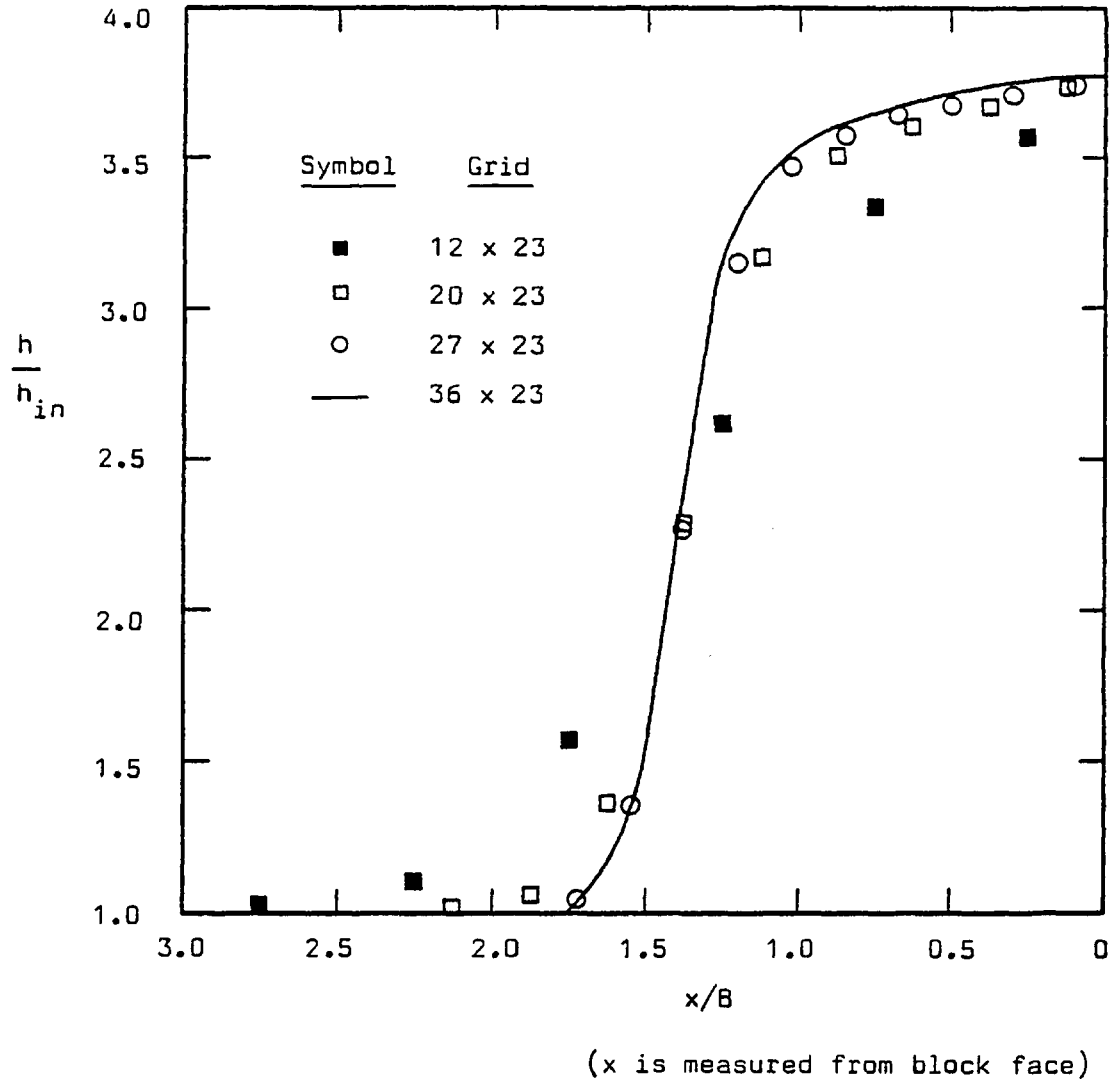
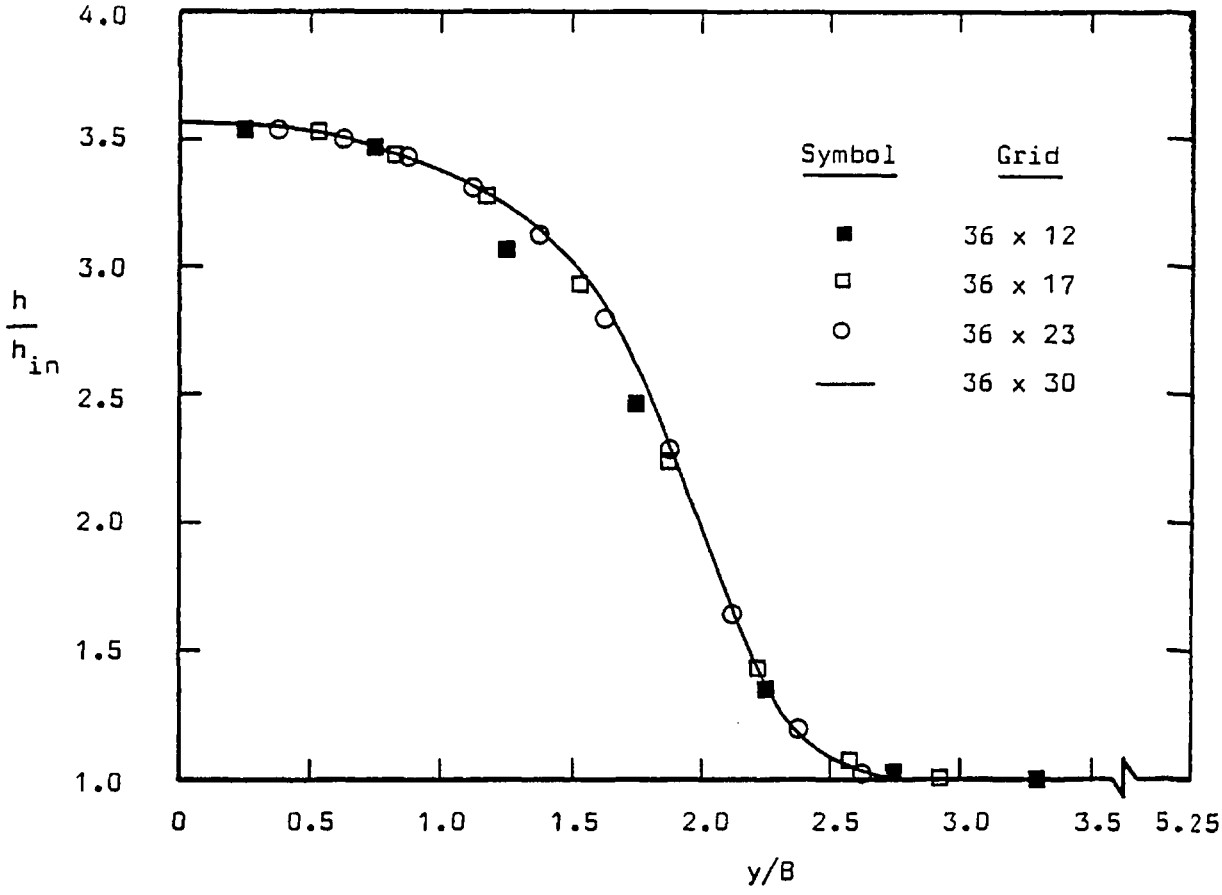
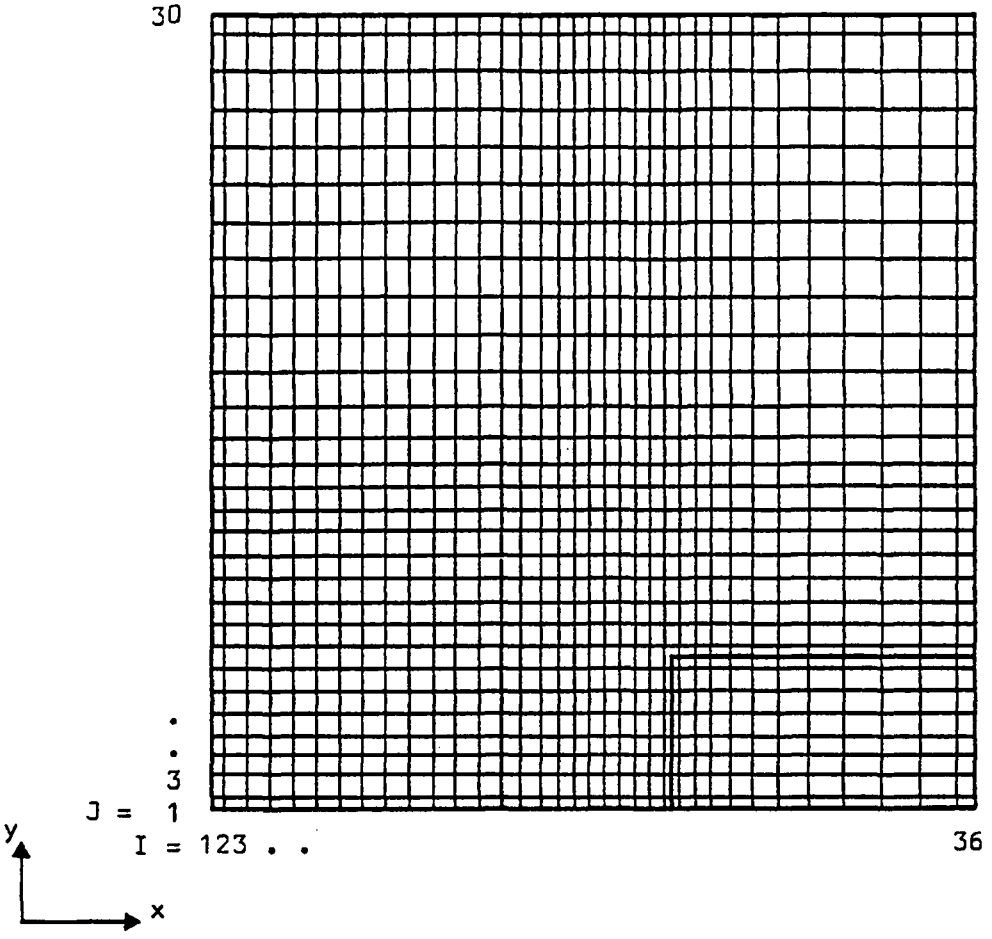


FIGURE 8.20 : COMPUTED CENTRE-PLANE DEPTH VARIATIONS FOR Fr_{in} = 2.8; FLOW IMPINGEMENT ON A RECTANGULAR BODY



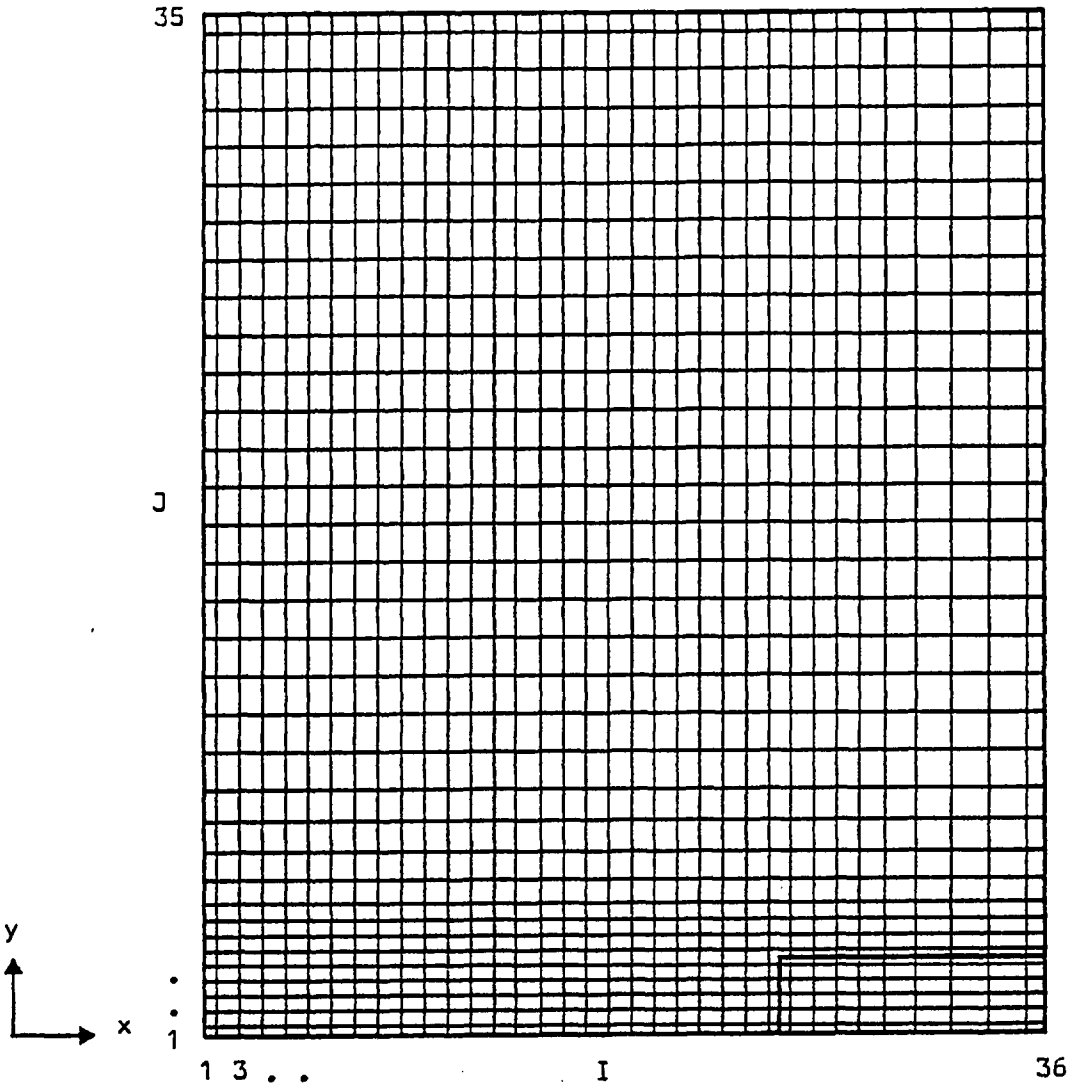
(Bow shock is at x/B = 1.4; x is measured from block face)

FIGURE 8.21 : COMPUTED CROSS-STREAM DEPTH VARIATIONS AT x/B = 1.0 FOR Fr_{in} = 2.8; FLOW IMPINGEMENT ON A RECTANGULAR BODY



I	x	I	x	J	y	J	y
1	0.00	19	0.98	1	0.00	19	1.06
2	0.03	20	1.02	2	0.03	20	1.15
3	0.09	21	1.06	3	0.09	21	1.25
4	0.15	22	1.10	4	0.14	22	1.35
5	0.21	23	1.14	5	0.19	23	1.45
6	0.27	24	1.18	6	0.25	24	1.55
7	0.33	25	1.22	7	0.31	25	1.65
8	0.39	26	1.26	8	0.37	26	1.75
9	0.45	27	1.30	9	0.43	27	1.85
10	0.51	28	1.35	10	0.49	28	1.95
11	0.57	29	1.41	11	0.55	29	2.05
12	0.63	30	1.48	12	0.61	30	2.10
13	0.69	31	1.56	13	0.67		
14	0.75	32	1.65	14	0.73		
15	0.80	33	1.75	15	0.79		
16	0.85	34	1.85	16	0.85		
17	0.90	35	1.95	17	0.91		
18	0.94	36	2.00	18	0.98		

FIGURE 8.22 : GRID USED TO PREDICT FLOW IMPINGEMENT ON A RECTANGULAR BODY FOR FREE-STREAM FROUDE NUMBER BETWEEN 2 AND 5.8



I	x	I	x	J	y	J	y
1	0.00	19	1.05	1	0.00	19	1.15
2	0.03	20	1.11	2	0.02	20	1.25
3	0.09	21	1.17	3	0.06	21	1.35
4	0.15	22	1.23	4	0.10	22	1.45
5	0.21	23	1.29	5	0.14	23	1.55
6	0.27	24	1.35	6	0.18	24	1.65
7	0.33	25	1.41	7	0.22	25	1.75
8	0.39	26	1.47	8	0.26	26	1.85
9	0.45	27	1.53	9	0.30	27	1.95
10	0.51	28	1.59	10	0.35	28	2.05
11	0.57	29	1.65	11	0.41	29	2.15
12	0.63	30	1.71	12	0.48	30	2.25
13	0.69	31	1.78	13	0.56	31	2.35
14	0.75	32	1.86	14	0.65	32	2.45
15	0.81	33	1.95	15	0.75	33	2.55
16	0.87	34	2.05	16	0.85	34	2.65
17	0.93	35	2.15	17	0.95	35	2.70
18	0.99	36	2.20	18	1.05		

FIGURE 8.23 : GRID USED TO PREDICT FLOW IMPINGEMENT ON A RECTANGULAR BODY FOR FREE-STREAM FROUDE NUMBER BETWEEN 1.3 AND 1.9

substantially by refining the grid. No significant change is observed by refining the grid from 27 x 23 to 36 x 23. Altering the number of nodes in the y-direction, from 17 to 23 and then to 30, produces an insignificant change in the cross-stream profile as seen in Figure 8.21. A grid of 27 x 17 can, thus, be considered to produce sufficiently grid-independent results. However, the grid of 36 x 30 was chosen so as to study the range of Fr_{in} between 2.0 and 5.8. A slightly larger grid was used to study the range of Fr_{in} between 1.3 and 1.9.

The effects of grid refinement show that the variation in shock location (L/B) between the coarsest and finest grids used is only 4%, which lies well within one cell length.

Figures 8.22 and 8.23 present the distributions of the finite-difference grids employed.

8.4.7 Concluding Remarks

With reference to the objectives laid down in Section 8.4.1, the following conclusions may be drawn:

(a) The computed results obtained from the modified hydraulic analogy have shown good agreement with experimental data and results from various theoretical approaches, by simulating supersonic flow impingement on rectangular bodies. This highlights the identical form of equations that govern the "modified" shallow-water equations and the compressible-gas flow equations for real gases.

(b) No non-linear instability was encountered and this allows the use of moderate under-relaxation factors. The convergence speed of the procedure was, thus, very satisfactory.

(c) Moderate grid sizes were employed and ensured sufficiently

grid-independent results. The shocks were, however, smeared over two cells but continuity and momentum have been conserved across the shocks. The computer time required to obtain a converged solution varies between 1 to 5 minutes on the CDC 6600 machine. This is compared to number of hours required by using the time-marching techniques.

8.5 CLOSURE AND GENERAL REMARKS

The finite-difference technique employed in the present study requires only a specification of the initial and boundary conditions. The technique requires neither information on whether a shock will appear nor knowledge of the shock location. The shock is an outcome of solving the governing equations over the entire region of interest.

As far as the analogy between free-surface and compressible-gas flows is concerned, it is shown that there is no necessity for the "analogous gas" to have a specific-heat ratio of 2. Minor modifications to the shallow-water flow equations are needed to bring them into conformity with the compressible-gas flow equations.

In all the examples given in the last three chapters, the computed results have shown a generally good agreement when compared to experimental and theoretical results. All disagreements found can be attributed to one or more of the following causes:

(a) Experimental uncertainties;

(b) approximations imposed on the mathematical formulation;

(c) assumptions made when discretizing the partial-differential equations into finite-difference equations; and

(d) boundary conditions employed and physical location of the computational boundaries.

The good agreement achieved in all studies, however, suggests that non of the above causes has been severly violated.

The numerical scheme used to solve the difference equations is based on the depth-correction technique, and is found to be stable, general, economical and capable of handling strong discontinuities.

C H A P T E R 9

CONCLUSIONS

9.1 ACHIEVEMENTS OF THE PRESENT STUDY

The main achievements of the present work and the conclusions thereof can best be summarized in relation to the objectives stated in Section 1.3.2, as follows:

(a) A mathematical model and solution procedure capable of predicting two-dimensional shallow-water flows were developed and presented in Chapters 3 and 4. Special features of the model include:

(i) Utilization of the widely used pressure-correction procedure of Patankar and Spalding (1972) for the determination of depth of flow. This involves:

- Implicit account of the depth variation in the formulation of the depth-correction equation.
- The use of upstream depths in evaluating the mass fluxes across the cell faces.
- Employment of Spalding's two-dimensional linear-equation solver for the solution of the depth-correction equations.

(ii) Utilization of a point-by-point solver for the solution of the momentum equations.

(iii) The method applies no restrictions on the value of Froude number; the same solution procedure applies to both subcritical and supercritical flows.

(iv) The model can handle both gradually and rapidly varied flows; hydraulic jumps are a natural outcome of the solution poced-ure. However, the model being depth-averaged, does not desc-ribe details of either the flow inside or the length of a hydraulic jump. As far as boundary conditions are concerned, the numerical stability of the procedure was enhanced for problems with fixed boundary conditions (e.g. prescribed free-stream conditions).

(v) The system is readily extendable to more complex physical processes (see next section on the suggestions for future work).

(vi) Compared to other calculation procedures, the present method is more general and economical.

(b) The comparisons of predictions with analytical results, published data and reliable solutions by others presented in Chapters 6 and 8, demonstrated the ability of the numerical procedure to accurately solve the finite-difference equations which describe the hydrodynamics. A modified hydraulic analogy was proposed and applied to the calculation of compressible-gas flows and resulted in accurate simulation.

(c) Experimental studies of supercritical flow and supercritical flow with hydraulic jumps, in channels of rectangular cross-section, were carried out to supplement the existing experi-mental information, and was described in Chapter 5.

(d) The results of the present experimental study were compared with predictions. These comparisons, presented in Chapter 7, showed that the numerical model simulated the physics of shallow-water flows fairly well.

9.2 SUGGESTIONS FOR FUTURE WORK

The following areas, arising from the present work, are considered useful for further investigation:

(a) The potential of the basic solution procedure is much greater than that demonstrated in this thesis. Subsequently, in order to realize this potential, the present procedure should be extended to:

(i) Solve for flows with heat transfer, for example, heated surface discharge into bodies of water and full-depth layer flows found in wind-stirred cooling ponds. Such flows involve one or more of the following additions to the model:

- temperature equation ,
- appropriate entrainment formula ,
- wind stresses, bed topography, etc.

(ii) Include unsteady effects, such as the simulation of tidal flows in coastal areas and estuaries.

(b) The inclusion of a suitable model of turbulence, based on depth-averaged quantities, is necessary to adequately describe the turbulent transfer of momentum, if important, in shallow-water flows.

(c) The extension of the present model to a multi-layer model for simulating three-dimensional effects, such as in stratified flows. The study would involve the interaction between layers through the exchange of mass and momentum across the interfaces.

(d) Consideration should also be given to the proper handling of irregular geometries. The use of a non-orthogonal numerical

mesh is expected to improve the accuracy and economy of the calculations for such geometries. Another possibility is to regard such irregularities as "blocked areas" to be accounted for implicitly when formulating the finite-difference coefficients for the boundary cells.

REFERENCES

(1) ABBOTT M B (1974)
"Continuous Flows, Discontinuous Flows and Numerical Analysis"
Journal of Hydraulic Research, Vol. 12, No. 4, pp. 417-467.

(2) ALLEN J & THANARAJAH J C M (1977)
"The Movement of Oil Slicks under the Action of the Wind"
IAHR, 17 th Congress, Vol. 3, pp. 195-202.

(3) AL-SANEA S A, PUN W M & SPALDING D B (1978)
"Computation of Two-Dimensional Elliptic Flows, Including Heat Transfer"
Imperial College, London, Mechanical Engineering Department Report No. HTS/78/5.

(4) ARUMUGAM K (1955)
"Surface Characteristics of Fast-Moving Water Emerging from a Sluice"
Ph.D. Thesis, University of London.

(5) AWN A G A (1979)
"Numerical Modelling of Flows with Moving Interfaces"
Ph.D. Thesis, University of London.

(6) BAGGE G & HERBICH J B (1967)
"Transitions in Supercritical Open-Channel Flow"
Journal of the Hydraulics Division, ASCE, Vol. 93, No. HY 5, pp. 23-41.

(7) BAGHDADI A H (1979)
"Numerical Modelling of Two-Phase Flow with Inter-Phase Slip"
Ph.D. Thesis, University of London.

(8) BAKHMETEFF B A & MATZKE A E (1936)
"The Hydraulic Jump in Terms of Dynamic Similarity"
Trans. ASCE, 101, pp. 630-680.

(9) BAZZHIN A P (1966)
in W.D. Hayes and R.F. Probstein (eds.), "Hypersonic Flow Theory", 2nd Edition, Vol. I, Academic Press, New York, p. 426.

(10) BLACK J & MEDIRATTA O P (1950-51)
"Supersonic Flow Investigations with a "Hydraulic Analogy" Water Channel"
The Aeronautical Quarterly, Vol. 2, Part IV, pp. 227-253.

(11) BREBBIA C A & PARTRIDGE P W (1976)
"Finite Element Simulation of Water Circulation in the North Sea"
Appl. Math. Modelling, 1, pp. 101-107.

(12) BROUDE B G (1956)
"Use of the Gas-Hydraulic Analog for the Study of Gas Dynamics"
Soviet Physics, Technical Physics, Vol. 1, Part 2, pp. 1538-1553.

(13) BRYANT R A A (1956)
"The One-Dimensional and Two-Dimensional Gas Dynamics Analogies"
Austral. J. Appl. Sci., Vol. 7, No. 4, pp. 296-313.

(14) BRYANT R A A (1960)
"The Hydraulic Analogy for External Flow"
Journal of the Aerospace Sciences, 27, pp. 148-149.

(15) BURGGRAF O R (1966)
"Analytical and Numerical Studies of the Structure of Steady Separated Flows"
J. Fluid Mech., Vol. 24, Part 1, pp. 113-151.

(16) BURSTEIN S Z (1966)
"Finite Difference Calculations for Hydrodynamic Flows Containing Discontinuities"
J. Comp. Phys., Vol. 1, No. 2, pp. 198-222.

(17) CARROLL G W (1980)
"Experimental and Theoretical Investigation of Three-Dimensional Turbulent Mixing in Jets and Ducts"
Ph.D. Thesis, University of London.

(18) CHENG R T, POWELL T M & DILLON T M (1976)
"Numerical Models of Wind-Driven Circulation in Lakes"
App. Math. Modelling, 1, pp. 141-159.

(19) CHOW V T (1959)
"Open-Channel Hydraulics"
McGraw-Hill Book Co., New York.

(20) CHOW W L & CHANG I S (1975)
"Mach Reflection Associated with Over-Expanded Nozzle Free Jet Flows"
AIAA Journal, Vol. 13, No. 6, pp. 762-766.

(21) CROSSLEY, Jr. H E & HARLEMAN D R F (1952)
"Studies on the Validity of the Hydraulic Analogy to Supersonic Flow"

Part V - Towed Model Investigation of Transonic Flow

M.I.T. Hydrodynamics Laboratory, Technical Report No. 11.

(22) DAKSHINAMOORTHY S (1977)

"High Velocity Flow through Expansions"

IAHR, 17th Congress, Vol. 2, pp. 373-380.

(23) DEMUREN A O (1979)

"Prediction of Steady Surface-Layer Flows"

Ph.D. Thesis, University of London.

(24) DRONKERS J J (1969)

"Tidal Computations for Rivers, Coastal Areas, and Seas"

Journal of the Hydraulics Division, ASCE, Vol. 95, No. HY 1, pp. 29-77.

(25) DUNN W E, POLICASTRO A J & PADDOCK R A (1975)

"Surface Thermal Plumes: Evaluation of Mathematical Models for the Near and Complete Field"

Argonne National Lab., Report ANL/WR-75-3.

(26) FERRI A (1949)

"Elements of Aerodynamics of Supersonic Flows"

The Macmillan Company, New York, pp. 172-178.

(27) FLOKSTRA C (1977)

"The Closure Problem for Depth-Averaged Two-Dimensional Flow"

IAHR, 17th Congress, Vol. 2, pp. 247-256.

(28) FORBES L K & SCHWARTZ L W (1981)

"Supercritical Flow Past Blunt Bodies in Shallow Water"

Journal of Applied Mathematics and Physics (ZAMP), 32, pp. 314-328.

(29) FRANCE P W (1981)

"Analysis of the Hydraulic Jump within a Diverging Rectangular Channel"

Proc. Instn Civ. Engrs., Vol. 71, Part 2, pp. 369-378.

(30) FRANKE P.-G. & VALENTIN F (1969)

"The Determination of Discharge Below Gates in Case of Variable Tailwater Conditions"

J. of Hydraulic Research, Vol. 7, No. 4, pp. 433-447.

(31) GILMORE F R, PLESSET M S & CROSSLEY, Jr. H E (1950)

"The Analogy between Hydraulic Jumps in Liquids and Shock Waves in Gases"

J. of Applied Physics, 21, pp. 243-249.

(32) GRIFFITH W (1952)

"Shock-Tube Studies of Transonic Flow over Wedge Profiles"

J. Aero. Sci., Vol. 19, No. 4, pp. 249-257.

(33) GROTKOP G (1973)

"Finite Element Analysis of Long-Period Water Waves"

Computer Methods in Applied Mechanics and Engineering, 2, pp. 147-157.

(34) HALL M G (1976)

"Transonic Flows"

in B.L. Hewitt, et al (eds.), "Computational Methods and Problems in Aeronautical Fluid Dynamics"

Academic Press, pp. 242-269.

(35) HARLOW F H & WELCH J E (1965)

"Numerical Calculation of Time-Dependent Viscous Incompressible Flow of Fluid with Free Surface"

The Physics of Fluids, Vol. 8, No. 12, pp. 2182-2189.

(36) HARTEN A & ZWAS G (1972)

"Self-Adjusting Hybrid Schemes for Shock Computations"

J. Comp. Phys., Vol. 9, pp. 568-583.

(37) HENRY H R (1950)

in discussion on "Diffusion of Submerged Jets" by M.L. Albertson, et al., Trans. ASCE, 115, pp. 687-697.

(38) HERBICH J B & WALSH P (1972)

"Supercritical Flow in Rectangular Expansions"

Journal of the Hydraulics Division, ASCE, Vol. 98, No. HY 9, pp. 1691-1700.

(39) HERBRAND K (1973)

"The Spatial Hydraulic Jump"

J. of Hydraulic Research, Vol. 11, No. 3, pp. 205-218.

(40) HOUGHTON D D & KASAHARA A (1968)

"Nonlinear Shallow Fluid Flow over an Isolated Ridge"

Communications on Pure and Applied Mathematics, 21, pp. 1-23.

(41) HOULT D P (1972)

"Oil Spreading on the Sea"

Annual Review of Fluid Mechanics, 4, pp. 341-368.

(42) HOYT J W (1962)

"The Hydraulic Analogy for Compressible Gas Flow"

Applied Mechanics Reviews, Vol. 15, No. 6, pp. 419-425.

(43) IPPEN A T (1942)

"Gas-Wave Analogies in Open-Channel Flow"

Proc. 2nd Hydraulics Conf., State University of Iowa, Studies in Engineering Bulletin, 27, No. 400, pp. 248-265.

(44) IPPEN A T (1950)

"Channel Transitions and Controls"

Chapter VIII in H. Rouse (ed.), "Engineering Hydraulics" John Wiley, New York.

(45) IPPEN A T (1951)

"Mechanics of Supercritical Flow"

Trans. ASCE, 116, pp. 268-295.

(46) IPPEN A T & DAWSON J H (1951)

"Design of Channel Contractions"

Trans. ASCE, 116, pp. 326-346.

(47) IPPEN A T & HARLEMAN D R F (1950)

"Studies on the Validity of the Hydraulic Analogy to Supersonic Flow"

Parts I, II and III
M.I.T. Hydrodynamics Laboratory, Technical Reports No. 1 and 4.

(48) IPPEN A T & HARLEMAN D R F (1956)

"Verification of Theory for Oblique Standing Waves"

Trans. ASCE, 121, pp. 678-694.

(49) JENNIONS I K (1980)

"The Impingement of Axisymmetric Supersonic Jets on Cones"

Ph.D. Thesis, University of London.

(50) JIRKA G H, ABRAHAM G & HARLEMAN D R F (1975)

"An Assessment of Techniques for Hydrothermal Prediction"

M.I.T., R.M. Parsons Lab. Report No. 203.

(51) JIRKA G H & HARLEMAN D R F (1979)

"Stability and Mixing of a Vertical Plane Buoyant Jet in Confined Depth"

J. Fluid Mech., Vol. 94, Part 2, pp. 275-304.

(52) KATOPODES N & STRELKOFF T (1979)

"Two-Dimensional Shallow Water-Wave Models"

Journal of the Engineering Mechanics Division, EM2, pp. 317-334.

(53) KAWAHARA M, TAKEUCHI N & YOSHIDA T (1978)
"Two Step Explicit Finite Element Method for Tsunami Wave Propagation Analysis"
Int. J. Numerical Methods in Engineering, Vol. 12, No. 2, pp. 331-351.

(54) KEDZIUR F, MOUSSIOPOULOS N, SCHUMANN U & STÖLTING K (1978)
"PWR-Depressurization and its Hydraulic Analogy"
Nuclear Engineering and Design, 47, pp. 25-34.

(55) KHALIFA A M & McCORQUODALE J A (1979)
"Radial Hydraulic Jump"
Journal of the Hydraulics Division, ASCE, Vol. 105, No. HY 9, pp. 1065-1078.

(56) KING H W & BRATER E F (1963)
"Handbook of Hydraulics"
5th Edition, McGraw-Hill.

(57) KNAPP R T (1951)
"Design of Channel Curves for Supercritical Flow"
Trans. ASCE, 116, pp. 296-325.

(58) KOLOSEUS H J & AHMAD D (1969)
"Circular Hydraulic Jump"
Journal of the Hydraulics Division, ASCE, Vol. 95, No. HY 1, pp. 409-422.

(59) KUIPERS J & VREUGDENHIL C B (1973)
"Calculations of Two-Dimensional Horizontal Flow"
Delft Hydraulic Laboratory, Report S 163 Part I.

(60) LAITONE E V (1952)
"A Study of Transonic Gas Dynamics by the Hydraulic Analogy"
Journal of the Aeronautical Sciences, 19, pp. 265-272.

(61) LANDRUM E J & MILLER D S (1981)
"Assessment of Analytical Methods for the Prediction of Supersonic Flow over Bodies"
AIAA Journal, Vol. 19, No. 2, pp. 160-164.

(62) LAUNDER B E & SPALDING D B (1972)
"Mathematical Models of Turbulence"
Academic Press, London and New York.

(63) LEENDERTSE J J (1970)

"A Water-Quality Simulation Model for Well-Mixed Estuaries and Coastal Seas: Vol. I, Principles of Computation"

The Rand Corporation, RM-6230-RC.

(64) LEENDERTSE J J & GRITTON E C (1971)

"A Water-Quality Simulation Model for Well-Mixed Estuaries and Coastal Seas: Vol. II, Computation Procedures"

The Rand Corporation, R-708-NCY.

(65) LEUTHEUSSER H J & ALEMU S (1979)

"Flow Separation Under Hydraulic Jump"

J. of Hydraulic Research, Vol. 17, No. 3, pp. 193-206.

(66) LEUTHEUSSER H J & KARTHA V C (1972)

"Effects of Inflow Condition on Hydraulic Jump"

Journal of the Hydraulics Division, ASCE, Vol. 98, No. HY 8, pp. 1367-1385.

(67) LIGGETT J A & VASUDEV S U (1965)

"Slope and Friction Effects in Two Dimensional, High Speed Channel Flow"

IAHR, 11th Congress, Vol. I, Paper No. 1.25.

(68) LIGGETT J A & WOOLHISER D A (1967)

"Difference Solutions of the Shallow-Water Equation"

Journal of the Engineering Mechanics Division, ASCE, Vol. 93, No. EM2, pp. 39-71.

(69) LOH W H T (1959)

"Hydraulic Analogy for Two-Dimensional and One-Dimensional Flows"

Journal of the Aerospace Sciences, 26, pp. 389-391.

(70) LONG R R (1954)

"Some Aspects of the Flow of Stratified Fluids: II. Experiments with a Two-Fluid System"

Tellus, Vol. 6, No. 2, pp. 97-115.

(71) McGUIRK J J & RODI W (1978)

"A Depth-Averaged Mathematical Model for the Near-Field of Side Discharges into Open Channel Flow"

JFM, Vol. 86, pp. 761-782.

(72) McGUIRK J J & RODI W (1979)

"Mathematical Modelling of Three-Dimensional Heated Surface Jets"

JFM, Vol. 95, Part 4, pp. 609-633.

(73) MAGALHAES L (1974)

"The Merging of Flow from a Sluice Gate with a Parallel Stream"

Ph.D. Thesis, University of London.

(74) MAXWELL T T (1977)

"Numerical Modelling of Free-Surface Flows"

Ph.D. Thesis, University of London.

(75) MOECKEL W E (1949)

"Approximate Method for Predicting Form and Location of Detached Shock Waves Ahead of Plane or Axially Symmetric Bodies"

NACA TN 1921.

(76) MOULT A, MARKATOS N C & SPALDING D B (1978)

"The Solution of Flow Problems in Highly Irregular Domains by the Finite-Difference Method"

in E. Alarcon and C.A. Brebbia (eds.), "Applied Numerical Modelling", Pentech Press, pp. 231-244.

(77) MURMAN E M (1972)

"Computational Methods for Inviscid Transonic Flows with Imbedded Shock Waves"

AGARD Lecture Series No. 48 on "Numerical Methods in Fluid Dynamics", Lecture No. 13.

(78) ORLIN W J, LINDNER N J & BITTERLY J G (1947)

"Application of the Analogy between Water Flow with a Free Surface and Two-Dimensional Compressible Gas Flow"

NACA, Report No. 875.

(79) PALUMBO D J & RUBIN E L (1972)

"Solution of the Two-Dimensional, Unsteady, Compressible Navier-Stokes Equations Using a Second-Order Accurate Numerical Scheme"

J. Comp. Phys., Vol. 9, pp. 466-495.

(80) PANDOLFI M & ZANNETTI L (1977)

"Numerical Investigation About the Predictions of Free Surface Shallow Water Motions"

Proc. 6th Australasian Hydraulics and Fluid Mechanics Conference, pp. 364-368.

(81) PATANKAR S V & SPALDING D B (1972)

"A Calculation Procedure for Heat, Mass and Momentum Transfer in Three-Dimensional Parabolic Flows"

Int. J. Heat Mass Transfer, 15, pp. 1787-1806.

(82) POSEY C J (1949)

"Gradually Varied Channel Flow"

in H.Rouse (ed.), "Engineering Hydraulics", John Wiley, p. 593.

(83) PREISWERK E (1940)

"Application of the Methods of Gas Dynamics to Water Flows with Free Surface"

Part (i) Flows with no Energy Dissipation
Part (ii) Flows with Momentum Discontinuities (Hydraulic Jumps)

NACA TM No. 934 and 935.

(84) PUN W M & SPALDING D B (1976)

"A General Computer Program for Two-Dimensional Elliptic Flows"

Imperial College, London, Mechanical Engineering Department Report No. HTS/76/2.

(85) RAJARATNAM N (1967)

"Hydraulic Jumps"

in V.T. Chow (ed.), "Advances in Hydroscience", Vol. 4, Academic Press, New York, pp. 197-280.

(86) RASTOGI A K & RODI W (1975)

"A Two-Dimensional Mathematical Model for the Dispersion of Heat in Rivers"

IAHR, 16th Congress, Vol. 4-5, pp. 146-153.

(87) RASTOGI A K & RODI W (1978)

"Predictions of Heat and Mass Transfer in Open Channels"

Journal of the Hydraulics Division, ASCE, Vol. 104, No. HY 3, pp. 397-420.

(88) RESCH F J & LEUTHEUSSER H J (1972)

"Reynolds Stress Measurements in Hydraulic Jumps"

J. of Hydraulic Research, Vol. 10, No. 4, pp. 409-430.

(89) ROACHE P J (1976)

"Computational Fluid Dynamics"

Hermosa Publications.

(90) RODI W (1978)

"Turbulence Models and their Application in Hydraulics - A State of the Art Review"

University of Karlsruhe, Report No. SFB 80/T/127.

(91) ROUSE H, BHOOTA B V & HSU E.-Y (1951)

"Design of Channel Expansions"

Trans. ASCE, 116, pp. 347-363.

(92) ROUSE H, SIAO T T & NAGARATNAM S (1959)

"Turbulence Characteristics of the Hydraulic Jump"

Trans. ASCE, 124, pp. 926-966.

(93) RUNCHAL A K (1971)

"A Review of the Problems Associated with Numerical Instabilities"

Imperial College, London, Department of Mechanical Engineering Report No. EF/IN/10.

(94) SAIVA G (1964)

"Hydraulic Analogy Studies of Shock Attachment to Wedges"

in R. Silvester (ed.), "Hydraulics and Fluid Mechanics" Pergamon Press, pp. 393-400.

(95) SCHLICHTING H (1968)

"Boundary-Layer Theory"

6th Edition, McGraw-Hill.

(96) SELLIN R H J (1969)

"Flow in Channels"

Macmillan and Co., London.

(97) SHEERAN W J & DOSANJH D S (1968)

"Observations on Jet Flows from a Two-Dimensional, Underexpanded, Sonic Nozzle"

AIAA Journal, Vol. 6, No. 3, pp. 540-542.

(98) SHUKRY A (1950)

"Flow around Bends in an Open Flume"

Trans. ASCE, 115, pp. 751-788.

(99) SIMONS T J (1972)

"Development of Numerical Models of Lake Ontario: Part 2"

Proc. 15th Conf. Great Lakes Res., Internat. Assoc. Great Lakes Res., pp. 655-672.

(100) SINGHAL A K (1977)

"Flow in Axial Turbomachinery Cascades"

Ph.D. Thesis, University of London.

(101) SINHA R, ZAKKAY V & ERDOS J (1971)

"Flowfield Analysis of Plumes of Two-Dimensional Underexpanded Jets by a Time-Dependent Method"

AIAA Journal, Vol. 9, No. 12, pp. 2363-2370.

(102) SMALL R D (1979)

"Overexpanded Two-Dimensional Transonic Free Jet"

AIAA Journal, Vol. 17, No. 3, pp. 307-309.

(103) SPALDING D B (1972)

"A Novel Finite Difference Formulation for Differential Expressions Involving both First and Second Derivatives"

Int. J. Num. Meth. Engng, Vol. 4, No. 4, pp. 551-559.

(104) SPALDING D B (1975)

"THIRBLE: Transfer of Heat in Rivers, Bays, Lakes and Estuaries"

Imperial College, Dept. of Mech. Eng., Rep. No. HTS/75/4.

(105) SPALDING D B (1976)

"Evironmental Impact of Energy Production: Heat and Mass Transfer Problems"

in J.C. Denton and N.H. Afgan (eds.), "Future Energy Production Systems, Heat and Mass Transfer Processes", Academic Press, Vol. II, pp. 729-745.

(106) SPALDING D B (1978)

Private communication.

(107) SPALDING D B (1979)

"Two-Dimensional Linear-Equation Solver"

Private communication, 9th Aug.

(108) SPALDING D B (1980)

"Mathematical Modelling of Fluid Mechanics, Heat Transfer and Mass Transfer Processes; a Lecture Course"

Imperial College, London, Mech. Eng. Dept. Rep. No. HTS/80/1.

(109) SPALDING D B (1981)

"The PHOENICS Computer Code"

Private communication.

(110) SRINIVAS K & GURURAJA J (1977)

"On the Computation of Two-Dimensional Compressible Flow Fields by the Modified Local Stability Scheme"

Computers and Fluids, Vol. 5, pp. 139-150.

(111) SRINIVAS K, GURURAJA J & PRASAD K K (1976)

"An Assessment of the Quality of Selected Finite-Difference Schemes for Time Dependent Compressible Flows"

J. of Computational Physics, Vol. 20, pp. 140-159.

(112) STEPHENSON G (1961)

"Mathematical Methods for Science Students"

Longman, p. 166.

(113) STOKER J J (1948)

"The Formation of Breakers and Bores - The Theory of Nonlinear Wave Propagation in Shallow Water and Open Channels"

Communications on Applied Mathematics, Vol. 1, pp. 1-87.

(114) STOLZENBACH K D, MADSEN O S, ADAMS E E, POLLACK A M & COOPER C K (1977)

"A Review and Evaluation of Basic Techniques for Predicting the Behavior of Surface Oil Slicks"

M.I.T., R.M. Parsons Lab. Report No. 222.

(115) TAYLOR T D, NDEFO E & MASSON B S (1972)

"A Study of Numerical Methods for Solving Viscous and Inviscid Flow Problems"

J. of Computational Physics, Vol. 9, pp. 99-119.

(116) TUCK E O (1978)

"Hydrodynamic Problems of Ships in Restricted Waters"

Ann. Rev. Fluid Mech., 10, pp. 33-46.

(117) VLIEGENTHART A C (1969)

"Dissipative Difference Schemes for Shallow Water Equations"

J. of Eng. Math., Vol. 3, No. 2, pp. 81-94.

(118) WANG J D & CONNOR J J (1975)

"Mathematical Modeling of Near Coastal Circulation"

M.I.T., R.M. Parsons Lab., TR. 200.

(119) WEARE T J (1976)

"Finite Element or Finite Difference Methods for the Two-Dimensional Shallow Water Equations ?"

Computer Methods in Applied Mechanics and Engineering, Vol. 7, pp. 351-357.

(120) WERLÉ H (1973)

"Hydrodynamic Flow Visualization"

Ann. Rev. Fluid Mech., 5, pp. 361-382.

(121) WERLE M J, SHAFFER D G & DRIFTMYER R T (1970)

"Freejet Terminal Shocks"

AIAA Journal, Vol. 8, No. 12, pp. 2295-2297.

(122) WILKINSON D L & WOOD I R (1971)
"A Rapidly Varied Flow Phenomenon in a Two-Layer Flow"
J. Fluid Mech., Vol. 47, Part 2, pp. 241-256.

(123) WILSON E H (1967)
"Location of the Hydraulic Jump in Open Rectangular Channels"
The Engineer, 223, pp. 145-149.

(124) XERIKOS J & ANDERSON W A (1962)
"A Critical Study of the Direct Blunt Body Integral Method"
Douglas Report No. SM-42603.

(125) YIH C.-S & GUHA C R (1955)
"Hydraulic Jump in a Fluid System of Two Layers"
Tellus VII, pp. 358-366.

(126) ZIENKIEWICZ O C & HEINRICH J C (1979)
"A Unified Treatment of Steady- State Shallow Water and Two-Dimensional Navier-Stokes Equations - Finite Element Penalty Function Approach"
Computer Methods in Applied Mechanics and Engineering, 17/18, pp. 673-698.

APPENDIX A

DERIVATION OF TWO-DIMENSIONAL SHALLOW-WATER EQUATIONS

In Chapter 3, Leibnitz's rule and the kinematic boundary conditions, at the bottom and surface of the water layer, were used in deriving the two-dimensional depth-averaged conservation equations (3.6) to (3.8) from the equation set (3.1) to (3.5). Details of this derivation are given below. The symbols used in this appendix are as used in the text and defined in Figure 3.1. Subscripts s and b define the variable values at the surface and bottom respectively. A general depth-averaged quantity ($\overline{\phi}$) is defined as follows:

$$\overline{\phi} = \frac{1}{h} \int_{z_b}^{z_b + h} \phi \, dz \qquad .(A1)$$

Leibnitz's Rule

This rule is used to change the order of integration and differentiation. Mathematically, if $f(x,\theta)$ is an integrable function of x in the range $a \leqslant x \leqslant b$ then by Leibnitz's rule (see, for example, Stephenson, 1961):

$$\frac{d}{d\theta} \int_a^b f(x,\theta)\, dx = f(b,\theta) \frac{db}{d\theta} - f(a,\theta) \frac{da}{d\theta} + \int_a^b \frac{\partial f(x,\theta)}{\partial \theta} dx \qquad .(A2)$$

The Kinematic Condition Representing the Surface

For a negligible loss or gain of mass (e.g. evaporation, rainfall), the kinematic condition is expressed as:

$$\frac{\partial h}{\partial t} + u_s \frac{\partial}{\partial x}(z_b + h) + v_s \frac{\partial}{\partial y}(z_b + h) = 0 \qquad .(A3)$$

The Kinematic Condition Representing the Bottom

The bottom surface is assumed rigid, impermeable, and stationary for which the kinematic condition is expressed as:

$$u_b \frac{\partial z_b}{\partial x} + v_b \frac{\partial z_b}{\partial y} = 0 \qquad .(A4)$$

Vertical Integration of the Continuity Equation

The continuity equation given by (3.1) is integrated, term by term, over the depth as follows:

$$\bullet \int_{z_b}^{z_b+h} \frac{\partial u}{\partial x}\, dz = \frac{\partial}{\partial x} \int_{z_b}^{z_b+h} u\, dz - u_s \frac{\partial}{\partial x}(z_b+h) + u_b \frac{\partial z_b}{\partial x} \qquad .(A5)$$

$$\bullet \int_{z_b}^{z_b+h} \frac{\partial v}{\partial y}\, dz = \frac{\partial}{\partial y} \int_{z_b}^{z_b+h} v\, dz - v_s \frac{\partial}{\partial y}(z_b+h) + v_b \frac{\partial z_b}{\partial y} \qquad .(A6)$$

Adding equations (A5) and (A6) and using equation (A1), one obtains:

$$\frac{\partial}{\partial x}(h\bar{u}) + \frac{\partial}{\partial y}(h\bar{v}) - \left[u_s \frac{\partial}{\partial x}(z_b+h) + v_s \frac{\partial}{\partial y}(z_b+h)\right] + \left[u_b \frac{\partial z_b}{\partial x} + v_b \frac{\partial z_b}{\partial y}\right] = 0 \qquad ,(A7)$$

The last two groups of terms in square brackets give $-\frac{\partial h}{\partial t}$ and 0 respectively, because of the kinematic conditions given by equations (A3) and (A4). The depth-averaged continuity equation is, therefore, given by:

$$\frac{\partial h}{\partial t} + \frac{\partial}{\partial x}(h\bar{u}) + \frac{\partial}{\partial y}(h\bar{v}) = 0 \qquad ,(A8)$$

This is equation (3.6) given in Chapter 3.

Vertical Integration of the u-Momentum Equation

The u-momentum equation given by (3.2) is integrated, term by term, over the depth as follows:

$$\bullet \int_{z_b}^{z_b+h} \left[\frac{\partial u}{\partial t} + \frac{\partial}{\partial x}(u^2) + \frac{\partial}{\partial y}(uv)\right] dz$$

$$= \frac{\partial}{\partial t}\int_{z_b}^{z_b+h} u \, dz + \frac{\partial}{\partial x}\int_{z_b}^{z_b+h} u^2 \, dz + \frac{\partial}{\partial y}\int_{z_b}^{z_b+h} uv \, dz$$

$$- u_s\left[\frac{\partial h}{\partial t} + u_s \frac{\partial}{\partial x}(z_b+h) + v_s \frac{\partial}{\partial y}(z_b+h)\right]$$

$$+ u_b\left[u_b \frac{\partial z_b}{\partial x} + v_b \frac{\partial z_b}{\partial y}\right] \qquad ,(A9)$$

The last two groups of terms in square brackets disappear because of the kinematic conditions given by equations (A3) and (A4).

$$\bullet \int_{z_b}^{z_b+h} -\frac{1}{\varrho}\frac{\partial p}{\partial x} \, dz = -gh\frac{\partial}{\partial x}(z_b+h) - \frac{h}{\varrho}\frac{\partial p_a}{\partial x} \qquad ,(A10)$$

where $\partial p/\partial x = \partial/\partial x\,(p_a + \varrho g h + \varrho g z_b)$.

$$\bullet \int_{z_b}^{z_b+h} f v \, dz = f\int_{z_b}^{z_b+h} v \, dz \qquad ,(A11)$$

$$\bullet \int_{z_b}^{z_b+h} \frac{1}{\varrho}\left(\frac{\partial \tau_{xx}}{\partial x} + \frac{\partial \tau_{xy}}{\partial y} + \frac{\partial \tau_{xz}}{\partial z}\right) dz =$$

$$\frac{1}{\rho}\frac{\partial}{\partial x}\int_{z_b}^{z_b+h}\tau_{xx}\,dz + \frac{1}{\rho}\frac{\partial}{\partial y}\int_{z_b}^{z_b+h}\tau_{xy}\,dz$$

$$-\frac{1}{\rho}\left[\tau_{xx_s}\frac{\partial}{\partial x}(z_b+h) + \tau_{xy_s}\frac{\partial}{\partial y}(z_b+h) - \tau_{xz_s}\right]$$

$$+\frac{1}{\rho}\left[\tau_{xx_b}\frac{\partial z_b}{\partial x} + \tau_{xy_b}\frac{\partial z_b}{\partial y} - \tau_{xz_b}\right] \qquad ,(A12)$$

The last two groups of terms in square brackets represent the surface and bottom stresses, $-\tau_{sx}$ and $-\tau_{bx}$ respectively.

Adding equations (A9), (A10), (A11) and (A12) together and using equation (A1), the depth-averaged u-momentum equation results in:

$$\frac{\partial}{\partial t}(h\bar{u}) + \frac{\partial}{\partial x}(h\bar{u}^2) + \frac{\partial}{\partial y}(h\overline{uv})$$

$$= -gh\frac{\partial}{\partial x}(z_b+h) - \frac{h}{\rho}\frac{\partial p_a}{\partial x} + f h \bar{v}$$

$$+\frac{1}{\rho}(\tau_{sx}-\tau_{bx}) + \frac{1}{\rho}\frac{\partial}{\partial x}(h\bar{\tau}_{xx}) + \frac{1}{\rho}\frac{\partial}{\partial y}(h\bar{\tau}_{xy}) \qquad ,(A13)$$

This is equation (3.7) given in Chapter 3.

Similarly, the v-momentum equation (3.3) can be integrated to yield equation (3.8).

It should be mentioned here that extra terms, due to non-uniform vertical distribution of the horizontal velocity components, may be added to the above depth-averaged momentum equations. They are neglected in this formulation on the assumption that the vertical profiles are uniform or nearly so. In the mathematical formulation made by , for example, Leendertse (1970), Kuipers and Vreugdenhil (1973), Wang and Connor (1975), these terms (called "dispersion" terms) were retained

in the depth-integrated momentum equations.

The above mentioned terms are modelled, as given by Leendertse, by expressing the distribution of the velocity components over the vertical as a function of the averages of these quantities, by introducing distribution coefficients ε_u and ε_v as follows:

$$u(z) = \bar{u}\left[1+ \varepsilon_u(z)\right] \quad ,$$

$$v(z) = \bar{v}\left[1+ \varepsilon_v(z)\right] \quad ,(A14)$$

or by splitting the local velocity components, as given by Kuipers and Vreugdenhil, into depth-averaged values and deviations as follows:

$$u = \bar{u} + (u-\bar{u}) \quad ,$$

$$v = \bar{v} + (v-\bar{v}) \quad .(A15)$$

The depth integration of the equations is then carried out. The form of the terms added to the depth-averaged u-momentum equation (A13), would be:

$$\frac{\partial}{\partial x}\int_{z_b}^{z_b+h} (u-\bar{u})^2 \, dz + \frac{\partial}{\partial y}\int_{z_b}^{z_b+h} (u-\bar{u})\,(v-\bar{v}) \, dz \quad .(A16)$$

However, these dispersion terms were neglected in the applications made by the above mentioned authors for the reasons of simplicity, inaccuracy that might result from choosing the distribution coefficients and being of little importance.

APPENDIX B

DERIVATION OF THE DEPTH-CORRECTION EQUATIONS

The role of the depth-correction equation along with its specific features have been explained in Section 4.2.4. This appendix presents its full derivation and clearly shows the contents of each term. Figure B1 depicts a typical continuity cell with mass fluxes (m) crossing its four cell faces. With no external sources or sinks of mass in the cell, the continuity conservation requires the balance of these fluxes over the cell faces. This is achieved, as indicated by the directions of the arrows, by:

$$m_e - m_w + m_n - m_s = 0 \qquad . \text{(B1)}$$

For constant density and by employing upstream depths throughout, equation (B1) becomes:

$$\delta y\, h_{p,E,u_e}\, u_e - \delta y\, h_{W,P,u_w}\, u_w + \delta x\, h_{p,N,v_n}\, v_n - \delta x\, h_{S,P,v_s}\, v_s = 0 \quad ,\text{(B2)}$$

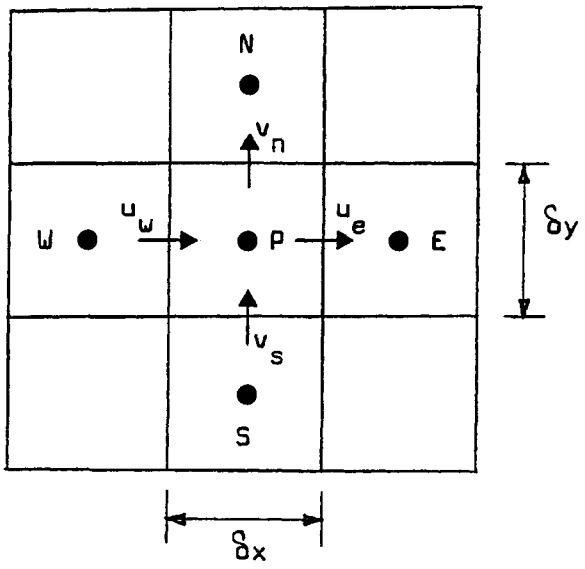


Figure B1 : Depth-correction cell

where the subscripts used for the depths have the following convention: the first and second subscripts indicate the two possible grid-node locations of the depth, either being chosen depending on the direction of velocity given in the third subscript. For positive or negative velocity, the depth takes the first or second subscript respectively.

The flow variables appearing in the above equation can be replaced by:

$$h = h^* + h' \quad ,$$

$$u = u^* + u' \quad ,$$

$$v = v^* + v' \quad , \tag{B3}$$

where the primed values are corrections added to the corresponding starred values during the solution process.

By substituting equations (B3) into equation (B2) and neglecting terms involving h'u' and h'v', one obtains:

$$\delta y\, h^*_{P,E,u_e}\, u'_e + \delta y\, h'_{P,E,u_e}\, u^*_e - \delta y\, h^*_{W,P,u_w}\, u'_w - \delta y\, h'_{W,P,u_w}\, u^*_w$$
$$+ \delta x\, h^*_{P,N,v_n}\, v'_n + \delta x\, h'_{P,N,v_n}\, v^*_n - \delta x\, h^*_{S,P,v_s}\, v'_s - \delta x\, h'_{S,P,v_s}\, v^*_s$$
$$= S_U \quad , \tag{B4}$$

where S_U is the continuity error given by:

$$S_U = \delta y\, h^*_{W,P,u_w}\, u^*_w - \delta y\, h^*_{P,E,u_e}\, u^*_e + \delta x\, h^*_{S,P,v_s}\, v^*_s - \delta x\, h^*_{P,N,v_n}\, v^*_n \quad . \tag{B5}$$

The primed velocities are related to the primed depths, using the truncated form of the momentum equations, by:

$$v'_n = D^v_n\,(h'_P - h'_N) \quad ,$$
$$v'_s = D^v_s\,(h'_S - h'_P) \quad ,$$
$$u'_e = D^u_e\,(h'_P - h'_E) \quad ,$$
$$u'_w = D^u_w\,(h'_W - h'_P) \quad , \tag{B6}$$

where the D coefficients are the same ones as those multiplying the depth-difference terms in the momentum equations.

Now, substituting equations (B6) into equation (B4) gives:

$$\underset{(1)}{\delta y\, h^{*}_{p,E,u_e}}\ \underset{(2)}{D^{u}_{e}\,(h'_{p} - h'_{E})} + \underset{(3)}{\delta y\, h'_{p,E,u_e}}\ \underset{(4)}{u^{*}_{e}} - \underset{(5)}{\delta y\, h^{*}_{W,P,u_w}}\ \underset{(6)}{D^{u}_{w}\,(h'_{W} - h'_{p})} - \underset{(7)}{\delta y\, h'_{W,P,u_w}}\ \underset{(8)}{u^{*}_{w}} + \underset{(9)}{\delta x\, h^{*}_{P,N,v_n}}\ \underset{(10)}{D^{v}_{n}\,(h'_{p} - h'_{N})} + \underset{(11)}{\delta x\, h'_{P,N,v_n}}\ \underset{(12)}{v^{*}_{n}} - \delta x\, h^{*}_{S,P,v_s}\, D^{v}_{s}\,(h'_{S} - h'_{p}) - \delta x\, h'_{S,P,v_s}\, v^{*}_{s} = S_{U} \qquad .(B7)$$

Equation (B7) contains twelve terms on the left-hand side. These can now be separated and written as:

u_e +ve (TERM1) $h'_{p} = (\ \delta y\, h^{*}_{p}\, D^{u}_{e}\ )\, h'_{p}$,

for

u_e -ve (TERM1) $h'_{p} = (\ \delta y\, h^{*}_{E}\, D^{u}_{e}\ )\, h'_{p}$,

u_e +ve (TERM2) $h'_{E} = (\ -\delta y\, h^{*}_{p}\, D^{u}_{e}\ )\, h'_{E}$,

for

u_e -ve (TERM2) $h'_{E} = (\ -\delta y\, h^{*}_{E}\, D^{u}_{e}\ )\, h'_{E}$,

u_e +ve (TERM3) $h'_{p} = (\ \delta y\, u^{*}_{e}\ )\, h'_{p}$,

for

u_e -ve (TERM3) $h'_{E} = (\ \delta y\, u^{*}_{e}\ )\, h'_{E}$,

u_w +ve (TERM4) $h'_{W} = (\ -\delta y\, h^{*}_{W}\, D^{u}_{w}\ )\, h'_{W}$

for

u_w -ve (TERM4) $h'_{W} = (\ -\delta y\, h^{*}_{p}\, D^{u}_{w}\ )\, h'_{W}$,

u_w +ve (TERM5) $h'_{p} = (\ \delta y\, h^{*}_{W}\, D^{u}_{w}\ )\, h'_{p}$,

for

u_w -ve (TERM5) $h'_{p} = (\ \delta y\, h^{*}_{p}\, D^{u}_{w}\ )\, h'_{p}$,

u_w +ve (TERM6) $h'_{W} = (\ -\delta y\, u^{*}_{w}\ )\, h'_{W}$,

for

u_w -ve (TERM6) $h'_{p} = (\ -\delta y\, u^{*}_{w}\ )\, h'_{p}$,

$$
\begin{aligned}
&v_n \text{ +ve} \qquad (\text{TERM7})\ h'_p = \left(\delta x\, h^*_p\, D^v_n \right) h'_p \quad , \\
&\text{for} \\
&v_n \text{ -ve} \qquad (\text{TERM7})\ h'_p = \left(\delta x\, h^*_N\, D^v_n \right) h'_p \quad , \\
&\\
&v_n \text{ +ve} \qquad (\text{TERM8})\ h'_N = \left(-\delta x\, h^*_p\, D^v_n \right) h'_N \quad , \\
&\text{for} \\
&v_n \text{ -ve} \qquad (\text{TERM8})\ h'_N = \left(-\delta x\, h^*_N\, D^v_n \right) h'_N \quad , \\
&\\
&v_n \text{ +ve} \qquad (\text{TERM9})\ h'_p = \left(\delta x\, v^*_n \right) h'_p \quad , \\
&\text{for} \\
&v_n \text{ -ve} \qquad (\text{TERM9})\ h'_N = \left(\delta x\, v^*_n \right) h'_N \quad , \\
&\\
&v_s \text{ +ve} \qquad (\text{TERM10})h'_S = \left(-\delta x\, h^*_S\, D^v_s \right) h'_S \quad , \\
&\text{for} \\
&v_s \text{ -ve} \qquad (\text{TERM10})h'_S = \left(-\delta x\, h^*_p\, D^v_s \right) h'_S \quad , \\
&\\
&v_s \text{ +ve} \qquad (\text{TERM11})h'_p = \left(\delta x\, h^*_S\, D^v_s \right) h'_p \quad , \\
&\text{for} \\
&v_s \text{ -ve} \qquad (\text{TERM11})h'_p = \left(\delta x\, h^*_p\, D^v_s \right) h'_p \quad , \\
&\\
&v_s \text{ +ve} \qquad (\text{TERM12})h'_S = \left(-\delta x\, v^*_s \right) h'_S \quad , \\
&\text{for} \\
&v_s \text{ -ve} \qquad (\text{TERM12})h'_p = \left(-\delta x\, v^*_s \right) h'_p \quad . \qquad (88)
\end{aligned}
$$

Equations (88) involve 24 operations. However, only twelve terms are needed to be evaluated and stored at any one time depending on the direction of the velocities. These terms will be needed in constructing the coefficients of the depth-correction equation as shown next.

The Final Form Of The Depth-Correction Equation

Equation (87) contains depth corrections at points P,N,S,E and W. This can now be simplified by grouping the coefficients for each depth-correction value and hence enable the h' equation to be put in the following form:

$$A_P h'_P = A_N h'_N + A_S h'_S + A_E h'_E + A_W h'_W + S_U \qquad ,(89)$$

this is equation (4.18) given in the main text at Section 4.2.4 in which:

$$A_N = - \text{TERM8} - \text{Min}(0, \text{TERM9}) \quad ,$$

$$A_S = - \text{TERM10} - \text{Min}(0, \text{TERM12}) \quad ,$$

$$A_E = - \text{TERM2} - \text{Min}(0, \text{TERM3}) \quad ,$$

$$A_W = - \text{TERM4} - \text{Min}(0, \text{TERM6}) \quad ,$$

$$\begin{aligned} A_P = {} & \text{TERM1} + \text{TERM5} + \text{TERM7} + \text{TERM11} \\ & + \text{Max}(0, \text{TERM3}) + \text{Max}(0, \text{TERM6}) \\ & + \text{Max}(0, \text{TERM9}) + \text{MAX}(0, \text{TERM12}) - S_P \end{aligned} \qquad ,(810)$$

where S_P is added as a part of the linearized source term. Its value is usually zero. It can be set to a large negative number for the grid nodes in the flow domain to ensure zero depth correction there, if required. S_U is the other part of the linearized source term which has been defined earlier and given by equation (85).

APPENDIX C

DEPTH-CORRECTION EQUATION AND ADJUSTMENT PROCEDURE FOR LOW FROUDE NUMBER FLOWS

Introduction

Low Froude number flows involve all subcritical flows and few supercritical ones in which Fr is not much greater than one. These flows are characterized in that the surface-elevation variation is not significant. This allows for a simpler, and hence cheaper, form of depth (pressure)-correction equation to be employed with a different adjustment procedure to solve for such flows as compared to the general form of the procedure used throughout the thesis and which is fully described in Appendix B. Its limited applicability, as far as Froude number is concerned, is demonstrated by a test case.

Strategy

The basic strategy is to regard the depth of flow that is used in the evaluation of the cell mass fluxes to be momentarily constant (equal to the previous iteration value). This allows for a simpler study of the effect of change in pressure (which is ultimately translated as a change in depth) on a corresponding change in flow rate through changes in velocities only.

It is particularly essential for this scheme to have two arrays for the depth, where the depth (h) is replaced by:

(i) "h", the depth used in the convection terms and

(ii) "p", the depth used in the momentum sources.

These two depths are separated and under-relaxed differently. The two fields will be different during the solution process but will be identical when a converged solution is obtained.

Derivation

This follows similar lines to those followed in the derivation of the general form of the h' equation given in Appendix B. The derivation yields a correction equation similar to equation (B9) and given by:

$$A_P p'_P = A_N p'_N + A_S p'_S + A_E p'_E + A_W p'_W + S_U \quad ,(C1)$$

but now with,

$$A_N = a_n D^v_n \quad ,$$
$$A_S = a_s D^v_s \quad ,$$
$$A_E = a_e D^u_e \quad ,$$
$$A_W = a_w D^u_w \quad ,$$
$$A_P = A_N + A_S + A_E + A_W - S_P \quad .(C2)$$

remarks

(i) S_U , S_P and the D's have the same meaning as in Appendix B.

(ii) The a's are the areas of the cell faces containing upstream depths (h) as given by equation (4.1).

(iii) The operations involved in evaluating the values of the coefficients are now much reduced (compare terms in equation C2 with their counterparts in equations B10 or 4.19). The storage needed for their saving is halved since the reciprocity rule is now applied.

(iv) The corresponding corrections to the velocities are the same as those given by equations (B3) and (B6).

Adjustment Procedure

The values obtained from solving equation (C1), using the same solver as described in Section 4.3.3, are the depth corrections to be added to the depths used in the momentum sources, i.e. p, as follows:

$$p_{new} = p_{old} + (\text{RELAXP})\, p' \quad ,(C3)$$

where RELAXP is the relaxation factor for p.

The corresponding velocity corrections are made in the same way as before.

Having obtained the p field, the h field is then allowed to change and calculated at the end of the iteration from:

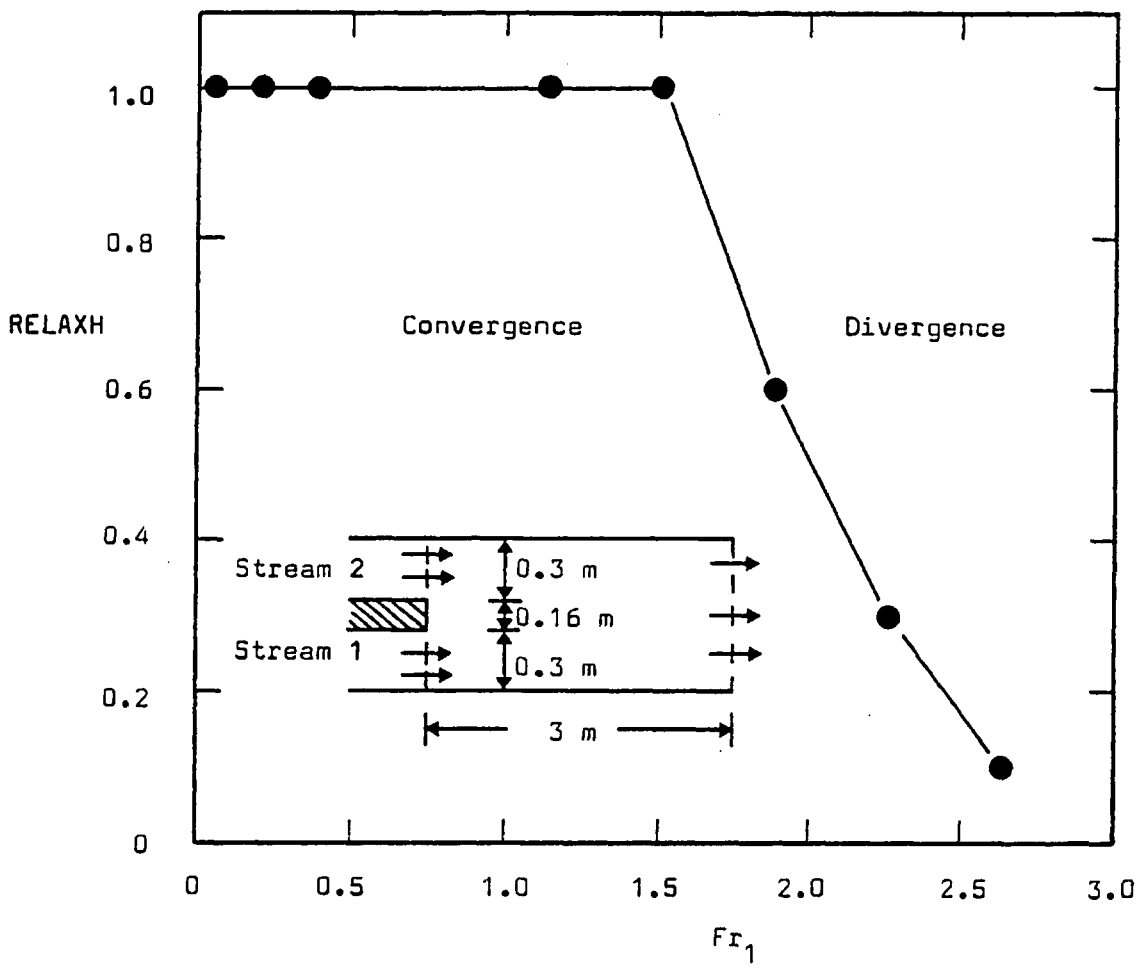
$$h_{new} = (RELAXH)\ p_{new} + (1- RELAXH)\ h_{old} \qquad ,(C4)$$

where RELAXH is the relaxation factor for h.
(RELAXH less than one implies that the depth values will change towards their corresponding effective pressure values but only gradually and become equal when a converged solution is obtained).

Performance of the Correction Procedure

The procedure is tested by applying it to simple flow situations; namely, laminar driven flow in closed square cavity, cavity flow with inflow and outflow boundaries and the flow situation described below. In all cases, converged and plausible results are obtained with a satisfactory convergence behaviour and the need to use moderate values of under-relaxation factors for all variables. Uniformly distributed grids are used throughout. For finer grids, smaller under-relaxation factors are needed. However, the performance deteriorates rapidly as Froude number increases, which is usually associated with larger variations in the surface elevation. This is cured by employing heavier under-relaxation factors on the depth changes. But with further increase in Fr, the relaxation factors needed for convergence become practically impossible to give a reasonable convergence speed.

Figure C1 shows the performance of this procedure for a uniform grid of 11x12 as applied for the physical problem presented in Section 7.3. The problem simulates the merging of two supercritical streams in a straight, rectangular and horizontal channel. The streams are separated



- Uniform grid: 11 x 12
- Relaxations for u,v and p = 0.1
- $\bar{h}_1$ = 3.1 cm , $\bar{h}_2$ = 5.5 cm
- $u_1 = u_2$; $Fr_2 = (\bar{h}_1 / \bar{h}_2)^{\frac{1}{2}} Fr_1$
- $v_1 = v_2 = 0$

FIGURE C1 : RELAXATION FACTOR FOR DEPTH VARIATION VERSUS FROUDE NUMBER

at the inlet by a thick wall. Problem specification and boundary conditions used are given in Section 7.3. The depths at the inlet of the two streams are kept constant, but different from each other; the inlet velocities are uniform. The investigation is carried out for a range of Fr between 0.05 and 3. The optimum under-relaxation factor used for the depth variation for each Fr investigated is recorded. The under-relaxation factors for u, v and p are kept constant, for consistency, at an optimum value of 0.1. As shown in the figure the solution diverges when Fr exceeds a value of about 2.8 even when employing very heavy relaxation on the depth variation (RELAXH = 0.01) which are calculated from the already relaxed pressure field, equations (C3) and (C4). For finer grids, the performance deteriorates even more.

Conclusions

(i) The procedure is simpler and cheaper to use as compared to the general purpose procedure. The ratio of the computing time per iteration per grid node is 1.0 : 1.32 for the two procedures respectively.

(ii) The procedure converges for subcritical flows and those at which Fr is not much greater than one.

(iii) Heavy under-relaxation factors are needed for all variables as Fr increases.

(iv) For even higher Fr, convergence is practically impossible.

(v) Its limited applicability, as far as Fr limitation is concerned, has made it improper to use in the present work and was indeed abandoned in favour of the more general one as described in Appendix B.

APPENDIX D

TABULATED EXPERIMENTAL DATA FOR 1D FLOWS

This appendix contains the data obtained in the experimental investigation reported in Section 5.2 and plotted in Figure 5.2. The tabulated values are the measured depths (h) at the specified locations (x), where x is measured from the sluice gate. In each case, the depth below the sluice (h_5) is 2.0 cm. The conjugate depths (h_1 and h_2), the distances to the toe and end of the jump (x_1 and x_2 respectively) and other pertinent data are given in each table. All dimensions are in centimeters. The variable names are as defined in the text and shown in Figure 5.1.

Set 1

This consists of five runs; namely, Runs 1.1 to 1.5. These are all for constant discharge per unit width (q) = 1.823×10^{-2} m^2/s ; Fr_3 = 3.88. The only parameter changed is h_t .

Table D1 : Run 1.1; h_4=11.8, h_t=4.46

x	15	50	100	150	201	222	230
h	1.30	1.46	1.72	2.01	2.20	4.46	4.46

x_1= 201 , x_2= 222 , h_1= 2.20 , h_2= 4.46.

Table D2 : Run 1.2; h_4=11.8, h_t=4.64

x	15	50	100	150	175	191	230
h	1.31	1.50	1.78	2.03	2.12	4.64	4.64

x_1= 175 , x_2= 191 , h_1= 2.12 , h_2= 4.64.

Table D3 : Run 1.3; h_4=11.8, h_t=5.34

x	15	50	75	118	133	230
h	1.32	1.51	1.57	1.86	5.34	5.34

x_1= 118 , x_2= 133 , h_1= 1.86 , h_2=5.34.

Table D4 : Run 1.4; h_4=11.8, h_t=5.60

x	15	50	84	100	230
h	1.32	1.49	1.64	5.60	5.60

x_1= 84 , x_2= 100 , h_1= 1.64 , h_2= 5.60.

Table D5 : Run 1.5; h_4=11.8, h_t=5.90

x	15	41	60	230
h	1.31	1.41	5.90	5.90

x_1= 41 , x_2= 60 , h_1= 1.41 , h_2= 5.90.

Set 2

This set also consists of five runs; namely, Runs 2.1 to 2.5. These are for constant tailwater depth (h_t) = 5.90. The only parameter changed is the upstream depth (h_4). The discharge (q) is per unit width and in m^2/s.

Table D6 : Run 2.1; h_4= 16.6, q= 2.196×10^{-2}, Fr_3= 4.68

x	15	50	90	120	150	192	207	230
h	1.32	1.50	1.67	1.77	1.94	2.03	5.90	5.90

x_1= 192 , x_2= 207 , h_1= 2.03 , h_2= 5.90.

Table D7 : Run 2.2; h_4= 14.7, q= 2.046×10^{-2}, Fr_3= 4.36

x	15	50	90	120	141	154	230
h	1.32	1.48	1.65	1.81	1.92	5.90	5.90

x_1= 141 , x_2=154 , h_1=1.92 , h_2= 5.90.

Table D8 : Run 2.3; h_4= 13.5, q= 1.951×10^{-2}, Fr_3= 4.16

x	15	50	90	118	133	230
h	1.32	1.48	1.68	1.82	5.90	5.90

x_1= 118 , x_2= 133 , h_1= 1.82 , h_2= 5.90.

Table D9 : Run 2.4; h_4= 12.7, q= 1.893×10^{-2}, Fr_3= 4.03

x	15	50	83	100	230
h	1.30	1.46	1.63	5.90	5.90

x_1= 83 , x_2= 100 , h_1= 1.63 , h_2= 5.90.

Table D10 : Run 2.5; h_4= 11.8, q= 1.823×10^{-2}, Fr_3= 3.88

x	15	41	60	230
h	1.31	1.41	5.90	5.90

x_1= 41 , x_2= 60 , h_1= 1.41 , h_2= 5.90.

NOTE : All dimensions are in cms.

APPENDIX E

TABULATED EXPERIMENTAL DATA FOR 2D FLOWS

This appendix contains the data obtained in the experimental investigation reported in Section 5.3. These data are shown in perspective views in Figures 5.5 and 5.6, they are plotted and compared with the calculations in Section 7.3. The tabulated values are the measured depths (h) at the specified x and y locations (see Figure 5.3). All dimensions are in centimeters. Full account of the test conditions is given in Table 5.2. The flow at the outlet boundary is being supercritical. The data are given here in tabular form, for both Runs 1 and 2 (slower and faster flows respectively), on the following pages.

Run 1 (All dimensions are in centimeters)

y	X=0 h	X=5 h	X=10 h	X=15 h	X=20 h	X=30 h	X=40 h
75.00	5.66	5.68	5.63	5.62	5.49	5.43	5.26
72.00	5.65	5.67	5.61	5.55	5.52	5.42	5.23
68.00	5.59	5.62	5.60	5.53	5.48	5.44	5.34
66.00	5.46	-	-	-	-	-	-
64.00	5.29	5.30	5.33	5.40	5.40	5.44	5.34
62.00	5.20	-	-	-	-	-	-
60.00	5.22	5.14	5.22	5.32	5.46	5.42	5.09
58.00	5.32	-	-	-	-	-	-
56.00	5.48	5.45	5.36	5.30	5.11	4.76	4.46
54.00	5.68	-	-	-	-	-	-
52.00	5.76	5.58	5.32	5.08	4.69	4.06	3.71
50.00	5.73	-	5.12	4.76	4.35	3.76	3.34
48.00	5.66	5.12	4.54	4.08	3.61	3.28	2.96
46.00	5.63	4.50	3.55	3.00	2.75	2.76	2.66
44.00	0.00	0.46	1.68	1.88	2.00	2.21	2.33
42.00	0.00	0.00	0.77	1.12	1.35	1.78	2.00
40.00	0.00	0.00	0.42	0.69	0.94	1.44	1.75
38.00	0.00	0.00	0.62	0.59	0.72	1.15	1.50
36.00	0.00	0.00	0.17	2.95	3.21	3.52	4.04
34.00	0.00	0.00	0.37	0.46	4.04	4.78	4.95
32.00	0.00	0.24	0.54	0.80	0.94	4.04	4.60
30.00	3.20	2.11	1.54	1.42	1.43	2.76	3.35
28.00	3.21	2.88	2.42	2.19	1.97	1.86	3.42
26.00	3.27	-	-	2.64	2.45	2.09	2.40
24.00	3.19	3.10	3.04	2.92	2.76	2.48	2.35
22.00	3.10	-	-	-	-	2.80	2.58
20.00	3.02	3.04	3.03	3.02	3.07	2.98	2.81
16.00	2.93	3.04	3.08	3.11	3.13	3.12	2.97
14.00	3.00	-	-	-	-	-	-
12.00	3.04	3.02	3.01	2.97	2.98	3.05	3.20
10.00	3.08	-	-	-	-	-	-
8.00	3.04	3.00	2.95	2.95	2.96	2.98	3.14
4.00	3.10	3.04	2.96	2.97	2.98	2.97	3.05
2.00	3.03	2.99	3.00	2.95	2.90	2.97	2.95
1.00	3.10	3.05	3.03	2.99	2.98	3.04	3.10

Run 1 (continued)

y	X=50	X=60	X=80	X=100	X=120	X=140	X=160
	h	h	h	h	h	h	h
75.00	5.07	4.80	4.37	3.47	2.75	2.40	2.19
72.00	5.04	4.77	4.19	3.40	2.79	2.40	2.10
68.00	5.06	4.74	3.95	3.29	2.74	2.46	2.15
64.00	4.96	4.44	3.76	3.18	2.80	2.48	2.19
60.00	4.43	3.95	3.49	3.06	2.78	2.48	2.49
58.00	-	-	-	-	-	-	2.65
56.00	4.02	3.52	3.22	2.92	2.74	2.60	3.49
54.00	-	-	-	-	-	2.71	3.75
52.00	3.48	3.15	2.92	2.75	2.69	3.22	3.68
50.00	3.08	-	-	2.65	2.83	3.88	-
48.00	2.78	2.66	2.59	2.62	3.62	4.00	3.58
46.00	2.48	-	2.45	2.79	3.96	3.95	-
44.00	2.20	2.14	2.44	3.73	4.10	3.96	3.76
42.00	2.03	1.97	3.31	4.02	-	-	-
40.00	1.86	2.14	3.93	4.08	4.16	4.07	3.97
38.00	2.80	3.36	-	-	-	-	-
36.00	3.66	3.40	4.12	4.18	4.22	4.16	3.98
34.00	4.70	4.17	-	-	-	-	-
32.00	4.64	4.32	3.92	4.34	4.25	4.19	4.06
30.00	4.18	4.00	-	-	-	-	-
28.00	4.17	4.20	4.00	4.40	4.32	4.19	4.19
26.00	3.64	4.35	-	-	-	-	-
24.00	2.60	4.02	4.05	4.29	4.32	4.18	4.53
22.00	2.32	2.92	-	-	-	-	-
20.00	2.44	2.36	4.35	4.14	4.31	4.22	5.00
18.00	2.57	2.40	-	-	-	-	5.34
16.00	2.74	2.54	4.03	4.04	4.27	4.48	5.60
14.00	-	-	3.20	-	-	-	5.96
12.00	3.00	2.75	2.74	4.23	4.14	4.91	6.22
10.00	-	-	2.67	4.35	-	5.21	5.95
8.00	3.08	2.94	2.63	4.24	4.16	5.60	5.51
6.00	-	-	-	3.10	4.24	6.55	5.29
4.00	2.90	2.85	2.77	2.90	4.56	6.17	5.38
2.00	2.84	2.89	2.82	2.78	5.20	5.38	6.00
1.00	2.85	2.96	2.90	2.84	6.55	5.24	6.24

Run 1 (continued)

y	X=180	X=200	X=220	X=230	X=240	X=250	X=260
	h	h	h	h	h	h	h
75.00	1.97	2.20	4.26	4.00	3.37	3.92	6.05
72.00	1.98	2.29	3.71	3.76	3.45	4.25	5.78
68.00	2.19	3.19	2.56	3.31	4.50	4.67	4.92
66.00	2.23	3.31	2.62	3.20	4.30	5.17	5.26
64.00	2.63	2.98	2.81	3.12	3.90	5.48	5.68
62.00	3.30	2.70	2.91	3.18	3.92	5.00	5.49
60.00	3.57	2.65	2.97	3.15	3.98	4.74	4.70
58.00	3.55	-	-	3.36	4.10	4.49	4.10
56.00	3.30	2.87	3.09	3.63	4.32	4.18	3.66
54.00	-	-	-	3.88	4.35	3.86	3.52
52.00	3.35	3.07	3.48	4.22	4.30	3.64	3.48
50.00	-	-	3.84	4.46	3.90	-	-
48.00	3.50	3.27	4.26	4.38	3.79	3.47	3.65
44.00	3.69	3.63	4.60	4.00	3.57	3.56	3.91
40.00	3.90	4.30	4.28	3.74	3.68	3.94	4.06
38.00	-	4.68	4.07	3.76	3.79	4.13	4.05
36.00	4.19	4.96	3.97	3.78	3.96	4.21	3.89
34.00	-	5.22	3.92	3.88	4.06	4.28	3.82
32.00	4.76	5.19	3.97	4.00	4.30	4.27	3.70
30.00	-	5.04	4.00	4.15	4.48	4.18	3.61
28.00	5.38	4.93	4.10	4.32	4.43	4.00	3.68
26.00	-	4.80	4.25	4.46	4.40	3.85	3.76
24.00	5.80	4.60	4.43	4.69	4.22	3.81	3.96
22.00	5.86	4.60	4.76	4.67	4.02	3.89	-
20.00	5.91	4.50	4.94	4.41	4.03	4.11	4.16
18.00	5.87	4.58	4.86	4.28	4.05	4.24	-
16.00	5.60	4.80	4.52	4.21	4.28	4.35	4.03
14.00	5.20	5.21	4.34	4.28	4.47	4.40	-
12.00	5.10	5.49	4.32	4.43	4.55	4.30	3.96
10.00	5.20	5.45	4.55	4.61	4.50	4.12	-
8.00	5.48	5.09	4.68	4.68	4.38	4.09	4.00
6.00	5.96	5.00	4.76	4.59	4.30	4.05	-
4.00	5.68	5.06	4.79	4.50	4.22	4.10	4.10
2.00	5.47	5.06	4.64	4.40	4.27	4.18	4.07
1.00	5.47	5.23	4.63	4.43	4.26	4.18	4.09

Run 1 (continued)

y	X=270 h	X=280 h	X=290 h	X=300 h
75.00	6.22	5.90	5.38	4.98
72.00	6.37	5.97	5.26	5.00
68.00	5.20	6.00	5.22	5.08
66.00	5.00	5.75	5.30	5.38
64.00	4.77	5.26	5.75	5.64
62.00	4.82	4.60	6.23	6.00
60.00	4.90	4.85	6.07	6.47
58.00	4.60	5.40	5.72	6.60
56.00	4.23	5.56	6.00	5.71
54.00	4.11	5.34	6.02	5.68
52.00	4.10	4.85	5.42	5.83
50.00	-	4.62	4.80	5.47
48.00	4.12	4.24	4.37	5.16
46.00	-	3.92	-	4.95
44.00	4.03	3.70	3.88	4.77
42.00	-	-	-	4.63
40.00	3.76	3.53	3.86	4.51
36.00	3.57	3.59	3.96	4.16
32.00	3.64	3.89	3.86	3.66
28.00	3.92	3.99	3.60	3.63
24.00	4.07	3.72	3.57	3.70
20.00	3.88	3.65	3.65	3.76
16.00	3.75	3.72	3.75	3.70
12.00	3.80	3.80	3.74	3.59
8.00	3.96	3.79	3.63	3.55
4.00	3.94	3.78	3.59	3.50
2.00	3.92	3.81	3.61	3.50
1.00	3.92	3.82	3.62	3.56

Run 2 (All dimensions are in centimeters)

y	X=0 h	X=5 h	X=10 h	X=15 h	X=20 h	X=30 h	X=40 h
75.00	5.87	6.02	6.10	6.16	6.20	6.17	6.10
72.00	5.81	5.96	5.98	5.99	6.10	6.05	5.92
68.00	5.56	5.61	5.65	5.58	5.61	5.77	5.82
64.00	5.53	5.48	5.44	5.36	5.35	5.33	5.40
60.00	5.46	5.43	5.34	5.36	5.23	5.15	5.10
56.00	5.49	5.46	5.42	5.36	5.30	5.04	4.88
54.00	-	-	-	-	5.38	5.11	4.80
52.00	5.40	5.32	5.36	5.41	5.43	5.07	4.66
50.00	-	-	-	5.12	4.95	4.63	4.24
48.00	5.52	5.28	4.90	4.37	3.92	3.65	3.54
46.00	-	0.00	3.65	3.57	3.02	2.75	2.76
44.00	0.00	0.00	1.50	2.10	2.09	2.21	2.34
42.00	0.00	0.00	0.00	0.83	1.24	1.65	2.02
40.00	0.00	0.00	0.00	0.42	0.73	1.20	1.58
38.00	0.00	0.00	0.00	0.29	1.90	0.84	1.32
36.00	0.00	0.00	0.00	-	0.39	4.39	4.14
34.00	0.00	0.00	0.00	0.40	-	-	4.92
32.00	0.00	0.00	0.44	0.54	0.70	1.04	4.49
30.00	-	0.00	2.00	1.38	1.29	1.44	1.75
28.00	3.04	2.91	2.64	2.36	2.30	2.03	1.94
26.00	-	-	-	-	2.81	2.47	2.29
24.00	3.10	3.13	3.09	3.01	2.93	2.78	2.61
22.00	-	-	-	-	-	2.94	2.79
20.00	3.06	3.04	3.06	3.03	3.08	3.08	3.05
16.00	3.09	3.04	3.05	3.05	3.00	3.08	3.15
12.00	3.02	3.02	3.06	3.08	3.12	3.14	3.22
8.00	2.99	3.06	3.08	3.13	3.02	3.31	3.36
4.00	3.18	3.10	3.05	3.02	3.06	3.12	3.24
1.00	3.20	3.19	3.13	3.06	3.11	3.23	3.33

Run 2 (continued)

y	X=50	X=60	X=80	X=100	X=120	X=140	X=160
	h	h	h	h	h	h	h
75.00	5.67	5.43	5.04	4.65	4.22	3.89	3.52
72.00	5.69	5.44	4.87	4.57	4.06	3.72	3.27
68.00	5.72	5.54	4.89	4.27	3.90	3.52	3.14
64.00	5.37	5.27	4.87	4.28	3.87	3.52	3.09
60.00	4.97	4.80	4.59	4.03	3.63	3.43	3.08
56.00	4.62	4.26	4.09	3.76	3.39	3.16	3.06
52.00	4.19	3.62	3.49	3.41	3.15	2.90	2.89
50.00	3.89	-	-	3.18	-	-	2.93
48.00	3.36	3.07	2.86	2.98	3.01	2.91	3.15
46.00	2.68	-	-	-	2.97	3.60	4.00
44.00	2.32	2.16	2.34	2.63	2.90	4.00	4.37
42.00	2.11	1.89	2.09	2.85	3.97	-	-
40.00	1.77	1.65	3.40	3.81	4.40	4.52	4.40
38.00	1.46	-	3.80	-	-	-	-
36.00	4.03	4.20	-	4.61	4.39	4.77	4.70
34.00	4.15	4.85	-	-	-	-	-
32.00	4.69	4.20	4.34	4.31	4.63	4.84	4.91
30.00	3.26	2.85	4.06	-	-	-	-
28.00	2.83	3.20	4.60	4.43	4.71	4.95	4.78
26.00	1.97	2.80	4.00	-	-	-	-
24.00	2.20	2.02	3.20	4.82	4.65	4.67	4.63
22.00	2.56	2.20	2.80	-	-	-	-
20.00	2.80	2.50	-	4.67	4.58	4.62	4.73
18.00	-	2.70	2.68	3.60	-	-	-
16.00	3.01	2.82	2.84	2.90	4.81	4.44	4.60
14.00	-	-	-	2.76	4.60	-	-
12.00	3.15	3.04	2.91	2.85	3.60	4.64	4.37
10.00	-	-	-	-	3.07	-	-
8.00	3.15	3.00	3.05	3.00	2.95	4.62	4.37
6.00	-	-	-	-	-	3.60	-
4.00	3.24	3.13	3.03	2.92	2.92	3.14	4.74
2.00	-	-	-	-	-	2.99	4.89
1.00	3.22	3.26	3.13	3.00	3.00	3.02	5.35

Run 2 (continued)

y	X=180 h	X=200 h	X=220 h	X=240 h	X=260 h	X=280 h	X=300 h
75.00	3.09	2.81	2.47	2.37	2.18	2.44	4.31
72.00	2.95	2.70	2.47	2.29	2.19	2.62	3.70
68.00	2.84	2.57	2.37	2.22	2.27	3.28	2.98
66.00	-	-	-	-	-	3.53	2.77
64.00	2.81	2.52	2.34	2.34	3.00	3.28	2.86
62.00	-	-	-	2.55	3.72	2.94	-
60.00	2.83	2.47	2.43	3.00	3.58	2.92	3.16
56.00	2.87	2.56	2.96	3.82	3.22	3.22	3.38
52.00	2.99	3.02	3.94	3.39	3.25	3.29	3.70
50.00	3.40	-	3.71	-	-	-	4.13
48.00	4.20	4.10	3.57	3.47	3.34	3.44	4.47
44.00	4.40	4.06	3.74	3.46	3.27	3.86	5.31
42.00	-	-	-	-	-	-	5.56
40.00	4.46	4.17	3.78	3.55	3.47	4.58	5.51
36.00	4.48	4.03	3.78	3.80	4.00	5.29	5.28
34.00	-	-	-	-	-	5.58	4.95
32.00	4.46	4.02	3.87	4.05	4.73	5.66	4.65
30.00	-	-	-	-	-	5.74	4.58
28.00	4.56	4.12	4.07	4.45	5.49	5.60	4.56
26.00	-	-	-	-	5.79	5.21	4.70
24.00	4.70	4.25	4.11	5.00	6.01	5.03	4.83
22.00	-	-	-	-	6.01	4.74	5.21
20.00	4.70	4.40	4.47	5.63	5.67	4.86	5.38
18.00	-	-	-	6.28	5.27	5.03	5.43
16.00	4.68	4.60	5.10	6.15	5.00	5.31	5.30
14.00	-	-	6.09	-	4.94	5.58	5.11
12.00	4.73	5.12	6.90	5.60	4.97	5.66	4.96
10.00	-	5.46	6.68	5.26	5.29	5.48	4.89
8.00	4.97	6.29	6.42	5.26	5.80	5.06	4.89
6.00	-	7.14	6.00	5.42	5.75	4.91	4.86
4.00	5.45	6.69	5.68	5.93	5.39	4.95	4.82
2.00	6.84	5.86	5.98	6.08	5.25	5.06	4.76
1.00	7.08	5.70	6.31	5.92	5.36	5.04	4.85